12-2012

# SYNTHESIS AND CHARACTERIZATION OF NANOSCALE FLUORESCENT POLYMER FILMS

Maryus Chyasnavichyus
*Clemson University*, cchyasn@clemson.edu

# SYNTHESIS AND CHARACTERIZATION OF NANOSCALE FLUORESCENT POLYMER FILMS

---

A Dissertation
Presented to
the Graduate School of
Clemson University

---

In Partial Fulfillment
of the Requirements for the Degree
Doctor of Philosophy
Materials Science and Engineering

---

by
Maryus Chyasnavichyus
December 2012

---

Accepted by:
Dr. Igor Luzinov, Committee Chair
Dr. Douglas Hirt
Dr. Stephen H. Foulger
Dr. Konstantin Kornev
Dr. Bogdan Zdyrko

## ABSTRACT

Performance of the chemical sensing devices is based sensitivity to the targeted analytes and accuracy of the measurements. Of many different types of chemical sensors, fluorescence based sensing devices draw much attention as efficient yet small and straightforward devices, capable of detection of various analytes at extremely small quantities.

Polymeric materials provide support for the fluorescent materials and usually serve as a host for the chromophores, protecting them from harsh environments, and serve as a transport media for the analyte.

In the present study thin fluorescent polymer films, sensitive to the environment are synthesized and studied. Poly(glycidyl methacrylate) was used as a host material and Rhodamine B (RhB) was used as a fluorescent material. PGMA-RhB polymer films deposited on the flat surface of silicon wafers and glass slides showed the ability to uptake vapor of organic solvents from the vapor phase. It was observed, that during the swelling of the film fluorescent emission of the RhB molecules changes.

Those changes were attributed to the variations in the RhB immediate environment, therefore confirming the sensitivity of the PGMA-RhB layer to the environmental changes. The fluorescent response of the PGMA-RhB layer was unique for each analyte used in the study and could be tuned by grafting of non-fluorescent layer to the surface of PGMA-RhB.

Four different polymers (polystyrene, poly(2-vinyl pyridine), polyacrylic acid, and polyethylene glycol) were grafted to the surface of PGMA-RhB and each of the polymers grafted induced unique changes of fluorescent response of the PGMA-RhB.

The attachment of the sensitive fluorescent layers to the surface of silica nanoparticles and fibers of Polyethylene terephthalate fabrics was performed. The sensitivity of the PGMA-RhB layers of structures with high roughness was improved, while the ability to tune the fluorescent response of the system was retained. Overall the studies have shown, that proposed method of fluorescent response tuning could be used in sensing applications.

## DEDICATION

I would like to devote this work to my parents Tatiana Chyanavichene and Kyastas Chyasnavichyus who have always believed in me, to my brother Julius Chyasnavichyus who have never left my side and to my closest friend, Daria Monaenkova, who was always there for me to share the worst and the best moments of my PhD journey. Thank you all for your patience and sacrifice you made in order to let this day happen.

## ACKNOWLEDGEMENTS

First of all I would like to acknowledge gratefully my advisor, Dr. Igor Luzinov, whose insightful mentorship, patience and encouragement helped me to find my way in science and complete my PhD trail in the most efficient way.

I appreciate the time as well as helpful suggestions on my work from my committee members, Dr. Bogdan Zdyrko, Dr. Stephen H. Foulger, Dr. Douglas E. Hirt, Dr. Konstantin Kornev. I owe a special acknowledgment to Dr. Stephen H. Foulger for providing access to the spectrophotometer and for multiple discussions on experimental methods I have used and underlying theory, for the criticism, which allowed me to deepen my knowledge and improve the quality of my work substantially. I also owe a special thanks to Dr. Bogdan Zdyrko who have helped me a lot with so many aspects of my research.

I would like to acknowledge Dr. Victor Klep for his guidance at the initial stage of this work, for multiple valuable advices and all the time he spent with me in the laboratory.

I am grateful to Dr. Volodymyr Tsyalkovskyfor sharing his experience and his willingness to discuss the progress of the project.

I am thankful for and would like to acknowledge the members of our research laboratory who helped me along the way: Dr. Ruslan Burtovyy, Dr. Olga Hoy, Dr. Oleksandr Burtovyy, Mr. Yura Galabura, Mr. Michael Seeber, Mr. James Giammarco, Ms. Fehime Vatansever, Ms. Tugba Demir and Ms. Anna Paola Soliani. Thank you for

fruitful discussions, brainstorms on Friday's group meetings, challenging questions and exciting mutual work.

Also, I would like to acknowledge the help of the intern students, who broadened the value of the work and helped me a lot with data acquisition: Ms. Carole Hubert, Mr. Levan Khulordava, Mr. David Kohen, Mr. Jacob Maggio, and Mr. Chad Cummings.

I would like to acknowledge my funding agency NSF, grants number CBET-0756457, CMMI-0825773, CMMI-0826067 for support of this research.

I would like to express my sincere gratitude to my mentors from IPMech RAN Dr. Robert Goldstein, Dr. Edward Teodorovich and Dr. Konstantin Ustinov, without whose support I would have never found a courage to pursue a Doctorate degree.

## TABLE OF CONTENTS

Page

Table of Contents (Continued)

Figure Page

Table of Contents (Continued)

Figure Page

Table of Contents (Continued)

Figure Page

Table of Contents (Continued)

Figure Page

## LIST OF TABLES

Table Page



## LIST OF FIGURES

Figure Page

List of Figures (Continued)

Figure Page

List of Figures (Continued)

Figure Page

List of Figures (Continued)

Figure Page

List of Figures (Continued)

Figure Page

List of Figures (Continued)

Figure Page

List of Figures (Continued)

Figure Page

# CHAPTER ONE

# INTRODUCTION

Chemical sensing devices are essential in many areas of scientific research and daily life ranging from health care to homeland security. Effectiveness of the sensing devices is defined by the sensitivity to the targeted analytes and accuracy against false-positive measurements. That is why sensing devices based on the fluorescence are widely used in modern chemical detection. Such devices are portable, precise, sensitive and easy to use.

However to achieve such high performance of these devices precise control over the properties of fluorescent material environment is needed. That is why much attention is devoted to the design of the host media for the fluorescent materials comprising the sensitive part of chemical detectors.

Of all the possible materials of the fluorophores encapsulation polymers draw the most attention due to their unique properties. Polymeric materials can bear multiple functionalities and can be attached to the variety of surfaces. Their properties can be tuned by the means of the chemical design to make them durable, adherent or conductive. Polymeric materials can also be responsive to the external stimuli, producing smart materials, which can adjust their properties during their use.

One of the foremost features of the polymeric materials is the possibility of their use in nanoscale amounts. Polymers can be applied to the surface of other materials as thin films with the thickness ranging from several nanometers to several microns. Despite

of the small amounts, polymer materials can drastically change the surface properties of underlying substrate. Nanoscale polymer films can cover the rough surfaces and nanoscale objects, which have high area to volume ratios. Since the surface of the material is primarily exposed to the environment, materials with large surface area covered with the fluorescent polymer films find multiple uses in sensing applications. However, to create high precision detecting devices it is necessary to understand the effects of host material on the behavior of the fluorescent molecules embedded in it.

The ultimate goal of current study is to fabricate and characterize thin fluorescent polymer films, sensitive to the environment, which could be employed for surface modification of the flat surfaces, rough materials, and nanoobjects. The present study also studies the possibility of tuning the fluorescent response of such polymer film by non-fluorescent grafting. Such tuning may be employed for the sensing applications to tailor the selectivity of the chemical detecting devices.

**Chapter 2** provides the brief overview of the fluorescent materials, their properties and the methods of the use of fluorescent materials in the sensing applications with the emphasis on the use of the thin polymer films in these applications. Also the current progress in polymer film preparation techniques, methods of the polymer film modification, and behavior of the polymer film subjected to the changing environment is discussed. Based on the techniques found in literature, **Chapter** 3 gives descriptions of the experimental techniques used in this work.

In the first part of this study experimental procedures for fluorescent film preparation are developed. Poly(glycidyl methacrylate) (PGMA) is used for the host

material for the fluorescent molecules of Rhodamine B (RhB). In **Chapter 4** deposition techniques and properties of the fluorescent films such as the PGMA-RhB layer uniformity and thickness are studied to design the method of deposition of uniform PGMA-RhB film with preset properties. Also the ability of the PGMA-RhB film to uptake the vapor of organic solvent and sensitivity of the fluorescent emission to the environmental changes are studied qualitatively to determine the possibility of use of such a film for sensing applications.

**Chapter 5** describes the synthesis and characterization of ultrathin PGMA-RhB films. Such ultrathin polymer layers can be applied to the objects with the nanoscale size features and are better suited for sensing applications than thicker films, because of fast response times. In this chapter the ability of ultrathin polymer films to uptake the analyte from the vapor phase is studied together with the variation of fluorescent emission response in changing environment. Also different solvents are compared in terms of emission intensity and polymer film thickness changes to investigate the possibility to distinguish between the analytes. In addition, the data processing methods are developed in this chapter to define the degree of the thickness changes, fluorescent emission variation and affinity of the solvent to the sensitive layer.

In **Chapter 6** the possibility of tuning fluorescent emission of the ultrathin PGMA-RhB film with the polymer grafting is studied. Techniques for the PGMA-RhB film modification with polystyrene (PS), poly(2-vinyl pyridine) (P2VP), polyacrylic acid (PAA), and polyethylene glycol (PEG) are developed. The separate studies on the thick films of these polymers are also performed in this chapter to study such properties as

refractive indexes and affinity to the solvents of different nature. The swelling of modified PGMA-RhB films is performed to study how the affinity of fluorescent layer to the solvent is changing upon polymer grafting. Also changes of PGMA-RhB fluorescent properties in the vapors of organic solvents are studied in order to investigate the influence of grafted non-fluorescent polymer layers of the fluorescent emission of PGMA-RhB film. To increase the sensitivity of the fluorescent emission change the incorporation of gold nanoparticles with distance dependent fluorescent quenching properties is studied.

The further tuning of the fluorescent properties of the modified PGMA-RhB films by variation of properties of the grafted layer is studied in **Chapter 7.** Specifically, changes in the grafting density of the non-fluorescent layer and variation of composition of the grafted layer are investigated.

In **Chapter 8** fluorescent sensitive layer application on silica nanoparticles and rough surface of fabric is investigated. It is shown how sensitivity of the PGMA-RhB films applied onto the materials with high surface-to-volume ratios increases for the analytes both in liquid phase and the vapor. Complex structure of PGMA-RhB modified nanoparticles attached to the fabric is designed to achieve high sensitivity of the fluorescent layers.

In conclusion, this dissertation will provide the fundamentals for fabrication and characterization of thin fluorescent polymer layers sensitive to the environment with controllable properties, which could be applied to the variety of surfaces.

# CHAPTER TWO

# LITERATURE REVIEW

The present research is devoted to the preparation of the thin fluorescent polymer films sensitive to the environment and to the study of their properties. Therefore, it is essential to know how the fluorescent properties can be given to polymer film and how these properties are affected when the film is subjected to the environmental changes. It is also essential to understand the principles of polymer film fabrication, polymer film characterization and behavior of the polymer film during the interaction with the environment.

To this end this chapter gives a brief overview of the fluorescent materials, their properties and the methods of the use of fluorescent materials in the sensing applications. Advantages of fluorescent materials incorporation into the polymer films for sensing purposes are discussed as well. Polymer film preparation techniques, methods of the polymer film modification, and behavior of the polymer film subjected to the changing environment are presented in this chapter to overview the state of the art in the field of surface modification with polymer films.

## 2.1. Fluorescent materials

Application of the fluorescent properties to the material significantly broadens the ways of materials possible applications. Fluorescence is the ability of the substance to emit light in response to excitation caused by the absorption of electromagnetic radiation [1]. Main characteristic of fluorescent material are the brightness of the emission and its

stability over time[2]. Brightness of the fluorescent materials depends on its quantum yield. Quantum yield is defined by as the ratio between the amount of photons emitted by the material to the amount of photons absorbed[3]. Quantum yield of the material is very sensitive to the environment, since various effects such as Forster resonance Energy Transfer (FRET), quenching, dimer formation and solvatochromism produce the means of non-radiative decay of the excited state, thus decreasing the photon emission probability[3]. This sensitivity can be used in the straightforvard and very simple in design, yet efficient sensing devices. For example, Chunga et al.[4] showed that thin fluorescent polymer films can be used as a crack sensor. The thin film made of cyclobutane-type dimers of cinamoyl groups was deposited on the surface of the plastic samples. When the samples were bent, the cracks in the polymer film mechanochemically cleaved cyclobutane links, producing highly fluorescent cinnamoyl groups. This way it is possible to straightforwardly visualize the crack in materials using fluorescent microscopy.

### 2.1.1. Types of fluorescent materials

There are two major types of fluorescent materials: quantum dots and organic dyes. Quantum dots are semi-conductor nanocrystals with the size less than 10 nm[5]. Effect of quantum confinement gives rise to unique optical properties, such as light emission upon excitation with the photon[6]. The modern production techniques of quantum dots are well developed, allowing creation of monodisperse quantum dots of well-defined sizes[7]. Quantum dots are very bright and stable over time, and find multiple uses in many technological applications, such as laser emitters[8], charge storage devices[9]

and quantum information processing[10]. However, due to the complex surface modification techniques and cytotoxicity, their use in bioengineering and medical applications is limited[11].

Organic fluorescent dye is nature created or human made organic molecule which can be excited to the higher energy state by light irradiation. When it reverts back to the ground state, such molecule can emit photon[12]. Organic dyes are less bright and less stable than quantum dots, however they have several important advantages: they are small in size (~0.5 nm), can have low toxicity and can be easily bound to biomolecules[13]. Modern technologies allow synthesis of the dye molecules with precisely controlled chemical and optical properties[12] as well as attachment of these molecules to the polymer chains[14], proteins and living cells[15], and nanoparticles[16].

### 2.1.2. Properties and applications

Due to the ability of fluorescent material to interact with the light and high sensitivity of the fluorescent emission to the environment of the emitters fluorescent materials are widely used in many applications[1]. Fluorescent materials are used for centuries for the food and textile coloration[17]. They also find multiple uses for the visualization in biology and medicine[18]. For example, organic dye labeled proteins can be used for the visualization of the protein migration during the embryo growth. In the work of Canaria and Lansford[19] confocal and multi-photon time-lapse microscopy was used to study cell behavior, and embryo development over time.

Organic fluorescent materials are widely used in the as organic light-emitting devices such as light emitting diodes and organic light-emitting transistors[20]. For example, in the work of Muccini et al.[21] an OLET with maximum efficiency exceeding 5% is shown. Organic dyes can be also incorporated as a component of photovoltaic cells [22], and sensing devices[23].

### 2.2. Sensing devices based on fluorescence

Sensing devices based of the external stimuli responsive changes of fluorescent properties of the material are extremely efficient[24]. Such sensing devices have several advantages over the other types of chemical sensors such as chromatography, spectrometry, and electrochemical sensors[25]. Fluorescence based optical sensors are highly sensitive, small and long lasting[26]. In addition, they are immune to electromagnetic interference, completely passive and, unlike some other types of sensors, have no moving parts, which could fail after a certain number of cycles[27].

Various characteristics of excitation and subsequent emission process (decay time, energy transfer and quenching efficiency, intensity of polarization and stokes shift)can be used for the sensing applications of fluorescent materials[28]. For example, non-radiative energy transfer from the excited fluorophores allows detection of oxygen[29], metal ions[30] and halogens[31].

Working principle of sensing devices for anion detection, according to Forster mechanism[32] is based on the electron transfer between fluorophores and anion. In case of chemosensors for the transition metal ions, the sensing system usually consists of the

active fluorescent unit, the spacer and the receptor unit[33]. In absence of the positively charged metal and protons, the fluorescence of the active units is quenched by the electron transfer process between negatively charged receptor unit and chromophore. When the positively charged metal ion binds to the receptor electron transfer becomes impossible and the intensity of the fluorescent emission increases.

The change of the energy levels of the fluorophores due to the variations of the polarity and chemical nature of the environment is used in polarity sensors[34] and in medical applications for cancer tissue detection[35]. In the work of Potter et al.[36] it is shown that fluorescent energy levels of 6-acyl-2-dimethylaminonaphthalen are affected by dipolar properties of the environment. The spectral shifts were observed when this fluorophore is placed in different solvents, therefore reflecting changes in solvent polarity.

The possibility of energy transfer between several different types of fluorophores allows targeted detection of toxins[37], molecular recognition[38] and to detect protein-protein interactions and conformational changes[39]. For example, in the work of Mauro et al[40], the sensor for the maltose is presented. This sensor has two parts: fluorescently labeled maltose binding protein (MBP) as donor and long wavelength-excitable cyanine dye as acceptor. In the absence of maltose FRET occurs between the MBP and cyanine dye resulting in low fluorescence of MBP unit. Upon addition of maltose the cyanine dye is displaced, resulting in increased labeled MBP donor emission.

The unique ability of fluorescent organic molecules to create non-fluorescent complexes allows extremely sensitive "turn-on" chemical detectors[41]. For example, such technique is employed for explosives sensing[42] and molecule recognition[43].

In the work of Whitten et al.[44], the ability of metal ions to completely quench fluorescent emission was used for monitoring of kinase and phosphatase activities. The sensing system consisted of fluorescently modified peptides and $Ga^{3+}$ ions. In the presence of kinase peptide phosphate group binds top the $Ga^{3+}$ ions, which induces strong fluorescent quenching. When the phosphatase is introduced to the system the fluorescence restores back to the initial state.

Another possibility for the sensing application is the distance dependent quenching of the fluorescent emission by metal nanostructures[45]. Using this phenomenon it is possible to design very sensitive devices for the biological applications. For instance, in the work of Ray et al.[46] concept of the fluorescence quenching by gold nanoparticles is used for the detection of the Hepatitis C Virus RNA. The sensing is based on the following principle. Complementary RNA to the Hepatitis C Virus was attached to the gold nanoparticle by thiol group on the one end and fluorescently labeled with cyanine dye on the other end. Due to the flexibility of the RNA molecule assumed arc-like structure and chromophores situated in the vicinity of isolated gold particles experienced quenching of the fluorescence. When the RNA hybridizes with Hepatitis C Virus the formed double helix assumes straight shape and the chromophore becomes separated from the gold nanoparticle and fluorescent emission quenching diminishes.

The similar technique was used by Hotchandani et al.[47]to study charging of the gold nanoparticles using fluorescent pyrene molecules. In this work (1-pyrenyl)-6-oxaheptanethiol functionalized gold nanoparticles were attached to the $TiO_2$ film on the optically transparent electrode. In the absence of applied potential gold quenches fluorescence of the pyrene molecules by electron transfer. However, when negative potential is applied to the system the interactions between the fluorophore and the gold nanocore become completely suppressed and the high fluorescent emission of chromophores is observed. Thus, this technique allows electrochemical modulation of the emission of a chromophore.

In some cases, a single molecule can cause quenching of hundreds of fluorophores. This benefit makes such a technique capable of detecting traces of chemicals within a very low concentration[26]. Enhancing of fluorescent emission of the organic fluorophores by coupling with noble metal nanoparticles can bring the detection limits even further, creating single molecule detection devices[48]. For example in the work of Lakowicz et al.[49] it was shown how the quartz slides with 20% surface covered with silver islands can increase emission intensity of the fluorescently labeled DNA adsorbed to the surface in 5 to 10 times.

### 2.2.1. Polymers in fluorescent sensing applications

When used as a single molecule, organic dyes lack brightness and stability [3]. The situation can be significantly improved by incorporation of the fluorophores into the rigid matrix. For instance, in the work of Ismail et al.[50]it was shown that intensity of the

fluorescent emission of the Rhodamine B can be significantly enhanced, if the Rhodamine B molecules are introduced into the rigid PMMA matrix.

For the protective matrix organic[23] and inorganic[51] materials can be used. For the sensing applications fluorophores incorporation into the polymer films attract great attention due to the ability of the polymer matrix to support the fluorophores, protect them from harsh environments and at the same time serve as a transport media for the analytes need to be detected[23].

For example, in the work of Yang et al.[52] thin polymer film with fluorescent pentiptycene moieties was used as a TNT sensing device, utilizing the ability of the explosive molecules to quench fluorescence of pentiptycene derivatives. Another research group developed a thin fluorescent polymer films capable of fluorescent emission intensity reduction due to nonspecific sugars binding with detectable changes of fluorescence observed at glucose concentrations of 10 mg/ml[53].

Analogous system of spin-coated thin films of poly(N-hydroxysuccinimidyl methacrylate) on the gold and silicon substrates was used to study immobilization of biomolecules by fluorescence microscopy and surface plasmon resonance enhanced fluorescence spectroscopy[54].

Another example of the simple sensing device is presented in the work of Zang et al.[55]. It was demonstrated, that ultrathin nanofibers fabricated from N-(1-hexylheptyl)perylene-3,4,9,10-tetracarboxyl-3,4-anhydride-9,10-imide allow detection of the amine vapor by the decrease in fluorescent emission of the fibril structure.

Swelling of the polymer film can induce conformational changes of the polymer molecules which in turn may result in the changes of fluorescent emission. This concept was used in the work of Fujiki et al.[56] where distance between polymer chains in the poly(phenylacetylene) film was changing due to the swelling in organic solvents, promoting the fluorescent emission intensity changes.

The sensing devices, presented above are capable of single analyte detection, however in some cases, when multiple substances can trigger the similar changes in the fluorescent properties of the materials more complex approach is needed to perform the detection of a single analyte from the mixture of substances[57]. This can be done by implementation of the concept of an "artificial nose"[58].

The basic idea behind this concept is analogous to the human olfactory system. An array of different types of sensors is exposed to the analyte material, and the response from each sensor is collected. A computer combines the individual responses from each sensor in the array to get a "fingerprint" for the analyte. To identify unknown substance computer performs fingerprint analysis, so the device should be "trained" in advance with various substance of interest to build a sample database[59]. The "artificial nose" concept is widely used in modern fluorescent sensing applications. For example, Anzenbacher et al.[60] showed a sensor array capable of differentiating between more than 20 different analytes including mixtures of substances. The sensing array consisted of eight meso-octamethylcalix-4-pyrrole derivatives, which showed anion-specific change in color. The similar concept can be applied for the detection of the protein macromolecules[61].

In the work of Mattoso et al.[62] electrospun nylon fibers are modified by fluorescent polymers using layer by layer assembly. Several different polymers were employed in the creation of the sensing array, which was used for the detection of pesticides in water. Principle component analysis was successfully employed to discriminate between very diluted paraoxon solutions and potable water from different sources.

However in all of the presented systems the tuning of the fluorescent properties or the analyte selectivity is done by tailoring of chemical composition of the organic dyes or the polymer matrix. To this end no study was performed on the investigation of the fluorescent property changes of fluorescent polymer materials with predefined fluorescent properties upon modification with non-fluorescent polymer grafting.

## 2.3. Polymer films

### 2.3.1. Properties and applications

Polymer films are the thin layers of polymer material with the thickness in the range of fractions of nanometer (monolayers) to several microns. Polymer films can be free standing[63] or be applied to the surface of variety of the materials such as flat and rough substrates, micro- and nano-objects, to change their surface properties[64]. Surface of materials fully defines many of their properties, such as wettability, adhesion, biocompatibility, friction, corrosion resistance and wear[65]. Therefore, application of polymer films onto substrate can regulate these properties, while the bulk properties of the material will remain the same.

For example, in the work of Blackwood et al.[66] protective conductive polymer films made of mixed polyaniline and polypyrrole were used to decrease corrosion of the carbon and stainless steel. It was found that for the case of stainless steel such polymer films can decrease corrosion rate a factor of 2000 at the same time providing good stability against delamination. Another example is the wear resistant protective coating designed for silicon-based micro-devices, described in the work of Tsukruk et al.[67]. This 20-30 nm thick polymer film with hard-soft-hard architecture significantly decreases wear of the substrate, at the same time improving the friction coefficient of the surface compared to the commonly used lubricants.

Described above surface properties variation with the polymer films is very cost-efficient due to the small amount of polymer used for the film fabrication[68]. Another advantage of polymer film compared to the other types of surface modification is the ease of deposition. For example using method developed by Messersmith et al.[64], it is possible to modify the surface of virtually any substrate by simply dipcoating it into the aqueous solution of dopamine and performing self-polymerization. The highly surface-adherent thin polymer coatings created in this way can be used for further surface modification. Even more elaborate polymer films with complex structures can be created in the single step process. As it is shown in work of Shimomura et al.[69] single step process can be used to apply porous transparent polymer films to create robust superhydrophobic surfaces.

Polymer films are able not only to change the material properties, but also bring the new functionalities to the surface of the material. Specifically designed polymer films can make the surface of the material to be conductive, reactive or fluorescent. This ability

brings many possible applications for thin polymer films in medical devices[70], electronics[71], food packaging[72], sensing devices[73] and many others.

### 2.3.2. Multicomponent polymer films

In most of the cases it is beneficial to have the polymer film composed of several different polymeric materials. This way it is possible to specifically tailor surface properties brought to the substrate by polymer film grafting. This is done, for example, in optical coatings to increase reflectivity of the surface by creation of multiple layers with different refractive indexes[74], in solar cells to increase dissociation of electron-hole pairs by introduction of a driving force for charge movement[75]. Multicomponent polymer films can be used as enrichment layers in the sensing devices, where each of the components of the polymer film attracts species of different type, therefore, increasing analyte interaction with the sensitive part of the detector[76]. Another type of coatings, which consists of several polyelectrolytes with different charges can serve as a protective barrier in the drug delivery systems[77].

The presence of several components in the polymer film allows creation of the "smart" coatings, which are capable of changing the surface properties in the response to the external stimuli[78]. For example, dual component polymer can be used to create a system with switching fluorescent properties. Such concept is presented in the work of Weber et al.[79], where distance between fluorescent molecules dispersed in the polymer matrix is controlled by solvent-vapor annealing. The properties of the polymer matrix define Förster Resonance Energy Transfer (FRET) between the donor and acceptor

molecules, therefore, controlling the energy (color) of the fluorescent emission. Another interesting application of multi-component polymer films is controllable adhesion of macromolecules. For example, in the work of Alexander et al.[80] it is shown that mixed polymer layer of Poly(N-isopropylacrylamide) (PNIPAm) and N,N,N',N',N''-Pentamethyldiethylenetriamine, (PMDETA) can exhibit switching protein adhesion behavior when going through a transitions at a lower critical solution temperature.

The mixed polymer layer systems can also be switched reversibly by solvent treatment. For example in work of Stamm et al.[81] the friction, wettability and adhesion properties of the polystyrene–poly(2-vinylpyridine) mixed polymer film were reversibly changed by the film exposure to the solvent selective for one of the components. Another types of external stimuli, besides the ones described above, that can be used to induce the property changes of smart multicomponent polymer films are light-irradiation[82], thermal treatment[83], electric field[84] changes and others.

The ability to bring forward the properties of either of the components of the polymer film when necessary is possible in all of the multicomponent film concepts presented above due to the high mobility of the polymers in thin films[85].

## 2.4. Fabrication of thin polymer films

### 2.4.1. Polymer application techniques

As it was mentioned above, one of the foremost features of polymer films is the ease of polymer film application[86]. Over the years multiple techniques for straightforward polymer film application were developed. Polymer films can be created from glow

discharge plasmas of organic compounds[87], adsorbed from vapor[88] or solution[89], and deposited by physically spreading polymer over the surface of the substrate by drop casting[90], spin coating[91] and dip coating[92]. All the methods, with exception of spin coating and drop casting, are extremely efficient in terms of the waste of material.

Using the methods mentioned above polymer films can be used to modify variety of substrates for multiple applications. Polymer films are known to be used for tuning the properties of not only the flat substrates[93], but also the rough surfaces of membranes[94], and fibers[95]. For example, in the work of Gupta et al.[96]it is shown how the solventless initiated chemical vapor deposition can be used for the coating of three dimensional structures with polymer films. Using such technique it is possible to create patterns of various polymers inside the structure of the hydrophilic chromatography paper.

Polymer coatings can be also applied to the surface of nanoparticles creating single component coatings[97] as well as elaborate multicomposite, nanostructured coatings[98].

### 2.4.2. Single component polymer films anchored to the surface

There are two general ways of polymer film attachment to the substrate: physisorption[99] and covalent attachment[100]. Since physisorption is reversible[101] it cannot be extensively used for creation of the robust stable polymer films. To overcome this limitation, polymers need to be covalently attached to the surface of the substrate.

For these purposes “grafting from” and “grafting-to” techniques are used. “Grafting from” technique employs covalent attachment of the initiator onto the substrate

with subsequent polymerization of the polymer chain from the initiator[102]. Synthesized polymer chains created in such way can have multiple functionalities, for example, using "grafting from" technique Muller and coworkers[103] introduced amphiphilic properties to the substrates, creating polymer brushes with hydrophilic and hydrophobic side chains.

Using "grafting from" technique it is possible to achieve very high polymer grafting density, if the density of initiating functionalities on the surface of the substrate is high. For example, this technique was used in the work of Lennox et al.[104]to attach polymer chains to the surface of gold nanoparticles. The achieved polystyrene grafting density was very high (in the order of 3.5 chains/$nm^2$). The main disadvantage of such an approach is the high polydispersity of grafted chains due to the limitations of the polymerization termination process and initiator efficiency[105].

Another polymer film synthesis method is "grafting to" technique. This technique involves attachment of presynthesized polymer chains with reactive groups to specially functionalized surface[106]. This method gives more precise control of the properties of the grafted polymer layers, such as molecular weight[105], since precisely characterized polymer chains are used for the attachment. The main limitation of the "grafting to" technique is the slow diffusion of the polymer chains to the reaction sites[107], therefore, to increase mobility of the polymer chains the polymer film synthesis can be conducted from melt[106].

Due to the control of the polymer layer properties "grafting to" method brings much attention in modern polymer film deposition techniques. For example, Akcora et al.[108] report deposition of tethered polystyrene chains to the surface of iron oxide

nanoparticles through ligand exchange reaction. It was discovered that nanoparticle aggregation depends on the grafting density and the molecular weight of the grafted polymer. Therefore, the properties of the suspension can be precisely tuned by variation of the properties of the grafted layer.

Both methods of the polymer grafting require special treatment of the substrate to have necessary functionalities[109]. Instead of the creation of the functional groups on the surface of the substrate, it is possible to attach reactive anchoring layer first, and then perform the grafting of the polymer to the anchoring layer[110]. Such technique targets universal method of polymer film deposition, since the reactive groups on the polymer chains to be grafted does not have to match directly the functionalities of the substrate [109].

The properties of grafted polymer layer can be varied using the single component polymer film. For example, this could be done by variation of the grafting density of the attached polymer. In the work of Luzinov et al.[111] high density polystyrene gradient was applied to the flat silicon wafers by annealing the substrate on the plate with temperature gradient. It is also possible to create orthogonal polymer gradients, with variation of two different properties in two perpendicular directions. For example, in the work of Genzer et al.[112] "grafting from" method was used to synthesize thin films of poly(2-(dimethylamino)ethyl methacrylate) with grafting density gradient along one direction and molecular weight gradient along perpendicular direction by surface-initiated atom transfer radical polymerization .

Another interesting technique is the synthesis of the patterned polymer layers. Such patterned structures can be used for microfluidic devices, biological sensors, and

tissues engineering[113]. Polymer layer patterns can be applied by various methods, such as electron beam lithography, laser-based lithography, and scanning probe lithography. For example Liu et al.[114] have reported the fabrication of nanostructured and gradient polymer brushes bydip-pen nanodisplacement lithography. The scientists developed a method to produce arbitrary patterned polymer brushes from a gray-scale image with ~25 nm resolution.

### 2.4.3. Multicomponent nanoscale polymer films

To create switchable, stimuli responsive polymer films or to apply several different properties to the surface of the material simultaneously multicomponent polymer grafting is usually used[115]. Multicomponent polymer films can be created in the ways similar to the single component coatings. To this end there are several different techniques of multicomponent film creation.

Polymer films can be assembled layer-by-layer, simply applying each subsequent layer on top of the previous one. Such technique allows precise control of the polymer film properties along the direction normal to the substrate[116]. For such deposition each layer should be attracted to previous one, therefore layer-by-layer assembly is usually used for the materials capable of hydrogen bonding[117] and polyelectrolytes[118]. Layer-by-layer assembly of polyelectrolyte material is presented in the work of Decher[116], where subsequent electrostatic driven attachment of poly(styrene sulfonate) and poly(allylamine hydrochloride) is performed. The polymers form even monolayers with total film thickness in the range 20-120 nm. Layered structures created using this technique are

used for materials separation, controlled permeation and release of target materials, and sensing[119].

Both “grafting to” and “grafting from” can be used to create mixed polymer layers and brushes. This can be done by subsequent grafting of several polymers to the functionalized substrate[120]. For example, mixed polystyrene–poly(2-vinylpyridine) brush can be created by subsequent grafting of end functionalized polymers to the anchoring layer[81]. The ratio of the grafted polymers can be controlled by changing the grafting density and/or molecular weight of the polymers used for the attachment[121]. Another way of mixed polymer film composition control is presented in the work of Beers et al.[122]. In this work monomer solution of n-butyl methacrylate and 2-(N,N-dimethylamino)ethyl methacrylatewith continuous composition gradient was created using microfluidic techniques. Due to the relatively slow liquid diffusion it was possible to perform polymerization before any significant change in the gradient profile is observed, creating mixed gradient polymer films. Temperature gradients can also be used to create mixed polymer bushes with composition gradients[123]. For example, in the work of Luzinov et al.[124]polymer film with composition gradient was applied to the flat surface of silicon wafer by subsequent application of two layers with the grafting density gradients induced by the differences in annealing temperature along the substrate.

### 2.5. Summary

This literature review indicates the importance of the fluorescent materials and sensing devices based on the principles of fluorescence due to their widespread

applications. Many approaches have been investigated for the creation of sensing devices. Among them, sensing devices based on the fluorescent polymer films present special interest. Analysis of literature indicates of many possibilities for the fabrication of the thin polymer films on the variety of substrates, which could be used for the sensing applications. Though theoretical aspects have been studied, much research is still necessary for the full understanding of the polymer matrix effect on the embedded chromophores in terms of their fluorescent properties. Therefore, existing knowledge should be further explored to fabricate efficient fluorescent polymer based sensing devices with tunable properties.

## 2.6. References


1. Valeur, B., *Molecular fluorescence : principles and applications*. Wiley-VCH: Weinheim; New York, 2002.

2. Burns, A.; Ow, H.; Wiesner, U., Fluorescent core-shell silica nanoparticles: towards "Lab on a Particle" architectures for nanobiotechnology. *Chemical Society Reviews* **2006,** *35* (11), 1028-1042.

3. Lakowicz, J. R., *Principles of fluorescence spectroscopy*. Kluwer Academic/Plenum: New York, 1999.

4. Cho, S.-Y.; Kim, J.-G.; Chung, C.-M., A fluorescent crack sensor based on cyclobutane-containing crosslinked polymers of tricinnamates. *Sensors and Actuators B: Chemical* **2008,** *134* (2), 822-825.

5. Alivisatos, A. P., Semiconductor Clusters, Nanocrystals, and Quantum Dots. *Science* **1996,** *271* (5251), 933-937.

6. Henglein, A., Small-particle research: physicochemical properties of extremely small colloidal metal and semiconductor particles. *Chemical Reviews* **1989,** *89* (8), 1861-1873.

7. Michalet, X.; Pinaud, F. F.; Bentolila, L. A.; Tsay, J. M.; Doose, S.; Li, J. J.; Sundaresan, G.; Wu, A. M.; Gambhir, S. S.; Weiss, S., Quantum Dots for Live Cells, in Vivo Imaging, and Diagnostics. *Science* **2005,** *307* (5709), 538-544.

8. Allen, C. N.; Poole, P. J.; Marshall, P.; Fraser, J.; Raymond, S.; Fafard, S., InAs self-assembled quantum-dot lasers grown on (100) InP. *Applied Physics Letters* **2002,** *80* (19), 3629-3631.

9. Bodefeld, M. C.; Warburton, R. J.; Karrai, K.; Kotthaus, J. P.; Medeiros-Ribeiro, G.; Petroff, P. M., Storage of electrons and holes in self-assembled InAs quantum dots. *Applied Physics Letters* **1999,** *74* (13), 1839-1841.

10. Loss, D.; DiVincenzo, D. P., Quantum computation with quantum dots. *Physical Review A* **1998,** *57* (1), 120-126.

11. (a) Costa-Fernández, J. M.; Pereiro, R.; Sanz-Medel, A., The use of luminescent quantum dots for optical sensing. *TrAC Trends in Analytical Chemistry* **2006,** *25* (3), 207-218; (b) Medintz, I. L.; Uyeda, H. T.; Goldman, E. R.; Mattoussi, H., Quantum dot bioconjugates for imaging, labelling and sensing. *Nat Mater* **2005,** *4* (6), 435-446.

12. Zollinger, H., *Color Chemistry: Syntheses, Properties, and Applications of Organic Dyes and Pigments*. Verlag Helvetica Chimica Acta: 2003.

13. Resch-Genger, U.; Grabolle, M.; Cavaliere-Jaricot, S.; Nitschke, R.; Nann, T., Quantum dots versus organic dyes as fluorescent labels. *Nat Meth* **2008,** *5* (9), 763-775.

14. Imai, Y.; Naka, K.; Chujo, Y., Isomerization Behavior of Azobenzene Chromophores Attached to the Side Chain of Organic Polymer in Organic−Inorganic Polymer Hybrids. *Macromolecules* **1999,** *32* (4), 1013-1017.

15. Miller, L. W.; Cornish, V. W., Selective chemical labeling of proteins in living cells. *Current Opinion in Chemical Biology* **2005,** *9* (1), 56-61.

16. Xiaoxiao, H.; Jinghua, D.; Kemin, W.; Weihong, T.; Xia, L.; Chunmei, H., A Novel Fluorescent Label Based on Organic Dye-Doped Silica Nanoparticles for HepG Liver Cancer Cell Recognition. *Journal of Nanoscience and Nanotechnology* **2004,** *4* (6), 585-589.

17. Hunger, K., *Industrial Dyes: Chemistry, Properties, Applications*. John Wiley & Sons: 2007.

18. (a) Thompson, N. L.; Lagerholm, B. C., Total internal reflection fluorescence: applications in cellular biophysics. *Current Opinion in Biotechnology* **1997,** *8* (1), 58-64; (b) Suzuki, T.; Matsuzaki, T.; Hagiwara, H.; Aoki, T.; Takata, K., Recent Advances in Fluorescent Labeling Techniques for Fluorescence Microscopy. *ACTA HISTOCHEMICA ET CYTOCHEMICA* **2007,** *40* (5), 131-137.

19. Canaria, C.; Lansford, R., Advanced optical imaging in living embryos. *Cellular and Molecular Life Sciences* **2010,** *67* (20), 3489-3497.

20. Tang, C. W.; VanSlyke, S. A., Organic electroluminescent diodes. *Applied Physics Letters* **1987,** *51* (12), 913-915.

21. Capelli, R.; Toffanin, S.; Generali, G.; Usta, H.; Facchetti, A.; Muccini, M., Organic light-emitting transistors with an efficiency that outperforms the equivalent light-emitting diodes. *Nat Mater* **2010,** *9* (6), 496-503.

22. Brabec, C. J., *Organic Photovoltaics: Concepts and Realization*. Springer: 2003.

23. Demchenko, A. P., *Introduction to Fluorescence Sensing*. Springer: 2008.

24. Rahman, M.; Kumar, P.; Park, D.-S.; Shim, Y.-B., Electrochemical Sensors Based on Organic Conjugated Polymers. *Sensors* **2008,** *8* (1), 118-141.

25. Wolfbeis, O. S., Chemical sensors — survey and trends. *Fresenius' Journal of Analytical Chemistry* **1990,** *337* (5), 522-527.

26. Heeger, P. S., Making sense of polymer-based biosensors. *Proceedings of the National Academy of Sciences* **1999,** *96* (22), 12219-12221.

27. Ho, C. K.; Itamura, M. T.; Kelley, M. J.; Hughes, R. C.; Sandia National Labs, A. N. M.; Sandia National Labs, L. C. A., *Review of Chemical Sensors for In-Situ Monitoring of Volatile Contaminants*. United States, 2001.

28. Wolfbeis, O. S., Materials for fluorescence-based optical chemical sensors. *Journal of Materials Chemistry* **2005,** *15* (27-28), 2657-2669.

29. Lippitsch, M. E.; Pusterhofer, J.; Leiner, M. J. P.; Wolfbeis, O. S., Fibre-optic oxygen sensor with the fluorescence decay time as the information carrier. *Analytica Chimica Acta* **1988,** *205* (0), 1-6.

30. Tumambac, G. E.; Rosencrance, C. M.; Wolf, C., Selective metal ion recognition using a fluorescent 1,8-diquinolylnaphthalene-derived sensor in aqueous solution. *Tetrahedron* **2004,** *60* (49), 11293-11297.

31. Chris, D. G., Optical halide sensing using fluorescence quenching: theory, simulations and applications - a review. *Measurement Science and Technology* **2001,** *12* (9), R53.

32. Förster, T., *Fluoreszenz Organischer Verbindungen*. Vandenhoeck & Ruprecht: 1982.

33. Prodi, L.; Bolletta, F.; Montalti, M.; Zaccheroni, N., ChemInform Abstract: Luminescent Chemosensors for Transition Metal Ions. *ChemInform* **2000,** *31* (44), no-no.

34. Valeur, B.; Bourson, J.; Pouget, J., Ion Recognition Detected by Changes in Photoinduced Charge or Energy Transfer. In *Fluorescent Chemosensors for Ion and Molecule Recognition*, American Chemical Society: 1993; Vol. 538, pp 25-44.

35. Bremer, C.; Ntziachristos, V.; Weissleder, R., Optical-based molecular imaging: contrast agents and potential medical applications. *European Radiology* **2003,** *13* (2), 231-243.

36. Prendergast, F. G.; Meyer, M.; Carlson, G. L.; Iida, S.; Potter, J. D., Synthesis, spectral properties, and use of 6-acryloyl-2-dimethylaminonaphthalene (Acrylodan). A thiol-selective, polarity-sensitive fluorescent probe. *Journal of Biological Chemistry* **1983,** *258* (12), 7541-7544.

37. Ma, G.; Cheng, Q., Manipulating FRET with Polymeric Vesicles: Development of a "Mix-and-Detect" Type Fluorescence Sensor for Bacterial Toxin. *Langmuir* **2006,** *22* (16), 6743-6745.

38. Ojida, A.; Mito-oka, Y.; Sada, K.; Hamachi, I., Molecular Recognition and Fluorescence Sensing of Monophosphorylated Peptides in Aqueous Solution by Bis(zinc(II)−dipicolylamine)-Based Artificial Receptors. *Journal of the American Chemical Society* **2004,** *126* (8), 2454-2463.

39. Truong, K.; Ikura, M., The use of FRET imaging microscopy to detect protein–protein interactions and protein conformational changes in vivo. *Current Opinion in Structural Biology* **2001,** *11* (5), 573-578.

40. Medintz, I. L.; Goldman, E. R.; Lassman, M. E.; Mauro, J. M., A Fluorescence Resonance Energy Transfer Sensor Based on Maltose Binding Protein. *Bioconjugate Chemistry* **2003,** *14* (5), 909-918.

41. Zhang, M.; Yu, M.; Li, F.; Zhu, M.; Li, M.; Gao, Y.; Li, L.; Liu, Z.; Zhang, J.; Zhang, D.; Yi, T.; Huang, C., A Highly Selective Fluorescence Turn-on Sensor for Cysteine/Homocysteine and Its Application in Bioimaging. *Journal of the American Chemical Society* **2007,** *129* (34), 10322-10323.

42. Andrew, T. L.; Swager, T. M., A Fluorescence Turn-On Mechanism to Detect High Explosives RDX and PETN. *Journal of the American Chemical Society* **2007,** *129* (23), 7254-7255.

43. Ojida, A.; Takashima, I.; Kohira, T.; Nonaka, H.; Hamachi, I., Turn-On Fluorescence Sensing of Nucleoside Polyphosphates Using a Xanthene-Based Zn(II) Complex Chemosensor. *Journal of the American Chemical Society* **2008,** *130* (36), 12095-12101.

44. Rininsland, F.; Xia, W.; Wittenburg, S.; Shi, X.; Stankewicz, C.; Achyuthan, K.; McBranch, D.; Whitten, D., Metal ion-mediated polymer superquenching for highly sensitive detection of kinase and phosphatase activities. *PNAS* **2004,** *101* (43), 15295-15300.

45. Schneider, G.; Decher, G.; Nerambourg, N.; Praho, R.; Werts, M. H. V.; Blanchard-Desce, M., Distance-Dependent Fluorescence Quenching on Gold Nanoparticles Ensheathed with Layer-by-Layer Assembled Polyelectrolytes. *Nano Letters* **2006,** *6* (3), 530-536.

46. Griffin, J.; Singh, A. K.; Senapati, D.; Rhodes, P.; Mitchell, K.; Robinson, B.; Yu, E.; Ray, P. C., Size- and Distance-Dependent Nanoparticle Surface-Energy Transfer (NSET) Method for Selective Sensing of Hepatitis C Virus RNA. *Chemistry – A European Journal* **2009,** *15* (2), 342-351.

47. Kamat, P. V.; Barazzouk, S.; Hotchandani, S., Electrochemical Modulation of Fluorophore Emission on a Nanostructured Gold Film. *Angewandte Chemie* **2002,** *114* (15), 2888-2891.

48. Aslan, K.; Wu, M.; Lakowicz, J. R.; Geddes, C. D., Fluorescent Core−Shell Ag@SiO2 Nanocomposites for Metal-Enhanced Fluorescence and Single Nanoparticle Sensing Platforms. *Journal of the American Chemical Society* **2007,** *129* (6), 1524-1525.

49. Lakowicz, J. R.; Malicka, J.; Gryczynski, I., Silver particles enhance emission of fluorescent DNA oligomers. *BioTechniques* **2003,** *34* (1), 62-6.

50. Fikry, M.; Omar, M.; Ismail, L., Effect of Host Medium on the Fluorescence Emission Intensity of Rhodamine B in Liquid and Solid Phase. *Journal of Fluorescence* **2009,** *19* (4), 741-746.

51. Mader, H.; Li, X.; Saleh, S.; Link, M.; Kele, P.; Wolfbeis, O. S., Fluorescent Silica Nanoparticles. *Annals of the New York Academy of Sciences* **2008,** *1130* (1), 218-223.

52. Yang, J.-S.; Swager, T. M., Fluorescent Porous Polymer Films as TNT Chemosensors: Electronic and Structural Effects. *Journal of the American Chemical Society* **1998,** *120* (46), 11864-11873.

53. Manju, S.; Hari, P. R.; Sreenivasan, K., Fluorescent molecularly imprinted polymer film binds glucose with a concomitant changes in fluorescence. *Biosensors and Bioelectronics* **2010,** *26* (2), 894-897.

54. Feng, C. L.; Zhang, Z.; Förch, R.; Knoll, W.; Vancso, G. J.; Schönherr, H., Reactive Thin Polymer Films as Platforms for the Immobilization of Biomolecules. *Biomacromolecules* **2005,** *6* (6), 3243-3251.

55. Che, Y.; Zang, L., Enhanced fluorescence sensing of amine vapor based on ultrathin nanofibers. *Chemical Communications* **2009,** (34), 5106-5108.

56. Kwak, G.; Lee, W.-E.; Jeong, H.; Sakaguchi, T.; Fujiki, M., Swelling-Induced Emission Enhancement in Substituted Acetylene Polymer Film with Large Fractional Free Volume: Fluorescence Response to Organic Solvent Stimuli. *Macromolecules* **2008,** *42* (1), 20-24.

57. Dickinson, T. A.; Michael, K. L.; Kauer, J. S.; Walt, D. R., Convergent, Self-Encoded Bead Sensor Arrays in the Design of an Artificial Nose. *Analytical chemistry* **1999,** *71* (11), 2192-2198.

58. Persaud, K.; Dodd, G., Analysis of discrimination mechanisms in the mammalian olfactory system using a model nose. *Nature* **1982,** *299* (5881), 352-355.

59. Pearce, T. C.; Schiffman, S. S.; Nagle, H. T.; Gardner, J. W., *Handbook of Machine Olfaction: Electronic Nose Technology*. John Wiley & Sons: 2006.

60. Palacios, M. A.; Nishiyabu, R.; Marquez, M.; Anzenbacher, P., Supramolecular Chemistry Approach to the Design of a High-Resolution Sensor Array for Multianion Detection in Water. *Journal of the American Chemical Society* **2007,** *129* (24), 7538-7544.

61. Miranda, O. R.; Creran, B.; Rotello, V. M., Array-based sensing with nanoparticles: 'Chemical noses' for sensing biomolecules and cell surfaces. *Current Opinion in Chemical Biology* **2010,** *14* (6), 728-736.

62. Oliveira, J. E.; Scagion, V. P.; Grassi, V.; Correa, D. S.; Mattoso, L. H. C., Modification of electrospun nylon nanofibers using layer-by-layer films for application in flow injection electronic tongue: Detection of paraoxon pesticide in corn crop. *Sensors and Actuators B: Chemical* **2012,** *171–172* (0), 249-255.

63. (a) Stroock, A. D.; Kane, R. S.; Weck, M.; Metallo, S. J.; Whitesides, G. M., Synthesis of Free-Standing Quasi-Two-Dimensional Polymers. *Langmuir* **2002,** *19* (6), 2466-2472; (b) Yamato, H.; Kai, K.-i.; Ohwa, M.; Asakura, T.; Koshiba, T.; Wernet, W., Synthesis of free-standing poly(3,4-ethylenedioxythiophene) conducting polymer films on a pilot scale. *Synthetic Metals* **1996,** *83* (2), 125-130.

64. Lee, H.; Dellatore, S. M.; Miller, W. M.; Messersmith, P. B., Mussel-Inspired Surface Chemistry for Multifunctional Coatings. *Science* **2007,** *318* (5849), 426-430.

65. (a) Mason, R.; Jalbert, C. A.; O'Rourke Muisener, P. A. V.; Koberstein, J. T.; Elman, J. F.; Long, T. E.; Gunesin, B. Z., Surface energy and surface composition of end-fluorinated polystyrene. *Advances in Colloid and Interface Science* **2001,** *94* (1–3), 1-19; (b) Somorjai, G. A.; Li, Y., Impact of surface chemistry. *Proceedings of the National Academy of Sciences* **2011,** *108* (3), 917-924.

66. Tan, C. K.; Blackwood, D. J., Corrosion protection by multilayered conducting polymer coatings. *Corrosion Science* **2003,** *45* (3), 545-557.

67. Sidorenko, A.; Ahn, H.-S.; Kim, D.-I.; Yang, H.; Tsukruk, V. V., Wear stability of polymer nanocomposite coatings with trilayer architecture. *Wear* **2002,** *252* (11–12), 946-955.

68. Karim, A.; Kumar, S., *Polymer surfaces, interfaces and thin films*. World Scientific: Singapore; River Edge, NJ, 2000.

69. Yabu, H.; Shimomura, M., Single-Step Fabrication of Transparent Superhydrophobic Porous Polymer Films. *Chemistry of Materials* **2005,** *17* (21), 5231-5234.

70. Vendra, V. K.; Wu, L.; Krishnan, S., Polymer Thin Films for Biomedical Applications. In *Nanotechnologies for the Life Sciences*, Wiley-VCH Verlag GmbH & Co. KGaA: 2007.

71. Stubb, H.; Punkka, E.; Paloheimo, J., Electronic and optical properties of conducting polymer thin films. *Materials Science Reports* **1993,** *10* (3), 85-140.

72. Appendini, P.; Hotchkiss, J. H., Review of antimicrobial food packaging. *Innovative Food Science & Emerging Technologies* **2002,** *3* (2), 113-126.

73. Harsányi, G., *Polymer films in sensor applications : technology, materials, devices and their characteristics*. Technomic Pub. Co.: Lancaster, Pa., 1995.

74. Weber, M. F.; Stover, C. A.; Gilbert, L. R.; Nevitt, T. J.; Ouderkirk, A. J., Giant Birefringent Optics in Multilayer Polymer Mirrors. *Science* **2000,** *287* (5462), 2451-2456.

75. Thompson, B. C.; Fréchet, J. M. J., Polymer–Fullerene Composite Solar Cells. *Angewandte Chemie International Edition* **2008,** *47* (1), 58-77.

76. Giammarco, J.; Zdyrko, B.; Petit, L.; Musgraves, J. D.; Hu, J.; Agarwal, A.; Kimerling, L.; Richardson, K.; Luzinov, I., Towards universal enrichment nanocoating for IR-ATR waveguides. *Chemical Communications* **2011,** *47* (32), 9104-9106.

77. Caruso, F.; Trau, D.; Möhwald, H.; Renneberg, R., Enzyme Encapsulation in Layer-by-Layer Engineered Polymer Multilayer Capsules. *Langmuir* **2000,** *16* (4), 1485-1488.

78. Stuart, M. A. C.; Huck, W. T. S.; Genzer, J.; Muller, M.; Ober, C.; Stamm, M.; Sukhorukov, G. B.; Szleifer, I.; Tsukruk, V. V.; Urban, M.; Winnik, F.; Zauscher, S.; Luzinov, I.; Minko, S., Emerging applications of stimuli-responsive polymer materials. *Nat Mater* **2010,** *9* (2), 101-113.

79. Kim, S.; Yoon, S.-J.; Park, S. Y., Highly Fluorescent Chameleon Nanoparticles and Polymer Films: Multicomponent Organic Systems that Combine FRET and Photochromic Switching. *Journal of the American Chemical Society* **2012**.

80. de las Heras Alarcon, C.; Farhan, T.; Osborne, V. L.; Huck, W. T. S.; Alexander, C., Bioadhesion at micro-patterned stimuli-responsive polymer brushes. *Journal of Materials Chemistry* **2005,** *15* (21), 2089-2094.

81. Kumar Vyas, M.; Schneider, K.; Nandan, B.; Stamm, M., Switching of friction by binary polymer brushes. *Soft Matter* **2008,** *4* (5), 1024-1032.

82. Feng, C. L.; Zhang, Y. J.; Jin, J.; Song, Y. L.; Xie, L. Y.; Qu, G. R.; Jiang, L.; Zhu, D. B., Reversible Wettability of Photoresponsive Fluorine-Containing Azobenzene Polymer in Langmuir−Blodgett Films. *Langmuir* **2001,** *17* (15), 4593-4597.

83. Abu-Lail, N. I.; Kaholek, M.; LaMattina, B.; Clark, R. L.; Zauscher, S., Micro-cantilevers with end-grafted stimulus-responsive polymer brushes for actuation and sensing. *Sensors and Actuators B: Chemical* **2006,** *114* (1), 371-378.

84. Lahann, J.; Mitragotri, S.; Tran, T.-N.; Kaido, H.; Sundaram, J.; Choi, I. S.; Hoffer, S.; Somorjai, G. A.; Langer, R., A Reversibly Switching Surface. *Science* **2003,** *299* (5605), 371-374.

85. Frank, B.; Gast, A. P.; Russell, T. P.; Brown, H. R.; Hawker, C., Polymer Mobility in Thin Films. *Macromolecules* **1996,** *29* (20), 6531-6534.

86. Brinker, C. J.; Hurd, A. J.; Schunk, P. R.; Frye, G. C.; Ashley, C. S., Review of sol-gel thin film formation. *Journal of Non-Crystalline Solids* **1992,** *147–148* (0), 424-436.

87. Yasuda, H., *Plasma polymerization*. Academic Press: Orlando, 1985.

88. Vaeth, K. M.; Jensen, K. F., Chemical vapor deposition of thin polymer films used in polymer-based light emitting diodes. *Advanced Materials* **1997,** *9* (6), 490-493.

89. Decher, G.; Hong, J. D.; Schmitt, J., Buildup of ultrathin multilayer films by a self-assembly process: III. Consecutively alternating adsorption of anionic and cationic polyelectrolytes on charged surfaces. *Thin Solid Films* **1992,** *210–211, Part 2* (0), 831-835.

90. Iovu, M. C.; Jeffries-El, M.; Sheina, E. E.; Cooper, J. R.; McCullough, R. D., Regioregular poly(3-alkylthiophene) conducting block copolymers. *Polymer* **2005,** *46* (19), 8582-8586.

91. Hall, D. B.; Underhill, P.; Torkelson, J. M., Spin coating of thin and ultrathin polymer films. *Polymer Engineering & Science* **1998,** *38* (12), 2039-2045.

92. Brinker, C. J.; Frye, G. C.; Hurd, A. J.; Ashley, C. S., Fundamentals of sol-gel dip coating. *Thin Solid Films Thin Solid Films* **1991,** *201* (1), 97-108.

93. Frank, C. W.; Rao, V.; Despotopoulou, M. M.; Pease, R. F. W.; Hinsberg, W. D.; Miller, R. D.; Rabolt, J. F., Structure in Thin and Ultrathin Spin-Cast Polymer Films. *Science* **1996,** *273* (5277), 912-915.

94. Tanaka, M.; Sackmann, E., Polymer-supported membranes as models of the cell surface. *Nature* **2005,** *437* (7059), 656-663.

95. Xue, P.; Tao, X. M., Morphological and electromechanical studies of fibers coated with electrically conductive polymer. *Journal of Applied Polymer Science* **2005,** *98* (4), 1844-1854.

96. Haller, P. D.; Flowers, C. A.; Gupta, M., Three-dimensional patterning of porous materials using vapor phase polymerization. *Soft Matter* **2011,** *7* (6), 2428-2432.

97. Kang, Y.; Taton, T. A., Core/Shell Gold Nanoparticles by Self-Assembly and Crosslinking of Micellar, Block-Copolymer Shells. *Angewandte Chemie* **2005,** *117* (3), 413-416.

98. Caruso, F., Nanoengineering of Particle Surfaces. *Advanced Materials* **2001,** *13* (1), 11-22.

99. Halperin, A.; Tirrell, M.; Lodge, T., Tethered chains in polymer microstructures

Macromolecules: Synthesis, Order and Advanced Properties. Springer Berlin / Heidelberg: 1992; Vol. 100, pp 31-71.

100. Hoffman, A. S., Surface modification of polymers: Physical, chemical, mechanical and biological methods. *Macromolecular Symposia* **1996,** *101* (1), 443-454.

101. Bug, A. L. R.; Cates, M. E.; Safran, S. A.; Witten, T. A., Theory of size distribution of associating polymer aggregates. I. Spherical aggregates. *The Journal of Chemical Physics* **1987,** *87* (3), 1824-1833.

102. Zhao, B.; Brittain, W. J., Polymer brushes: surface-immobilized macromolecules. *Progress in Polymer Science* **2000,** *25* (5), 677-710.

103. Cheng, G.; Böker, A.; Zhang, M.; Krausch, G.; Müller, A. H. E., Amphiphilic Cylindrical Core−Shell Brushes via a "Grafting From" Process Using ATRP. *Macromolecules* **2001,** *34* (20), 6883-6888.

104. Corbierre, M. K.; Cameron, N. S.; Lennox, R. B., Polymer-Stabilized Gold Nanoparticles with High Grafting Densities. *Langmuir* **2004,** *20* (7), 2867-2873.

105. Brittain, W. J.; Minko, S., A structural definition of polymer brushes. *Journal of Polymer Science Part A: Polymer Chemistry* **2007,** *45* (16), 3505-3512.

106. Minko, S.; Patil, S.; Datsyuk, V.; Simon, F.; Eichhorn, K.-J.; Motornov, M.; Usov, D.; Tokarev, I.; Stamm, M., Synthesis of Adaptive Polymer Brushes via "Grafting To" Approach from Melt. *Langmuir* **2002,** *18* (1), 289-296.

107. Luzinov, I.; Julthongpiput, D.; Malz, H.; Pionteck, J.; Tsukruk, V. V., Polystyrene Layers Grafted to Epoxy-Modified Silicon Surfaces. *Macromolecules* **2000,** *33* (3), 1043-1048.

108. Jiao, Y.; Akcora, P., Assembly of Polymer-Grafted Magnetic Nanoparticles in Polymer Melts. *Macromolecules* **2012,** *45* (8), 3463-3470.

109. Zdyrko, B.; Luzinov, I., Polymer Brushes by the "Grafting to" Method. *Macromolecular Rapid Communications* **2011,** *32* (12), 859-869.

110. Iyer, K. S.; Zdyrko, B.; Malz, H.; Pionteck, J.; Luzinov, I., Polystyrene Layers Grafted to Macromolecular Anchoring Layer. *Macromolecules* **2003,** *36* (17), 6519-6526.

111. Liu, Y.; Klep, V.; Zdyrko, B.; Luzinov, I., Synthesis of High-Density Grafted Polymer Layers with Thickness and Grafting Density Gradients. *Langmuir* **2005,** *21* (25), 11806-11813.

112. Bhat, R. R.; Tomlinson, M. R.; Genzer, J., Assembly of Nanoparticles using Surface-Grafted Orthogonal Polymer Gradients. *Macromolecular Rapid Communications* **2004,** *25* (1), 270-274.

113. Lin, X.; He, Q.; Li, J., Complex polymer brush gradients based on nanolithography and surface-initiated polymerization. *Chemical Society Reviews* **2012,** *41* (9), 3584-3593.

114. Liu, X.; Li, Y.; Zheng, Z., Programming nanostructures of polymer brushes by dip-pen nanodisplacement lithography (DNL). *Nanoscale* **2010,** *2* (12), 2614-2618.

115. Ejaz, M.; Yamamoto, S.; Tsujii, Y.; Fukuda, T., Fabrication of Patterned High-Density Polymer Graft Surfaces. 1. Amplification of Phase-Separated Morphology of Organosilane Blend

Monolayer by Surface-Initiated Atom Transfer Radical Polymerization. *Macromolecules* **2002,** *35* (4), 1412-1418.

116. Decher, G., Fuzzy Nanoassemblies: Toward Layered Polymeric Multicomposites. *Science* **1997,** *277* (5330), 1232-1237.

117. Kharlampieva, E.; Kozlovskaya, V.; Sukhishvili, S. A., Layer-by-Layer Hydrogen-Bonded Polymer Films: From Fundamentals to Applications. *Advanced Materials* **2009,** *21* (30), 3053-3065.

118. Decher, G.; Eckle, M.; Schmitt, J.; Struth, B., Layer-by-layer assembled multicomposite films. *Current Opinion in Colloid & Interface Science* **1998,** *3* (1), 32-39.

119. Ariga, K.; Hill, J. P.; Ji, Q., Layer-by-layer assembly as a versatile bottom-up nanofabrication technique for exploratory research and realistic application. *Physical Chemistry Chemical Physics* **2007,** *9* (19), 2319-2340.

120. Barbey, R.; Lavanant, L.; Paripovic, D.; Schüwer, N.; Sugnaux, C.; Tugulu, S.; Klok, H.-A., Polymer Brushes via Surface-Initiated Controlled Radical Polymerization: Synthesis, Characterization, Properties, and Applications. *Chemical Reviews* **2009,** *109* (11), 5437-5527.

121. Müller, M., Phase diagram of a mixed polymer brush. *Physical Review E* **2002,** *65* (3), 030802.

122. Xu, C.; Barnes, S. E.; Wu, T.; Fischer, D. A.; DeLongchamp, D. M.; Batteas, J. D.; Beers, K. L., Solution and Surface Composition Gradients via Microfluidic Confinement: Fabrication of a Statistical-Copolymer-Brush Composition Gradient. *Advanced Materials* **2006,** *18* (11), 1427-1430.

123. Genzer, J., *Soft matter gradient surfaces : methods and applications*. Wiley: Hoboken, N.J., 2012.

124. Ionov, L.; Sidorenko, A.; Stamm, M.; Minko, S.; Zdyrko, B.; Klep, V.; Luzinov, I., Gradient Mixed Brushes: "Grafting To" Approach. *Macromolecules* **2004,** *37* (19), 7421-7423.

# CHAPTER THREE

# EXPERIMENTAL

## 3.1. Chemical reagents used

Hydrogen peroxide:

Company Identification: Acros Organics.

MSDS Name: Hydrogen Peroxide (30% in Water) (Without Stabilizer), Reagent ACS.

CAS Number: 7722-84-1

Sulfuric acid 98%:

Company Identification: Acros Organics.

MSDS Name: Sulfuric acid, reagent ACS.

CAS Number: 7664-93-9

Chloroform:

Company Identification: VWR International LLC.

MSDS Name: Chloroform, ACS.

CAS Number: 67-66-3

Toluene:

Company Identification: Acros Organics.

MSDS Name: Toluene, reagent ACS.

CAS Number: 108-88-3

Methyl ethyl ketone:

Company Identification: Acros Organics.

MSDS Name: 2-Butanone, 99+%.

CAS Number:78-93-3

Ethanol:

Company Identification: Mallinckrodt Baker Inc.

MSDS Name: Reagent alcohol, ACS.

CAS Number: 64-17-5

Methanol:

Company Identification: VWR International LLC.

MSDS Name: Methanol, ACS.

CAS Number: 67-56-1

Acetone:

Company Identification: VWR International LLC.

MSDS Name: Acetone, ACS.

CAS Number:67-64-1

Cyclohexane:

Company Identification: Acros Organics.

MSDS Name: Cyclohexane, 99.5%

CAS Number:110-82-7

Tetrahydrofuran:

Company Identification: Alfa Aesar.

MSDS Name: Tetrahydrofuran, 99.8%

CAS Number: 109-99-9

N-Methyl-2-pyrrolidone (NMP):

Company Identification: Alfa Aesar.

MSDS Name: N-Methyl-2-pyrrolidone, 99+%

CAS Number: 872-50-4

Ether:

Company Identification: : VWR International LLC.

MSDS Name: Ether, Stabilized. ACS

CAS Number:60-29-7

Rhodamine B:

Company Identification: Alfa Aesar.

MSDS Name: Rhodamine B

CAS Number:81-88-9

Succinic anhydride:

Company Identification: Sigma-Aldrich

MSDS Name: Succinic anhydride

CAS Number:108-30-5

Gold nanoparticles:

Company Identification: Sigma-Aldrich

MSDS Name: Gold Nanoparticles

CAS Number: 7440-57-5

### 3.2. Polymers used for surface modification

Poly(glycidyl methacrylate) (PGMA)

Several different PGMA were used:

1) Mn=382,000 g/mol with polydispersity 2.5, before RhB attachment

Mn=402,000 g/mol with polydispersity 2.2, after RhB attachment

2) Mn=63,000 g/mol with polydispersity 1.9, before RhB attachment

Mn=80,000 g/mol with polydispersity 2.57, after RhB attachment

3) Mn=300,000 g/mol with polydispersity 2.14, before RhB attachment

Mn=405,000 g/mol with polydispersity 3.81, after RhB attachment

PGMA was synthesized by solution radical polymerization and purified by multiple precipitations by Dr. B. Zdyrko according to procedure reported elsewhere[1], School of Materials Science and Engineering, Clemson University.

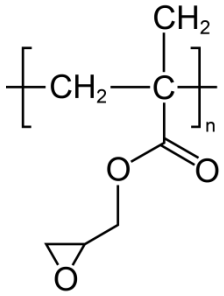


**S. 1**

Carboxy terminated Polystyrene (PS)

Carboxyl terminated Polystyrene with molecular weight Mn=48,000 g/mol with polydispersity 1.05 was obtained from Polymer Source Inc., Canada.

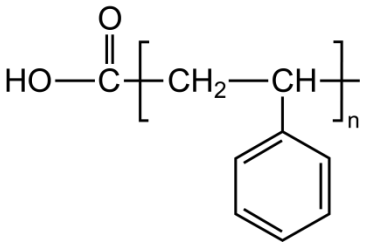

**S. 2**

Carboxy terminated Poly(2vinyl pyridine) (PVP)

Carboxyl terminated Poly(2vinyl pyridine) with molecular weight Mn=53,000 g/mol with polydispersity 1.06 was obtained from Polymer Source Inc., Canada.

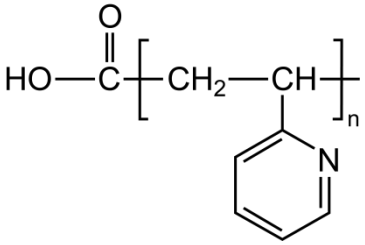

**S. 3**

Carboxy terminated Polyethylene glycol (PEG)

Poly(ethylene glycol) monomethyl ether with molecular weight Mn=5,000 was obtained from Sigma-Aldrich and modified with succinyl anhydrideto form carboxyl terminated derivative by Dr. B. Zdyrko according to procedure reported elsewhere[2], School of Materials Science and Engineering, Clemson University.

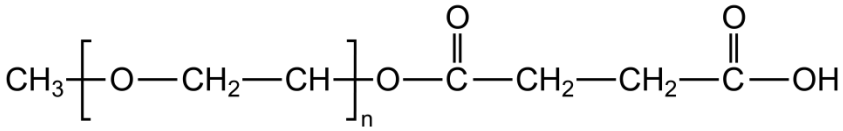

**S. 4**

Poly acrylic acid (PAA)

PAA with molecular weight Mw=100,000 was obtained from Sigma-Aldrich.

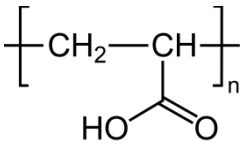

**S. 5**

### 3.3. Principal experimental techniques

#### 3.3.1. Coating techniques

##### 3.3.1.1 Dip coating

Dip coating is the process of film deposition on a substrate. During dip coating, a substrate is immersed into a liquid coating solution and subsequently withdrawn at controlled speed. After solvent evaporation, the substrate remains covered with a dry polymer coating. All the steps are schematically shown in **Figure 3.1.** To achieve uniform films, this technique should be applied in a clean environment with precise control. If there is no evaporation, the thickness of the obtained film can be estimated as[3]:

$$h = 0.944 \cdot \left(\frac{\eta v}{\rho g}\right)^{1/2} \left(\frac{\eta v}{\sigma}\right)^{1/6} \qquad \textbf{Eq. 3.1}.$$

where $\eta$ is the dynamic viscosity of the solvent, $v$ is the withdrawal speed, $\rho$ is the liquid density, $g$ is the acceleration of gravity, and $\sigma$ is the liquid surface tension. For the polymer solutions the thickness of the film after evaporation will be approximately equal to $h \cdot c$, where $c$ is the volumetric content of the polymer in the solution. A Mayer Fientechnik D-3400 dip coater was used for the coating fabrication. Dip coating was performed in a clean room to avoid solution and dry film contamination. To protect the drying film from unwanted airflow, both the substrate and the liquid coating solution were covered with a transparent box. Coating thickness variation was achieved by

changes in the viscosity of the solution. For this purpose, solutions of different concentrations of polymer were used.

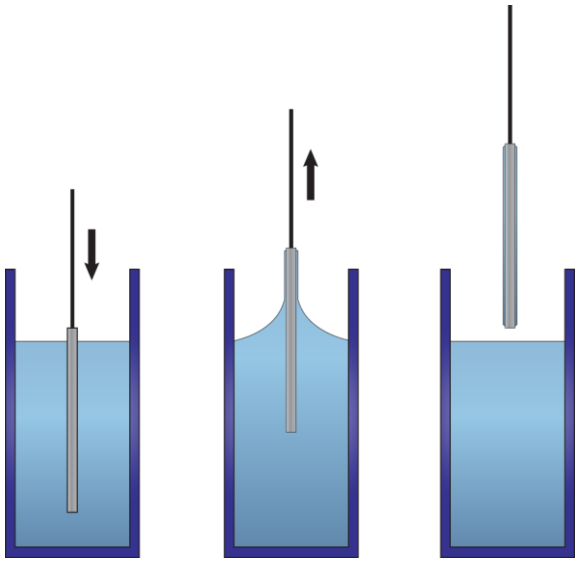

**Figure 3.1.** Schematic of film deposition by dip coating technique

#### 3.3.1.2. Spin coating

Spin coating is a batch process used to create solidified thin coatings on flat or slightly curved surfaces[4]. A liquid coating solution is deposited on the substrate, which is subsequently rotated at high speeds. The process can be divided into four stages[5]: deposition, spin-up, spin-off, and evaporation (**Figure 3.2**). The resulting film thickness depends almost solely on the spin-off stage, during which the uniform film thins down constantly during rotation. The evolution of the film thickness in this process can be described by the equation[4]:

$$h(t) = \frac{h_0}{\sqrt{1 + 4\rho\omega^2 h_0^2 t/3\eta}} \qquad \textbf{Eq. 3.2}.$$

where$h_0$ is the initial uniform thickness, $\rho$ is the density of the liquid coating, $\omega$ is the angular velocity, and $\eta$ is the liquid viscosity. Uniformity is achieved by the balance between the two forces acting in the horizontal direction: rotation-induced centrifugal force and resisting viscous force. Film wrinkling can be caused by forces perpendicular to the plane of rotation, which arise only in case of contamination or differential evaporation. If these two factors are avoided, uniform coatings are always formed. In this study, a spin coater (Headway Research Inc.) was used for the polymer film deposition from solution onto the surface of glass microscope slides and silicon wafers. Rotation speed was kept constant at 900 rpm and the polymer concentration in the solution was varied in order to change the solution's viscosity, thus tuning the resulting film thickness.

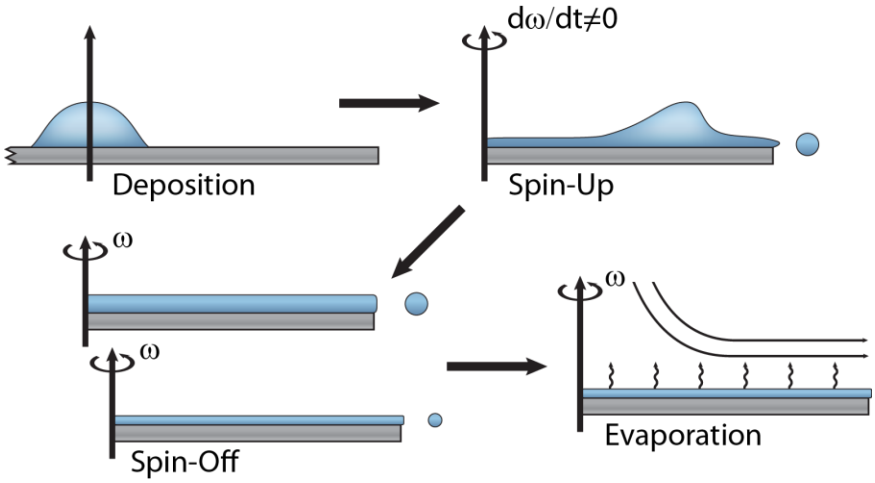


**Figure 3.2.** Four stages of spin coating (Redrawn after [4])

### 3.3.2. Atomic Force Microscopy

Atomic Force Microscopy (AFM) is a set of techniques for measuring surface topography and properties on a submicron scale[6].

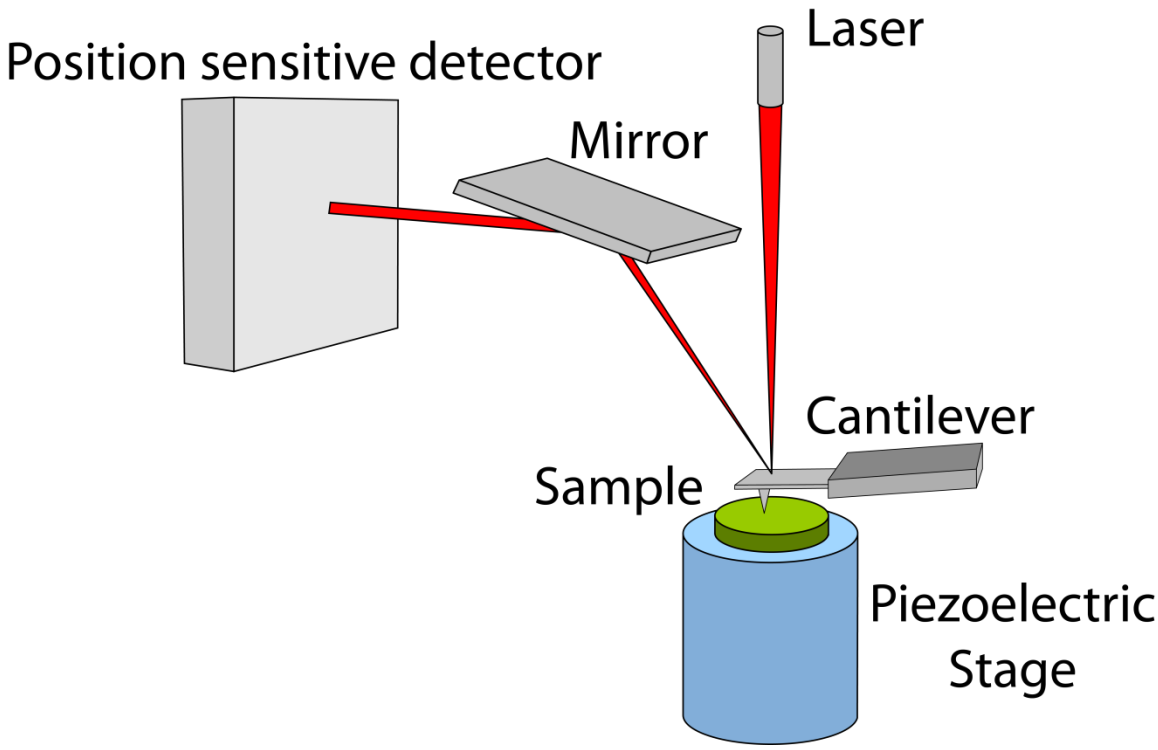


**Figure 3.3.** AFM schematics

The structure of a simplified AFM setup is presented in **Figure 3.3.** During AFM measurements, a sharp probe moves across the sample surface and interactions between the probe and the surface are recorded. These interactions can be used to study the morphology and physical properties of the sample, such as surface conductivity, elastic moduli, localized friction, adhesion, and others. In this work, AFM studies were performed using a Dimension 3100 (Digital Instruments, Inc.) microscope. A tapping mode was used to study the surface morphology of the samples in ambient air. Silicon tips from MicroMasch with spring constants of 50 N/m were used. Imaging was done at

scan rates in the range of 1 - 2 Hz. Nanoscope III 5.12r3 software was used for image processing and roughness calculation.

### 3.3.3. Ellipsometry

Ellipsometry is an optical measurement technique that characterizes thin films and surfaces by measuring light reflection from a sample[7]. The values used to characterize the sample in this technique are related to changes in the properties of polarized light upon light reflection on a sample. In particular, ellipsometry measures two parameters: Ψand Δ. These values represent the amplitude ratio Ψ and the phase difference Δ between p-polarized (in plane with the light beam) and s-polarized (perpendicular to the plane of the light beam) light waves. The values for Ψ and Δ are related to the ratio of Fresnel reflection coefficients $R_p$ and $R_s$ for p-polarized and s-polarized light, respectively:

$$tan(\Psi)e^{i\Delta} = R_p/R_s \qquad \textbf{Eq. 3.3}.$$

The remarkable features of ellipsometry are the high precision of the measurements and the high sensitivity to thickness in the order of angstroms. A major drawback of this technique is that measurements of sample properties are indirect; therefore, data analysis requires an optical model and tends to be complicated. In this work, ellipsometric measurements were performed on a single wavelength (651 nm) COMPEL automatic ellipsometer (InOmTech, Inc.) at an angle of incidence of 70°. To increase the precision of the measurements, a compensator was used when the values of Δwere close to 0° or 180°. For the measurements of changes to the sample's properties during vapor absorption, a closed glass cuvette with light-permeable windows

perpendicular to the beam was fabricated. The vapors of the water and organic solvents were introduced to the cuvette from a small bucket filled with a liquid.

### 3.3.4. Total Internal Reflectance Fluorescence

The Total Internal Reflectance Fluorescence (TIRF) measurement technique allows observations of the interactions of molecules with a solid surface. In particular, the technique is applicable to in situ studies of changes in the fluorescent properties of solid surfaces in flowing systems[8].

A TIRF apparatus, custom-built by Dr. Bogdan Zdyrko (Clemson University) was used in this study. A DPGL Series Modulated Green Laser Modulus (Part No.: DPGL-01S-TTL) was used to generate a monochromatic 532 nm laser signal (**Figure 3.4.**). The fluorescence detector (Si Photodiode, diameter is 1.0 mm, from Edmund Optics) was used to collect fluorescent signals from the polymer films.

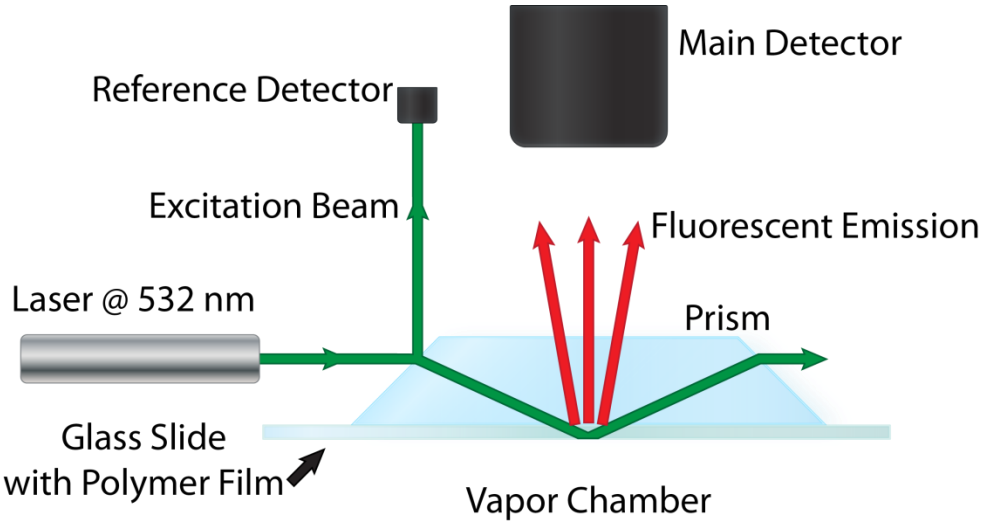


**Figure 3.4.** Main components of the TIRF apparatus

The cuvette designed for the measurements is presented in **Figure 3.5.** A glass prism was used to split the beam and serve as an optically dense light-conducting material for the total internal reflection. FisherFinest Premier microscope slides (Cat. No. 12-544-1) of nearly the same refractive index as the prism were used for the fluorescent polymer deposition. Glass slides with polymer films on the inner surface were placed in the flowing cell made of Teflon. The Teflon holder has a cavity with inlet and outlet channels on the sides. A glass slide was pressed to the holder using a metal plate. A rubber ring was placed between the glass slide and the Teflon to prevent glass fracture. The glass prism was covered with a refractive index matching oil (Cargille Immersion Oil, Type DF) and placed on top of the glass slide. Saturated vapors of water and various organic solvents were pumped at 10 ml per minute through the cuvette using a pump (ISMATEC, Inc.) connected to the cell with polyethylene tubing. Time-dependent fluorescent emission changes upon absorption of vapors by the polymer film were monitored and analyzed using LabView software.

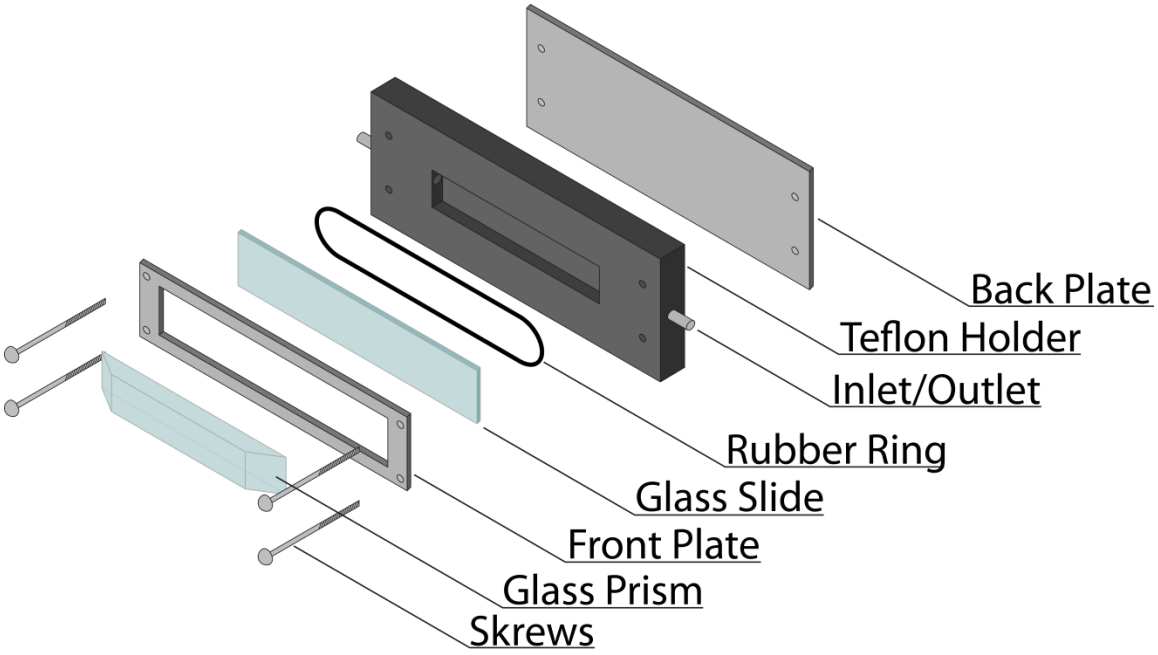


**Figure 3.5.** Schematic diagram of the cuvette for the TIRF measurements.

The following theory stands behind the total internal reflection phenomena used in this study. Upon total reflection of the laser beam from the optically less dense material, a small portion of reflected light penetrates through the interface, creating an electromagnetic field, as schematically shown in **Figure 3.6.** This field is usually called the evanescent field.

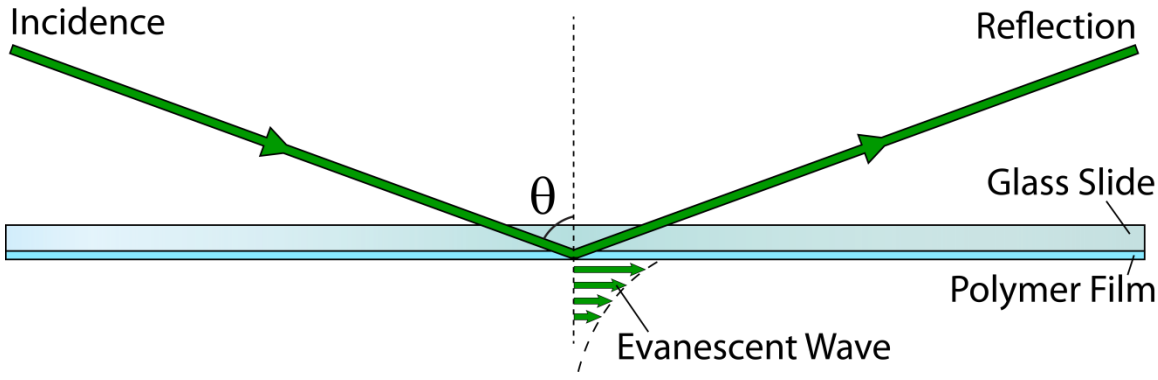


**Figure 3.6.** Pathway of the light beam during total internal reflection

The theory predicts an exponential decrease of intensity of this field in the direction perpendicular to the surface. The characteristic depth of penetration $d_p$ is the depth at which evanescent field intensity is reduced to $1/e = 0.367879441$ times its initial value, which can be calculated as [9]:

$$d_p = \frac{\lambda}{2\pi}\sqrt{n_1^2 sin^2\theta - n_2^2} \qquad \textbf{Eq. 3.4}.$$

where $n_1$ and $n_2$ are refractive indexes of more dense and less dense material, respectively; $\lambda$ is the wavelength of the incident beam; and $\theta$ is the angle of incidence. For the setup used ($n_1 = 1.52$, $n_2 \sim 1$, $\lambda = 532nm, \theta = 72.7°$), $d_p$ is approximately 88 nm.

### 3.3.5. Spectrophotometry

Spectrophotometry is a type of spectroscopy that measures the radiant energy transmitted or reflected by the sample as a function of wavelength. In particular, spectrofluorometry deals with fluorescent materials. Fluorescence spectrophotometers measure the excitation and emission spectra of a material as the intensity of absorption and emission as a function of wavelength[10]. A Jobin Yvon Fluorolog 3–222Tau spectrofluorometer was used in this study. The setup of the spectrophotometer apparatus is presented schematically in **Figure 3.7.**

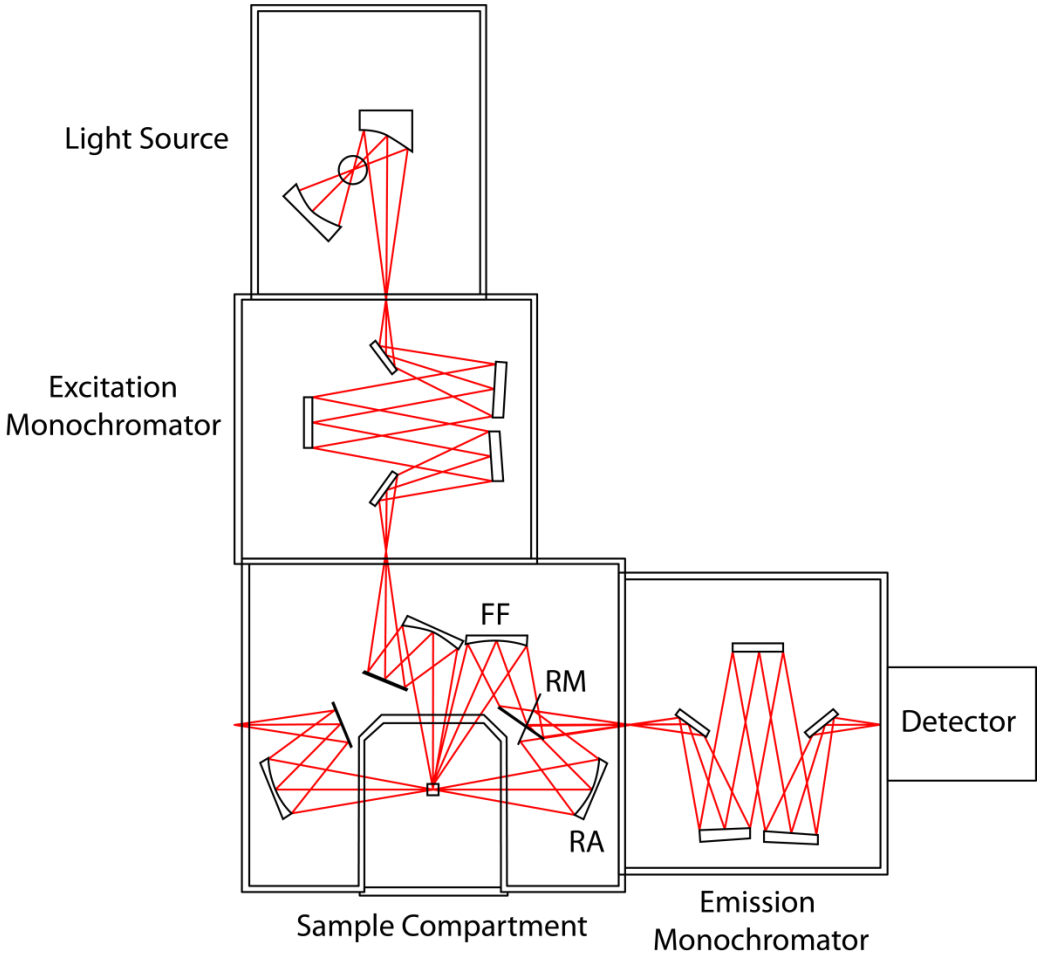


**Figure 3.7.** Schematic of the spectrophotometer

In this setup, the light source is a 450 W ozone-free xenon lamp. Light from the source passes the excitation monochromator and enters the sample chamber. There, a light beam passes through the sample and excites the fluorophores within the sample. Fluorescent emission then passes the emission monochromator and is finally collected by the detector.

There are two modes of spectrophotometer operation. In the first mode, emission is collected at 90° to the pathway of the excitation beam (Right Angle mode (RA)). This mode is generally used in the case of transparent liquid solutions. In the second mode,

emission is collected at the front-face (Front Phase mode (FF)). This mode is used for the reflective or strongly absorbant samples. The switching between the two modes of operation can be done using a rotating mirror (RM) (**Figure 3.7.**)

Collected light first passes the emission monochromator and then reaches the detector. The resulting measurement is presented as the number of photons of defined energy reaching the detector per unit of time. As previously mentioned, a spectrophotometer has two modes of operation. In the first mode, the wavelength of excitation is kept constant and fluorescent emission is collected as a function of photon energy. In the second mode, the sample is excited by the range of wavelengths, and emission is collected at a single wavelength. Since fluorescent emission is always proportional to the sample's absorbance, the second mode of operation produces an excitation spectrum. OriginLab Origin software was used to collect, monitor, and plot the results of measurements.

For spectroscopic measurements of fluorescent solutions, standard quartz cuvettes were used for sample containment. To perform in situ measurements of the fluorescent emissions of the fluorescent film in the saturated solvent vapors, a special cuvette was designed (**Figure 3.8**).

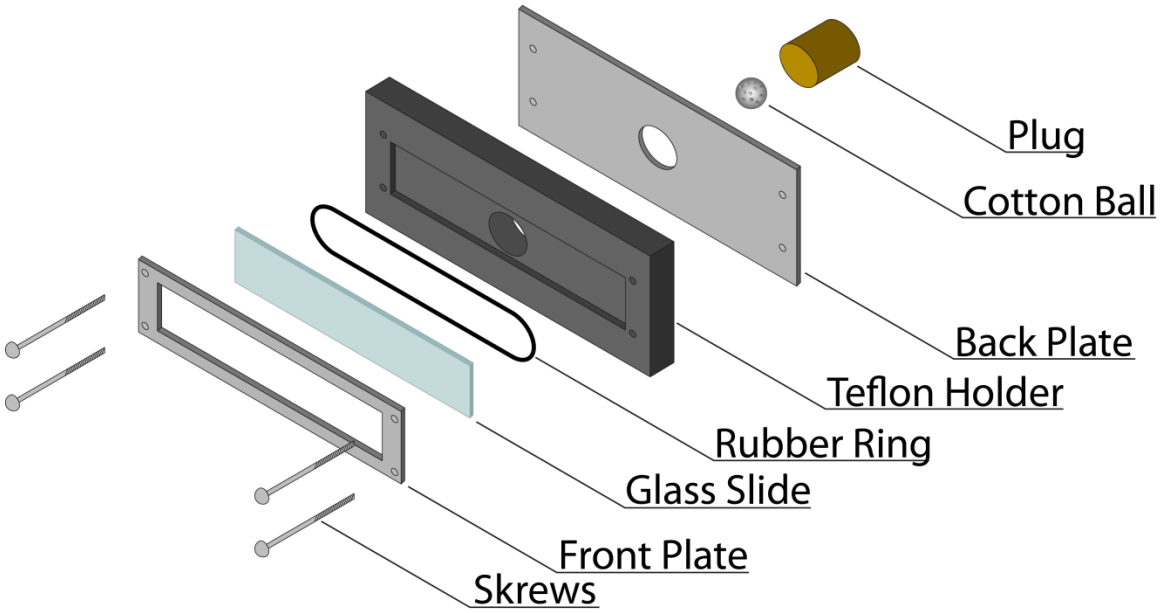


**Figure 3.8.** Schematic diagram of custom-made cuvette for spectrophotometry measurements.

A glass slide with a fluorescent film was sandwiched between the front metal plate and the Teflon holder with the cavity. A rubber ring was placed between the glass slide and the Teflon holder to distribute load and prevent glass fracture. Four screws tightly pressed the front plate towards the back plate so the fluorescent film on the inner surface of the glass slide was exposed to the environment established inside the cavity of the Teflon holder. Analyte vapors were introduced to the cuvette by a cotton ball soaked with the solvent, which was inserted into the cavity from the back side of the Teflon holder. To prevent solvent evaporation, the cavity was tightly sealed with a plug.

To prevent variations in the fluorescent signal, glass position was maintained for each swelling experiment. A fully assembled cuvette with a dry cotton ball inside was inserted into the sample compartment of the spectrophotometer, as shown in **Figure 3.8**. Measurements were conducted in front-face mode. After all measurements of the

fluorescent emission of the film in the dry state were performed, solvent was injected into the cotton ball using a pipette without detaching the assembly from the sample compartment of the spectrophotometer. The cuvette was then sealed with a plug and measurements for the film in the swollen state were performed. After each measurement, the cuvette was disassembled and purged with nitrogen. The glass slide was taken out of the cuvette to let the polymer film de-swell for at least 30 minutes. Ellipsometry studies on the de-swelling of the fluorescent polymer films used in this study have shown that 30 minutes is enough for the film to return to the dry state (**Section 4.3.5.**).

### 3.3.6. Electron Microscopy

Electron microscopy is a type of microscopy that uses an electron beam to illuminate a sample[11]. It is possible to achieve a much higher resolution with electron microscopy than with regular light microscopy due to the shorter wavelength of the electron beam. This beam is produced by an electron gun, accelerated by the electrical potential difference and focused on the sample with electrostatic lenses. Two electron microscopy techniques were used in this study: Scanning Electron Microscopy (SEM) and Transmission Electron Microscopy (TEM). In the SEM technique, an electron beam with energy between 0.2 keV and 40 keV hits the sample, producing secondary electrons and back-scattered electrons. These can be used to reconstruct the topology, composition, and conductivity of the sample. In some cases, if the sample is non-conductive, an additional conductive coating is needed. For TEM, an electron gun is connected to a much higher voltage source (usually 100 - 300 keV). A focused beam of accelerated

electrons penetrates through the sample and hits the fluorescent screen. On the resulting TEM image, brightness represents the density of the sample; darker parts of an image represent denser areas of the sample where electron beam scatters more. Special conductive grids are used to hold the sample for TEM imaging.

Electron microscopy was performed using devices available in the Advanced Materials Research Laboratory (AMRL), Research Park, Clemson University. A Hitachi S4800 was used for SEM imaging. All samples were coated with platinum to increase sample conductivity using a Hummer 6.2 Sputtering System for approximately 2 minutes. A Hitachi H7600T was used for TEM imaging of nanoparticles. A nanoparticle suspension was deposited onto copper TEM grids and measurements were performed after solvent evaporation.

## 3.4. General experiment procedures

### 3.4.1. Cleaning of glass slides and silicon wafers

Silicon wafers (SHE America Inc.) and premium microscope glass slides (Fisher Scientific Inc.) were initially cleaned with deionized water for 30 min in a sonicator (75HT, VWR International LLC). During the sonication process, water was changed 3 times. After, the sonication samples were placed into the piranha solution (concentrated sulfuric acid with 30% hydrogen peroxide at a ratio of 3:1) at 80 °C for 2 hours for wafers and 1 hour for glasses. Samples were then rinsed with deionized water. Water leftovers were blown away with the steam of high purity nitrogen (National Specialty

Gases). To prevent surface contamination, glasses and wafers were used for film deposition right after cleaning.

### 3.4.2. Fabric cleaning and surface activation

Polyethylene terephthalate (PET) fabrics (Test Fabric Inc.) were used in this study. Prior to coating deposition, fabric samples were cleaned and activated following the procedure reported in[12]. Each fabric sample was rinsed in several solvents (DI water, methanol, toluene, and acetone) to remove any finishes or contaminants. Subsequently, fabrics were treated with 40% sodium hydroxide solution (40/30/30 wt % of NaOH/Methanol/DI water; ethanol was added to improve the wetability of the fabric) for 2 minutes at room temperature, and then were rinsed with DI water until all the residues were removed. Such treatment creates groups (carboxylic and hydroxilic) that are reactive to the PET yarn surface[13] and makes them active for further modification. To prevent surface contamination, fabrics were used for surface modification right after cleaning and drying at room temperature for 2 hours.

## 3.5. Polymer film characterization

### 3.5.1. Surface morphology characterization

The AFM measurements were used for surface characterization using a Dimension 3100 (Digital Instruments, Inc.) microscope. The root mean square roughness of the film surface was computed from the AFM images using NanoScope version 5.3.0r3.sr3 software (Veeco Instruments, Inc.). The formula used for calculation is [14]:

$$RMS = \sqrt{\frac{1}{n}\sum_{i=1}^{n}\left(h_i - \bar{h}\right)^2} \qquad \textbf{Eq. 3.5.}$$

where$h_i$ is the height of the i-th point of the total $n$ points on the AFM image and $\bar{h}$ is the arithmetic mean height of all $n$ points. The root mean square roughness calculated in this way would characterize statistically how the surface profile of the film deviates from the ideally flat.

### 3.5.2. Film thickness and refractive index measurement

All films deposited on silicon wafers and glass slides produced in this study were characterized using the same procedures. The thickness of the film was determined by scratching the surface using a sharp razor blade and acquiring the topographic profile along the scratch using AFM. The profile was then analyzed using Gwyddion software and the film thickness was estimated. Ellipsometric measurements were then taken using the model for calculation with known thickness and unknown refractive index of the film. The refractive index of the polymer film was calculated from these measurements.

### 3.5.3. Grafting density calculation

To characterize grafted polymer films, several parameters were used, including surface coverage and grafting density[15]. The surface coverage Γ and the amount of the material grafted per unit area in $mg/m^2$was calculated from known film thickness $h$ and polymer density as:

$$\Gamma = \rho \cdot h$$ **Eq. 3.6**.

The grafting density Σ calculated as the number of polymer chains grafted to the substrate surface per unit area in $chains/nm^2$ was calculated as:

$$\Sigma = \Gamma N_A / M_n$$ **Eq. 3.7**.

where$N_A$is the Avogadro's number and $M_n$ is the molecular weight of the grafted polymer.

### 3.6. Reproducibility of spectrophotometric measurements

To estimate the repeatability of the spectrophotometric measurements of the fluorescent emission intensity changes during the vapor uptake, the intensity changes for the same PGMA-RhB film of 5 nm thick were measured in chloroform and water vapors, as these solvents present the highest positive and negative emission intensity changes respectively. The measurements were repeated four times for each of the solvents. Resulting relative intensity changes calculated using the **Eq.5.10.** were 0.03±0.002 for chloroform vapor and -0.061±0.003. Here the value after ± sign represents the standad error of the measurements. Therefore the standard error of the relative intensity change calculation in these solvents was less than 7%.

For the PGMA-RhB films with nonfluorescent polymer grafting the repeatability of the fluorescent emission changes was examined by performing several experiments for the emission intensity changes. For each of the polymer grafted (PS, P2VP, PEG and PAA) at least three measurements were performed in selected solvents. The errors in of these measurements were less than 10% for all samples.

## 3.7. References


1. Zdyrko, B.; Swaminatha Iyer, K.; Luzinov, I., Macromolecular anchoring layers for polymer grafting: comparative study. *Polymer* **2006,** *47* (1), 272-279.

2. Zdyrko, B.; Klep, V.; Luzinov, I., Synthesis and Surface Morphology of High-Density Poly(ethylene glycol) Grafted Layers. *Langmuir* **2003,** *19* (24), 10179-10187.

3. Crawford, L. J.; Edmonds, N. R., Calculation of film thickness for dip coated antireflective films. *Thin Solid Films Thin Solid Films* **2006,** *515* (3), 907-910.

4. Scriven, L. E., Physics and Applications of DIP Coating and Spin Coating. *MRS Proc. MRS Proceedings* **1988,** *121*.

5. Bornside, D. E.; Macosko, C. W.; Scriven, L. E., ON THE MODELING OF SPIN COATING. *Journal of Imaging Technology* **1987,** *13* (4), 122-130.

6. Poggi, M. A.; Gadsby, E. D.; Bottomley, L. A.; King, W. P.; Oroudjev, E.; Hansma, H., Scanning probe microscopy. *Analytical chemistry* **2004,** *76* (12), 3429-43.

7. Fujiwara, H., *Spectroscopic ellipsometry : principles and applications*. John Wiley & Sons: Chichester, England; Hoboken, NJ, 2007.

8. Lok, B., Total internal reflection fluorescence: a technique for examining interactions of macromolecules with solid surfaces. *Journal of Colloid and Interface Science Journal of Colloid and Interface Science* **1983,** *91* (1), 87-103.

9. Lassen, B.; Malmsten, M., Competitive Protein Adsorption Studied with TIRF and Ellipsometry. *Journal of Colloid and Interface Science* **1996,** *179* (2), 470-477.

10. Lakowicz, J. R., *Principles of fluorescence spectroscopy*. Kluwer Academic/Plenum: New York, 1999.

11. Bozzola, J. J.; Russell, L. D. Electron microscopy principles and techniques for biologists. http://search.ebscohost.com/login.aspx?direct=true&scope=site&db=nlebk&db=nlabk&AN=25575

12. Ramaratnam, K.; Iyer, S. K.; Kinnan, M. K.; Chumanov, G.; Brown, P.; Luzinov, I., Ultrahydrophobic textiles: Lotus approach. *Aatcc Review* **2008,** *8* (1), 42-48.

13. Hauser, P. J., *Textile dyeing*. InTech: Rijeka, Croatia, 2011.

14. Poon, C. Y.; Bhushan, B., Comparison of surface roughness measurements by stylus profiler, AFM and non-contact optical profiler. *Wear* **1995,** *190* (1), 76-88.

15. Henn, G.; Bucknall, D. G.; Stamm, M.; Vanhoorne, P.; JГ©rГrme, R., Chain End Effects and Dewetting in Thin Polymer Films. *MACROMOLECULES* **1996,** *29* (12), 4305-4313.

# CHAPTER FOUR

# FABRICATION AND CHARACTERIZATION OF SUBMICRON FLUORESCENT FILMS

## 4.1. Introduction

Crosslinked thin polymer films provide the unique ability to modify a surface of various materials[1]. Deposition of the crosslinked polymer network creates a soft stable surface with known controllable physical, mechanical, and biochemical properties[2]. Such coatings offer significant opportunities for various applications.

For example, the coating may be used as a host material for a drug or protein for medical applications[3]. Crosslinked polymer networks can protect the material from harsh environments or provide essential functionality for the material surface[4]. The submicron dimensions of such polymer films make them useful in micro and nanoscale technology[5]. The ability of the polymer network to swell reversibly in response to external stimuli allows the employment of crosslinked coatings as sensors and actuators[6].

In particular, the use of polymer films in sensing applications is a very promising field of study due to the ability of the polymer network to concentrate the analyte during absorption of the target substance from the vapor or liquid phase[7]. Of all types of sensing devices, fluorescent sensors draw special attention due to the unique properties of fluorescence, such as high sensitivity, the small size of the emitters, and their immunity to electromagnetic interference[8].

The present work targets environment-sensitive fluorescent polymer films that, in principle, can be used in sensor devices. The operating principle of such a film is based

on the ability of the vapors of an analyte to be absorbed by the polymer network and change the emissive characteristics of the fluorescent dye molecules embedded in the film. The first step on the way to making a sensoric system based on fluorescent polymer films is deposition of the films on a substrate. The second step is qualitative measurements of the changes in optical properties during solvent absorption.

With this in mind, the objective of this part of the work was to synthesize and characterize fluorescent polymer films. The thickness of the films was targeted to be in the order of hundreds of nanometers. On the one hand, this is relatively low, so created polymer films have nanoscale dimensions. On the other hand, the amount of fluorophores embedded into the film should be enough for high signal-to-noise ratios of the fluorescent signal. Poly(glycidyl methacrylate) PGMA was chosen as a matrix polymer since it has a set of unique properties well suited for hosting fluorophores[9]: As can be seen from the structure of the polymer in **Figure 4.1.**,each monomeric unit of PGMA contains an epoxy group that is known to be highly reactive[10]. This reactivity is employed to chemically bond polymer chains to the substrate and crosslink the polymer chains to create a chemically stable polymer network. Unreacted groups are still present in the polymer network after the crosslinking due to the high number of epoxy functionalities[11]. This allows further chemical modification to the stable polymer network.

In order to make the film fluorescent, the polymer used for the film fabrication needs to be labeled with fluorescent molecules. In the present study, Rhodamine B (**Figure 4.1. left**)was chosen for this purpose. Rhodamine B (RhB) is known to be highly fluorescent, has very low photo bleaching over time, and has a carboxylic group in its

molecular structure[12], which allows chemical attachment of RhB molecules to the epoxy group of the PGMA.

The PGMA films were deposited on the surface of silicon wafers and glass slides. The studies on the morphology and the optical characteristics were conducted using AFM and ellipsometry. Since the polymer films are targeted for use in sensing applications with volatile organic solvents as analytes, the amount of solvent intake from the vapor phase will be one of the key parameters governing the sensitivity of the system. To this end, the proof of concept experiments on analyte (chloroform) intake from saturated chloroform vapors were performed using ellipsometry. To study the fluorescent properties of the films in the dry state and to determine how the signal changes during the vapor intake, spectrophotometry and Total Internal Reflectance Fluorescence (TIRF) measurements were used.

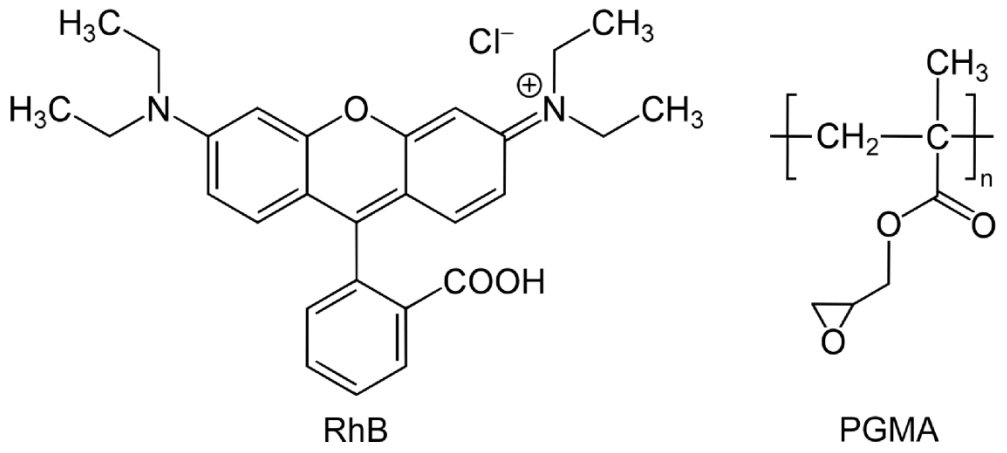


**Figure 4.1.** Structures of Rhodamine B (RhB) (left) and poly (glycidyl methacrylate) (PGMA) (right)

## 4.2. Experimental

### 4.2.1. Fluorescent polymer labeling

Chemical attachment of RhB to PGMA (Mn= 382,000 g/mol, PDI 2.5) was performed according to the previously developed procedure[13]. The labeling was conducted from the MEK solution (17:1 RhB:PGMA molar ratio). The reaction between the carboxylic group of RhB and the epoxy group of PGMA was allowed to proceed for 24 h at 70 °C. The polymer was then purified by multiple precipitations from the MEK solution into diethyl ether. The precipitate was extracted from diethyl ether using a centrifuge (Precision Durafuge 100). The GPC analysis of the labeled PGMA-RhB showed a Mn of 402,000 g/mol and a PDI of 2.2. For the developed fluorescent labeling procedure, elemental analysis showed attachment of one RhB molecule per 311 monomeric units of PGMA[13].

### 4.2.2. Deposition of the polymer film

Prior to the film deposition, silicon wafers and glass slides were cleaned according to the procedure described in **Section 3.4.1.** Florescent polymer films were deposited on the substrates from a 1% w/w PGMA solution in chloroform using a spincoater (Headway Research Inc.). Spincoating was performed at 900 rpm for 30 seconds and solution concentration was varied to achieve the desired dry film thickness. After the spincoating, films were annealed in a vacuum oven at 120 °C for 8 h to crosslink and chemically attach the film to the substrate. After annealing, unattached

polymer chains were removed by rinsing the sample with chloroform three times for 30 minutes on a shaker.

### 4.2.3. Characterization of the polymer film in the dry state

The morphology of resulting polymer film and its thickness were characterized using a Dimension 3100 (Digital Instruments, Inc.) atomic force microscope. Films deposited on the glass slides and silicon wafers under the same conditions were compared to ensure that the deposited film properties were independent from the substrate type. The thickness of the film and its refractive index were examined with a COMPEL automatic ellipsometer (InOmTech, Inc.) using silicon wafers as a substrate and an angle of incidence set to 70°. Glass slides were used as a substrate for measuring fluorescent properties. The fluorescent properties of the dry film were studied using measurements from a custom-built TIRF apparatus and a Jobin Yvon Fluorolog 3–222Tau spectrofluorometer.

### 4.2.4. Measurements of the film properties during vapor intake

To examine in situ changes of the film properties, films were subjected to saturated chloroform vapor. For thickness measurements during the swelling process, ellipsometry was used. Silicon wafers were placed in a closed cuvette together with a small (2 ml) aluminum bucket. After the thickness of the film was measured in the dry state, the bucket was filled with chloroform and the cuvette was tightly sealed with the cap using grease (Krytox, Dupont) to prevent solvent evaporation. Ellipsometric

parameters Ψ and Δ were measured as a function of time. The position of the sample was not changed during the measurement. Next, the acquired parameters were fitted using the program supplied with the device.

For the TIRF measurements, saturated chloroform vapors were pumped through the Teflon cuvette holding the glass slide to the polymer film using a peristaltic pump (ISMATEC Inc.) at 10 ml/min. Exposures to the chloroform vapors were repeated several times to determine the reversibility and repeatability of the measurements.

## 4.3. Results and Discussion

### 4.3.1. Selection of substrate and deposition technique

To investigate the fluorescent properties of the RhB-labeled PGMA,the polymer was deposited by spin coating a film on flat substrates. For the fluorescent properties examination, Total Internal Reflectance Fluorescence (TIRF) and spectrophotometry measurements were used. Both methods require a transparent substrate for the measurement. Moreover, both techniques are used to study the changes in the polymer film environment and only one side of the substrate is subjected to changing conditions. This implies that only one side of the substrate should be covered with fluorescent polymer film, otherwise additional constant fluorescent emission will be observed during experiments.

For measurements of the film thickness and refractive index, ellipsometric measurements were performed using an ellipsometer with an angle of incidence set to 70°. For effective measurements at this angle the following condition should be satisfied:

if the substrate used for the film under investigation is relatively thin (less than several centimeters) it should not be transparent for the light beam. Otherwise, the light beam reflected from the back side of the substrate will give rise to significant measurement error[14].

Considering all arguments presented above, silicon wafers were chosen as substrates for the ellipsometric measurements, and glass microscope slides were chosen for the fluorescent measurements. Silicon wafers are well suited for ellipsometric measurements due to their low roughness and well known optical properties[15]. Glass microscope slides are good candidates for fluorescence measurements because these substrates are transparent in the visible region. Since the surface chemistry of silicon wafers and glass slides are similar[16], the same technique for film deposition was used for both types of substrates.

Spin coating was selected as a film deposition technique for this part of the study. The choice was based on the previously mentioned argument that for the fluorescent measurements only one side of the surface should be covered with fluorescent film. Due to the fact that deposited film properties are only affected by the viscosity of the polymer solution used for the coating and the rotation speed[17], spincoated films on both kinds of substrate should have the same thickness if the same deposition conditions are maintained.

### 4.3.2. Selection of solvent for the PGMA-RhB deposition

Selection of the solvent used for the film deposition was governed by the solubility of the PGMA-RhB. PGMA shows good solubility in several organic solvents.

Affinity of the solvent to the polymer can be found during the polymer swelling experiments[18], as described in detail in **Section 5.3.6.** Polymer films swell more in good solvents and show almost no swelling in solvents that are poor for the polymer. Swelling experiments showed good solubility of PGMA-RhB in several organic solvents. Among these, chloroform and MEK showed the best affinity to PGMA.

Therefore, polymer films were spincoated from a 1% w/w solution of PGMA-RhB in these two solvents at 900 rpm and annealed for 8h at 120°C. Polymer film annealing is an essential processing step for PGMA-RhB films. Without annealing, the PGMA will not attach itself to the substrate and will not form a chemically stable polymer network. Since these films are targeted for use in sensing applications with volatile organic solvents as analytes, polymer films not bonded chemically to the substrate can dewet or detach from the substrate surface during analyte intake.

After annealing the polymer film, unattached polymer chains left within the film structure must be removed. If this is not done, these chains can migrate during the swelling more easily than the polymer chains that belong to the crosslinked polymer network. This may cause unwanted interference with the fluorescent signal in the course of analyte intake.

The AFM imaging of the PGMA-RhB film surface is shown in **Figure 3.2.** It can be seen from the images that by using both solvents, flat films were obtained on the

surface of the silicon wafers. However, there were a significant number of pores in the film created from the MEK solution (**Figure 3.2.left**). The presence of pores in the resulting polymer film originates from the presence of small amounts of water in the MEK. As the film is created MEK evaporates from the film rapidly, while water droplets stay longer in the film. As a result holes are left in the film after water evaporation, since PGMA-RhB is insoluble in water[19]. On the other hand, chloroform does not contain water, and evaporation of the solvent from the drying film after deposition from chloroform solution takes place in a uniform fashion, decreasing the roughness of film surface (**Figure 3.2.right**). Thus, for the rest of the work chloroform was used as a solvent for polymer film deposition.

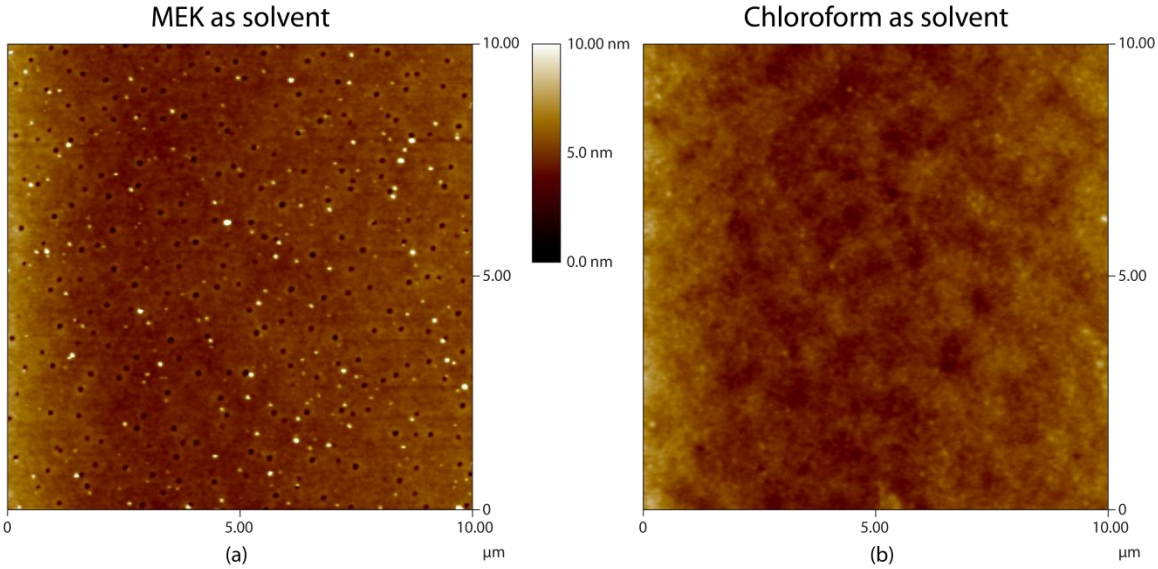


**Figure 4.2**AFM images of the surface of PGMA thin film. Polymer film prepared using MEK (left) and Chloroform (right) as a solvent.

### 4.3.3. Measurements of the thickness of PGMA-RhB film

The thickness of the films was measured with ellipsometry and cross-checked with AFM using profiling over the scratch approach. The AFM thickness and morphology measurements were performed on both the glass slides and the silicon wafers for comparison between the two types of substrates. Film morphology was found to be the same and the measured thickness was determined to be 55 nm for both substrates.

The thickness of the films was measured using ellipsometry and compared with AFM using the profile over the scratch approach. Ellipsometric measurements showed good correspondence with the AFM measurements. The refractive index of the PGMA-RhB film was determined to be 1.51 from the fitting of ellipsometric data with the thickness value found using AFM measurements.

This proves independence of the deposited film thickness and morphology on the substrate for the listed substrate types. This important result allows investigation of the properties of the film, selecting the most convenient substrate type for the measurement technique: wafers for the thickness measurements using ellipsometry, and glass slides for fluorescent properties measurements using the spectrophotometer and a TIRF setup.

### 4.3.4. Tuning the thickness of PGMA-RhB film

To evaluate the possibility of tuning the thickness of the dry PGMA-RhB film created using a spin coating technique, the PGMA films were spincoated on silicon wafers using a constant rotation speed and a solution of PGMA-RhB with different concentrations.

The viscosity of the PGMA-RhB solution depends on the polymer concentration[18] and, as **Eq. 3.2** suggests, viscosity governs the thickness of the deposited layer if the other parameters are kept constant. So, by varying the film concentration it is possible to tune the thickness of the resulting polymer film.

After annealing and subsequent removal of unattached polymer chains, the thickness of the films was measured using ellipsometry and was cross-checked with AFM using the profiling over the scratch approach. Once again, the ellipsometric measurements showed good correspondence with the AFM measurements. **Figure 4.3** shows the linear dependence of the resulting thickness on the PGMA-RhB concentration, making it clear that any desired thickness can be achieved using the proposed technique.

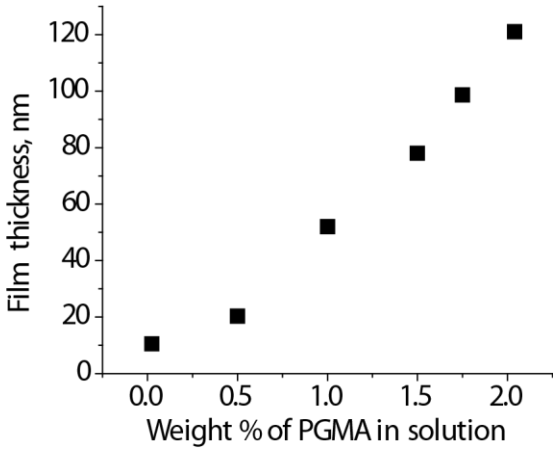


**Figure 4.3.** Dependence of the thickness of dry PGMA film on the concentration of PGMA in solution

From the combined AFM and ellipsometry measurements, the refractive index of the PGMA-RhB film was determined to be 1.51, independent of the film's thickness. It is known that the refractive index depends on the crosslinking density and the free volume fraction within the polymer network[20]. Therefore, independence of the refractive index

from the achieved polymer film thickness means close chemical composition, polarity, and density of the polymer network for each film.

### 4.3.5. Swelling of PGMA-RhB film

One of the tasks of this work is to study the behavior of fluorescent polymer films in different environments. Specifically, we expect that in different environments the fluorescent signal produced by the dye molecules embedded in the polymer film will be different. Therefore, it is important to determine the PGMA film's response to environmental changes. Does PGMA protect RhB molecules from the environment or does it swell, hence exposing the RhB molecules to the analyte? To answer this question and find out how the solvent enters the film from the vapor phase, swelling experiments were performed using an ellipsometer. For this purpose, a sealable transparent cuvette was created (**Figure 4.4.left**). The cuvette was designed such that two transparent windows are perpendicular to the laser beam and do not alter its polarization state. First, the sample was put into the cuvette and the dry thickness of the film was measured. Next, a small bucket with a solvent (e.g. chloroform) was introduced into the cuvette and ellipsometric measurements were conducted for 30 minutes as the film absorbed the solvent. After the acquisition, raw data was fitted using ellipsometer software.

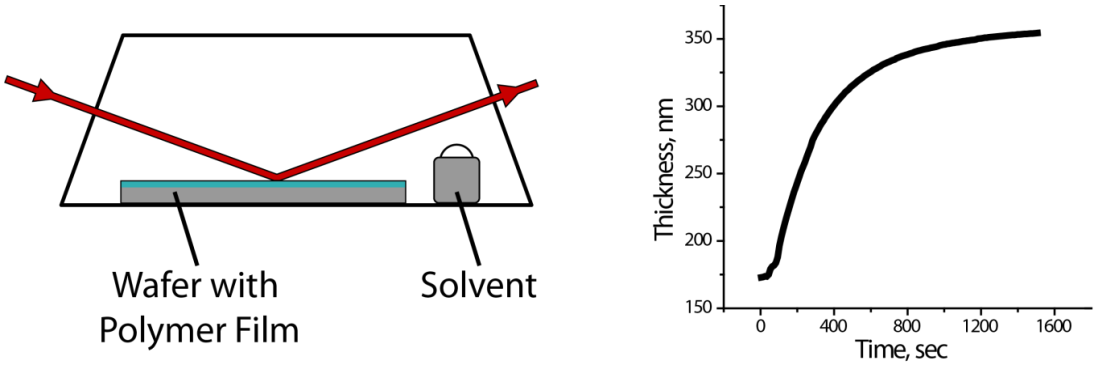


**Figure 4.4.** Schematic of the glass cuvette for solvent absorption measurements using an ellipsometer (left). Thickness change of the 170 nm thick PGMA-RhB film upon exposure to saturated chloroform vapors (right).

Swelling measurements show that the thickness of the PGMA-RhB film increases when the film is subjected to chloroform vapor. The swelling curve for this experiment, presented in **Figure 4.4.right,** shows a thickness increase of 2.04 times after 25 minutes of exposure. This suggests that with a high amount of the solvent within the film, the environment around the RhB molecules should change upon vapor absorption.

As discussed above, the refractive index of the dry polymer film depends on the crosslinking density and the density of polymer chain packing. All PGMA-RhB films reported were obtained using the same annealing time and temperature. They had the same refractive index and therefore the same crosslinking density. This fact implies that the polymer film should swell to the same extent, independent of the thickness, since the rate of solvent absorption is governed by the nature of the polymer and the crosslinking density of the polymer network [21]. For the thin films under consideration, the presence of the rigid substrate surface could also influence the extent of swelling for films of different thicknesses[22].

To determine how the relative amount of solvent absorbed by the PGMA-RhB film depends on the film thickness, the swelling experiment was repeated under the same conditions (using saturated chloroform vapor) for PGMA-RhB films of several thicknesses. The obtained results (**Figure 4.5.**) show, that the relative amount of swelling is the same for all films within the studied thickness range. Since relative swelling of the film depends on the crosslinking density within the polymer network[23] and the influence of the substrate surface[24], which is rigid and restricts polymer chain motion, the results

presented in **Figure 4.5** suggest the same crosslinking density for the PGMA-RhB network and the same surface influence for the series.

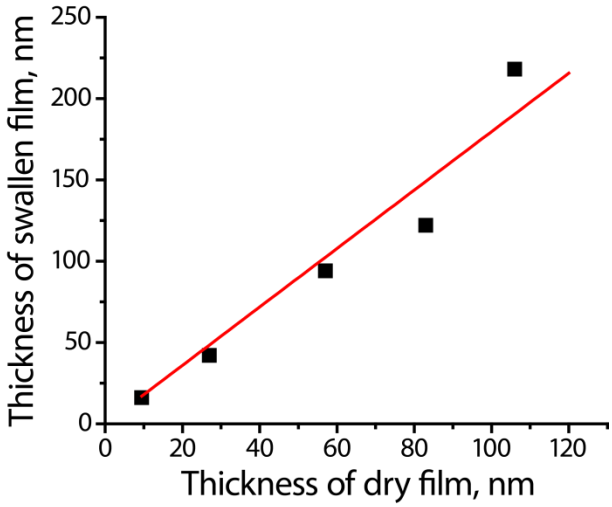


**Figure 4.5.** Swelling behavior of several PGMA-RhB films in saturated chloroform vapor

### 4.3.6. Kinetics of PGMA-RhB film swelling

Since one of the possible applications of fluorescent PGMA-RhB films is in vapor sensing, it is important to know how fast the film can reach a saturated state, since the maximum analyte content within the film is achieved when the film is fully saturated. The driving force for the polymer film to swell is the pressure of the solvent in the vapor phase[25]. Since the solvent is introduced to the cuvette as a liquid, vapor fills the cuvette over a period of time. Thus, the pressure of the vapor in the cuvette is constantly changing until saturation is reached. Therefore, the kinetics of polymer film swelling will depend not only on the rate of absorption of the analyte by the polymer film, but also on the solvent's evaporation rate.

To investigate the factors affecting the swelling rate of the flexible polymer film in the changing vapor pressure rates it is useful to consider the simple case first. The following discussion is valid for the simplified case of constant vapor pressure and rigid film.

It is known that the amount of the solvent $M$ which enters the film at the time $t$ for the terminal stages of the swelling can be described by the equation[26]:

$$\frac{M}{M_\infty} = 1 - \frac{8}{\pi^2}\exp[-\frac{D\pi^2 t}{4h_0^2}] \qquad \textbf{Eq. 4.1}.$$

where $M_\infty$ is the amount of solvent contained within the film at equilibrium, $D$ is the diffusion coefficient, and $h_0$ is the thickness of the film, which stays the same during the vapor intake. It can be seen from the equation that the time needed to achieve the ratio $M/M_\infty$ should be higher for the thick film than for a thin film, since $t/h_0^2$ should stay the same, assuming that there is no change in the diffusion coefficient.

Because of the changing pressure and moving boundary, swelling of the polymer film is much more complicated case than the one presenter above. However since in the case of the polymer film swelling the amount of the solvent in the film $M/M_\infty$ is proportional to the change of the film thickness $h/h_\infty$, where $h_\infty$ is the thickness at the equilibrium, if is possible to compare the kinetics of swelling for films of different thickness using the swelling curves. In **Figure 4.6**, the relative thickness change for 9 nm and 106 nm thick PGMA-RhB film in chloroform vapors is shown. For comparison purposes the swelling curves were rescaled using the equation $(h - h_0)/(h_\infty - h_0)$ to

range from 0 to 1, where 0 is the thickness in the dry state and 1 is the thickness in the fully swollen state.

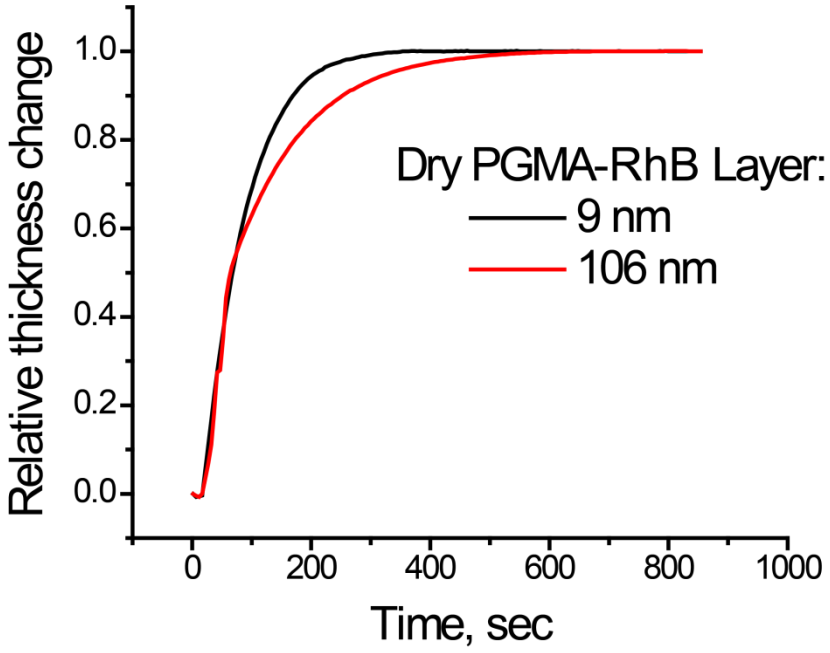


**Figure 4.6.** Relative swelling of PGMA-RhB layers of different thickness as a function of time.

It can be seen from the graph above that the thin PGMA-RhB layer reaches equilibrium swelling in a shorter time than the thick film. This phenomenon can be explained by the fact that the diffusion time for the small molecules into the film depends on the thickness of the film.

One important conclusion could be made from the results of this experiment: thinner films reach a saturation state more quickly than thick films. This can be used as an advantage for applications where it is favorable to have a fast system response to the target analyte.

### 4.3.7. Fluorescent measurements

#### 4.3.7.1. RhB concentration in the PGMA-RhB film

The next step of this study was to examine the fluorescent characteristics of dry PGMA-RhB film. It is known that the fluorescent properties of the fluorophores depend on their concentration: if the distance between fluorophores is short, multiple effects such as inner filter effects and dimer formation may occur[27]. The inner filter effect is the decrease of the emission collected from the sample due to the reabsorption of the emitted light at high dye concentrations[28]. Dimer formation can decrease the fluorescent emission of the sample when the dimers of the fluorophores have a lower quantum yield then the fluorophores themselves[29]. These effects depend on the proximity of the fluorescent molecules in the system, so it is important to estimate the distance between the RhB molecules in the PGMA-RhB film. The RhB concentration in the film can be calculated using the formula:

$$c_0 = \frac{\rho * N_A}{M * 311} \qquad \textbf{Eq. 4.2.}$$

where $\rho = 1.08\ \mathrm{g/cm^3}$ is PGMA density[30], $N_A$ is the Avogadro's number, $M = 142\ \mathrm{g/mol}$ is the molecular weight of the PGMA monomeric unit, and the factor of 311 originates from the fact that the labeling technique attached an average of one RhB molecule per 311 monomeric units of PGMA. The approximate RhB molecule concentration is therefore $c_0 = 1.52 \cdot 10^{-2} nm^{-3}$. The distance between the RhB molecules can be estimated as $s = \sqrt[3]{1/n} \approx 4\ nm$.

#### 4.3.7.2. Forster Resonance Energy Transfer (FRET)

Due to the low thickness of the polymer film, there is almost no inner filter effect[31], as only a very small number of the RhB molecules get excited and the chance of reabsorption of light emitted by the fluorophores is very low. However, since the absorption spectrum overlaps the fluorescent emission spectrum, Forster Resonance Energy Transfer (FRET) can occur between RhB molecules.

The FRET is an energy transfer that can occur between fluorophores due to dipole-dipole coupling[32]. The efficiency of such a transfer can be estimated as[33]:

$$E = \frac{1}{1 + (r/R_0)} \qquad \textbf{Eq. 4.3.}$$

where$r$ is the distance between fluorophores, and $R_0$ is the Forster radius. From **Eq. 4.2,** it can be seen that when the distance between the fluorophores is equal to the Forster radius, the efficiency of the FRET is 50%.

The formula for the Forster radius is[34]:

$$R_0^6 = \frac{9Q(ln10)\kappa^2 J}{128\pi^5 n^4 N_A} \qquad \textbf{Eq. 1.4.}$$

where $Q$ is the quantum yield of the fluorophore, $\kappa$ is the orientation factor, $n$ is the refractive index of the host medium, $N_A$ is the Avogadro's number, and $J$ is the normalized spectral overlap between the emission and excitation spectra.

Normalized spectral overlap $J$ can be calculated using the equation[34]:

$$J = \int_0^\infty F(\lambda) * A(\lambda)\lambda^4 d\lambda \qquad \textbf{Eq. 4.5.}$$

where $A(\lambda)$ is the molar extinction coefficient, $\lambda$ is the wavelength of light, and $F(\lambda)$ is the normalized emission intensity, calculated from the acquired emission intensity $I(\lambda)$ as[34]:

$$F(\lambda) = \frac{I(\lambda)}{\int_0^\infty I(\lambda)d\lambda} \qquad \textbf{Eq. 4.6.}$$

Units of $J$are $nm^4/(M * cm)$. Since $\sqrt[6]{\frac{9*\ln(10)}{128*\pi^5 N_A}} = 0.2108$, **Eq. 4.3.**can be rewritten in the form:

$$R_0 = 0.02108 * \sqrt[6]{\frac{Q\kappa^2 J}{n^4}} nm \qquad \textbf{Eq. 1.7.}$$

As an example, the Forster radius can be calculated for the RhB molecules in ethanol. The quantum yield for RhB molecules in pure ethanol is $Q = 0.4935$; the orientation factor can be assumed to be equal to $\kappa^2 = 2/3$, as for the free molecule[36]; the refractive index for ethanol is $n = 1.36$.

Using the absorption and emission spectra of RhB in ethanol (**Figure 4.6.**) from[37], the spectral overlap can be calculated as $J = 2.3 * 10^{15} nm^4 * M^{-1} cm^{-1}$. Using this value, the Forster distance can be estimated as $R_0 \approx 5.1\ nm$.

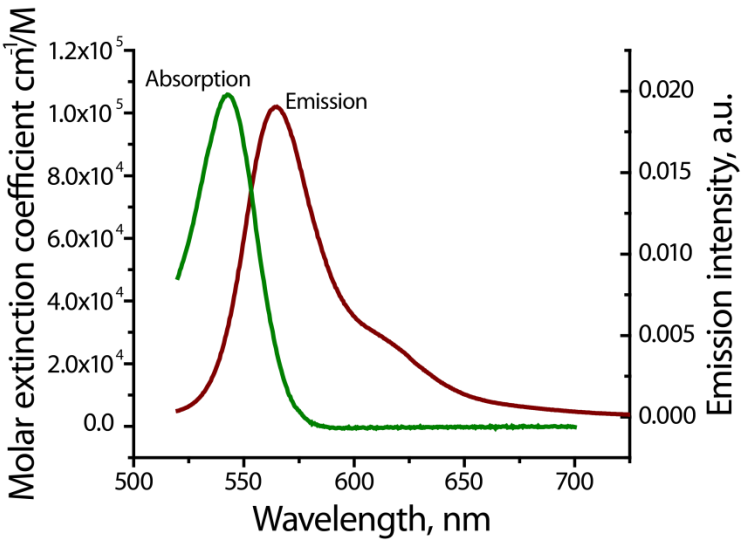


**Figure 4.7.** Absorption and emission spectra of RhB in ethanol from [37]

It can be seen that both estimations, for the distance between RhB molecules in the PGMA film and the Forster distance for the RhB molecules in ethanol, gave values of the same order. Therefore, there is a possibility of Homo-FRET between the RhB molecules in the film. Thus, a special experiment is needed to determine if FRET is in effect. This technique will be described in detail in **Section 4.3.7.5.**

#### 4.3.7.3. Fluorescent measurements of PGMA-RhB film in the dry state

The fluorescent emission of the dry film was collected using a spectrophotometer. Glass slides with PGMA-RhB films were placed in the spectrophotometer sample chamber at 45° to the incident light. Emission from the dry PGMA-RhB film was collected in the front face mode. The excitation spectrum showed the absorption peak at

532 nm and the emission spectrum showed the emission peak at 582 nm. Typically, RhB molecules have a single emission peak around 580 ± 20 nm depending on the environment and the RhB concentration[38]. The shapes of the acquired emission and excitation spectra of the PGMA-RhB films were characteristic for the RhB molecules[37]. Since the non-labeled PGMA is not fluorescent, the presence of fluorescent emission confirms the chemical attachment of the RhB to the PGMA. Spectrophotometry measurements of PGMA-RhB films with different thicknesses were conducted in order to study photoluminescence dependence on thickness. The results are shown in **Figure 4.8.**It can be observed that the spectra shift up with the thickness increase, meaning increased photon emission counts at each wavelength. To compare the emission intensity, the area under the peak can be calculated[39], which represents the total number of photons collected by the detector at all wavelengths.

The total area under the emission spectra was calculated and plotted as a function of the film thickness (**Figure 4.8.right**).The plot reveals the linear variation of the emission with the thickness. Since the fluorescent emission intensity depends on the RhB molecule packing, as was discussed in **Section 4.3.7.2.**, the results presented in **Figure 4.8.**suggest that the packing of RhB molecules is independent of the thickness of the film and is a constant for all samples in the series.

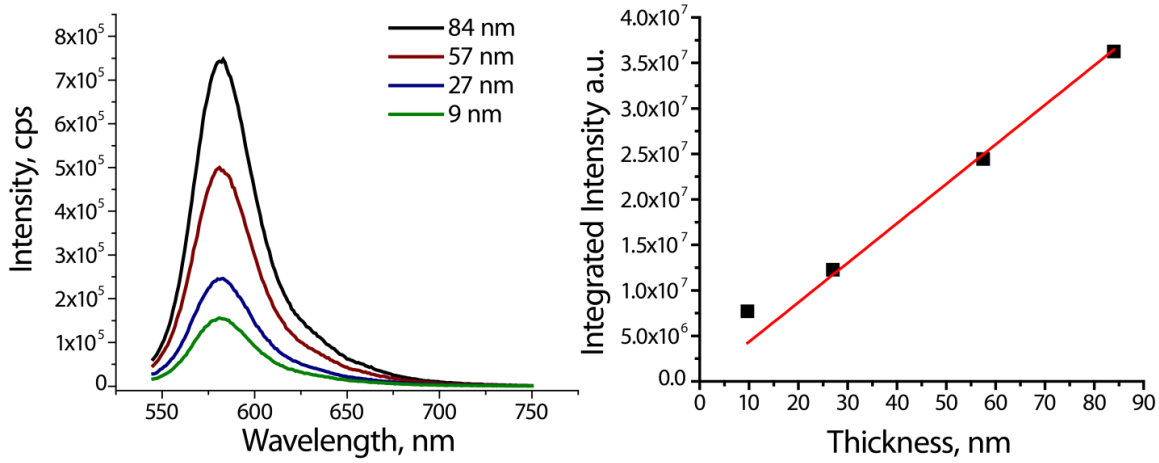


**Figure 4.8.** Emission spectra of the PGMA-RhB films with various thicknesses (left). Integrated area under the emission spectrum as a function of the PGMA-RhB film thickness (right)

#### 4.3.7.4. Change of fluorescent emission upon vapor intake

Measurement of fluorescent emission changes was performed using a TIRF setup. First, the fluorescent emission intensity of the dry polymer films was investigated in order to establish a baseline intensity to which the intensity in the swollen state could be compared. Again, it was plotted as a function of the film thickness (**Figure 4.9.left**). It could be seen that there is a linear dependence of the emission intensity on the film thickness analogous to what was observed during the spectrophotometry measurements. However, in the case of the TIRF measurements, the line has a $y = Ax + B$ type of dependence, with $B>0$. This means that when the film thickness approaches zero, the emission intensity has a non-zero value. This non-zero intensity is produced by the part of the excitation beam that scatters from the surface of the glass. Some fraction of this scattered light is not blocked by the optical filter and causes the increased intensity to be

measured. Nevertheless, this addition depends on the geometry of the setup, therefore it has to be the same for all the samples measured with the device and can be easily subtracted from the acquired signal.

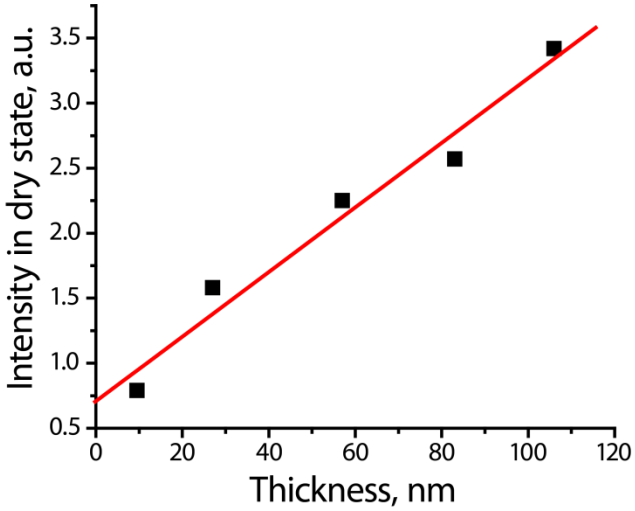


**Figure 4.9.** TIRF measurements for the PGMA-RhB films: intensity in the dry state for films of different thickness

As shown by ellipsometry, chloroform enters the PGMA-RhB film from the vapor phase and should therefore expose RhB molecules to chloroform molecules. If the fluorescence of the RhB molecules is affected by chloroform, the described TIRF setup should be able to reveal the changes in the intensity of fluorescent emission.

**Figure 4.10.left** shows how the emission intensity measured by the detector using the TIRF setup changes when the chloroform vapors are pumped through the cuvette containing the glass slide with the PGMA-RhB film. It can be seen that the emission intensity increases in a way similar to the thickness change measured by ellipsometry (compare with **Figure 4.4.right**). This suggests that emission intensity change depends

on the amount of chloroform entering the film, and that the change is the highest at the point of maximum chloroform intake.

The results presented in **Figure 4.10. left** confirm the sensitivity of 120 nm thick PGMA-RhB film to the presence of the analyte in the vapor phase surrounding the polymer film. The direction and magnitude of the change in fluorescent emission intensity depend on the quantum yield and the amount of solvent in proximity to the RhB molecules. These properties will be discussed in detail in **Chapter 5**.

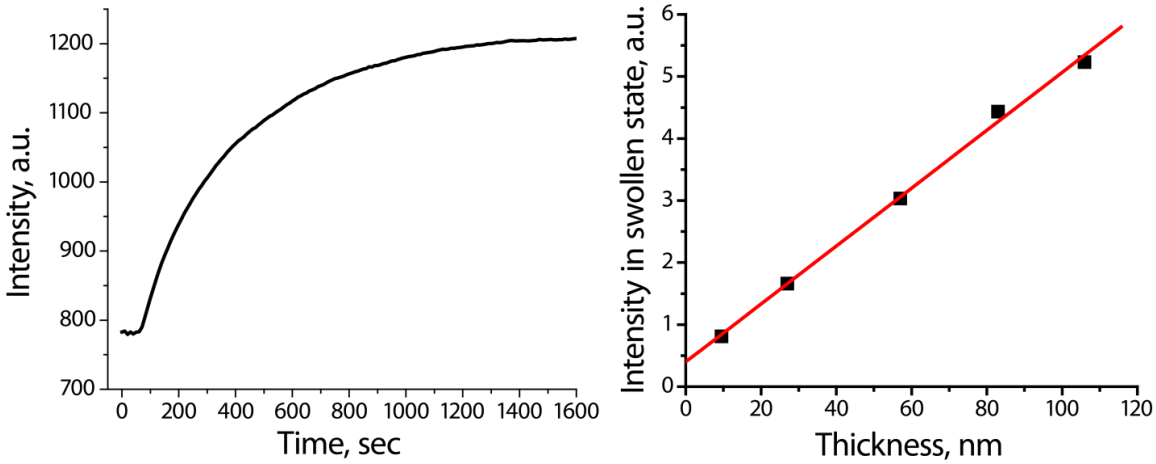


**Figure 4.10.** Intensity change during chloroform intake by 120 nm thick PGMA-RhB film (left), dependence of this intensity at equilibrium on the dry PGMA-RhB film thickness (right).

The same measurements of fluorescent emission intensity during swelling of PGMA-RhB in chloroform vapors were repeated for several films of different thickness. The results shown in **Figure 4.10.right** reveal the linear dependence of the emission intensity in the fully swollen state on the initial film thickness. Similar to what was observed for the films in the dry state, this result suggests that RhB molecule packing is the same for each PGMA-RhB film in the swollen state. This means that each RhB

molecule changes its fluorescent emission independently of all the other RhB molecules during film swelling.

This important conclusion means that it is possible to adjust the parameters of the film (for example, the thickness of the PGMA-RhB film) for a particular problem without affecting the RhB response, as long as it is allowed by the sensitivity of the detector.

#### 4.3.7.5. Effect of concentration of RhB on fluorescent emission

During the solvent intake by the polymer film, the PGMA molecules are moving apart and thus the distance between the RhB molecules is increasing. As discussed in **4.3.7.2.**, the distance change between the fluorophores should result in changes to FRET efficiency. **Eq. 4.2.** shows that FRET efficiency is highest when the RhB molecules are close to each other; therefore it is highest for the dry film and decreases during the film swelling.

FRET efficiency is an important term in the fluorescent emission intensity calculation; however, at large distances this term becomes very small due to the $1/r^6$distance dependence. It is thus important to determine whether the initial RhB concentration in the polymer film in the dry state is high enough for efficient FRET. For this purpose, the following experiment was conducted.

Several films of the same thickness were prepared using PGMA with varying RhB concentrations. The fluorescent emission of these films was then measured as a function of the RhB concentration. In the absence of all concentration-dependent effects, the fluorescent emission intensity of the PGMA-RhB films should be a linear function of

the RhB concentration [40]. However, when FRET is taken into consideration, nonlinear effects can be observed with RhB concentration variation.

To produce PGMA-RhB films with fluorophore concentration variation, RhB-labeled PGMA-RhB was mixed with non-fluorescent unlabeled PGMA at different ratios. Polymer films of the same thickness (120 nm) were deposited on the surface of silicon wafers and glass slides from the 2% w/w chloroform solutions of these blends using spin coating at 900 rpm. After annealing (120 °C, 8 h) and unattached polymer chain removal, thefluorescent emission intensity of the dry films with known relative labeled PGMA concentrations was measured. The results show the linear dependence of the emission intensity of the RhB molecules up to the concentration present in the pure labeled PGMA-RhB (**Figure 4.11.**). Relative concentration of the RhB molecules in the film was calculated as $c/c_0$, where $c$ is the concentration of the RhB molecules in the mixture of labeled and unlabeled PGMA and $c_0$ is the concentration of the RhB molecules in the labeled PGMA (**Section 4.3.7.1**). Assuming uniform RhB mixing in the polymer blend and no aggregation of RhB molecules, this result leads to an important conclusion: for PGMA-RhB film in the dry state, the distance between RhB molecules it too large for an efficient FRET. During the swelling of the polymer film, the distance will only grow, therefore FRET has no effect on the emission intensity change during the solvent absorption.

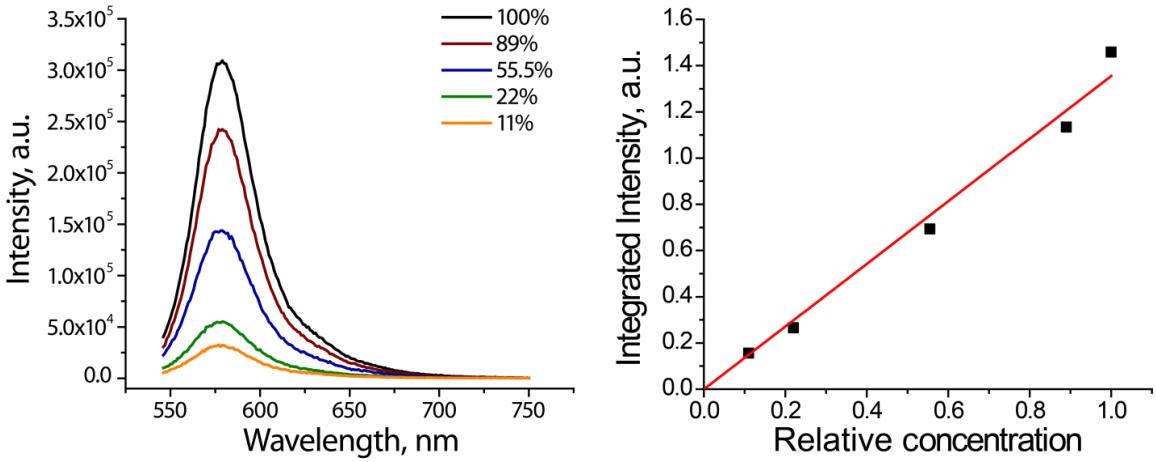


**Figure 4.11.** Fluorescent spectra of the PGMA-RhB films of different ratios of labeled to unlabeled PGMA in the dry state (left), integrated area of these spectra as a function of PGMA-RhB concentration (right)

#### 4.3.7.6. Repeatability and reversibility of the method

For prospective sensing applications it is important that the PGMA-RhB film can be reused after exposure and give the same results for succeeding exposures. To check the repeatability and reversibility of the observed signal change, the film was exposed to alternating chloroform vapors and air. Each exposure was 5 minutes long. The result is shown in **Figure 4.12.**It can be seen that each signal change was fully reversible. A small overall drift of signal can be seen; however the amplitude of this drift is much lower than the total signal change.

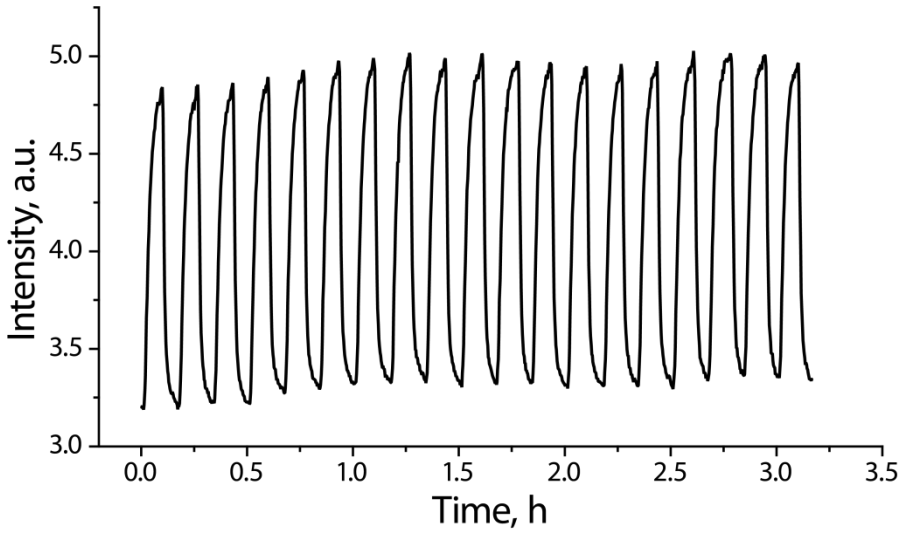


**Figure 4.12.** Emission intensity variation observed with TIRF measurements during alternating 5 minute exposures of PGMA-RhB films to saturated chloroform vapors and air.

### 4.4. Conclusions

PGMA was fluorescently labeled with RhB molecules with approximately one RhB molecule per 311 PGMA monomeric units. Relatively thick crosslinked PGMA-RhB films were synthesized from the PGMA-RhB solution. Spin coating was selected as a deposition technique and silicon wafers and glass slides were chosen as substrates.

The deposition technique allowed flexibility in the created film thickness in the tens to hundreds of nanometers range. Synthesized polymer films were characterized with AFM and the deposition technique was further adjusted to achieve even, uniform films with low roughness.

Ellipsometry measurements in the presence of saturated chloroform vapor revealed that the PGMA-RhB film is able to absorb solvent from the vapor phase. The relative thickness change upon liquid absorption was not varied for films of different

thicknesses, suggesting the same crosslinking density of the PGMA-RhB film produced with the proposed deposition technique.

Spectrophotometry, as well as the TIRF measurements, confirmed the fluorescent emission from the PGMA-RhB film. Both methods showed that the fluorescent characteristics of RhB molecules are not affected by film thickness. Homo-FRET efficiency was found to be negligibly small using measurements of the emission intensity of dry PGMA-RhB films with a difference in distance between RhB molecules.

A TIRF apparatus was employed to conduct the measurements of the fluorescent emission of the film during the exposure to the saturated chloroform vapors. As the PGMA-RhB film was subjected to chloroform vapor, prominent reversible and repeatable fluorescent emission intensity changes were observed. Emission intensity showed linear dependence on the thickness of the film, indicating that it is linearly proportional to the number of emitting RhB molecules. Therefore, locally, the environment of RhB molecules upon swelling changes in the same way independent of film thickness.

### 4.5. References

1. Tsui, O. K. C.; Russell, T. P. Polymer thin films. http://public.eblib.com/EBLPublic/PublicView.do?ptiID=477256.

2. Grundke, K.; Adler, H. J.; Stamm, M. Characterization of Polymer Surfaces and Thin Films. http://dx.doi.org/10.1007/b104970.

3. Vendra, V. K.; Wu, L.; Krishnan, S., Polymer Thin Films for Biomedical Applications. In *Nanotechnologies for the Life Sciences*, Wiley-VCH Verlag GmbH & Co. KGaA: 2007.

4. Pauleau, Y.; Barna, P. B., *Protective coatings and thin films : synthesis, characterization, and applications*. Kluwer Academic Publishers: Dordrecht; Boston, 1997.

5. Herold, K. E.; Rasooly, A., *Lab on a chip technology Vol. 1, Fabrication and microfluidics*. Caister Academic Press: Norfolk, UK, 2009.

6. Osada, Y.; De Rossi, D. E., *Polymer sensors and actuators*. Springer: Berlin; New York, 2000.

7. Giammarco, J.; Zdyrko, B.; Petit, L.; Musgraves, J. D.; Hu, J.; Agarwal, A.; Kimerling, L.; Richardson, K.; Luzinov, I., Towards universal enrichment nanocoating for IR-ATR waveguides. *Chemical Communications* **2011,** *47* (32), 9104-9106.

8. Thomas, S. W., III; Joly, G. D.; Swager, T. M., Chemical Sensors Based on Amplifying Fluorescent Conjugated Polymers. *ChemInform* **2007,** *38* (31), no-no.

9. Iyer, K. S.; Zdyrko, B.; Malz, H.; Pionteck, J.; Luzinov, I., Polystyrene Layers Grafted to Macromolecular Anchoring Layer. *Macromolecules* **2003,** *36* (17), 6519-6526.

10. Blank, W.; He, Z.; Picci, M., Catalysis of the epoxy-carboxyl reaction. *Journal of Coatings Technology* **2002,** *74* (926), 33-41.

11. Luzinov, I.; Iyer, S.; Klep, V.; Zdyrko, B. Surface modification of substrates. 20060154081, 2006.

12. (a) Beaumont, P. C.; Johnson, D. G.; Parsons, B. J., Photophysical properties of laser dyes: picosecond laser flash photolysis studies of Rhodamine 6G, Rhodamine B and Rhodamine 101. *Journal of the Chemical Society, Faraday Transactions* **1993,** *89* (23), 4185-4191; (b) Smart, P. L.; Laidlaw, I. M. S., An evaluation of some fluorescent dyes for water tracing. *Water Resour. Res.* **1977,** *13* (1), 15-33.

13. Tsyalkovsky, V.; Klep, V.; Ramaratnam, K.; Lupitskyy, R.; Minko, S.; Luzinov, I., Fluorescent Reactive Core–Shell Composite Nanoparticles with A High Surface Concentration of Epoxy Functionalities. *Chemistry of Materials* **2007,** *20* (1), 317-325.

14. Synowicki, R. A., Suppression of backside reflections from transparent substrates. *physica status solidi (c)* **2008,** *5* (5), 1085-1088.

15. Landgren, M.; Joensson, B., Determination of the optical properties of silicon/silica surfaces by means of ellipsometry, using different ambient media. *The Journal of Physical Chemistry* **1993,** *97* (8), 1656-1660.

16. Greenwood, N. N.; Earnshaw, A., *Chemistry of the elements*. Pergamon Press: 1984.

17. Bornside, D. E.; Macosko, C. W.; Scriven, L. E., ON THE MODELING OF SPIN COATING. *Journal of Imaging Technology* **1987,** *13* (4), 122-130.

18. Sperling, L. H., *Introduction to physical polymer science*. Wiley: New York, 1986.

19. Ham, H. T.; Chung, I. J.; Choi, Y. S.; Lee, S. H.; Kim, S. O., Macroporous Polymer Thin Film Prepared from Temporarily Stabilized Water-in-Oil Emulsion. *The Journal of Physical Chemistry B* **2006,** *110* (28), 13959-13964.

20. (a) Krevelen, D. W. v., *Properties of polymers : their correlation with chemical structure*. Elsevier Scientific Publ. Co.: Amsterdam [u.a.], 1972; (b) Lam, K.-Y.; Afromowitz, M. A., Fiber-optic epoxy composite cure sensor. I. Dependence of refractive index of an autocatalytic reaction epoxy system at 850 nm on temperature and extent of cure. *Appl. Opt.* **1995,** *34* (25), 5635-5638.

21. Ding, Z. Y.; Aklonis, J. J.; Salovey, R., Model filled polymers. VI. Determination of the crosslink density of polymeric beads by swelling. *Journal of Polymer Science Part B: Polymer Physics* **1991,** *29* (8), 1035-1038.

22. Toomey, R.; Freidank, D.; Rühe, J., Swelling Behavior of Thin, Surface-Attached Polymer Networks. *Macromolecules* **2004,** *37* (3), 882-887.

23. Flory, P. J., Statistical Mechanics of Swelling of Network Structures. *The Journal of Chemical Physics* **1950,** *18* (1), 108-111.

24. Toomey, R.; Freidank, D.; RΓjhe, J., Swelling Behavior of Thin, Surface-Attached Polymer Networks. *Macromolecules* **2004,** *37* (3), 882-887.

25. Russell, S. P.; Weinkauf, D. H., Vapor sorption in plasma polymerized vinyl acetate and methyl methacrylate thin films. *Polymer* **2001,** *42* (7), 2827-2836.

26. Crank, J., *The mathematics of diffusion*. Clarendon Press: Oxford, [Eng], 1975.

27. Fikry, M.; Omar, M. M.; Ismail, L. Z., Effect of host medium on the fluorescence emission intensity of rhodamine B in liquid and solid phase. *J Fluoresc Journal of Fluorescence* **2009,** *19* (4), 741-746.

28. Kubista, M.; Sjoback, R.; Eriksson, S.; Albinsson, B., Experimental correction for the inner-filter effect in fluorescence spectra. *Analyst* **1994,** *119* (3), 417-419.

29. Arbeloa, F. L.; Ojeda, P. R.; Arbeloa, I. L., Dimerization and trimerization of rhodamine 6G in aqueous solution. Effect on the fluorescence quantum yield. *Journal of the Chemical Society, Faraday Transactions 2: Molecular and Chemical Physics* **1988,** *84* (12), 1903-1912.

30. Zdyrko, B.; Varshney, S. K.; Luzinov, I., Effect of Molecular Weight on Synthesis and Surface Morphology of High-Density Poly(ethylene glycol) Grafted Layers. *Langmuir* **2004,** *20* (16), 6727-6735.

31. Kao, S.; Asanov, A. N.; Oldham, P. B., A Comparison of Fluorescence Inner-Filter Effects for Different Cell Configurations. *Instrumentation Science & Technology* **1998,** *26* (4), 375-387.

32. Förster, T., Zwischenmolekulare Energiewanderung und Fluoreszenz. *Annalen der Physik* **1948,** *437* (1-2), 55-75.

33. Valeur, B., *Molecular fluorescence : principles and applications*. Wiley-VCH: Weinheim; New York, 2002.

34. Gadella, T. W. J. FRET and FLIM techniques. http://site.ebrary.com/id/10305649.

35. Casey, K. G.; Quitevis, E. L., Effect of solvent polarity on nonradiative processes in xanthene dyes: Rhodamine B in normal alcohols. *The Journal of Physical Chemistry* **1988,** *92* (23), 6590-6594.

36. Yang, H., The Orientation Factor in Single-Molecule Förster-Type Resonance Energy Transfer, with Examples for Conformational Transitions in Proteins. *Israel Journal of Chemistry* **2009,** *49* (3-4), 313-321.

37. Prahl, S. Rhodamine B. http://omlc.ogi.edu/spectra/PhotochemCAD/html/009.html.

38. Van der Auweraer, M.; Verschuere, B.; De Schryver, F. C., Absorption and fluorescence properties of Rhodamine B derivatives forming Langmuir-Blodgett films. *Langmuir* **1988,** *4* (3), 583-588.

39. Fery-Forgues, S.; Lavabre, D., Are Fluorescence Quantum Yields So Tricky to Measure? A Demonstration Using Familiar Stationery Products. *Journal of Chemical Education* **1999,** *76* (9), 1260.

40. Lakowicz, J. R., *Principles of fluorescence spectroscopy*. Kluwer Academic/Plenum: New York, 1999.

# CHAPTER FIVE

# FABRICATION AND CHARACTERIZATION OF NANOSCALE FLUORESCENT POLYMER FILMS

## 5.1. Introduction

In the previous chapter, it was concluded that PGMA-RhB film, in orders of hundreds of nanometers thick, is sensitive to the environment. The sensitivity of the film is manifested through changes in the rate of fluorescent emissions when the vapor of an analyte enters the film. Since the signal change increases as the solvent enters the film, the most prominent signal variation is achieved after a significant amount of time, when the film fully swells with the analyte. However, in many applications, such as analyte detection, it is important that the response is as low as possible without a sacrifice in the signal-to-noise ratio.

It is possible to decrease the response time of the PGMA-RhB system by decreasing the thickness of the film. There are several advantages to this approach. First, it is known that for thin polymer films the swelling kinetics under the same conditions are faster than for the thick polymer films[1]. Therefore, shorter times are needed for the analyte molecules to diffuse to the fluorophore sites, so response times for thin films are shorter.

Second, such films can be applied to nanoscale objects[2], therefore the surface-to-volume ratio can be significantly enhanced. Also, ultrathin films have high surface influence[3]; in other words, it is possible to tune the properties of the film by modifying its surface. However, one downside of thin films is the magnitude of the fluorescent

emission: since the number of fluorophores in thin films is lower, high sensitivity methods must be used to study fluorescent emission variations.

The objective of this part of the work was to synthesize and characterize ultrathin (in the order of several nanometers) fluorescent polymer films. Fluorescently labeled polymer, namely PGMA-RhB (see **Section 4.2.1.** for description and labeling), was used. PGMA-RhB films 5 nm thick were synthesized and characterized.

Ellipsometry measurements of the swelling of ultrathin films in chloroform vapor confirmed an increase in the swelling kinetics with a decrease in the film thickness. Florescent properties were studied using TIRF and spectrophotometry measurements. It was discovered that the sensitivity of the TIRF measurements is not high enough for precise fluorescent emission collection during film swelling, so a special cuvette for in situ measurements of the emission under changing environmental conditions was built for the spectrophotometer.

The sensitivity of the ultrathin PGMA-RhB film was studied for different environments. For this purpose, spectrophotometric and ellipsometric measurements were performed for a variety of solvents with different chemical natures. Each of the solvents induced a distinct response from the PGMA-RhB system during the measurements.

## 5.2. Experimental

### 5.2.1. Synthesis of ultrathin PGMA-RhB film

The fluorescently labeled PGMA-RhB (Mn= 80,000 g/mol with polydispersity 2.57) was deposited onto the surface of cleaned silicon wafers and glass microscope

slides (see **Section 3.4.1.** for cleaning procedure). Drop casting was used as a deposition technique. After the deposition, PGMA-RhB film was annealed at 100 °C for 30 minutes to allow film crosslinking and attachment to the substrate. Unattached polymer chains were removed by rinsing the sample with chloroform three times for 30 minutes on a shaker.

### 5.2.2. Characterization of PGMA-RhB films

Next, polymer films were characterized by ellipsometry and AFM: film thickness, refractive index, and surface roughness were estimated. Ellipsometry was then used to study the film behavior in the saturated vapor of several organic solvents, namely chloroform, acetone, toluene, water, and cyclohexane. The same procedure was used for each swelling experiment. The sample was placed into the glass cuvette and the thickness of the PGMA-RhB layer was measured in the dry state. Next, solvent was introduced to the cuvette. Changes to the ellipsometric parameters were recorded as the polymer film absorbed the solvent. After the data acquisition, these parameters were fitted using an enhanced algorithm coupled with an effective medium approximation (see **Section 5.3.4.1.** for details). The swelling of the ultrathin films was compared to the swelling of thicker film to investigate the effect of the deposited polymer thickness on solvent absorption.

### 5.2.3. Environmental sensitivity measurements

Fluorescent signal change during solvent absorption was measured using both a TIRF setup and spectrophotometry. In the TIRF setup, chloroform-, acetone-, toluene-, water-, and cyclohexane-saturated vapors were pumped at 10 ml/min through the cuvette with the 5nm thick PGMA-RhB film on the glass microscope slide. After each solvent was introduced, air was pumped through the cuvette to bring the polymer film back to the dry state.

For spectrophotometry on the Jobin Yvon Fluorolog 3–222Tau, a special cuvette was designed to perform in situ measurements of the fluorescent emission from the PGMA-RhB film in the saturated solvent vapors (**Section 3.3.4.**). The cuvette was placed into the sample compartment of the device as shown in **Figure 5.1.,** and fluorescent emission measurements of the PGMA-RhB film were performed both in the dry and swollen state.

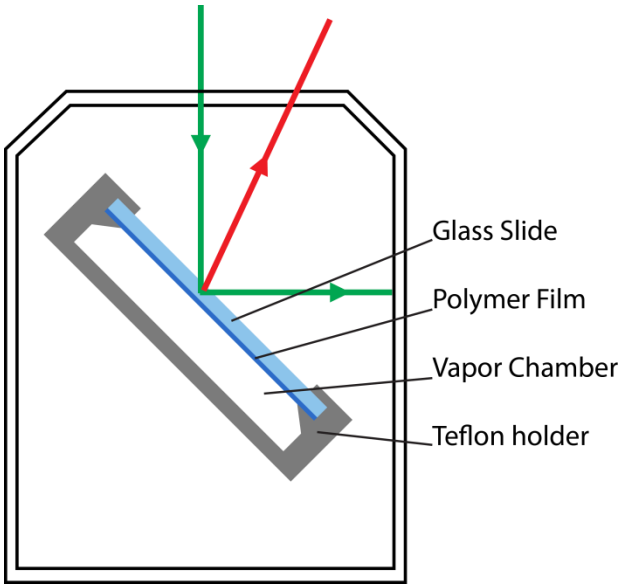


**Figure 5.1.** Positioning of the sample in the sample compartment of the spectrophotometer.

Fluorescent signal change was recorded using the area under the emission spectrum as a measure of the emission intensity. For the cases in which equilibrium was not achieved during the measurement, emission intensity at the point of equilibrium was calculated using the fitting of the intensity change curve. Each solvent induced changes in the fluorescent emission of the PGMA-RhB film. Using acquired data, sensitivity to the changes in fluorescent emission of ultrathin PGMA-RhB film using the spectrophotometry method was compared to the results from the TIRF method.

### 5.2.4. Quantum yield measurements for Octadecyl Rhodamine B (R18)

To determine the driving force of fluorescent emission changes, relative quantum yields were estimated for PGMA-RhB using a technique found in the literature[4].

Octadecyl Rhodamine B (R18) was used as a model fluorophore, as its chemical structure is close to the fluorescent unit in PGMA-RhB. Standard quartz 1 cm cuvettes were used for the quantum yield measurements. Absorption spectra for the dye solutions were acquired from aUV-3101PC UV-VIS-NIR scanning spectrophotometer from Shimadzu using an excitation wavelength of 532 nm. Emission spectra were collected using a Jobin Yvon Fluorolog 3–222Tauspectrofluorometerwith the same excitation wavelength.

For each solvent-dye combination, dye solutions of several concentrations were prepared. To exclude concentration-dependent effects, the amount of dye in the solution was kept at a low level. Specifically, the highest concentration used in the series was always lower than the concentration that would bring optical density of the solution above 0.1.

Both absorption and emission spectra were integrated and the emission was plotted as a function of the absorbance for the concentrations used. The slope of the plot defined the relative quantum yield for the dye. The absolute quantum yield was calculated through this relative value using known standards. Technique feasibility was verified using dye solutions with known quantum yields (RhB in water and RhB in ethanol 95%) for reference. Quantum yields for R18 solutions in chloroform, acetone, toluene, water, and cyclohexane were calculated and compared with the fluorescent emission intensity changes.

## 5.3. Results and discussion

### 5.3.1. Synthesis of ultrathin PGMA-RhB films

Synthesis of ultrathin films differs from that of thicker films. Owing to its chemical nature, PGMA starts chemical crosslinking in the vicinity of the substrate surface after the deposition onto the surface activated with the hydroxylic groups[5]. First, PGMA chains attach to the surface. As can be seen from the chemical equation (**Scheme.5.1.**), after the epoxy ring opening, a new hydroxylic group is produced. This hydroxylic group can induce another reaction.

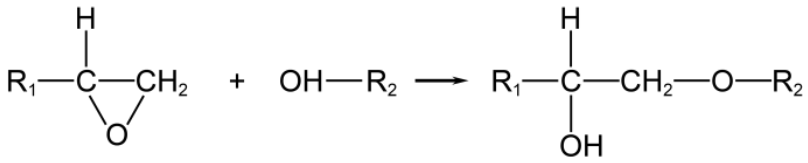


**Scheme 5.1.** Epoxy group reaction with hydroxylic group

The epoxy group opening can therefore propagate through the film from the substrate towards the outer surface of the polymer film. It is possible to stop the crosslinking process at its earlier stages, when the crosslinked part of the film is only several nanometers thick. This is schematically illustrated in **Figure 5.3. A** layer of PGMA is deposited onto the surface activated with the hydroxylic groups. When the film is annealed, the PGMA chains start to chemically bond to the substrate, creating reactive sites for the epoxy group attachment. This process repeats itself and when the desired thickness of the crosslinked layer is achieved, the reaction can be stopped and unattached polymer chains can be removed from the film. One useful advantage of this technique is the independence of the quality of the film from the morphology of the top layers of the

initially deposited film, since the top portion of the film does not contribute to the deposited PGMA layer.

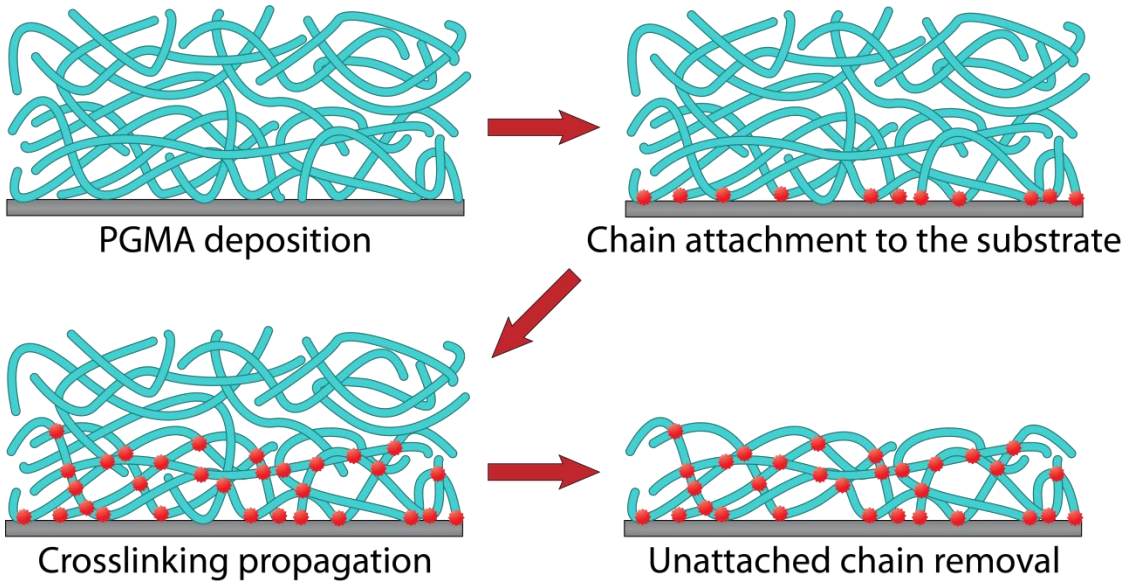


**Figure 5.2.** Schematic diagram of the synthesis of ultrathin PGMA film

### 5.3.2. Variation of PGMA-RhB film thickness

An important conclusion can be made from the previous section: films of various thicknesses can be synthesized using the same PGMA solution and the same deposition procedure. The thickness of the films can be controlled by changing the crosslinking time, allowing more or less polymer to be attached to the substrate. To check the possibility of such a method, several PGMA-RhB films were created on the surface of the cleaned silicon wafers from the 1% w/w solution via drop casting. The drop casting technique was selected instead of spin coating because it is a less labor and time consuming technique, since, as was pointed out above, the morphology of the top portion of the film should not influence the resulting film thickness. After the deposition, the

polymer films were annealed. In order to control the annealing with higher precision (the chemical reaction slows down when the temperature is decreased [5]), the annealing temperature was decreased from 120°C, which was used for thick film annealing, to 100 °C. The annealing was performed for several different durations (30 min, 1 h, 2 h, and 3 h) in a vacuum oven. Unattached polymer chains were then removed by rinsing the polymer films with chloroform.

The thickness of the polymer films was measured by ellipsometry. The results shown in **Figure 5.4.**reveal that the thickness of the attached layer depends nonlinearly on the annealing time: the thickness grow rate increases at longer annealing times. This phenomenon can be explained by the fact that chain movement is restricted by the surface of the wafer[6], so the above-discussed crosslinking reaction propagation through the film is more efficient far away from the substrate surface.

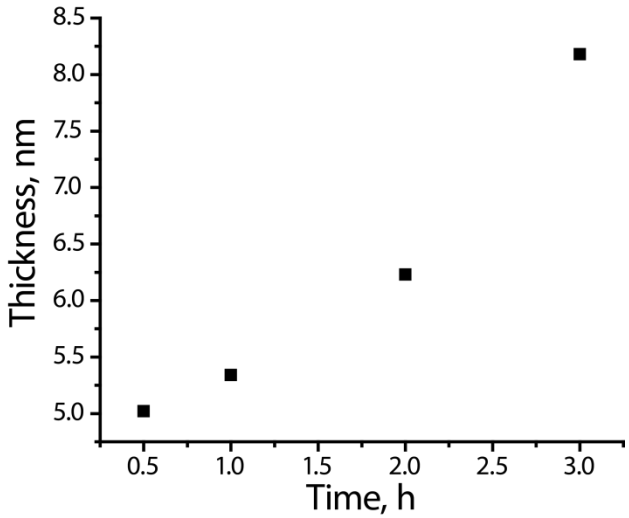


**Figure 5.3.** Dependence of the thickness of the attached layer of PGMA-RhB on the film annealing time

Therefore, unlike for the thicker films, in order to perform the ultrathin film synthesis it is not necessary to spin coat the film on the substrate. It is sufficient to dropcast a polymer film on the substrate: since the top part of the polymer film will be removed, its morphology should not affect the roughness of the resulting ultrathin film.

### 5.3.3. Properties of ultrathin PGMA-RhB film

For further study, film with the least thickness from the series (5 nm) was selected. AFM imaging of the film surface was conducted (**Figure 5.4.**). In fact, dropcasted polymer films annealed for 30 min at 100°C produced uniform, even films with a roughness of less than 1 nm. Next, the refractive index was measured with an ellipsometer using the dry thickness of the film obtained from AFM measurements of the profile over a scratch on the ultrathin film surface. The refractive index was found to be the same as for the thicker polymer film: 1.51 at 651 nm (wavelength of the beam used for ellipsometry measurements).

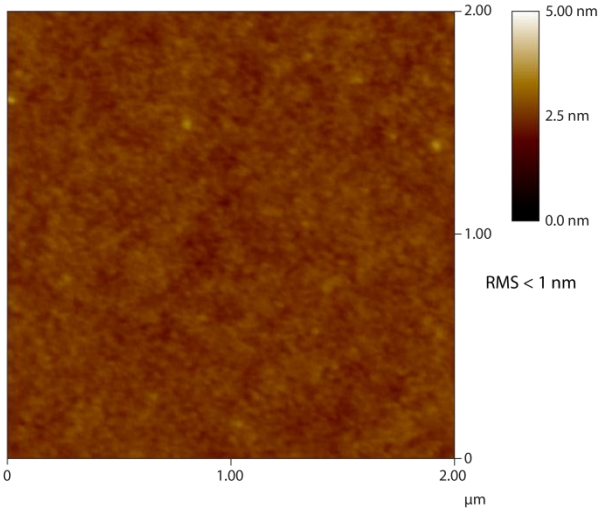


**Figure 5.4.** AFM image of the surface morphology of the 5 nm thick PGMA-RhB film.

As was pointed out in **Section 4.3.5.,** this result suggests that the density, free volume, and crosslinking density of the ultrathin PGMA-RhB film is close to that of the 100 – 120 nm PGMA-RhB film.

### 5.3.4. Swelling of ultrathin PGMA-RhB films

#### 5.3.4.1. Algorithm of ellipsometric calculations

To verify that ultrathin polymer film retains the ability to absorb solvents from the vapor phase, ellipsometric swelling experiments were conducted. The 5 nm thick PGMA films were subjected to the saturated vapors of organic solvents and water. It is known that during solvent absorption the refractive index of the polymer film changes[7]. This means that during the swelling of the PGMA-RhB film, each pair ($\Psi$,$\Delta$) measured by the ellipsometer should be fitted using two unknown variables: current thickness of the film $h$ and its refractive index. Due to the lower precision of the measurements in the low thickness region, the program supplied with the ellipsometer was unable to correctly fit $\Psi$ and $\Delta$ to both unknown variables.

To overcome this difficulty, a known relation between the thickness and the refractive index of the film during swelling was utilized. It is known that when two or more substances are ideally mixed the following Bruggemans effective medium approximation (EMA) applies[8]:

$$0 = \nu_1 \frac{n_1^2 - \langle n \rangle^2}{n_1^2 + 2\langle n \rangle^2} + \nu_2 \frac{n_2^2 - \langle n \rangle^2}{n_2^2 + 2\langle n \rangle^2} + \cdots \qquad \textbf{Eq.5.1.}$$

where $\langle n \rangle$ is the refractive index of the mixture; $n_1, n_2, \ldots$ are the refractive indexes of the components comprising the mixture; and $\nu_1, \nu_2, \ldots$ are the volume fractions of the components in the mixture.

This equation is widely used to model the porosity of silicon with void content up to 50% [9], as well as conductivity of linear composites[10] and transport properties of composites[11]. This approximation was also extensively used for refractive index calculation for the inorganic[12] and organic[13] coatings. It is known that the Bruggemans equation is a simplified theory and gives errors for high concentrations of the mixing substances [14]; however, it can still be used as a first approximation for the swelling of polymer films with high equilibrium solvent content[15].

If during the swelling of the film no changes in the lateral direction are observed, then the volume fractions of the polymer and the solvent within the film can be described as $\nu_1 = \nu_p = h_0/h$ and $\nu_1 = \nu_s = (h - h_0)/h$, respectively. Here, $h$ is the current film thickness and $h_0$ is the thickness of the film in the dry state. **Eq.5.1.**can be then rewritten in the form:

$$\frac{h}{h_0} = 1 - \left( \frac{n_0^2 - n^2}{n_0^2 + 2n^2} \Big/ \frac{n_s^2 - n^2}{n_s^2 + 2n^2} \right) \qquad \textbf{Eq.5.2.}$$

where $n_0$ is the refractive index of the dry polymer film, $n_s$ is the refractive index of the solvent, and $n$ is the effective refractive index of the film in a given swollen state. This

equation can provide additional relationships between $h$ and $n$ in fitting calculations for Ψ and Δ.

As shown in **Section 4.3.5.**, the precision of measurements for thick polymer films is high enough to fit the ellipsometric parameters Ψ and Δ using for calculation of both thickness and refractive index of the film with high precision. The algorithm of these calculations is described in detail in the **Appendix** (**Figure A2**). The fitting shows how the thickness of the film changes over time (**Figure 4.4. right**). It is therefore possible to check if the PGMA-RhB film follows the proposed effective medium approximation. Using the refractive index values acquired from the measurement and the following constants: $n_s = 1.445$ (chloroform), $n_0 = 1.51$, $h_0 = 106$ nm, it is possible to compare the thickness change measured from the ellipsometry experiment with the thickness change calculated from **Eq.5.2.** The results are shown in **Figure 5.5.left.** It can be seen that the thickness change calculated by the Bruggemans approximation closely follows the measured values of the thickness.

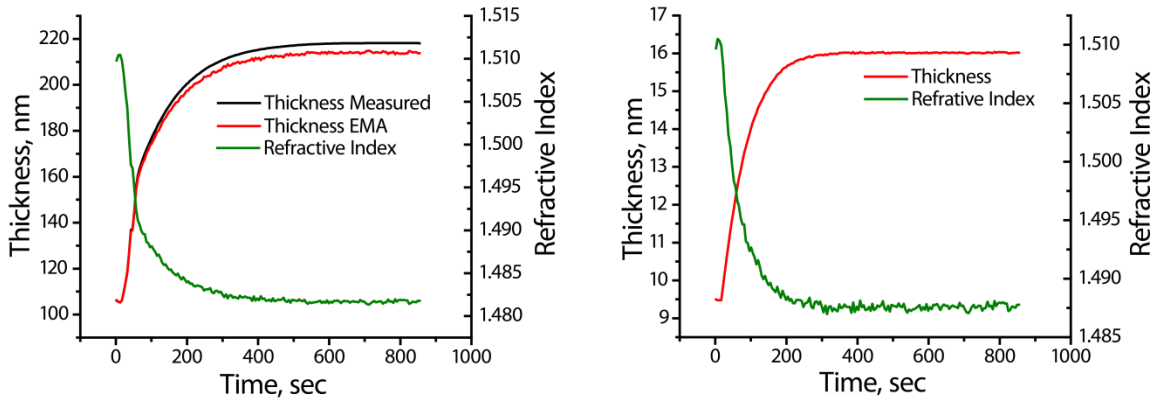


**Figure 5.5.** Ellipsometric measurements of the PGMA-RhB film during the absorption of the chloroform vapor. Thickness and refractive index measured for 106 nm thick PGMA-RhB film and thickness change calculated through Bruggemans EMA (left). Thickness

and refractive index change calculated through improved algorithm using Bruggemans EMA (right).

This result shows that during the swelling of the PGMA-RhB film, the thickness and refractive index are bound by **Eq.5.2.**, so the proposed EMA can be used to fit the ellipsometric data for the thin films.

To calculate the thickness and refractive index of the thin film, a program was written using MATLAB software. The algorithm for the calculations is shown in details in **Appendix** (**Figure A3**). This program refines the known approach of $h$ and $n$ calculations[16] from the known values of Ψ and Δ, where Fresnell's equations are used to calculate the reflected components of the beam for the multilayer film. Calculated thickness and refractive index are then bound together with **Eq.5.2.,** using the least square method. This way, the Bruggemans effective medium approximation helps reduce the errors in thickness and refractive index calculations.

The result of such a fitting is presented in **Figure 5.5.right** for the 9 nm thick PGMA-RhB film. It can be seen from the plot how the thickness of the polymer film increases and at the same time the refractive index of the film decreases.

#### 5.3.4.2. Kinetics of the swelling of ultrathin PGMA-RhB films

It was observed that the kinetics of swelling were different for PGMA-RhB films of various thicknesses (**Figure 4.6.**). It is also known that the rate of solvent intake by the polymer film depends on the diffusion of the solvent molecules, vapor pressure, and the solvent's affinity for the polymer[17]. Therefore, the swelling rate of the PGMA-RhB films will be different for various solvents.

To check this hypothesis, the swelling experiment was performed for 55 nm thick PGMA-RhB film in saturated vapors of chloroform, acetone, toluene, cyclohexane, and water. A fitting algorithm with EMA was used for fitting the ellipsometric data.

The thickness of the PGMA-RhB film was rescaled in order to compare the swelling rate: the thickness of the film changes in the range from 0 to 1, where 0 is the thickness of the film in the dry state and 1 is the thickness of the swollen film. As expected, the results shown in **Figure 5.6.**demonstrate variations in the swelling rate with respect to the solvent used. For example, it can be seen that during the swelling in acetone, equilibrium is reached after 10 minutes, but for the swelling in toluene, equilibrium is still not reached after 50 minutes.

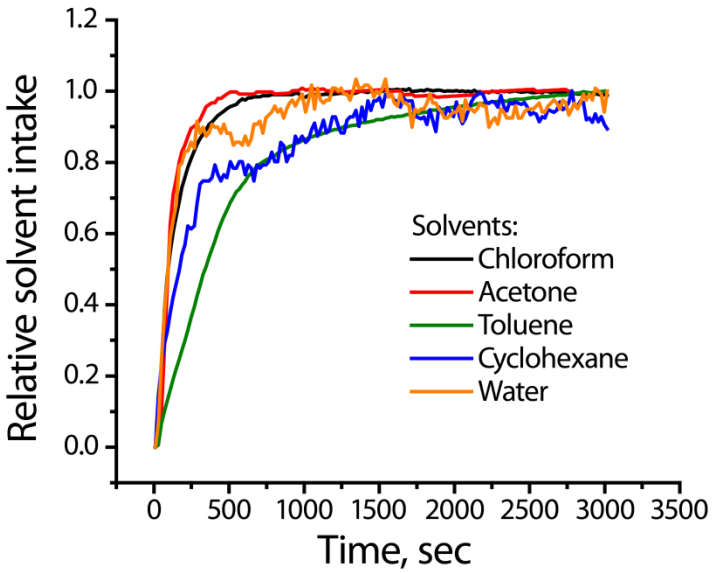


**Figure 5.6.** Rescaled swelling curves for 55 nm thick PGMA-RhB film in the vapors of chloroform, acetone, toluene, cyclohexane, and water.

To compare the amount of swelling, some parameter that characterizes the polymer swelling independent of time should be developed. It was decided that relative

swelling at equilibrium would be such a parameter. Effectively, the state of equilibrium is achieved at an infinitely long swelling period; however, it is not feasible to perform a swelling experiment for such long time. Instead, it is possible to fit the acquired swelling curve to achieve equilibrium thickness $h_\infty$18.

#### 5.3.4.3. Swelling curve fitting

In **Section 4.3.6.**, it was shown that at the final stages of the solvent absorption for rigid film the solvent intake exhibits exponential behavior (see **Eq. 4.1.**). Since the amount of solvent absorbed by the film is proportional to the thickness of the film, similar behavior for the PGMA-RhB system can be assumed. The following expression can describe the thickness $y$ of the PGMA-RhB film:

$$y' = P_1(1 - \exp[-P_2 t]) \qquad \textbf{Eq.5.3.}$$

where$y' = y - y_0$ is the reduced film thickness, $y_0$ is the thickness of the film in the dry state, and $P_1$ and $P_2$ are the fitting parameters, which account for deviations from the case of the rigid film presented in **Eq. 4.1**.

The proposed fitting was done using Origin software (OriginLab).The thickness of the film in the equilibrium state can be estimated as $h_\infty = P_1 + y_0$ once the parameters $P_1$ and $P_2$ are found. Before the application of the proposed method for $h_\infty$ determination, the validity of the fitting algorithm was examined using the swelling data where polymer film reaches complete saturation during the experiment. Specifically, the swelling of 45 nm thick PGMA-RhB film in chloroform vapor was examined. As can be seen from the

swelling curve (**Figure 5.7.**), the thickness of the film reaches maximum saturation after 20 minutes.

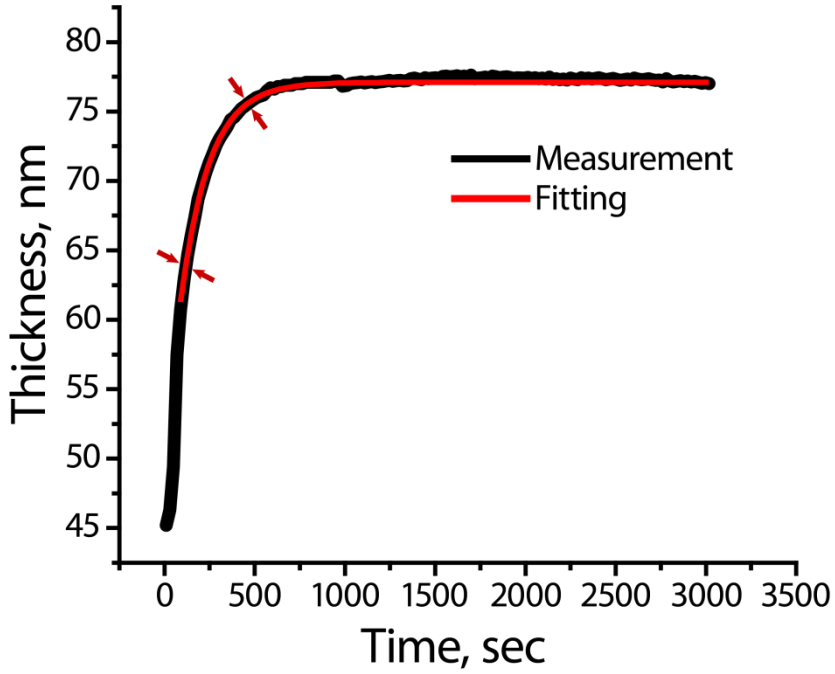


**Figure 5.7.** Swelling curve and the result of the curve fitting. Arrows show the range of the values used for the fitting

To check the applicability of the fitting algorithm, a part of the curve was fitted using **Eq.4.3.**, and the fitting was then compared with the measured equilibrium swelling. The part of the curve selected for the fitting is marked with the arrows in **Figure 5.7.**The starting point was selected at approximately 60% of the total swelling increase. This first point selection was selected for two reasons: first, **Eq. 4.3**. is known to describe only the terminal stages of the swelling (the beginning of the vapor absorption is known to have square root kinetics)[19]; second, the pressure of the solvent inside the cuvette does not reach saturation instantly; therefore, in the initial period the driving force for the swelling changes constantly and **Eq.4.3.**does not account for such changes.

After acquisition of the unknown parameters $P_1$and $P_2$, the swelling of the polymer film beyond the region used for the fitting can be constructed. **Figure 5.7.**showsthe results of the fitting overlapped with measured data. It can be seen that the fitted curve follows the real data with good agreement. This result means that for the substances with low vapor pressure, swelling equilibrium can be obtained in a relatively short experiment.

#### 5.3.4.4. Equilibrium relative thickness change

When the swelling at equilibrium $h_\infty$ is known, the relative thickness change (RTC) at equilibrium can be used as the above-mentioned parameter for comparing the swelling between various film-solvent pairs. This value is defined as:

$$RTC = h_\infty / h_0 \qquad \textbf{Eq.5.4.}$$

Using the relative thickness change, it is possible to compare the solvents together in relation to the particular PGMA-RhB film by the amount of solvent absorbed by the film.

With all necessary procedures developed, it is now possible to examine the swelling of the ultrathin 5 nm thick PGMA-RhB layer. Swelling experiments were conducted for this film in the saturated vapors of five analytes (chloroform, acetone, toluene, water, and cyclohexane). The swelling curves were constructed from raw ellipsometry data using the improved calculation algorithm. Next, swelling curves were fitted using **Eq.5.2.**and the relative thickness change was calculated. The final result is presented in **Figure 5.8.** Reversibility and repeatability of these measurements were

verified for selected solvents. It can be observed from the results that there are vast variations in the swelling ratios among the analytes. For example, the PGMA-RhB films swell to more than double in chloroform vapor and only several percent in water vapor.

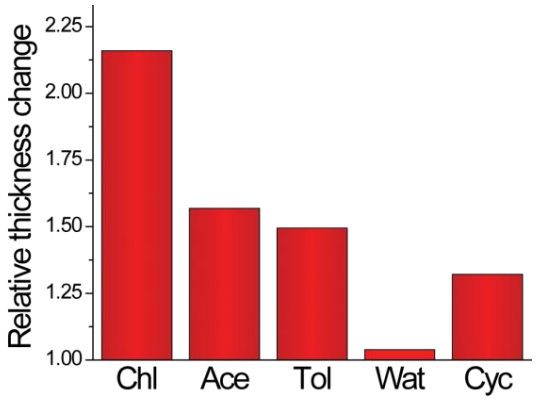


**Figure 5.8.** Relative thickness change for PGMA-RhB film in vapors of 5 various solvents: chloroform, acetone, toluene, water, andcyclohexane.

### 5.3.5. Polymer-solvent interaction

The behavior of the PGMA-RhB layer in various solvents has paramount significance for this work: ultrathin polymer film expresses selective affinity to particular analytes. It is known that the affinity of the polymer to the particular chemical substance can be described by the amount of absorption of this substance by the polymer. This affinity can be expressed in terms of the so-called effective interaction parameter[20] $\chi$. According to the Flory-Huggins theory, the energy change for a solvent molecule transferred from a pure solvent to a pure polymer equals $kT\chi$, where $k$ is the Boltzmann constant and $T$ is the temperature. It is therefore more favorable for the polymer to absorb solvent molecules if the $\chi$ for the solvent-polymer pair is low, since less energy is required for the solvent to enter the polymer film.

The interaction parameter is known to be concentration-dependent[21]. Such dependence can be described as $\chi = \chi_0 + \chi_1\varphi + \chi_2\varphi^2$, where $\varphi$ is the volume fraction of the polymer in the swollen state. Since in this study only equilibrium swellings in saturated solvent vapors are considered, the $\chi$ will be estimated at a single point $\varphi$ and will be assumed to be independent of polymer concentration. This will allow qualitative comparison of different polymer-solvent pairs.

There are several ways to estimate the Flory-Huggins interaction parameter: osmotic pressure, vapor sorption, or inverse gas chromatography[22].

For this particular study, the most practical way is to calculate $\chi$ from the solvent absorption experiment[23]. Since the Flory-Huggins theory does not account for the free volume, in all calculations listed below free volume was assumed to be constant during the polymer swelling. When the solvent molecules are mixed with polymer chains, the change to their chemical potential $\mu$ relative to some reference state $\mu^0$ can be described as[24]:

$$\frac{\mu - \mu^0}{RT} = \chi\varphi^2 + \ln(1-\varphi) + (1 - 1/N)\varphi \qquad \textbf{Eq. 5.5.}$$

where $N$ is the degree of polymerization of the polymer chains. It is known that change in the chemical potential of the solvent (assuming ideal gas behavior) can be described through the vapor pressure of the solvent vapor above a polymer solution $P$ relative to that of the pure solvent $P^0$ at reference state [24]:

$$\frac{\mu - \mu^0}{RT} = ln\left(\frac{P}{P^0}\right) \qquad \textbf{Eq. 5.6.}$$

Since in all experiments performed in this study $\frac{1}{N} \ll 1$, **Eq.5.5**. yields:

$$ln\left(\frac{P}{P^0}\right) = \chi\varphi^2 + \ln(1-\varphi) + (1 - 1/N)\varphi \qquad \textbf{Eq. 5.7.}$$

The reference state is taken to be 25°C, which is very close to the temperature at which the swelling experiments were conducted. During the swelling experiments there were observed no solvent condensation on the sample or the walls of the cuvette, thus it was assumed that some amount of the solvent escapes cuvette. Therefore it was assumed that the pressure inside of the cuvette is very close to the saturated vapor pressure, but never reaches it. Under this assumption $\frac{P}{P^0}$ in **Eq.5.7.** was set to be very close to unity, and the estimation of the interaction parameter was done using the equation:

$$\chi = -\frac{\ln(1-\varphi) + \varphi}{\varphi^2} \qquad \textbf{Eq. 5.8.}$$

Due to the limitations of the Flory-Huggins theory[25] and the assumptions mentioned above, this equation does not give precise values for $\chi$ parameter. However, the estimation of $\chi$ from **Eq.5.8.** can be used for comparison of solvent-polymer pairs as it qualitatively describes the affinity of the given solvent to the polymer. It can be seen from **Eq.5.7.**that for the thermodynamically good solvent, a high amount of solvent enters the polymer network and $\varphi$ is low, $\chi \to 0.5$. When the polymer does not dissolve in solvent $\varphi$ is close to unity and $\chi$ is high.

### 5.3.6. Interaction parameter calculation from swelling experiments

Data presented in **Figure 5.8.**was used for the estimations of the effective interaction parameter $\chi$. Since it is assumed that during the swelling the film does not expand in the lateral direction, the polymer volume fraction at equilibrium $\varphi$ can be calculated as

$$\varphi = \frac{h_0}{h_\infty} = RTC^{-1} \qquad \textbf{Eq.5.9.}$$

Therefore, using **Eq.5.8.**, the effective interaction parameter can be calculated from the relative thickness change. The calculated values of $\chi$ for PGMA-RhB and the 5 different solvents used in the swelling experiments for 5 nm thick film are presented in **Figure 5.9.** The interaction parameter can now be used to characterize polymer-solvent pairs in terms of the polymer affinity to the solvent. It can be seen that chloroform has the highest affinity to the PGMA-RhB system, with the lowest $\chi$. This explains why chloroform works well as a solvent during PGMA-RhB deposition. Toluene, acetone, and cyclohexane have close values for $\chi$, around 1, and water has the highest value: $\chi = 2.5$, which is much higher than the rest of the solvents, meaning that water has the lowest affinity to the PGMA-RhB system.

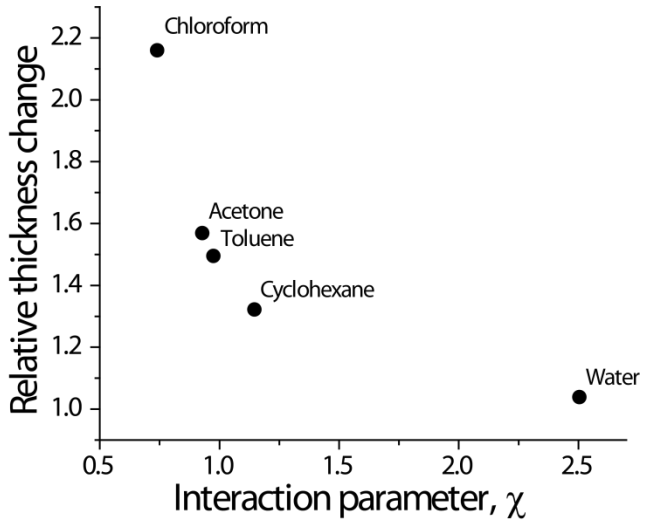


**Figure 5.9.** Effective interaction parameter $\chi$ calculated for the interaction between PGMA-RhB and 5 different solvents: chloroform, acetone, toluene, cyclohexane, and water.

### 5.3.7. Fluorescent properties of ultrathin PGMA-RhB film

#### 5.3.7.1. TIRF measurements

As shown in **Chapter 4**, the fluorescent emission of the PGMA-RhB film changed when the film was subjected to chloroform vapor. Since the PGMA-RhB film retained the ability to absorb a substantial amount of solvent after a reduction in the thickness to 5 nm, it is expected that the ultrathin films will exhibit environmental emission sensitivity as well.

However, much more interesting is the difference among the fluorescent responses induced by different analytes. To examine if such a difference exists, the swelling of the PGMA-RhB film on glass slides was performed using a TIRF setup. In **Figure 5.10.,** the fluorescent emission intensity of the 5 nm thick PGMA-RhB film is

shown. Vapors from 5 different analytes were pumped through the cuvette. A baseline of about 130 a.u., shown in **Figure 5.9.**, corresponds to the PGMA-RhB film in the dry state.

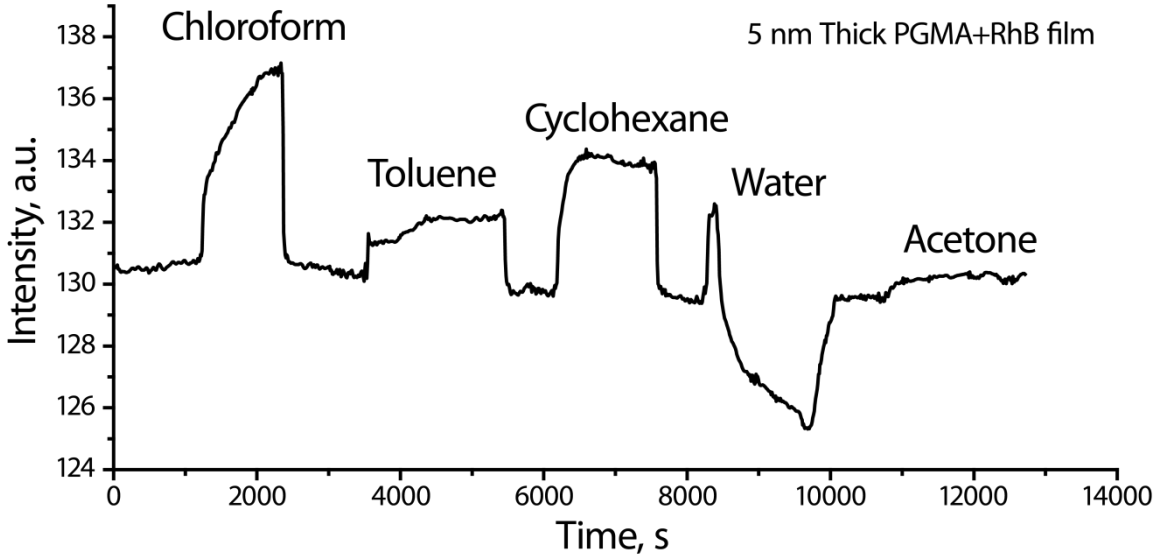


**Figure 5.10.** Fluorescent emission intensity change for 5 nm thick PGMA-RhB film measured using a TIRF setup. Vapors of chloroform, acetone, toluene, water, and cyclohexane were used as the analytes.

When the vapors of the analytes were introduced to the cuvette, an emission signal change was immediately observed. The rate of the signal change and the magnitude was different for each solvent. For example, the rate of the observed signal change was slower for chloroform and faster for cyclohexane and toluene. For all the solvents the signal change was positive, but for water, the signal increased first and then decreased. After the air was pumped through the cuvette, the swollen film almost immediately reverted to its dry state and the emission value returned to baseline.

As discussed earlier, ultrathin polymer films have several advantages over thick films. However, as was shown in **Section 4.3.7.5.**, the fluorescent emission in the dry and

saturated state is proportional to the number of RhB molecules exposed to the excitation beam. This means that the sensitivity of the detector is the major factor, which determines the possibility of using ultrathin films for vapor sensing. It can be seen from the comparison of the signal change for thick film of 120 nm thick (**Figure 4.10.**) with the signal for the ultrathin 5 nm film (**Figure 5.10.**) that the signal-to-noise ratio decreases significantly with the thickness of the PGMA-RhB layer.

Because of the presence of high amounts of noise, it was decided to perform the same measurements using blank glass slides to see if there was any interference induced by the interaction of the solvent with the surface of the glass. The results of these measurements are shown in **Figure 5.11.** It can be seen from the plot that after the introduction of the solvent vapor, the emission intensity jumps almost instantaneously. Another interesting tendency is the equality of the magnitude and direction for the signal change (increase) for each solvent used.

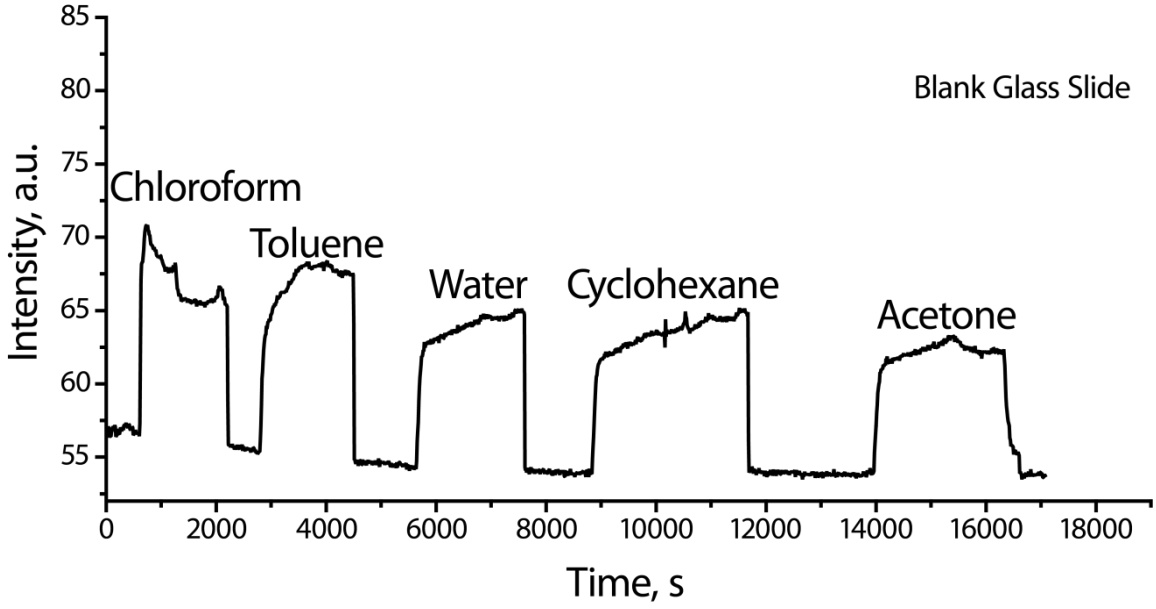


**Figure 5.11.** Intensity change measured by the detector when the vapors of chloroform, acetone, toluene, water, and cyclohexane are pumped through the cuvette onto a blank glass slide.

These two observations help identify the cause of the interference of the blank glass slide with the fluorescent emission of the ultrathin PGMA-RhB film. The detector used in the TIRF setup is sensitive to the photons of various energies in the visible region, including the laser excitation beam and the fluorescent emission of the PGMA-RhB film. Since only the fluorescent emission of RhB is of interest, the detector is protected from the excitation radiation by a filter. The filter, however, is designed to block only the radiation perpendicular to its surface[26], therefore scattered light from the excitation source can reach the detector as it passes the filter at a non-zero angle of incidence.

As discussed above, emission intensity experiences a jump as soon as the vapors of the solvents are pumped through the system. This means that the presence of the vapor

causes a scattering of the excitation beam at the point of reflection from the glass surface. Such scattering can be caused by the condensation of the solvent into small droplets on the surface of the glass.

The vapor condensation is, in turn, caused by the Joule-Thompson effect[27]: when the vapors of the solvent are pushed out of the tubing into the cavity inside of the closed cuvette, cooling of the vapors occurs. Vapor cooling favors condensation, thus causing droplet formation, excitation beam scattering, and ultimately a shift in the emission intensity collected by the detector.

As opposed to the thick films, the interference caused by vapor precipitation is comparable with the signal change for the ultrathin film and can become a source of significant errors. Since it is impossible to measure the exact change of the signal due to vapor condensation and simply subtract it from the measured signal change for the PGMA-RhB ultrathin films, such errors obstruct precise fluorescent emission measurement. To overcome this difficulty, it was decided to conduct the intensity measurements using spectrophotometry.

#### 5.3.7.2. Spectrophotometry measurements

##### 5.3.7.2.1. Selection of the technique for introduction of the analyte to the PGMA-RhB film

For the spectrophotometry measurements, a special Teflon cuvette was designed. (**Section 3.3.5.**) The cuvette can be positioned in the sample compartment of the

spectrophotometer at a 45° angle to the incident light. The measurements were conducted in the front face mode.

The main difference between the spectrophotometry technique and the TIRF measurement is the use of monochromators for emission and excitation beams. Monochromators allow radiation measurements to be recorded as a function of wavelength[28]. The presence of monochromators in the system completely eliminates the influence of the scattered excitation beam from the measured fluorescent emission of the RhB molecules due to the difference in the wavelengths of the excitation and emission.

However, despite the use of monochromators, scattering of the beam at the surface of the glass still has an indirect impact on the emission measurement: if during the swelling experiment the excitation beam becomes scattered from the glass surface, it can excite a larger number of fluorophores, thus producing greater emission intensity from the polymer film. Therefore, the solvent introduction method had to be modified to prevent droplet formation on the surface of the glass.

A cotton ball soaked with the solvent was chosen as a source for the saturated solvent vapors. When the solvent evaporates from the cotton ball, there is no volume change for the vapors so there are no temperature gradients in the cuvette and no condensation should occur.

Thus, the constructed cuvette was well suited to performing the fluorescent emission measurements in the changing environment. To measure the sensitivity of the 5 nm thick PGMA-RhB film, the following experiment was performed.

First, the fluorescent emission of the PGMA-RhB film in the dry state was acquired and then solvent vapors (chloroform) were introduced to the cuvette. After 30 minutes of swelling, the second emission spectrum was collected. The resulting spectra are presented in **Figure 5.12.**Significant changes can be seen in fluorescent emissions upon film swelling. The main change in the spectrum is a shift of the whole curve upwards, meaning an increase in the photon counts at all wavelengths. There was almost no horizontal shifting of the peak, which is usually observed when the fluorophores are subjected to the solvents with a different polarity[29]. This can be explained by the firm chemical attachment of the RhB molecules to the relatively rigid polymer network and restriction of the relaxation of energetic levels of the molecule[30].

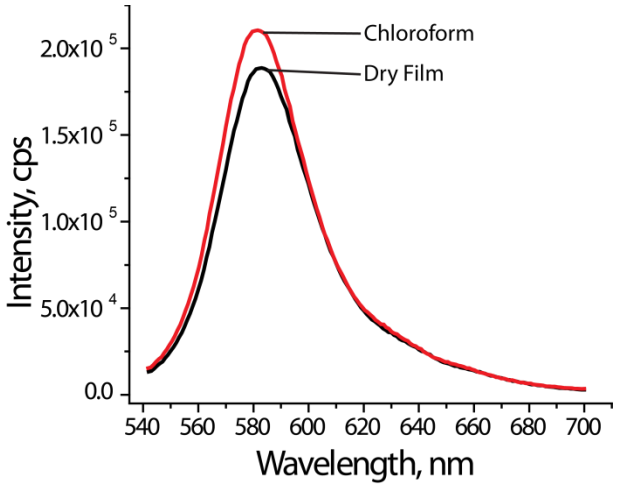


**Figure 5.12.** The shift of the fluorescent emission spectrum of 5 nm thick PGMA-RhB film due to exposure to chloroform vapors

#### 5.3.7.2.2. Selection of the spectrum range for the measurements

As in case of ellipsometric measurements, it would be interesting to have a curve representing the change of fluorescent signal over time. By fitting such a curve using the

same method as was shown in **Section 5.3.4.3.**, it would be possible to calculate the emission intensity at infinite swelling time, which can be further used as a characteristic parameter for the particular polymer-solvent system. It would also be possible to study the rate of the fluorescent emission intensity change and the factors affecting this rate.

However, measurement of the whole spectrum takes a considerable amount of time, usually several minutes depending on the integration time. Since the swelling of ultrathin films is a fast process, it is more convenient to measure a narrow part of the spectrum in order to decrease the measurement time. One downside of this approach is the possibility that the measured part of the spectrum will not represent the whole spectrum in terms of the fluorescent emission intensity change.

Therefore, before such a method could be used, its applicability had to be checked. As previously mentioned, the polarity of the solvent is the main reason for the emission spectrum shift that causes distortion of the spectrum. Measurement of part of the spectrum will only represent the full spectrum if there are no significant shifts. For validation, most of the polar solvents that were used throughout this work were selected: chloroform, acetone, and water. The relative polarities of these solvents are 0.259, 0.355, and 1, respectively (the polarities of cyclohexane and toluene are 0.006 and 0.099, respectively)[31].

First, fluorescent emission in the dry state was measured. Next, measurements of the signal change were conducted for chloroform, acetone, and water, using full spectrum acquisition (540 nm – 700 nm). The resulting emission spectra of the 5 nm thick PGMA-RhB film in the dry state and after 20 min of solvent exposure are shown in **Figure**

**5.13.left.** For comparison purposes the spectra for the swellings in acetone and water were rescaled so the intensity of the dry state would coincide with the dry state intensity for the measurement of chloroform intake.

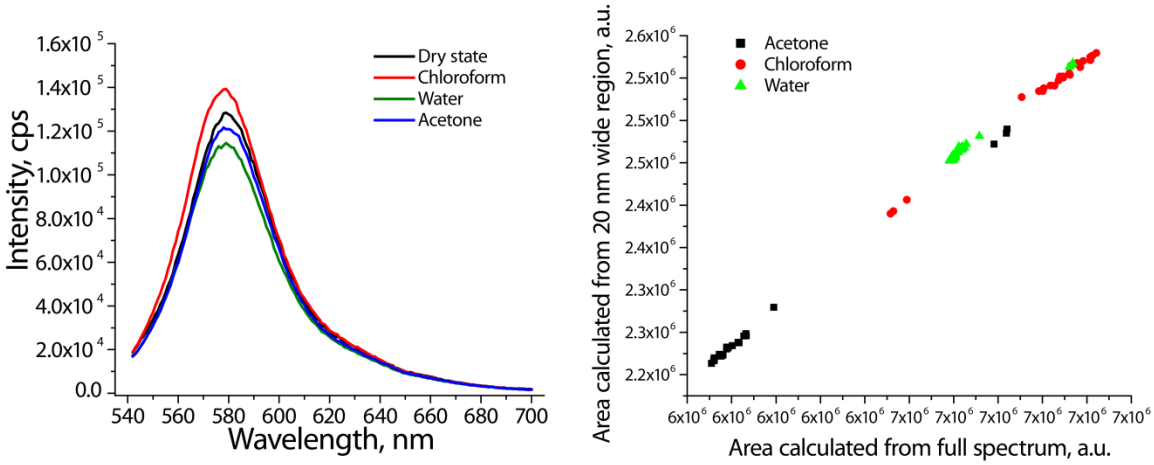


**Figure 5.13.** Changes in the emission spectrum of 5 nm thick PGMA-RhB film in chloroform, acetone, and water vapors (left). Plot of the area under 20 nm wide part of the spectrum vs. the area of the full spectrum (right).

It can be seen that a small peak shift occurs for chloroform and water. It can also be seen that the direction and change of the intensity magnitude is different for the solvents. These differences will be discussed later in **Section 5.3.8.,** when equilibrium intensity changes for the swollen film will be compared.

Using the data presented in **Figure 5.13. left,** it is possible to calculate how the intensity of the PGMA-RhB film changes by calculating the area under the emission spectrum. Next, the 20 nm wide part of the spectrum right under the emission peak (580 nm) was cut out and used for the area calculation as well.

The relative intensity change for the 20 minutes of exposure in the vapors of chloroform, acetone and water was calculated for the 20 nm region and the full spectrum. Next the area under the 20 nm region was plotted as the function of the area calculated

under the full spectrum (**Figure 5.13. right**). Calculations show a 1.35% standard deviation from a perfect match between the 20 nm wide region under the emission peak and the intensity change calculated from the full spectrum.

This result means that for the PGMA-RhB film, the 20 nm part of the spectrum under the peak fully represents the changes in the PGMA-RhB emission. The measurements for such a narrow region take only 30 sec, with a 1 second/nm integration time (an additional 10 seconds are needed to reset the monochromators). Therefore, using the measurements in the short wavelength region, it is possible to observe changes in the intensity of the fluorescent emission of the PGMA-RhB film with higher precision in the time interval.

#### 5.3.7.2.3. Relative intensity change measurements

It is now demonstrated that the proposed method of using a narrow region of the spectrum for fluorescent emission characterization is valid. First, the full spectrum of the PGMA-RhB film in the dry state was acquired. Next, the solvent was introduced to the cuvette and a continuous scan was performed using the Fluorolog software. The typical plot for the changes of the area over time are presented in **Figure 5.14.** In the plot presentedan intensity change for the 5 nm thick PGMA-RhB film in chloroform vapors. A 20 nm region (570 nm – 590 nm) was used for the intensity calculations. It can be seen from the plot that the emission intensity change and the thickness change measured using ellipsometry (**Figure 5.5.** (**right)**) have a similar appearance. This proves the previously

suggested hypothesis that the fluorescent emission intensity change is proportional to the amount of the analyte within the film.

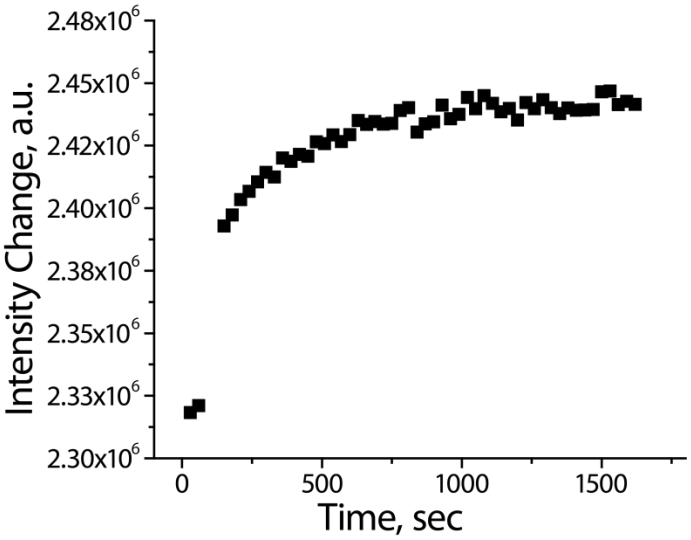


**Figure 5.14.** Relative intensity change for 5 nm thick PGMA-RhB film exposed to chloroform vapors.

This also indicates that the same fitting technique that was used for ellipsometric measurements (**Section 5.3.4.3.**) can be used to calculate the intensity of the PGMA-RhB film at equilibrium $I_\infty$. However, as was previously observed (**Figure 5.13.**), the magnitude of the emission intensity change can be negative (as opposed to ellipsometry measurements).

To account for this phenomenon, the following equation was used for the relative intensity change (RIC):

$$RIC = I_\infty / I_0 - 1 \qquad \textbf{Eq. 5.10.}$$

where$I_0$ is the intensity of the film in the dry state.

The sign for this value characterizes the direction of the emission intensity change: it will be positive if the emission intensity increases upon polymer film swelling and negative otherwise. Using the same measurement technique for the rest of the solvents and fitting the resulting intensity change with **Eq.5.2.** (curves with a decrease in emission intensity were flipped vertically for the fitting).

**Figure 5.15.**presents the results of the calculations for the relative intensity change for 5 nm thick PGMA-RhB film in chloroform, acetone, toluene, water, and cyclohexane. It can be seen that the signal change is different for each solvent used in the study. In addition, the magnitude of the signal variation changes sign: it is positive for chloroform and cyclohexane and negative for acetone, toluene, and water. This important result confirms the sensitivity of the proposed PGMA-RhB system to changes in the environment.

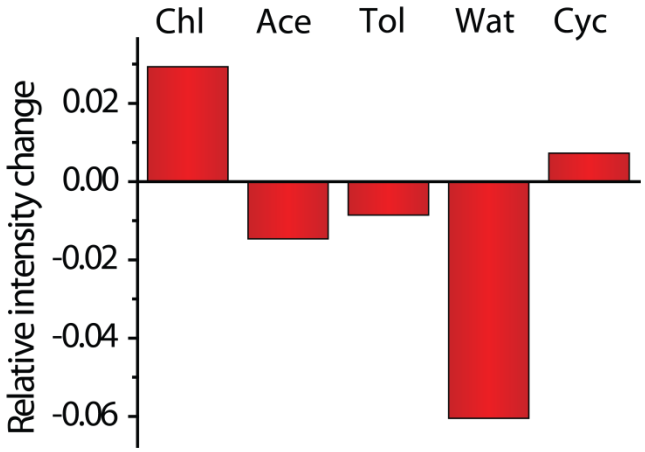


**Figure 5.15.** Relative intensity change for 5 nm thick PGMA-RhB film in chloroform, acetone, toluene, water, and cyclohexane.

The rate of the intensity change varied for the PGMA-RhB film exposed to the same analyte (due to the solvent deposition technique, the intensity change rate is very

sensitive to the cotton ball position, size, and amount of solvent introduced), the final relative intensity change was consistent for several measurements.

#### 5.3.7.3. Quantum yield calculations

The question immediately arises: what is the driving force for the change in the fluorescent emission response? As shown in **Section 5.3.7.2.2.**, there is almost no shift in the spectrum. This suggests that there is almost no change in the structure of the energy levels of the RhB molecules. Excluding the FRET and inner filter effect (**Section 4.3.7.5.**) only one possibility for the emission intensity change remains.

In is known that the fluorescent emission intensity of the fluorophore is governed by its quantum yields in its current environment[32]. The quantum yield for fluorescent material is defined as the number of photons emitted by the material divided by the number of photons absorbed[30]. From this definition, it follows that changes in the quantum yield of the RhB molecules upon PGMA-RhB exposure to the vapor of a solvent will define the emission intensity of the PGMA-RhB film.

Measurement of the absolute quantum yield of the fluorophore is a difficult and labor-intensive task. To do that, one needs to know the exact number of excited molecules and collect all the emission photons from the excited molecules (**Figure 5.16. left**).

Instead, for most applications it is more feasible to calculate relative quantum yields[4]. In the relative measurement technique, quantum yields for two dyes (a dye with an unknown quantum yield and a reference dye with a known quantum yield) are

calculated using a device that accounts for some part of all the photons contributing to fluorescence (**Figure 5.16.**, **right**). The key feature of this technique is the fact that the solid angle in which the photons are collected is the same for both measurements, since the same setup is used for photon calculation.

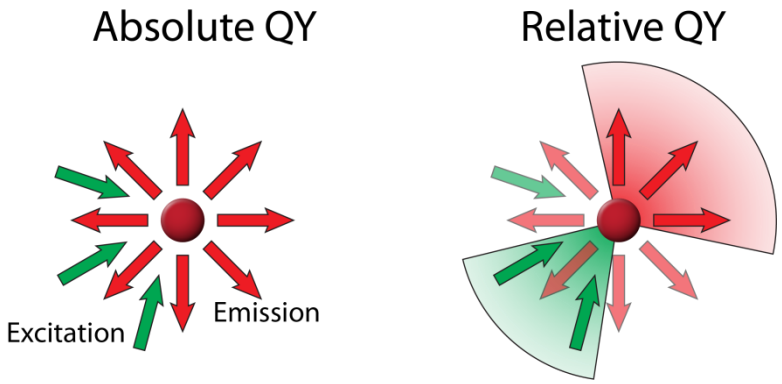


**Figure 5.16.** Schematics of Absolute (left) and Relative (right) quantum yield measurements

The quantum yield for unknown material$\Phi_x$ can be calculated using the reference value of the known standard $\Phi_{st}$ through the equation[4]:

$$\Phi_x = \Phi_{ST}\left(\frac{I_x/A_x}{I_{ST}/A_{ST}}\right)\left(\frac{n_x^2}{n_{ST}^2}\right) \qquad \textbf{Eq. 5.11.}$$

where$I_x$ and $A_x$ are the fluorescent emission and absorption of dye under investigation;$I_{ST}$ and $A_{ST}$ are those of the reference; $n_x$ and $n_{ST}$ are the refractive indexes of the solvents used for dye solutions for the dye with an unknown quantum yield, and the reference, respectively. The accuracy of the relative quantum yield measurements strongly depends on the methodology of the measurements and is estimated to be 10%.

To apply the relative quantum yield measurement technique to the present work, its accuracy was first verified by using two dyes with known quantum yield values. For

this purpose, Rhodamin B solutions in ethanol (95%) and water were used. The quantum yields for these systems are well studied and can be found in literature: the quantum yield for RhB in water[33] is 0.31and the quantum yield for RhB in ethanol[34] is 0.68. Five solutions of RhB in each of the solvents were prepared. The concentration of dye in these solutions was low enough that there was no interference of the inner filter effects with absorption and emission measurements for any of these solutions (absorption showed linear dependence on concentration, as shown in **Figure 5.17. left**). The results are plotted in **Figure 5.17. right**. It can be seen that the emission intensity has linear dependence on absorption for all concentrations used, confirming the absence of concentration-dependent effects. The slopes of these curves can be used to calculate the quantum yield of the RhB molecules in one solvent relative to another. Using the acquired data, the quantum yield of RhB in water was calculated through the known value of the quantum yield for RhB in ethanol using **Eq.5.10.** The calculations showed a value of 0.328, which is very close to the value of 0.31 found in the literature. This proves that the technique is accurate and feasible for quantum calculations.

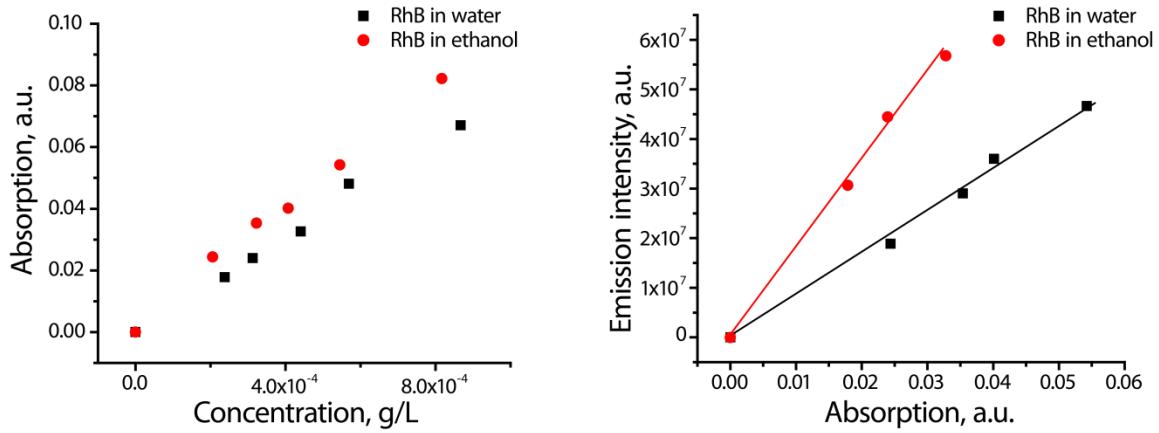


**Figure 5.17.** Absorption of the RhB solution vs. the concentration in water and ethanol (95%)(left).Emission intensity plotted as a function of absorption for the solutions of RhB in water and ethanol (95%) (right)

For estimations of quantum yield, the fluorescence of a substance should be measured in solution. As swelling experiments show, PGMA has a very low affinity to several analytes (toluene, cyclohexane, and water)and therefore is insoluble in these solvents. Thus, quantum yield measurements were performed for Octadecyl Rhodamine B (R18) instead. The chemical structure of this dye is shown in **Figure 5.18.left**. It can be seen from the structure that this dye is a very close chemical analog to the RhB molecule attached to the PGMA chain (outlined in F**igure 5.18, right**) and it is soluble in all of the used solvents.

Quantum yields for R18 dissolved in chloroform, acetone, toluene, water, and cyclohexane were calculated using the technique described above. For each solvent, 5 solutions of different concentrations were performed. Absorption for each of the solvents was verified to be linearly dependent on concentration in order to exclude inner filter effects. Solutions of RhB in water were used as a reference. The results of the quantum yield calculations are presented in **Figure 5.18. right.** It can be seen that for the solvents

used there is diverse variation in quantum yields. For example, the quantum yield of R18 in chloroform in almost 100% compared to the quantum yield of R18 in water, which is only 6%. Selected solvents cover the range of all possible values for the quantum yield of R18.

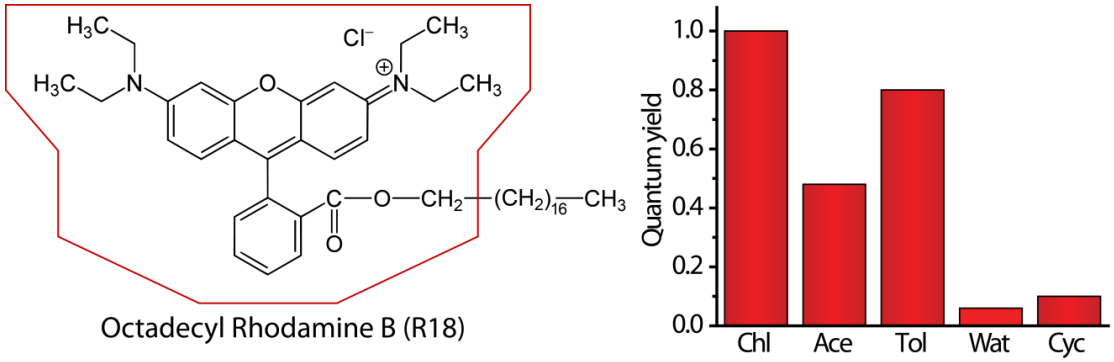


**Figure 5.18.** Structure of Octadecyl Rhodamine B (R18). Outlined is the structure of the fluorescent unit of PGMA-RhB (left). Quantum yields for the R18 solutions in chloroform, acetone, toluene, water, and cyclohexane (right)

### 5.3.8. Causes of emission intensity variation

It is now possible to draw an analogy between quantum yields and the variation of the emission intensity for the ultrathin PGMA-RhB layer. The comparison between the quantum yields and the relative intensity change values (**Figure 5.15.**) reveals that there is a close correlation between the two. The relative intensity change decreases as the quantum yield decreases: it is greatest for chloroform, then acetone, toluene, and water. However, the RIC of cyclohexane does not follow the pattern. The quantum yield in cyclohexane is almost the same as in water; whereas the relative intensity changefor cyclohexane is small and positive, as opposed to relative intensity change in water, which has a high magnitude and is negative.

It is possible to use the estimated effective interaction parameter to see if there is any correlation between the emission intensity change and the affinity of the solvent to the polymer. Integration of the calculations shown in **Figure 5.9.**into the relative intensity change is presented in **Figure 5.19.**It can be concluded from the plot that polymer-solvent interaction does not explain the behavior of the PGMA-RhB layer discussed in the previous paragraph.

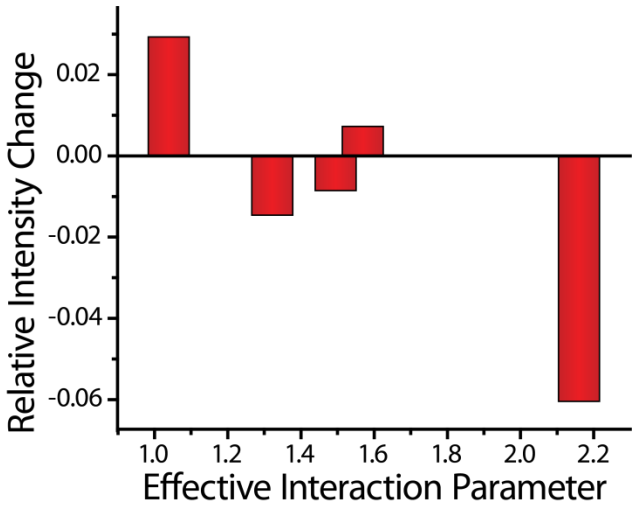


**Figure 5.19.** Relative intensity change for 5 nm thick PGMA-RhB film as a function of the effective interaction parameter for the polymer-solvent pair.

The presented data shows that that there is no direct relation between the relative intensity change and the solvent affinity to the PGMA-RhB layer. In particular, **Figure 5.8.**shows that the affinity of PGMA-RhB to cyclohexane is higher than for water; however, the intensity change is much greater for water than for cyclohexane.

This leads to an important conclusion that there is yet another factor affecting fluorescent emission intensity change besides the amount of the solvent present in the film and the quantum yield of the dye in the solvent. During the polymer film swelling,

along with the penetration of solvent molecules through the film to the RhB attachment sites, PGMA conformation also changes. The effect of such conformation changes can be described in the following example.

If one considers two swelling experiments where two different solvents, A and B (A is a good solvent for PGMA and B is not), are used, polymer film behavior can be represented using the following schematic drawn in **Figure 5.20**. It can be seen from the figure that when the PGMA chains are subjected to the solvent, separation of the polymer chains occurs. This separation is greater for the solvent with better affinity to PGMA because more molecules enter the film, as was described above (**Section 5.3.6.**).

This difference in PGMA chain conformation affects the proximal environment of the RhB molecules. It can be seen that in case of solvent A, the RhB molecule is surrounded with more of the solvent molecules, and in the case of B, the RhB molecule is surrounded with more of the PGMA chains. This would mean that the change in the conformation of the PGMA, along with the presence of the solvent, determines the closest environment and therefore the emission intensity of the RhB[35].

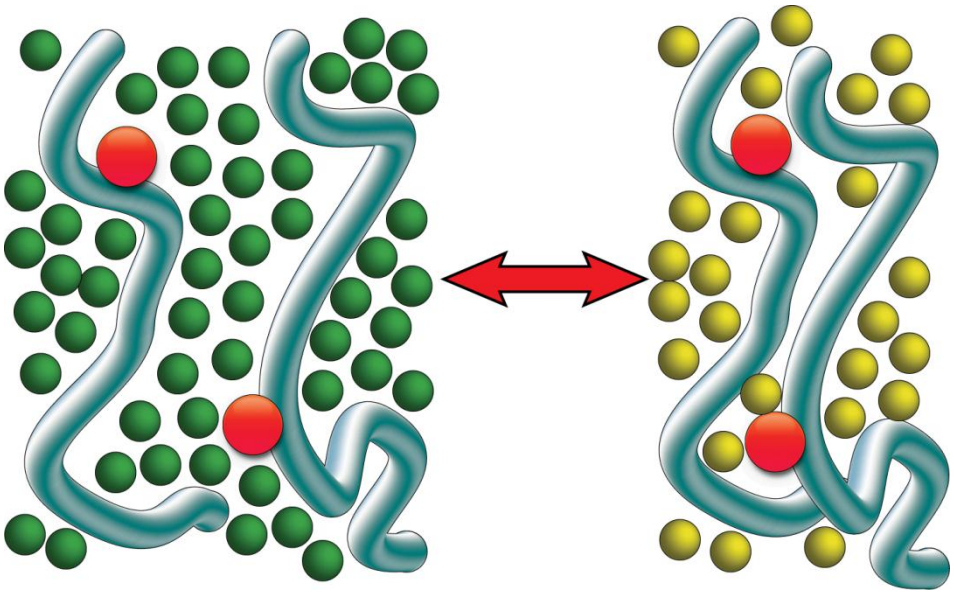

**Figure 5.20.** Schematic of PGMA chain conformation changes relative to the RhB molecules in two different solvents: a good solvent for PGMA (left) and a bad solvent for PGMA (right)

### 5.3.9Affinity of the RhB molecules to the environment

Another important feature is the affinity of the fluorescent units of the PGMA-RhB polymer to the particular analyte. For example, during the polymer film swelling, monomeric units of PGMA can "shield" the RhB molecules from a solvent that has low affinity to the fluorescent unit of PGMA-RhB.

To evaluate the affinity of the fluorescent unit of PGMA-RhB to the solvents used for the research, enthalpies of mixing ware calculated. The RhB attached to the PGMA (as outlined in **Figure 5.18.**) was used as a fluorescent unit of the polymer. For the calculations of the enthalpy of mixing$\Delta H_M$, the following equation was used[21]:

$$\Delta H_M = \varphi_1 \varphi_2 \left[ (\delta_{d1} - \delta_{d2})^2 + \left(\delta_{p1} - \delta_{p2}\right)^2 + (\delta_{h1} - \delta_{h2})^2 \right] \quad \textbf{Eq.5.12.}$$

where, respectively, $\varphi_1$ and $\varphi_2$ are the concentrations of the mixing substances; and$\delta_d$, $\delta_p$, $\delta_h$ are contributions to solubility from dispersion forces, polar forces, and hydrogen bonding (the Hansen solubility parameters). The values for the solubility parameter contributions for all of the solvents used (chloroform, acetone, toluene, water, and cyclohexane) were found in literature[36]. For the fluorescent unit, these values were calculated using the Bicerano method[37]. The enthalpy of mixing was then calculated on the assumption of equal amounts of mixing substances. The results are summarized in the **Table 5.1.,** together with the values of the Hansen solubility parameters. High values of the mixing energies in the table mean poor affinity between the solvent and the fluorescent unit of the PGMA-RhB.

**Table 5.1.** Hansen solubility parameters and enthalpy of mixing calculated for the mixing of fluorescent unit of PGMA-RhB with chloroform, acetone, toluene, cyclohexane, and water in a 50/50 mixing ratio.

| | $\delta_d, (J/cm^3)^{1/2}$ | $\delta_p, (J/cm^3)^{1/2}$ | $\delta_h, (J/cm^3)^{1/2}$ | $\Delta H_M$, $(J/cm^3)$ |
|---|---|---|---|---|
| RhB | 16.9 | 7.6 | 6.9 | 0 |
| Chloroform | 17.8 | 3.1 | 5.7 | 5.625 |
| Acetone | 15.5 | 10.4 | 7 | 2.45 |
| Toluene | 18 | 1.4 | 2 | 15.91 |
| Cyclohexane | 16.8 | 0 | 0.2 | 25.6 |
| Water | 15.6 | 16 | 42.3 | 331.35 |

It can be seen from the table that the value of the energy of mixing for water is very high compared to all other solvents. This seems to be untrue, since water is a very good solvent for RhB molecules[38]. Such high energy of mixing is caused by large differences among the $\delta_h$ values. For the rest of the solvents, calculations have shown reasonable values. It can be seen that acetone has the best affinity to RhB, and cyclohexane has the worst.

Results of the calculations were qualitatively checked by dissolving 1% w/w of RhB molecules in all the solvents from **Table 5.1.** The RhB molecules were readily and completely dissolved in water and acetone. On the contrary, poor solubility was observed for chloroform and toluene and almost no RhB was dissolved in cyclohexane. These results confirm the validity of the estimations presented in **Table 5.1.**for all solvents except water, which seems to be the best solvent for RhB.

Results of the solubility measurements for the RhB units, together with the hypothesis that PGMA monomeric units affect fluorescent emission, lead to the idea that non-fluorescent polymer chains could be used to tune the fluorescent response of the polymer in a changing environment. The presence of a polymer that is different in chemical nature from the PGMA in the PGMA-RhB system will, on the one hand, affect the conformational changes of the PGMA itself and, on the other hand, will modify the closest environment of the RhB molecules. Such tuning of fluorescent emission intensity variation in a changing environment is reported in the chapters that follow.

## 5.4. Conclusion

In conclusion, ultrathin fluorescent polymer films (5 nm thick) were synthesized on the surface of silicon wafers and glass slides. The films were characterized using ellipsometry and AFM.

The films were able to absorb solvents from the vapor phase, which changed the thickness reversibly and repeatably, as confirmed by ellipsometry. The thickness change observed was different for each solvent used in the study. The fluorescent emission changes were recorded using spectrophotometry and TIRF measurements and also showed distinctive responses to the analytes. Quantum yields of the model dye (R18) were calculated using the relative quantum yield measurement technique.

There were two factors affecting fluorescent emission: the relative solvent uptake and the quantum yield were compared to the relative intensity changes for the PGMA-RhB films. The quantum yield was found to have the most influence on fluorescent emission of the film. However, another factor, the conformation of the matrix polymer, was also assumed to have an influence on the fluorescent emission. This leads to the ability to change the emission intensity of the PGMA-RhB with non-fluorescent polymer grafting.

## 5.5. References

1. Stamatialis, D. F.; Wessling, M.; Sanopoulou, M.; Strathmann, H.; Petropoulos, J. H., Analysis of the kinetics of vapor absorption/desorption in/from silicone rubber and cellulose acetate membranes in the presence of stagnant boundary layers. *Journal of Membrane Science* **1997,** *125* (1), 165-175.

2. Godovsky, D., Device Applications of Polymer-Nanocomposites. Springer Berlin / Heidelberg: 2000; Vol. 153, pp 163-205.

3. Hamley, I. W., *The physics of block copolymers*. Oxford University Press: Oxford; New York, 1998.

4. Ltd, J. Y. A Guide to Recording Fluorescence Quantum Yields. http://www.horiba.com/fileadmin/uploads/Scientific/Documents/Fluorescence/quantumyieldstrad.pdf.

5. Liu, Y.; Klep, V.; Zdyrko, B.; Luzinov, I., Synthesis of High-Density Grafted Polymer Layers with Thickness and Grafting Density Gradients. *Langmuir* **2005,** *21* (25), 11806-11813.

6. Toomey, R.; Freidank, D.; Rühe, J., Swelling Behavior of Thin, Surface-Attached Polymer Networks. *Macromolecules* **2004,** *37* (3), 882-887.

7. (a) Arwin, H., Is ellipsometry suitable for sensor applications? *Sensors and Actuators A: Physical* **2001,** *92* (1–3), 43-51; (b) Pristinski, D.; Kozlovskaya, V.; Sukhishvili, S. A., Determination of film thickness and refractive index in one measurement of phase-modulated ellipsometry. *Journal of the Optical Society of America. A, Optics, image science, and vision* **2006,** *23* (10), 2639-44.

8. Bruggeman, D. A. G., Berechnung verschiedener physikalischer Konstanten von heterogenen Substanzen. I. Dielektrizitätskonstanten und Leitfähigkeiten der Mischkörper aus isotropen Substanzen. *Annalen der Physik* **1935,** *416* (7), 636-664.

9. Aspnes, D. E.; Theeten, J. B.; Hottier, F., Investigation of effective-medium models of microscopic surface roughness by spectroscopic ellipsometry. *Physical Review B* **1979,** *20* (8), 3292-3302.

10. Stroud, D., The effective medium approximations: Some recent developments. *Superlattices and Microstructures* **1998,** *23* (3–4), 567-573.

11. Das, P. K.; Li, X.; Liu, Z.-S., Effective transport coefficients in PEM fuel cell catalyst and gas diffusion layers: Beyond Bruggeman approximation. *Applied Energy* **2010,** *87* (9), 2785-2796.

12. Prevo, B. G.; Hwang, Y.; Velev, O. D., Convective Assembly of Antireflective Silica Coatings with Controlled Thickness and Refractive Index. *Chemistry of Materials* **2005,** *17* (14), 3642-3651.

13. (a) Hennig, A.; Eichhorn, K. J.; Staudinger, U.; Sahre, K.; Rogalli, M.; Stamm, M.; Neumann, A. W.; Grundke, K., Contact Angle Hysteresis: Study by Dynamic Cycling Contact Angle Measurements and Variable Angle Spectroscopic Ellipsometry on Polyimide. *Langmuir* **2004,** *20* (16), 6685-6691; (b) Pantelic, N.; Seliskar, C. J., Anomalous Diffusion in Poly(vinyl alcohol)в€'Poly(acrylic acid) Thin Films. *The Journal of Physical Chemistry C* **2007,** *111* (5), 2054-2062.

14. Chýlek, P.; Videen, G., Scattering by a composite sphere and effective medium approximations. *Optics Communications* **1998,** *146* (1–6), 15-20.

15. Tang, Y.; Lu, J. R.; Lewis, A. L.; Vick, T. A.; Stratford, P. W., Swelling of Zwitterionic Polymer Films Characterized by Spectroscopic Ellipsometry. *Macromolecules* **2001,** *34* (25), 8768-8776.

16. Fujiwara, H., *Spectroscopic ellipsometry : principles and applications*. John Wiley & Sons: Chichester, England; Hoboken, NJ, 2007.

17. Russell, S. P.; Weinkauf, D. H., Vapor sorption in plasma polymerized vinyl acetate and methyl methacrylate thin films. *Polymer* **2001,** *42* (7), 2827-2836.

18. Schott, H., Swelling kinetics of polymers. *Journal of Macromolecular Science, Part B* **1992,** *31* (1), 1-9.

19. Crank, J., *The mathematics of diffusion*. Clarendon Press: Oxford, [Eng], 1975.

20. (a) Sperling, L. H., *Introduction to physical polymer science*. Wiley: New York, 1986; (b) Flory, P. J.; Krigbaum, W. R., Thermodynamics of High Polymer Solutions. *Annu. Rev. Phys. Chem. Annual Review of Physical Chemistry* **1951,** *2* (1), 383-402.

21. Krevelen, D. W. v.; Nijenhuis, K. t. Properties of polymers their correlation with chemical structure; their numerical estimation and prediction from additive group contributions.

22. Orwoll, R. A., The Polymer-Solvent Interaction Parameter X. *Rubber Chemistry and Technology* **1977,** *50* (3), 451-479.

23. Elbs, H.; Krausch, G., Ellipsometric determination of Flory-Huggins interaction parameters in solution. *Polymer* **2004,** *45* (23), 7935-7942.

24. Gaskell, D. R., *Introduction to the Thermodynamics of Materials*. Taylor & Francis: 2003.

25. Favre, E.; Nguyen, Q. T.; Schaetzel, P.; Clement, R.; Neel, J., Sorption of organic solvents into dense silicone membranes. Part 1.-Validity and limitations of Flory-Huggins and related theories. *Journal of the Chemical Society, Faraday Transactions* **1993,** *89* (24), 4339-4346.

26. Price, R. L.; Jerome, W. G. Basic confocal microscopy. http://public.eblib.com/EBLPublic/PublicView.do?ptiID=763390.

27. Kelvin, W. T., *On the dynamical theory of heat.* Printed for the Society by Neill and Co.: Edinburgh, 1852.

28. DeCusatis, C.; Optical Society of, A., *Handbook of applied photometry*. AIP Press ; Optical Society of America: Woodbury, N.Y.; Washington, DC, 1997.

29. Hinckley, D. A.; Seybold, P. G.; Borris, D. P., Solvatochromism and thermochromism of rhodamine solutions. *Spectrochimica Acta Part A: Molecular Spectroscopy* **1986,** *42* (6), 747-754.

30. Lakowicz, J. R., *Principles of fluorescence spectroscopy*. Kluwer Academic/Plenum: New York, 1999.

31. Reichardt, C., *Solvents and solvent effects in organic chemistry*. VCH: Weinheim, Federal Republic of Germany; New York, NY, USA, 1988.

32. Kubin, R. F.; Fletcher, A. N., Fluorescence quantum yields of some rhodamine dyes. *Journal of Luminescence* **1982,** *27* (4), 455-462.

33. Magde, D.; Rojas, G. E.; Seybold, P. G., Solvent Dependence of the Fluorescence Lifetimes of Xanthene Dyes. *Photochemistry and Photobiology* **1999,** *70* (5), 737-744.

34. Snare, M. J.; Treloar, F. E.; Ghiggino, K. P.; Thistlethwaite, P. J., The photophysics of rhodamine B. *Journal of Photochemistry* **1982,** *18* (4), 335-346.

35. Sarzi Sartori, S.; De Feyter, S.; Hofkens, J.; Van der Auweraer, M.; De Schryver, F.; Brunner, K.; Hofstraat, J. W., Host Matrix Dependence on the Photophysical Properties of Individual Conjugated Polymer Chains. *Macromolecules* **2002,** *36* (2), 500-507.

36. Brandrup, J.; Immergut, E. H., *Polymer handbook*. Wiley: New York, 1989.

37. Bicerano, J., *Prediction of polymer properties*. Marcel Dekker: New York, 1993.

38. Ramette, R. W.; Sandell, E. B., Rhodamine B Equilibria. *Journal of the American Chemical Society* **1956,** *78* (19), 4872-4878.

# CHAPTER SIX

# TUNING FLUORESCENT RESPONSE OF NANO-SCALE FILM WITH POLYMER GRAFTING

## 6.1. Introduction

As discussed in Chapter 2, the conformation of non-fluorescent polymer chains in the vicinity of RhB molecules influences the fluorescent response of fluorophores. It is also known that the behavior of ultrathin films is influenced by their high surface-to-volume ratio[1] and polymers grafted to the crosslinked PGMA layer may interpenetrate the polymer network to a certain extent[2]. Therefore, grafting non-fluorescent polymers to ultrathin polymer films may affect the intensity of fluorescent emissions through changes to the environment of the RhB molecules[3].

The concept of tuning the fluorescent response of ultrathin polymer films with grafting is illustrated in **Figure 6.1.** First, an ultrathin fluorescent film is grafted to the surface of a silicon wafer or a glass slide (**Section 3.2.1.**). Next, several different polymers are grafted to the ultrathin PGMA-RhB. After the grafting, the fluorescent response of the film exposed to a particular analyte becomes different for each unique combination of the fluorescent layer and the non-fluorescent polymer graft. In the presented concept, each analyte becomes more distinct in its fluorescent emission response, since for each analyte several unique emission changes can be observed. Therefore, this concept can be incorporated into sensing systems for detecting a single substance from a substance mixture or for substance identification.

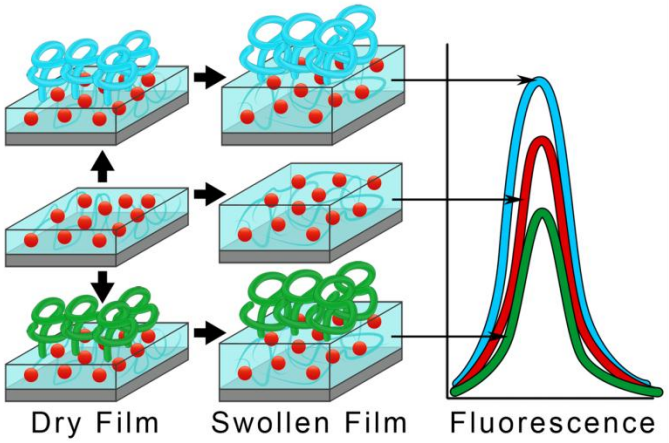


**Figure 6.1.** Schematic of the concept of tuning the fluorescent response of the PGMA-RhB with non-fluorescent polymer grafting

To this end, the objective of this part of the work was to investigate the influence of surface modification of PGMA-RhB films with grafts of non-fluorescent polymer on the fluorescent properties of the films. For the surface modification, the following polymers were selected: polystyrene (PS), poly(2-vinyl pyridine) (P2VP), polyacrylic acid (PAA), and polyethylene glycol (PEG). These polymers differ significantly in chemical structure, polarity, and affinity to the solvents used throughout the presented research (chloroform, acetone, toluene, cyclohexane, and water). PEG has good affinity to all solvents, PAA and P2VP have more affinity to polar solvents such as water and acetone, and PS has more affinity to low-polarity solvents such as cyclohexane and toluene. In addition, the molecular weight of the polymers also varied: PS and P2VP were approximately the same molecular weight of 50 kDa; PEG had shorter chains and PAA had longer chains than the rest of the polymers.

Ultrathin PGMA-RhB film with the surface modified with polymer grafting can be approximated as a two-layered system with some degree of grafted polymer

penetration into the PGMA network[2]. There are several possible ways the grafted non-fluorescent polymer affects the fluorescent emission response of the PGMA-RhB layer during film swelling. First, due to the differences in solvent absorption, there will exist deformations of the interfacial region between the two layers [4]. These deformations can be large enough to cause conformational disturbances to the polymer chains surrounding the RhB molecules, which is not the case for graft-free PGMA-RhB layers. As shown above (**Section 5.4.**), such conformational changes may influence the fluorescent emissions of the RhB molecules. Second, since there is some degree of grafted layer penetration to the PGMA-RhB network, some RhB molecules may be contacted by the monomeric units of a grafted polymer. These units will cause changes in the chemical nature of the PGMA network and, consequently, will change the affinity of the polymer film to the solvent vapors compared to the single layer PGMA-RhB film.

In all of the possible cases listed above, the key feature is the affinity of the target analyte to each of the polymers in the system. Similar to what was shown for the PGMA-RhB layer in **Section 5.3.6.,** the affinity of grafted polymer layers to analytes can be described by polymer-solvent interaction parameters. In this part of the work, ellipsometry was used to investigate polymer-solvent interactions through the swelling of thick films of the polymers that were used for grafting.

Variations in emission intensity for the modified PGMA-RhB films were studied using the spectrophotometry method for several analytes (chloroform, acetone, toluene, water, and cyclohexane). Causes of variations in fluorescent emissions were investigated by comparing the effects produced by the same solvents on PGMA-RhB films with

different surface modifications. These studies revealed that changes in the affinity of PGMA-RhB film to the solvent caused by the surface modification strongly influence the fluorescent response of the film.

## 6.2. Experimental

### 6.2.1. Grafting of Non-fluorescent polymer layer to the ultrathin PGMA-RhB film

The main fluorescent layer was composed of 5-nanometer thick PGMA-RhB films. The film synthesis is described in detail in **Chapter 3**. PGMA-RhB of Mn= 80,000 g/mol with polydispersity of 2.57 was used. Four polymers were grafted to the surface of the PGMA-RhB film. These were carboxyl-terminated versions of PS (Mn = 48,000 g/mol), P2VP (Mn=53,000 g/mol), and PEG (monomethyl ether Mn=5,000 g/mol). The fourth chosen polymer, PAA (Mw=100,000 g/mol),has a reactive carboxyl group in each monomeric unit (For polymer description see **Chapter 2**).

The PGMA-RhB films were covered with layers of the polymers to be grafted via dipcoating at 5 mm/sec. A 1% solution was used for each polymer: chloroform was used as a solvent for PS, and methanol was used for P2VP, PAA, and PEG. Next, the films were annealed (PGMA-RhB-PS and PGMA-RhB-P2VP at 120°C for 8 h; PGMA-RhB-PAA at 40°C for 2h) to allow polymer attachment to PGMA-RhB through a reaction with the epoxy groups of PGMA. Deposition of PEG was done from melt. Polymer melt was contained between the substrate and the cleaned glass slide. Annealing of PGMA-RhB-PEG was done at 120°C for 8 h.

After annealing, the unattached polymer chains were removed by rinsing the substrates covered with the polymer films in good solvents for the grafted layers (chloroform for PS and methanol for P2VP, PAA, and PEG) 3 times for 30 min each.

### 6.2.2. Deposition of non-fluorescent polymer films

For the investigation of the properties of the polymers used for grafting, such as refractive index and polymer-solvent interaction parameters, relatively thick polymer films were obtained. The thick polymer films were deposited on the surface of the cleaned silicon wafers (for the cleaning procedure see **Section 3.4.1.**). Two series of the films were manufactured. The first series was created using deposition by dip coating at 5 mm/sec from a 2% solution of each of the polymers: PS (carboxyl terminated, Mn = 48,000 g/mol) in chloroform, P2VP (carboxyl terminated, Mn = 53,000 g/mol) in methanol, PEG (carboxyl terminated, Mn = 5,000 g/mol) in methanol, and PAA (Mw = 100,000 g/mol) in methanol. All samples in the series showed dewetting when they were subjected to chloroform vapors. To suppress dewetting, higher molecular weight polymers were used. The second series of films was created using deposition by dip coating at 5 mm/sec from a 2% solution of each of the polymers: PS (Mn = 285,000 g/mol) in chloroform, P2VP (Mn = 150,000 g/mol) in methanol, PEG (Mn = 1,000,000 g/mol) in methanol, and PAA (Mw = 100,000 g/mol) in methanol. These polymer films exhibited no dewetting in any of the solvent vapors used throughout the research. Swelling experiments were performed right after the film deposition without cleaning the

sample as was done for the rest of the experiments, since these layers were not chemically attached to the substrates.

### 6.2.4. Film characterization techniques

Surface roughness and morphology was investigated by AFM. To find the refractive index of the grafted layers, an AFM of the profile over the scratch was performed, coupled with ellipsometry measurements (**Section 3.5.2.**) of the thick PS, P2VP, PAA, and PEG films. Next, the same measurements were performed on thin PGMA-RhB films with polymer grafting. For these measurements the refractive indexes calculated for thick polymer films were used during the ellipsometric fitting process.

Investigation of the swelling of modified PGMA-RhB films and thick one-component polymer films was performed via ellipsometry. See the detailed ellipsometric setup description in **Section 4.3.5.** First, the polymer-solvent interaction for each possible combination of polymer and solvent was studied by swelling the single thick layers of the polymers (PS, P2VP, PEG, and PAA) in the solvents used in the study (chloroform, acetone, toluene, water, and cyclohexane). Next, swelling experiments for the ultrathin polymer films were performed. The polymer solvent interaction of the one-component layer was combined to study grafting-layer interpenetration into the polymer network.

Fluorescent properties of the system were studied using the spectrophotometer. Fluorescent emission of PGMA-RhB with the grafted non-fluorescent polymer layers was measured for the dry polymer films as well as for the films subjected to the saturated vapors of organic solvents and water. The same setup as in **Chapter 5** was used. The

changes in fluorescent response upon solvent absorption were compared for the films of different composition in order to study the tuning of intensity changes with non-fluorescent polymer grafting.

## 6.3. Results and discussion

### 6.3.1. Selection of deposition technique

There are two major ways to graft non-fluorescent polymer chains to the surface of PGMA-RhB[5]. The first method is a "grafting from" technique. In this method, a polymer chain is polymerized from the initiating group on the surface of the substrate. The second method is a "grafting to" technique. In contrast to "grafting from", in this method polymer chains with functional groups are attached to the complementary groups on the substrate surface[6]. For this study, the "grafting to" method was selected, since it allows straightforward one-step surface modification using polymers with predefined properties.

It has been shown that PGMA-RhB serves as a suitable surface for such modification. As previous work performed in our group shows, after the surface attachment and crosslinking, PGMA still has a significant number of unreacted epoxy groups within its network[7]. These epoxy groups serve as attachment sites for the grafted polymer layers, providing the ability to modify the PGMA surface with polymer layers of high grafting density.

Another advantage of the "grafting to" approach is dependence of the grafting density on the time and temperature of the chain attachment reaction[8]. This important

feature not only allows grafting of polymer layers with controllable properties, but also allows grafting of mixed polymer layers to the PGMA anchoring layer[9]. This can be achieved by two subsequent surface modifications of PGMA. In this case, the first polymer is grafted at a lower grafting density, leaving some surface functional groups unreacted. Through these unreacted groups, subsequent grafting of the second polymer is performed. It was shown that mixed polymer brushes created by the "grafting to" approach have an ability to switch the surface composition through changes in the film environment[10]. This ability may further improve the sensitivity of the PGMA-RhB system in terms of the uniqueness of its fluorescent response.

### 6.3.2. Synthesis of grafted polymer layers

To start with, it was decided that two polymers with very close physical properties and chemical structures would be selected for grafting. For this purpose, carboxyl-terminated PS and P2VP were selected. These aromatic macromolecules are very similar, apart from the fact that the presence of a nitrogen atom in the aromatic pyridine ring makes P2VP more polar and basic in nature, capable of hydrogen bonding. The other two polymers chosen were carboxyl-terminated PEG, and PAA, which has long chains and a reactive group in each monomeric unit. As the chemical structure suggests, these polar polymers are significantly different from each other and also significantly dissimilar to PS and P2VP.

Dipcoating was selected as the deposition technique for PS, P2VP, and PAA, instead of the spin coating previously used in this study. Compared to spin coating, this

technique consumes less solution per deposited film[11]. Dip-coated flat substrates have a polymer coating on both sides; however, since only one side of the substrate is covered with reactive PGMA-RhB film, the deposited non-fluorescent polymer coating can be easily removed from the other side of the glass slide after grafting by washing the substrate. This ensures that there is no interference with fluorescent emission from the coating on the back side of the glass during the fluorescent measurements.

Dip-coated layers were annealed for different lengths of time and under different conditions, taking into consideration the nature of the polymer used for deposition (**Section 6.2.1.**). PS and P2VP have long polymer chains and only one reactive group per chain. This means that to attach them to a PGMA chain, they must first be diffused to some extent into the polymer film in order to reach the reactive site[12]. To facilitate polymer chain movement, a temperature higher than the glass transition temperature should be selected[13]. It is known that both polymers exhibit reduction of glass transition temperature with polymer layer thickness compared to bulk polymer[14]. Glass transition temperature for the bulk P2VP film is 93 °C[15] and for PS is 100 °C [16]. Therefore, 120 °C was selected as an annealing temperature. High annealing times (8 h) were selected for these two polymers to allow diffusion of the reactive group into the polymer film to the reaction site[9]. The glass transition temperature for PAA is 105 °C[17]; however, since each monomeric unit of PAA contains a reactive group, the annealing temperature was set to 40°C and the time was decreased to 2 h to prevent very strong crosslinking of the polymer chains[18].

With regard to PEG, dip coating has been found to be an inappropriate method of deposition. It is known that upon deposition of a thin layer of relatively short polymer chains on the substrate, dewetting usually occurs[19]. Consequently, due to the low molecular weight of the PEG chains, dewetting was observed during annealing, producing non-uniform PEG layers.

To overcome this difficulty, bulk PEG was deposited on the surface of PGMA-RhB film in the form of dry flakes. To hold the melted polymer in place and prevent dewetting upon melting, a cleaned glass slide was put on top of the PEG layer. However, even with this setup dewetting is possible if air bubbles are trapped within the polymer melt. So, the oven was vacuumed after the PEG deposition and the polymer melt was covered with the glass slide. As in the case of PS and P2VP, a long annealing time (8 h) was selected due to the fact that the reactive group is positioned at the end of the polymer chain. The melting temperature of PEG is around 70°C[20], so the PGMA-RhB-PEG film was annealed at 120°C.

### 6.3.3. Morphology of the films

The morphology of the film surface was examined by AFM (**Figure 6.2.**). Measurements showed that all polymers evenly covered the surface of the glass slides and silicon wafers. The PGMA-RhB-PS and PGMA-RhB-P2VP films showed a roughness of around 0.5 nm, whereas the PGMA-RhB-PAA and PGMA-RhB-PEG films showed a somewhat higher roughness of around 1.5 nm. The higher roughness for PAA and PEG can be explained by the ability of these two polymers to form crystals[18]. As can

be seen in **Figure 6.2.,** (d) and (e), PAA and PEG form small clusters, which increase the roughness of the grafted surface.

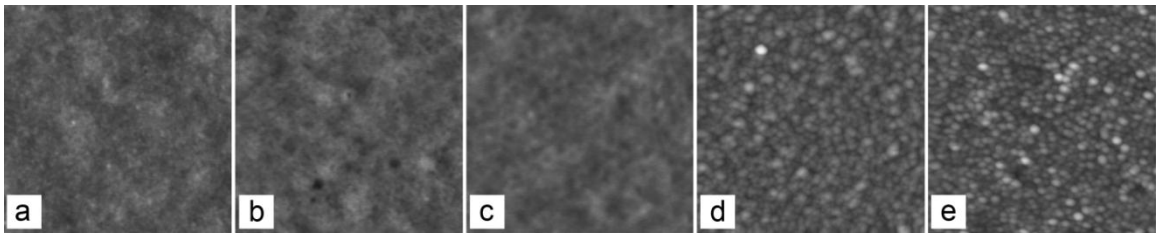


**Figure 6.2.** AFM topography images: a) PGMA-RhB film deposited on a glass slide; PGMA-RhB film grafted with b) P2VP, c) PS, d) PAA, and e) PEG. Image size: 1x1 μm. Vertical scale: a) 5 nm; b) and c) 10 nm; d)and e) 15 nm

### 6.3.4. Refractive index of the grafted polymers

It is known that the sensitivity of ellipsometry is low for thin films[21] and refractive index calculations lack precision. Therefore, to estimate the refractive index for the grafted layer, thick films of the same polymer were used.

The thickness of the layer for the refractive index estimations was at least ten times higher than the thickness of the grafted layer. Deposited thick polymer layers were examined using both AFM, with the thickness calculated from the profiling over the scratch approach (**Section 3.5.2.**)and ellipsometry. From these measurements, the thickness and refractive indexes of the films were found. The calculated refractive indexes are listed in **Table 6.1.** The values of the refractive indexes were found to be in good agreement with the results found in literature (PS[22], P2VP[23], PEG [Supplier Information], PAA[24]) for the bulk polymers. As described in **Section 4.3.4.,**this implies that the density of the polymers within the polymer film should be the same as in the bulk

material. Therefore, the same refractive indexes could be used for the ultrathin layers of these polymers grafted to the PGMA-RhB layer.

### 6.3.5. Properties of grafted layers

Using the refractive index data collected from the thick film measurements, it was possible to characterize the grafting results for the ultrathin PGMA-RhB films with modified surfaces using ellipsometry.

The thickness of the films was calculated in two steps. First, several ultrathin PGMA-RhB layers were created and their thickness was calculated to be 5 nm (see **Chapter 2** for details). The deposition procedure used in the synthesis of the PGMA-RhB layer was the same for all films in the series, so the same values of thickness were achieved for all the films.

During the next step, non-fluorescent polymer was grafted to the surface of the PGMA-RhB layer. To calculate the thickness for modified films in the dry state, ideal two-layer morphology was assumed. In this morphology, the PGMA-RhB layer and the top non-fluorescent layer have no interpenetration into each other, as schematically shown in **Figure 6.3.**

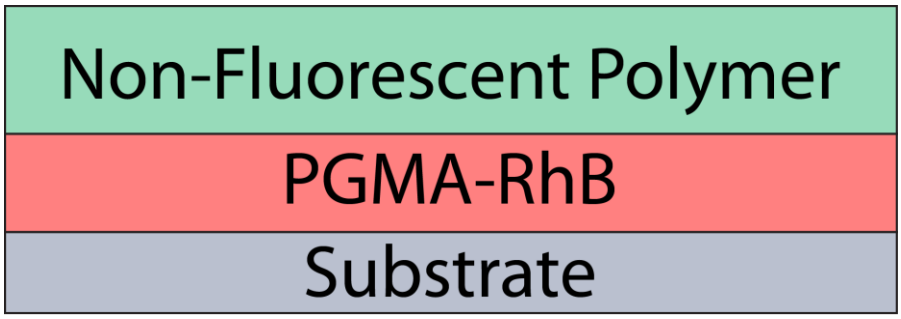


**Figure 6.3.** Structure of the PGMA-RhB film with non-fluorescent polymer grafting

For ellipsometric measurements, therefore, a two-layered structure with a known thickness and refractive index was used for the PGMA-RhB layer. The refractive index for the second layer was taken from the measurements of the thick single-layer polymer films. Therefore, the only unknown parameter was the thickness of the second grafted layer. This was determined by fitting the measurement data using the standard program supplied with the device. The resulting thickness of the grafted layer was consequently used to calculate the grafting density for the polymer chains. Calculations were performed using **Eq.3.6**. The density for the polymers was approximated as 1 $g/cm^3$.The results are summarized in **Table 6.1.**

**Table 6.1.** Parameters of film layers calculated from ellipsometry measurements

| Polymer | Refractive Index | Thickness, nm | Grafting density, chains/$nm^2$ |
|---|---|---|---|
| PGMA-RhB | 1.51 | 5 | 0.21 |
| PS | 1.58 | 14 | 0.18 |
| P2VP | 1.56 | 13 | 0.14 |
| PEG | 1.46 | 22 | 2.7 |
| PAA | 1.52 | 4 | 0.025 |

It can be seen from **Table 6.1.**that PS and P2VP, which have close molecular weights, are grafted to almost the same thickness, with close grafting density, whereas

PAA and PEG differ greatly both in grafting density and thickness. This result comes from the fact that the grafting density depends on the length of the polymer chains and the rate of polymer chain attachment to PGMA-RhB. Since PS and PVP have similar chain lengths and similar chemical structure, grafting of these two polymers occurs in a similar fashion. PAA has longer chains and it is harder for PAA to reach the grafting sites. In addition, PAA is grafted at a much lower temperature, which slows down the polymer chain diffusion and reaction rates. Consequently, the density of PAA grafting is much lower than that of the rest of polymers. In contrast, PEG has very short chains so it has the ability to move freely even when some PEG chains are already attached to the PGMA-RhB. This gives PEG the ability to have very densely packed grafting sites.

However, the two-layer model presented above is just an approximation of the real case where an intermediate phase exists between the polymer layers[25]. Even if two polymers are immiscible, they interpenetrate each other to a certain extent. This phenomenon will be addressed in **Section 6.3.9.**

### 6.3.6. Swelling of polymers used for PGMA-RhB modification

Prior to investigation of the swelling for modified PGMA-RhB films, solvent intake was studied for the thick one-component films made of the same polymers that were used for grafting. It is known that thin polymer films that are not chemically crosslinked could dewet from the substrate surface[26]. The main factor affecting the dewetting process is chain mobility; therefore, dewetting is more likely to occur for low molecular weight polymers and thin films. Also, the greater the swelling ratio of the film

in a particular solvent, the greater the driving force for dewetting, since the mobility of the chains increases.

Thus, the thickness of the layers obtained to study the swelling of the one-component uncrosslinked polymer layers was selected to be at least 10 times higher than the thickness of the layers of these polymers used for the PGMA-RhB modification. For this purpose, dip coating was used to create thick films on the surface of silicon wafers from 2% w/w solutions of the polymers. Since these films were supposed to be used for the swelling experiments, the mobility of the chains was reduced by increasing the molecular weight of the polymer. Since the interaction between the polymer and the solvent is not affected by the molecular weight of the polymer at high molecular weights[27], swelling of polymer films made of these polymers would give an estimation for the polymer-solvent interaction.

The thickness of the achieved films was: P2VP - 215 nm; PS - 175 nm; PAA - 60 nm; PEG - 140 nm. When it was certain that the polymer films from the second series would not dewet in the saturated vapors of any of the analytes used in the study, swelling experiments were performed. The swelling procedure was the same as described in **Section 5.3.4.** The results are summarized in **Figure 6.4.**The results for 5 nm PGMA film swelling were added to the plot for comparison. In can be seen from the **Figure 6.4.**that each polymer has a unique pattern of swelling in the 5 solvents used as analytes. The relative change in thickness is consistent with the nature of the polymers. For example, of all the polymers, the least polar, PS, swells the most in cyclohexane and toluene, and the

more polar P2VP, PEG, and PAA swell in water. It can be seen that for most polymers, except PAA, chloroform is a very good solvent.

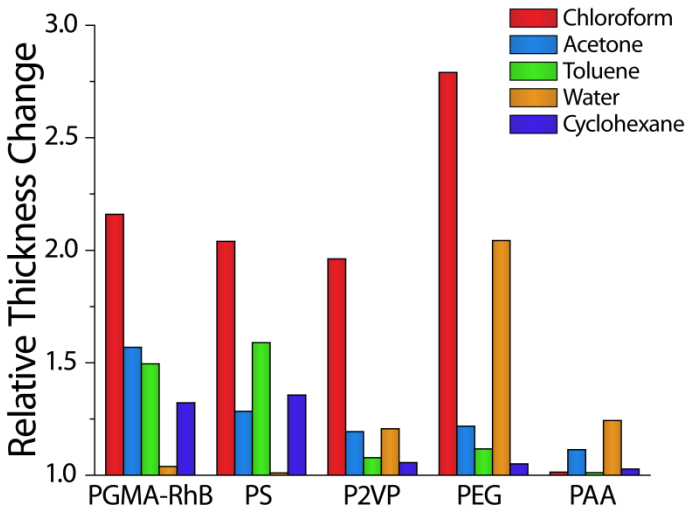


**Figure 6.4.** Relative thickness change for the single-layer polymer films in chloroform, acetone, toluene, water, and cyclohexane vapors. Relative thickness change for the 5 nm thick PGMA-RhB layer film in the same solvents is shown for comparison.

The pattern of the swelling ratios for the single polymer layers of PS, P2VP, PEG, and PAA is clearly different from that of PGMA; therefore, grafting these polymers to the ultrathin PGMA-RhB layer will likely change the swelling behavior of the PGMA-RhB and influence the amount of solvent entering the RhB sites, thus affecting fluorescence.

### 6.3.7. Effective interaction parameter

As described in **Section 5.3.5.,** using the swelling data it is possible to calculate the polymer-solvent interaction parameter, which will allow comparison of the polymer-solvent pair in terms of their affinity to one other. The swelling data presented above (**Figure 6.4.**) can be converted into effective interaction parameters using **Eq.5.8.** The

results of these calculations are presented in **Table 6.2.**below. As in the case of swelling, the effective interaction parameters for the 5 nm thick PGMA-RhB layer are included for comparison.

**Table 6.2.** Effective interaction parameters calculated for single-layer polymer films.

| | Chloroform | Acetone | Toluene | Water | Cyclohexane |
|---|---|---|---|---|---|
| PGMA-RhB | 1.039 | 1.32178 | 1.49505 | 2.15944 | 1.56864 |
| P2VP | 0.78152 | 1.16037 | 1.36426 | 1.83618 | 2.21903 |
| PS | 0.76379 | 1.20343 | 0.91682 | 3.69788 | 1.20508 |
| PEG | 0.66479 | 1.33436 | 1.69807 | 0.76315 | 2.30659 |
| PAA | 3.38935 | 1.72059 | 3.52985 | 1.27886 | 2.8107 |

As previously discussed, the higher values of interaction parameters mean poor swelling of a polymer in the particular solvent. Values from **Table 6.2.**will be used later in the chapter to compare the influence of solvents on changes in fluorescent emission intensity during the swelling of the PGMA-RhB films modified with grafting.

### 6.3.8. Swelling of the modified PGMA-RhB film

To study how the solvent intake by the film changes upon non-fluorescent polymer grafting, swelling experiments were performed for the modified PGMA-RhB layers using ellipsometry. As mentioned above (**Section 5.3.4.1.**), for the single layer it is possible to fit ellipsometric data (Ψand Δ) to find the thickness and refractive index of the film. However, during the two-layer polymer film swelling, the thickness and refractive index of both layers changes, increasing the number of unknown variables to four. It is impossible to fit ellipsometric data with four unknowns, so the following simplification was applied.

Instead of a two-layer structure, a single effective layer structure was assumed. For this effective layer, the thickness $h$ is the sum of the thicknesses of the PGMA-RhB layer $h_1$ and the grafted layer $h_2$ in the dry state. The refractive index $n$ for this layer is calculated as a linear combination of the refractive indexes of the layers[28]:

$$n = \frac{h_1}{h} n_1 + \frac{h_2}{h} n_2 \qquad \textbf{Eq. 6.1.}$$

It is known that such an assumption gives a good prediction for refractive index calculations of multilayer films, with small errors in the order of several percent[29].

Next, the measured values of Ψ and Δ were fitted in order to calculate how the thickness changes during the swelling of this single effective layer. From the swelling curves, the relative thickness change was found by fitting the swelling curve and calculating the equilibrium swelling (**Section5.3.4.3.**).

Results of these calculations are presented in **Figure 6.5.**Alterations in relative thickness changes after the grafting of P2VP and PS layers are shown in **Figure 6.5.left**. As discussed above, the main difference between the two grafted layers is in the chemical structure. It can be seen that non-polar PS molecules do not bring affinity for the polar water molecules: relative swelling for water decreases after the PS layer grafting. On the contrary, affinity for toluene increases compared to the unmodified film. The more polar P2VP molecules show a decrease in relative thickness change for toluene and cyclohexane, but an increase for water. It is noticeable that the overall relative thickness change decreases after grafting; for example, the equilibrium swelling ratio is very close for chloroform in PGMA-RhB, P2VP, and PS (**Figure 6.4.**). However, when PS and

P2VP are grafted to the PGMA-RhB layer, the relative thickness change decreases for chloroform. This can be explained by the fact that, upon grafting, additional rigidity is introduced to the PGMA-RhB film in the region of the PS attachment sites. Nevertheless, in some cases this reduction is overcome by an increased swelling ratio of the grafted polymers. This happens for the swelling of PGMA-RhB-PS in cyclohexane and PGMA-RhB-P2VP in water, where the relative thickness change actually increases upon polymer grafting.

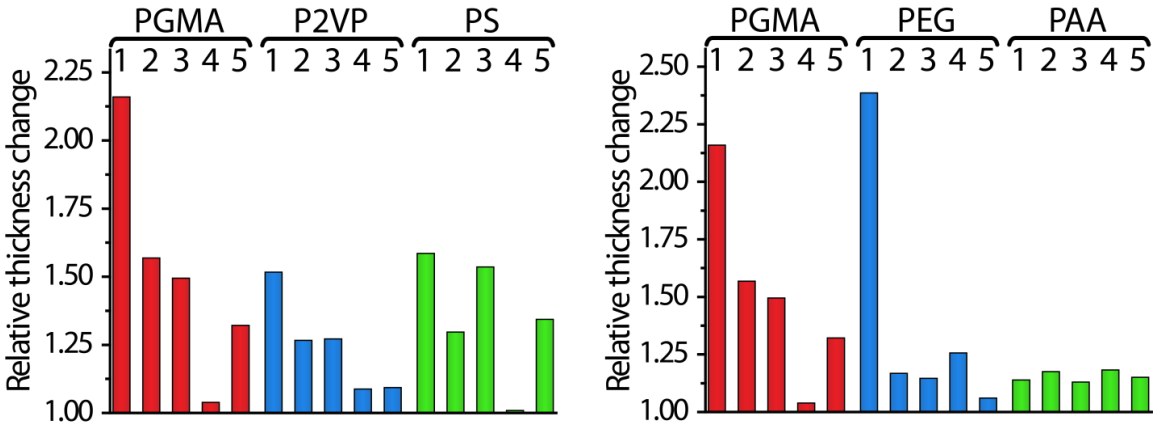


**Figure 6.5.** Relative thickness change for different layered systems. Comparison between PGMA-RhB and modified PGMA-RhB-P2VP and PGMA-RhB-PS films (Left). Comparison between PGMA-RhB and modified PGMA-RhB-PEG and PGMA-RhB-PAA films (Right). Solvents used: 1 - Chloroform, 2 - Acetone, 3 - Toluene, 4 - Water, 5 - Cyclohexane.

In **Figure 6.5.right,** the effects of PEG and PAA grafting are compared. Due to the difference in grafting density and thickness of PGMA-RhB-PEG and PGMA-RhB-PAA films, the results of the grafting of these two polymers influences the relative swelling differently. It can be seen that the overall decrease in the relative swelling ratios is again prominent, especially for PGMA-RhB-PAA. This can be explained by the

previously mentioned ability of PAA to form a "crust" on the surface of the PGMA-RhB, which decreases swelling.

Due to the high affinity of PEG to chloroform and water, the thickness of the PGMA-RhB-PEG changes more in these solvents. However, due to the fact that PEG molecules enter the PGMA-RhB network and stretch the PGMA molecules, the relative thickness change decreases for the rest of the solvents. Due to the high polarity of PAA, the relative thickness change in water increases after grafting. For the rest of the solvents, the swelling decreases.

### 6.3.9. Estimation of the thickness of the interpenetration region

As mentioned above, during the annealing of the grafted layer, chains of the attached polymer penetrate into the PGMA-RhB network. It is known that the thickness of the interpenetration region depends on the miscibility of the polymers; it is higher for the more similar chains. It is possible to estimate interpenetration zone thickness using a formula derived by Helfand and coworkers[25]:

$$D = 2a/\sqrt{6\chi} \qquad \textbf{Eq. 6.2.}$$

where$a$ is the statistical segment length and $\chi$ is the polymer-polymer interaction parameter. This interaction parameter can be estimated from the polymer solubility parameters as[30]:

$$\chi = \frac{V(\delta_1 - \delta_2)}{RT} \qquad \textbf{Eq. 6.3}.$$

where$V$ is the mean molar volume of the monomeric units of the polymers, $\delta_1$ and $\delta_2$ are the solubility parameters of both polymers in the mixture, $R$ is the gas constant, and $T$ is the temperature.

It can be seen from equations **Eq. 6.2**.and**Eq. 6.3.**that for polymers with high affinity to each other (solubility parameters are close), the interaction parameter is small and the thickness of the interpenetration zone is significant. The values for the solubility parameters were found in literature. The PGMA, PS, and PEG solubility parameters were calculated using the Askadskii method and were found to be 20.49, 18.65, and 22.01 $(J/cm^3)^{1/2}$, respectively[20]. For P2VP and PAA, the Van Krevelen method was used and the values were 21.8 and 23.6 $(J/cm^3)^{1/2}$, respectively[31]. Statistical segment length is known to be close for most vinyl polymers; therefore, a value of 0.65 nm (statistical segment length for PMMA) was used[30]. The statistical segment length for PEG (0.7 nm) was found in literature[32]. The molar volume was calculated as $V = M/\rho$, where $M$ is the molecular weight of the monomeric unit of the polymer and $\rho$ is the density. Density was assumed to be $1\ \mathrm{g/cm^3}$for all polymers.

For each polymer-polymer pair, using the mean value of the molar volumes of the components and the temperature of annealing as $T$, the interpenetration zone thickness was calculated using equations **Eq. 6.2.**and**Eq. 6.3.** The resulting values for calculated thickness were 1.48, 2.07, 0.87, and 2.07 nm for PS, P2VP, PAA, and PEG, respectively.

It is important to point out that the formula for the interpenetration thickness was derived for the case where no reaction between the polymers occurred. Since constant chemical attachment of the grafted chains to the bottom layer occurs in the case of grafting a polymer layer to the PGMA-RhB, the mobility of the chains decreases. However, **Eq. 6.2.**can still be used as an estimation to compare the grafted layers in terms of their interaction with the PGMA-RhB layer.

Comparison shows that of all four polymers, PAA has the lowest value of interpenetration region thickness, and considering the above statements, the depth of the PAA penetration is only a small fraction of the PGMA-RhB thickness. Conversely, P2VP and PEG have the highest interpenetration regions. Since the thickness of the PGMA-RhB layer is only 5 nm, this means that a substantial part of the bottom layer is penetrated by the grafting polymer; therefore, it is probable that the RhB molecules will be directly subjected to the monomeric units of the grafted layer. As hypothesized in **Chapter 5,** this could result in variations in the fluorescent emission of the PGMA-RhB layer upon swelling. This will be verified experimentally in the next section.

### 6.3.10. Fluorescent measurements for PGMA-RhB layers with surface modification

To study how the grafted layers affect the fluorescent emission intensity changes during swelling, spectrophotometry experiments were performed for the PGMA-RhB films modified with non-fluorescent polymers. All measurements and calculation

procedures were conducted in the same way as was done for the ultrathin 5 nm thick PGMA-RhB films (**Section 5.3.7.2.3.**).

First, the effect of the PS and P2VP layers, which have very similar structures, was examined (**Figure 6.6.**). In the figure, fluorescent emission changes during solvent uptake by PGMA-RhB film is compared to the modified version of the same film. It can be seen that after the polymer grafting the fluorescent response of the films changed significantly compared with the original PGMA-RhB film. There is a noteworthy difference between PS- and P2VP-modified films with respect to the fluorescent signal produced by water, chloroform, and acetone. On the other hand, the signal for toluene and cyclohexane was close for both modified films. These results prove the hypothesized ability of the grafted polymer layers to tune the reaction of the RhB to the presence of the solvent molecules.

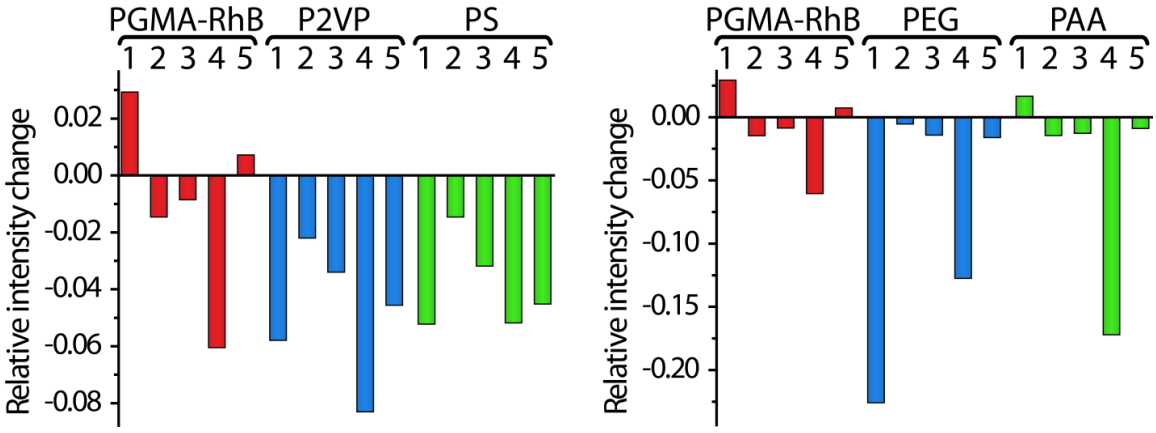


**Figure 6.6.** Effect of non-fluorescent polymer grafting on the fluorescent emission of ultrathin PGMA-RhB film.Relative intensity change after PS and P2VP (left) and after PEG and PAA (right) grafting.Solvents used: 1 - Chloroform, 2 - Acetone, 3 - Toluene, 4 - Water, 5 - Cyclohexane.

To further study this, fluorescent emission changes during solvent absorption were studied for the PGMA-RhB film with two other layers grafted: PAA and PEG. As the results show (**Figure 6.6.right**), these two polymers produce significant deviations in the fluorescent emissions from the unmodified PGMA-RhB layer upon exposure to the analytes. The fluorescent responses of PGMA-RhB-PAA and PGMA-RhB-PEG are very dissimilar between these two films, as opposed to the PGMA-RhB-PS and PGMA-RhB-P2VP pair, which showed similar trends in the solvent fingerprints.

### 6.3.11. Comparison of non-fluorescent modification effects

The fluorescent emission intensity variation discussed above needs to be examined in detail to understand the reason for the direction and magnitude of these changes. In general, the fluorescent emission intensity of the swollen polymer film is lower than that of the polymer in the dry state [33]. This is related to the flexibility of the fluorescent unit of the polymer[34]: high flexibility gives fluorophores the ability to dissipate the excited state energy non-radiatively, thus reducing its quantum yield. This explains the general trend for most of the films used in the study: upon swelling, the relative emission intensity change is negative. However, there are particular cases where this is not true; therefore, it is useful to examine the effects of surface modification on the relative emission intensity changes separately.

In the present section, relative emission intensity changes for modified derivatives of ultrathin 5 nm thick PGMA-RhB film are discussed. To compare the measured emission, the responses of the modified films are grouped by the analyte used in the

experiment. The vertical axis shows the relative intensity change measured for the 5 nm thick PGMA-RhB film modified with a particular non-fluorescent polymer. The horizontal axis shows the effective interaction parameter of the grafted polymer with the analyte. The values for the effective interaction parameters were taken from **Table 6.2.** The relative intensity change for the original PGMA-RhB film used for the modification and its interaction parameter with the analyte are added to the plot for comparison.

In this representation, according to the above discussion of effective interaction parameters, all polymers with an interaction parameter higher than that of PGMA-RhB have less affinity to the particular analyte and swell less than PGMA-RhB. Conversely, all polymers with a lower interaction parameter swell more in the same analyte. As noted in **Section 6.3.9.,** each of the polymers grafted to the initial film penetrates into the PGMA-RhB network. Therefore, the position of the particular polymer along the horizontal axis relative to the PGMA-RhB layer describes the changes in the affinity of the interpenetration zone to the analyte. Again, for all polymers with an interaction parameter higher than that of PGMA-RhB, this affinity decreases, and vice versa.

In **Figure 6.7.left,** the relative emission intensity changes for chloroform are shown. It can be seen from the figure that all of the grafted polymers with a high penetration zone thickness have a higher affinity to chloroform. This means that a high amount of the solvent will enter the interpenetration zone, bringing mobility to the polymer chains, in particular to the fluorescent units of the PGMA-RhB. It was shown in **Section 5.3.7.3.** that the quantum yield is very high for model dye in chloroform; however, in accordance with the hypothesis proposed in the last section of the previous

chapter, upon grafting non-fluorescent polymer the immediate environment around the RhB molecules changes. It was also mentioned that RhB showed low solubility in chloroform (**Section 5.3.8.**); therefore, upon swelling in chloroform vapors, RhB molecules will be mostly surrounded by the monomeric units of the grafted polymers. It can be seen from **Figure 6.7.**that the intensity decrease is greatest for PGMA-RhB-PEG, which has the highest affinity for chloroform; therefore it swells more and brings the most flexibility to the RhB molecules, increasing the probability of non-radiative relaxation to the excited RhB molecules. The PEG-modified film is followed by PGMA-RhB-P2VP and PGMA-RhB-PS, which have a lower affinity to chloroform and, therefore, a less prominent intensity decrease. As calculations show, PAA does not penetrate as much into the PGMA-RhB network and, in addition, it has lower affinity to chloroform, so the intensity change for PGMA-RhB-PAA is very close to that of the initial PGMA-RhB film.

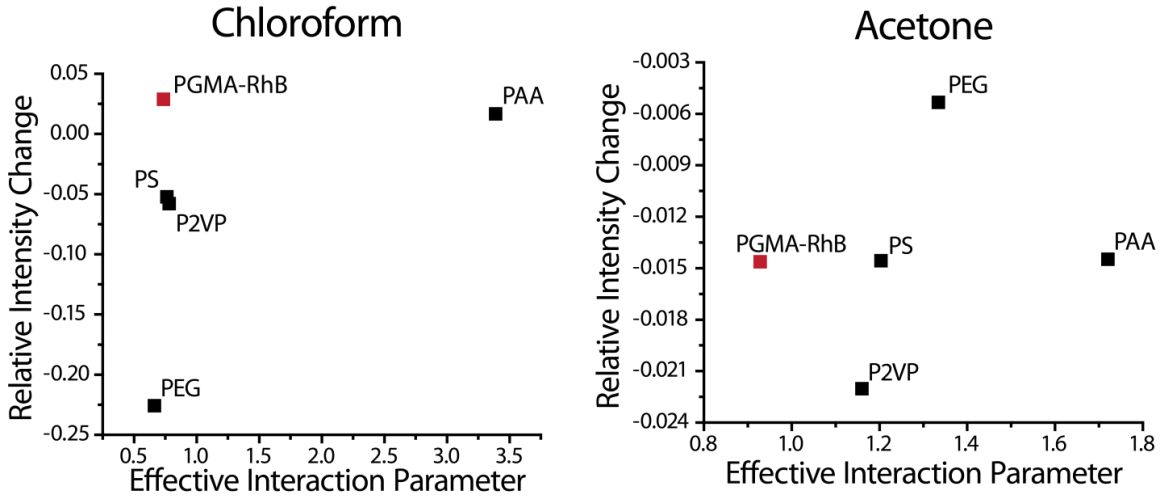


**Figure 6.7.** Relative intensity change variation after the modification of ultrathin PGMA-RhB dependence on the affinity of the grafted polymers to chloroform (left) and acetone (right). Value for PGMA-RhB layer is added for comparison.

Results for acetone are presented in **Figure 6.7.right**. The quantum yield in acetone (0.48) is much lower than for chloroform; therefore, the intensity of the emission decreases for all of the films. In addition, as opposed to chloroform, RhB itself is soluble in acetone, which favors the presence of acetone in the RhB environment. However, the amount of chain flexibility brought by the swelling in acetone is much lower compared to chloroform, due to the lower affinity of all the polymers to this solvent.

It can be seen that after grafting PS and P2VP, which swell more in acetone, there is additional flexibility and a greater amount of solvent reaches the PGMA-RhB layer, which decreases the relative intensity change. For PGMA-RhB-PEG, the intensity is not as low because less acetone enters the film due to the lower affinity of PEG to that solvent. The affinity of PAA to acetone is higher compared to PGMA-RhB; however, due to minimal penetration and increased rigidity (PAA forms a high number of crosslinks on the PGMA surface), the PAA grafting shows almost no effect on the fluorescent emission.

The situation for toluene is very close to that of chloroform (**Figure 6.8.**).The quantum yield is relatively high for toluene (0.8) and RhB itself is not soluble in toluene. However, the main difference between the two is that the affinity of the PGMA-RhB layer to toluene is much lower. For the grafted polymers with a higher affinity to toluene (PS and P2VP), more toluene is introduced to the film and the intensity decreases. For the polymers with low affinity (PEG and PAA), the intensity decrease is not as prominent.

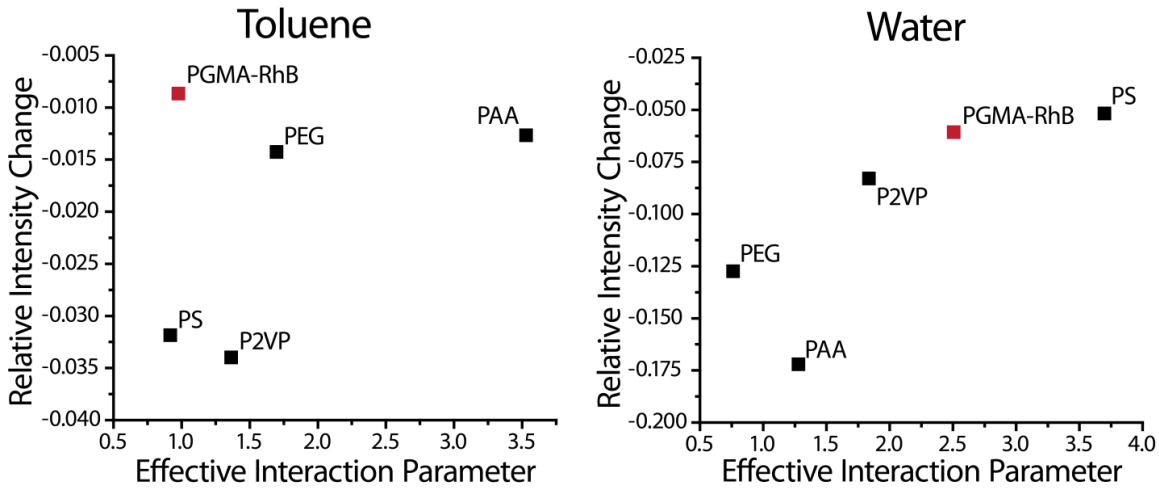


**Figure 6.8.** Relative intensity change variation after the modification of ultrathin PGMA-RhB dependence on the affinity of the grafted polymers to toluene (left) and water (right). Value for PGMA-RhB layer is added for comparison.

Water gives the pronounced intensity decrease for a single PGMA-RhB layer due to two factors: the low quantum yield of model dye in water (0.06) and the fact that water is the best solvent for RhB. However, since the PGMA-RhB network has a poor affinity to water, a single PGMA-RhB layer has low water content even in equilibrium with saturated water vapor. **Figure 6.8.right** shows that upon grafting of the polymers that have a high affinity to water (PEG and PAA), it is possible to increase the water content within the film, thus decreasing the relative intensity change. The effect of PAA is higher compared to PEG. This may be explained by the fact that PEG penetrates more into the PGMA-RhB network, partially shielding the RhB molecules from the water, whereas PAA increases the water content within the film without much interaction with the PGMA-RhB network. PS swells the least in water; therefore, this polymer protects the

RhB molecules from water, so the lowest intensity decrease is observed in the PGMA-RhB-PS system subjected to water vapors.

For cyclohexane (**Figure 6.9.**), the relative intensity changes are very similar to those for toluene and chloroform (with the exception of an even lower quantum yield (0.1) and swelling for most of the polymers): as the effective interaction parameter increases, less solvent enters the polymer film and the intensity decrease upon swelling is lower. For the most polar polymers, PAA and PEG, the changes are approaching zero. The highest change is observed for the PGMA-RhB-RS system, which swells the most in cyclohexane.

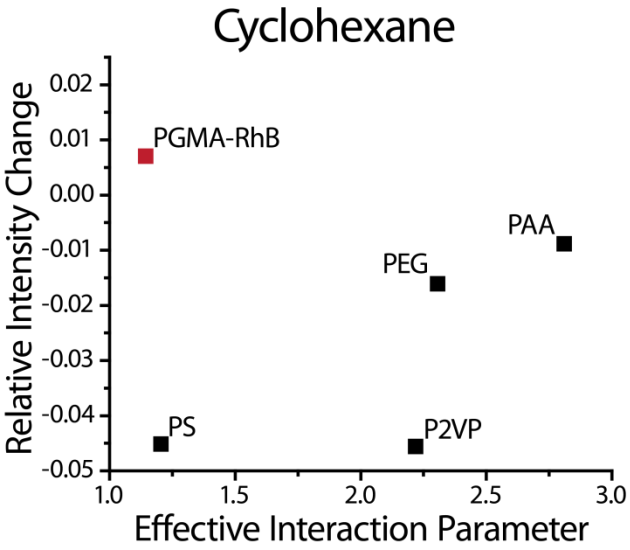


**Figure 6.9.** Relative intensity change variation after the modification of ultrathin PGMA-RhB dependence on the affinity of the grafted polymers to cyclohexane. Value for PGMA-RhB layer is added for comparison

Overall, the general trend is consistent in all of the experiments listed above: high affinity to the analyte, together with high penetration depth, increases the solvent content

within the film and the chain flexibility. These factors in turn cause a decrease in the emission of the fluorescent units of the PGMA-RhB film.

There is yet another way to represent the data from the emission intensity measurements. **Figure 6.10.**shows all fluorescent experiments combined on one plot, with results rearranged to group responses to the same solvent. An important conclusion can be made from this plot: for the set of five different films, the "fingerprint" response to each of the solvents used in the present study is unique and completely distinguishable from the others. This suggests that the proposed technique of tuning the fluorescent reaction of the fluorophores to environmental changes could be used in applications where environmental identification is needed.

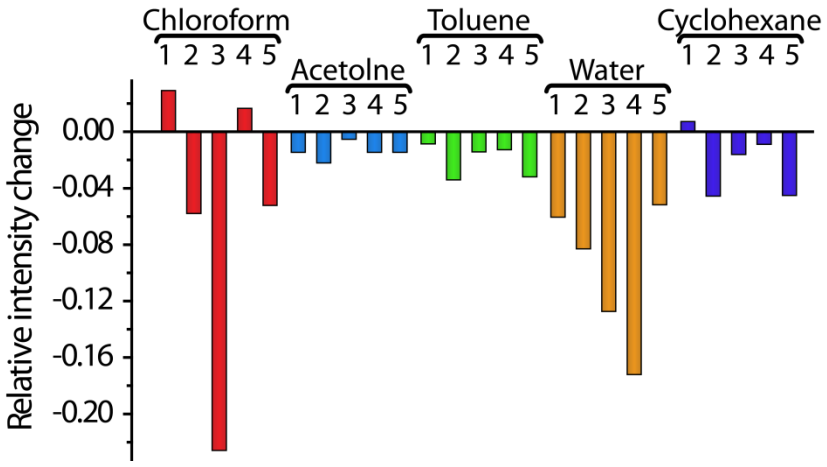


**Figure 6.10.** Relative intensity change grouped by the solvents used in the measurements. The fluorescent films used in the experiments were: 1 – PGMA-RhB, 2 – PGMA-RhB-P2VP, 3 – PGMA-RhB-PEG, 4 – PGMA-RhB-PAA, 5 – PGMA-RhB-PS.

### 6.5. Conclusions

Thin grafted layers were deposited onto the surface of ultrathin PGMA-RhB films via dip coating. The deposited layers had low roughness and evenly covered the surface

of the PGMA-RhB film. The properties of the grafting layers, such as thickness, grafting density, and presence of the interpenetration region were examined via ellipsometry. The parameters necessary for fitting ellispometric data were obtained utilizing thick films made of the same polymers that were used for the grafting.

From the swelling experiments, solvent affinity to the polymers used in the study was calculated in terms of the effective interaction parameter. Calculations involving polymer-polymer interactions revealed the presence of the interpenetration region in the two-layer modified PGMA-RhB films.

The spectrophotometry measurements for the modified PGMA-RhB films confirmed the hypothesis that non-fluorescent polymer films grafted to the surface of ultrathin fluorescent films influence the emission of the fluorophores embedded in the prime layer. Results showed that the similar polymers, PS and P2VP, produced similar changes in the pattern of the emission response of PGMA-RhB film, while the dissimilar polymers, PAA and PEG, showed very diverse changes for each of the solvents. Close studies on the nature of the fluorescent emission changes revealed complex influence of the solvent-dye and solvent-polymer interactions of the fluorescent emission of the modified films. Changes in the affinity of the PGMA-RhB film to the solvent, caused by the surface modification, strongly influenced the fluorescent response of the film.

Another important result was the uniqueness of the pattern of responses for each of the analytes. This feature allows the use of presented response-tuning technique for substance identification applications.

## 6.4. References


1. Keddie, J. L.; Jones, R. A. L.; Cory, R. A., Interface and surface effects on the glass-transition temperature in thin polymer films. *Faraday Discussions* **1994,** *98*, 219-230.

2. Zdyrko, B.; Klep, V.; Luzinov, I., Synthesis and Surface Morphology of High-Density Poly(ethylene glycol) Grafted Layers. *Langmuir* **2003,** *19* (24), 10179-10187.

3. Chyasnavichyus, M.; Tsyalkovsky, V.; Zdyrko, B.; Luzinov, I., Tuning Fluorescent Response of Nanoscale Film With Polymer Grafting. *Macromolecular Rapid Communications* **2012,** *33* (3), 237-241.

4. Christodoulou, K. N.; Lightfoot, E. J.; Powell, R. W., Model of stress-induced defect formation in drying polymer films. *AIChE Journal* **1998,** *44* (7), 1484-1498.

5. Minko, S., Grafting on Solid Surfaces: "Grafting to" and "Grafting from" Methods
Polymer Surfaces and Interfaces. Stamm, M., Ed. Springer Berlin Heidelberg: 2008; pp 215-234.

6. Zdyrko, B.; Luzinov, I., Polymer Brushes by the "Grafting to" Method. *Macromolecular Rapid Communications* **2011,** *32* (12), 859-869.

7. Zdyrko, B.; Swaminatha Iyer, K.; Luzinov, I., Macromolecular anchoring layers for polymer grafting: comparative study. *Polymer.* **2006,** *47* (1), 272-279.

8. Liu, Y.; Klep, V.; Zdyrko, B.; Luzinov, I., Synthesis of High-Density Grafted Polymer Layers with Thickness and Grafting Density Gradients. *Langmuir* **2005,** *21* (25), 11806-11813.

9. Ionov, L.; Sidorenko, A.; Stamm, M.; Minko, S.; Zdyrko, B.; Klep, V.; Luzinov, I., Gradient Mixed Brushes: "Grafting To" Approach. *Macromolecules* **2004,** *37* (19), 7421-7423.

10. Minko, S., Responsive Polymer Brushes. *Journal of Macromolecular Science, Part C: Polymer Reviews* **2006,** *46* (4), 397-420.

11. Bhuiyan, M. S.; Paranthaman, M.; Salama, K., Solution-derived textured oxide thin films—a review. *Superconductor Science and Technology* **2006,** *19* (2), R1.

12. Jones, R. A. L.; Lehnert, R. J.; Schonherr, H.; Vancso, J., Factors affecting the preparation of permanently end-grafted polystyrene layers. *Polymer* **1999,** *40* (2), 525-530.

13. Luzinov, I.; Klep, V.; Minko, S.; Iyer, K. S.; Draper, J.; Zdyrko, B., Synthesis of responsive polymer brushes via macromolecular anchoring layer. *Abstr. Pap. Am. Chem. Soc.* **2004,** *227*, U509-U509.

14. (a) Efremov, M. Y.; Olson, E. A.; Zhang, M.; Allen, L. H., Glass transition of thin films of poly(2-vinyl pyridine) and poly(methyl methacrylate): nanocalorimetry measurements. *Thermochimica Acta* **2003,** *403* (1), 37-41; (b) Jiang, Q.; Lang, X. Y., Glass Transition of Low-Dimensional Polystyrene. *Macromolecular Rapid Communications* **2004,** *25* (7), 825-828.

15. Papadopoulos, P.; Peristeraki, D.; Floudas, G.; Koutalas, G.; Hadjichristidis, N., Origin of Glass Transition of Poly(2-vinylpyridine). A Temperature- and Pressure-Dependent Dielectric Spectroscopy Study. *Macromolecules* **2004,** *37* (21), 8116-8122.

16. Krevelen, D. W. v.; Nijenhuis, K. t. Properties of polymers their correlation with chemical structure; their numerical estimation and prediction from additive group contributions.

17. Maurer, J. J.; Eustace, D. J.; Ratcliffe, C. T., Thermal characterization of poly(acrylic acid). *Macromolecules* **1987,** *20* (1), 196-202.

18. Li, Z. Protein interactions with mixed poly(ethylene glycol)/polyacrylic acid brushes.

19. Henn, G.; Bucknall, D. G.; Stamm, M.; Vanhoorne, P.; Jérôme, R., Chain End Effects and Dewetting in Thin Polymer Films. *Macromolecules* **1996,** *29* (12), 4305-4313.

20. Zdyrko, B.; Swaminatha Iyer, K.; Luzinov, I., Macromolecular anchoring layers for polymer grafting: comparative study. *Polymer* **2006,** *47* (1), 272-279.

21. Fujiwara, H., *Spectroscopic ellipsometry : principles and applications*. John Wiley & Sons: Chichester, England; Hoboken, NJ, 2007.

22. Ashby, M. F.; Shercliff, H.; Cebon, D., *Materials : engineering, science, processing and design*. Butterworth-Heinemann: Oxford, 2007.

23. Tam, T. K.; Ornatska, M.; Pita, M.; Minko, S.; Katz, E., Polymer Brush-Modified Electrode with Switchable and Tunable Redox Activity for Bioelectronic Applications. *The Journal of Physical Chemistry C* **2008,** *112* (22), 8438-8445.

24. Gooch, J. W. Encyclopedic dictionary of polymers. http://www.myilibrary.com?id=135062.

25. Broseta, D.; Fredrickson, G. H.; Helfand, E.; Leibler, L., Molecular weight and polydispersity effects at polymer-polymer interfaces. *Macromolecules* **1990,** *23* (1), 132-139.

26. Gabriele, S.; Damman, P.; Sclavons, S.; Desprez, S.; Coppée, S.; Reiter, G.; Hamieh, M.; Akhrass, S. A.; Vilmin, T.; Raphaël, E., Viscoelastic dewetting of constrained polymer thin films. *Journal of Polymer Science Part B: Polymer Physics* **2006,** *44* (20), 3022-3030.

27. Wolf, B.; Wolf, B. A.; Enders, S., Making Floryr–Huggins Practical: Thermodynamics of Polymer-Containing Mixtures
Polymer Thermodynamics. Springer Berlin / Heidelberg: 2011; Vol. 238, pp 1-66.

28. Tikhonravov, A. V.; Trubetskov, M. K.; Amotchkina, T. V.; Kokarev, M. A.; Kaiser, N.; Stenzel, O.; Wilbrandt, S.; Gдbler, D., New optimization algorithm for the synthesis of rugate optical coatings. *Appl. Opt.* **2006,** *45* (7), 1515-1524.

29. Miller, M. D.; Bruening, M. L., Correlation of the Swelling and Permeability of Polyelectrolyte Multilayer Films. *Chemistry of Materials* **2005,** *17* (21), 5375-5381.

30. Sperling, L. H., *Introduction to physical polymer science*. Wiley: New York, 1986.

31. Yu, K.; Wang, H.; Xue, L.; Han, Y., Stimuli-Responsive Polyelectrolyte Block Copolymer Brushes Synthesized from the Si Wafer via Atom-Transfer Radical Polymerization. *Langmuir* **2006,** *23* (3), 1443-1452.

32. Zhang, H.-Y.; Hill, R. J., Lipopolymer electrophoresis in supported bilayer membranes. *Soft Matter* **2010,** *6* (21), 5625-5635.

33. Fikry, M.; Omar, M. M.; Ismail, L. Z., Effect of host medium on the fluorescence emission intensity of rhodamine B in liquid and solid phase. *J Fluoresc Journal of Fluorescence* **2009,** *19* (4), 741-746.

34. Ronova, I. A.; Pavlova, S. S. A., The effect of conformational rigidity on several physical properties of polymers. *High Performance Polymers* **1998,** *10* (3), 309-329.

# CHAPTER SEVEN

# EFFECT OF NON-FLUORESCENT GRAFTED POLYMER LAYER THICKNESS AND COMPOSITION ON THE RESPONSE OF THE FLUORESCENT LAYER

## 7.1 Introduction

It was demonstrated (**Chapter 6)** that grafting of non-fluorescent polymers to the surface of the PGMA-RhB layer changes the optical response of one-component PGMA-RhB film to the saturated vapor of solvents. As it was concluded in **Section 6.3.11.**,grafting non-fluorescent polymers to the surface of PGMA-RhB affects emission intensity in two possible ways. First, it changes the affinity of the solvent to the modified PGMA-RhB film, thus changing the swelling of the film. Second, depending on the nature of the solvent, it either shields or exposes fluorescent units of the PGMA-RhB to the solvent molecules.

The next question arises: Is it possible to tune the effect of the grafting layer on the fluorescent properties of the PGMA-RhB film? The ability to perform such tuning would be beneficial for prospective applications. For example, with such a tuning it might be possible to maximize the polymer layer sensitivity to the particular analyte in the mixture by increasing the magnitude of the fluorescent response changes upon solvent intake. This method is known to be used in the detection of explosives[1]. Conversely, one could design a grafting that would reduce the systems sensitivity to the components of the mixture that do not need to be detected. This technique was used in the work of Liu et al.[2]. However, in most cases such tuning is done by chemical modification of the host material. With the method described in the present work, it could be done without

chemical modification of the matrix polymer or fluorescent molecules with straightforward grafting of premade material. This method of tuning may also make it possible to generate an array of fluorescent films with unique fluorescent responses using one polymer for the grafting.

The tuning proposed above can be realized in several ways. The first possible method is to vary the amount of the polymer grafted to the surface. This can be done using the fact that the chemical reaction between the fluorescent polymer and the polymer being grafted is not instantaneous; it takes place over a period of time. Therefore, by varying the rate of the reaction or the reaction time, it is possible to graft different amount of the material to the anchoring fluorescent layer [3]. In addition, mobility of the polymer chains can be adjusted by varying the molecular weight of the polymer. This will affect the reaction rate, as shorter molecules reach reaction sites faster than longer ones[4]. Moreover, variations in the grafted polymer chain length will also change the thickness of the interpenetration zone, where the grafted chains penetrate deeper to the fluorescent polymer layer since shorter molecules have a greater ability to diffuse deeper into the base layer network[5].

The second possible method to change the fluorescent properties of the base fluorescent layer is to modify its nature by grafting the mixed polymer layer[6]. Polymer film created in this way is shown schematically in **Figure 7.1.** In this method, two or more different polymers are grafted to the same fluorescent polymer layer. This is done by sequential grafting of the polymers to the reactive layers surface[7]. With grafting of the mixed polymer layer, fluorescent emission of the base layer can be subjected to the

multiple effects brought by each of the grafted polymers. In addition, the ratios between the polymers can be varied in the same way as was described for single polymer grafting since each of the polymers is grafted to the base layer separately.

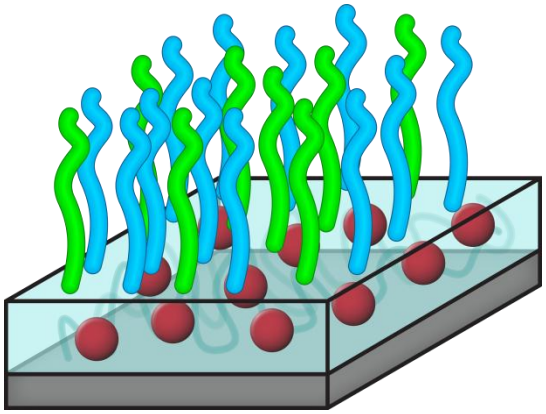

**Figure 7.1.** Schematic of the mixed polymer layer grafted to the surface of the PGMA-RhB.

In this part of the work, variation in the grafted layers properties (thickness and composition) on the PGMA-RhB films fluorescent emission response to the several analytes is examined. Specifically, the effects of changes in both the amount of the grafted polymer and its nature are studied. PS and P2VP macromolecules were selected for the variation. Grafted layers of these two polymers with different grafting densities as well as mixed grafted layers were obtained. During the grafting of each of the polymers, the reaction time was varied to create grafted layers of different grafting densities.

Fluorescent properties of the PGMA-RhB films with the different grafted layers were studied using spectrophotometry in a saturated vapor of chloroform, acetone, toluene, water, and cyclohexane. It was observed that the fluorescent response of the film varied significantly with the nature and the thickness of the grafting layer for several

solvents, confirming the validity of the proposed technique for tuning fluorescent responses of base polymer layers.

## 7.2. Experimental

### 7.2.1. Deposition of PGMA-RhB film

Base layer for the grafting of non-fluorescent polymers was created using PGMA-RhB with Mn=405,000 g/mol and polydispersity 3.81. The same deposition technique described in **Section 5.2.1.**was used. The thickness of the PGMA-RhB layer was 6.5 nm.

### 7.2.2. One-component grafted layer

Carboxyl terminated PS (48,000 g/mol) and carboxyl terminated P2VP (53,000g/mol) were used for the grafting. Layers of the polymers were deposited onto the surface of the PGMA-RhB layer by dipcoating at 5 mm/sec. PS was deposited from a 1% solution in chloroform and P2VP was deposited from 1% solution in MEK. Variation of grafting density for the non-fluorescent polymer was achieved by annealing polymer films at different times. A temperature of 120 °C was used for annealing in a vacuum oven (**Section 6.2.1.**)

After the annealing, unattached polymer chains were removed by rinsing the substrates covered with the polymer films in good solvents for the grafted layers (chloroform for PS and methanol for P2VP) three times for 30 min each.

### 7.2.3. Grafting of mixed polymer layers

Mixed polymer layers were deposited using a technique described elsewhere[7]. In brief, the first series of the PGMA-RhB films with PS layers of various grafting densities was created using the method described above (**Section 7.2.2.**). Next, the P2VP layer was deposited by dipcoating at 5 mm/sec from a 1% solution of P2VP in methanol. The resulting film was annealed at 120°C in a vacuum oven for 8h to graft P2VP at the maximum possible density. After the annealing, unattached polymer chains were removed by rinsing the substrates covered with the polymer films in methanol three times for 30 min each.

### 7.2.4. Characterization of polymer film

The thickness of the films was examined with ellipsometry, and surface morphology was studied using AFM.

The films fluorescent properties and variations in the emission intensity in vapor of chloroform, acetone, and cyclohexane were studied by spectrophotometry using the same procedure described in **Section 5.2.3.**

### 7.2.5. Modification of the PGMA-RhB-P2VP with gold nanoparticles

Samples with 6.5 nm thick PGMA-RhB layer and 11, 8.5, and 5.3 nm thick P2VP grafting were used. Attachment of the gold nanoparticles (Sigma-Aldrich Co. LLC.) of 7-10 nm in size was performed in suspension at room temperature for 48 h. After the attachment grass slides were rinsed three times for 30 min in DI water.

## 7.3. Results and discussion

### 7.3.1. Selection of the polymers for variations in grafted layer properties

For the investigation of the variation in the grafted layers properties on the PGMA-RhB layers fluorescent emission response, PS and P2VP were selected. These were the same polymers as were used in **Chapter 6**. As discussed above (**Section 6.3.2.**), these two polymers of different polarities possess similar physical properties; therefore, grafted layers of the two polymers will have a similar morphology. It was also demonstrated above that the grafting of these two polymers dramatically changes the fluorescent response of the PGMA-RhB layer (**Section 6.3.11.**).

These two polymers are also well suited for the investigation of the mixed grafting effect on the fluorescent properties of PGMA-RhB, since, due to the similarities discussed above, there will be no dramatic property variations in the mixed layer consisting of these two polymers.

The PS-P2VP mixed grafted layer is a well-studied system with known behaviors[8]. Due to the immiscibility between the two polymers at room temperature, there is a local phase separation between the two polymers after grafting. In addition, selective swelling of one of the polymers can be observed while the chains of the other will remain a shrunken state[9]. If such behavior of the grafted layer has the potential to influence fluorescent characteristics of the base fluorescent layer, one could significantly enhance the systems selectivity for mixture analysis.

### 7.3.2. Deposition and characterization of grafted layer

#### 7.3.2.1. One component polymer layers

It is well known that by varying the annealing temperature, it is possible to graft polymer layers to a different grafting density[10]. It is also possible to vary the grafting density by annealing polymers at the same temperature but at different times[11]. Due to the possible temperature gradients inside the oven used for the annealing, the latter method of grafting density variation was selected.

After the unattached polymer chains were removed, the grafted layers surface morphology was examined with AFM. Results showed no significant variation in the roughness of layers related to the annealing time. In fact, all calculated roughness values were virtually the same as those of the layers grafted to the maximum grafting density studied in **Section 6.3.3.**

The grafting layers thickness was measured by ellipsometry. Results of these measurements are shown in **Figure 7.2.** It can be seen from the measurements for the both PS and P2VP grafted layers that the chain attachment rate decreases over time. This phenomenon can be explained by the consumption of the reactive sites for the grafted polymers. Thus, at the long grafting times most initially active attachment sites are already occupied by polymer chains, and it is harder for the additional polymer chains to diffuse for the remaining unreacted epoxy groups. Moreover, already attached polymer chains become less mobile, and the grafting process slows down even more at latter stages.

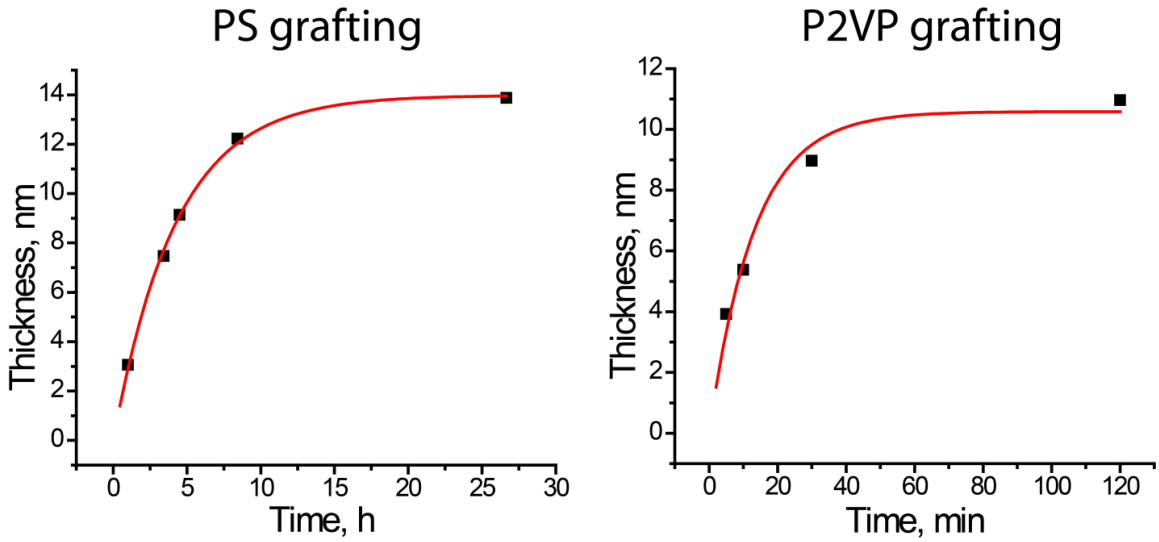


**Figure 7.2.** Thickness of PS (left) and P2VP (right) grafted layers attached to 6.5 nm thick PGMA-RhB film. Black squares represent the ellipsometry measurements; solid lines represent results of the curve fitting with **Eq.7.1.**

A comparison of the two types of grafted polymers shows that the rate of the P2VP attachment is much higher than that of PS. This can be explained by the basic nature of P2VP chains, which are known to catalyze the reaction between carboxylic and epoxy groups[12].

Mathematically, the dependence of the thickness $y$ of grafted layers with time $t$ can be expressed in the form:

$$y = P_1(1 - e^{-P_2 t}) \qquad \textbf{Eq.7.1.}$$

where$P_1$and $P_2$ are the fitting parameters. $P_1$describes the maximum grafted layer thickness and $P_2$ describes the rate of the chain attachment. The measured thickness of grafted layers was fitted with **Eq.7.1**. Resulting curves for both polymers are shown as solid lines in **Figure 7.2.** Using these curves it is possible to graft layers of PS and P2VP

of necessary thickness constrained by the maximum grafting thickness for a particular polymer.

To estimate the thickness of the penetration zone, an assumption was made that the penetration depth for the grafted polymer chains increases in the same fashion as the thickness of the grafting layer, reaching the value calculated in **Section 6.3.9.**at the infinite time of grafting. Mathematically, this can be described by **Eq.7.1.**with parameter $P_1$ equal to the maximum penetration depth (1.48 nm for PS and 2.07 nm for P2VP) and the same parameter $P_2$ that was estimated for the changes in thickness. Results of the calculation are shown in **Figure 7.3.**

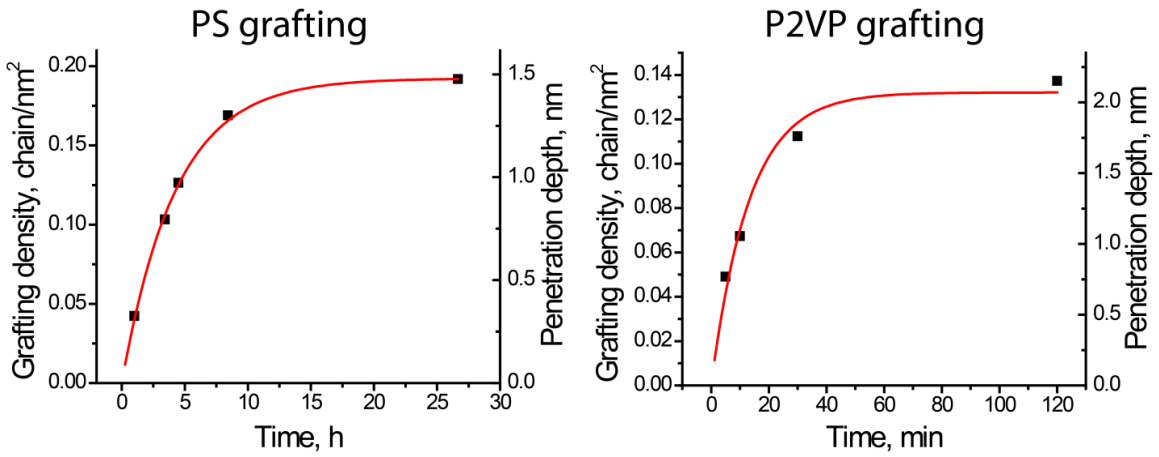


**Figure 7.3.** Variations in grafting density and chain penetration depth with time for PS (left) and P2VP (right)

Grafting density calculations were performed in the same manner as in **Section 6.3.5** using **Eq.3.6.**Results are plotted in **Figure 7.3.** It can be seen that at short annealing times, grafting density and penetration depth are well below the maximum levels for both polymers.

#### 7.3.2.2. Mixed polymer layers

After PS grafting at short annealing times, the non-reactive epoxy groups in the PGMA-RhB network can be used for the P2VP attachment. The previously reported technique was used for the mixed brush application[7]. First, a series of films with PS grafted at different grafting densities was synthesized. Next, a P2VP layer was applied to the film and annealed. During annealing, P2VP chains diffused through the grafted PS chains to the reaction sites. Thus, films with both PS and P2VP chains attached to the PGMA-RhB at various ratios were created. The same series of PGMA-RhB-PS films as shown in **Figure 7.2.left** and **Figure 7.3.left** was used for P2VP attachment.

**Figure7.4.**shows AFM images of a series of PGMA-RhB films with PS-P2VP grafting. The thickness of the P2VP layer was measured with ellipsometry as an addition to the thickness of the PGMA-RhB-PS layer used for grafting.

It can be seen from the figure that the phase separation occurs between PS and PVP as these polymers are immiscible[7]. When the amount of PS is low (top left), it forms islands that extend from the continuous P2VP phase. As the concentration of PS increases, these islands grow in the continuous phase (**Figure 7.4.** top right). When the thickness of the grafted layer of PS reaches 12 nm (grafting density of PS at this point is 0.17 chains/$cm^2$), the attached P2VP chains are almost completely hidden below the PS layer (bottom left). After PS is grafted to the highest grafting density of the series (bottom right), the amount of grafted P2VP becomes so small that the interphase region between PS and P2VP cannot be observed from the image.

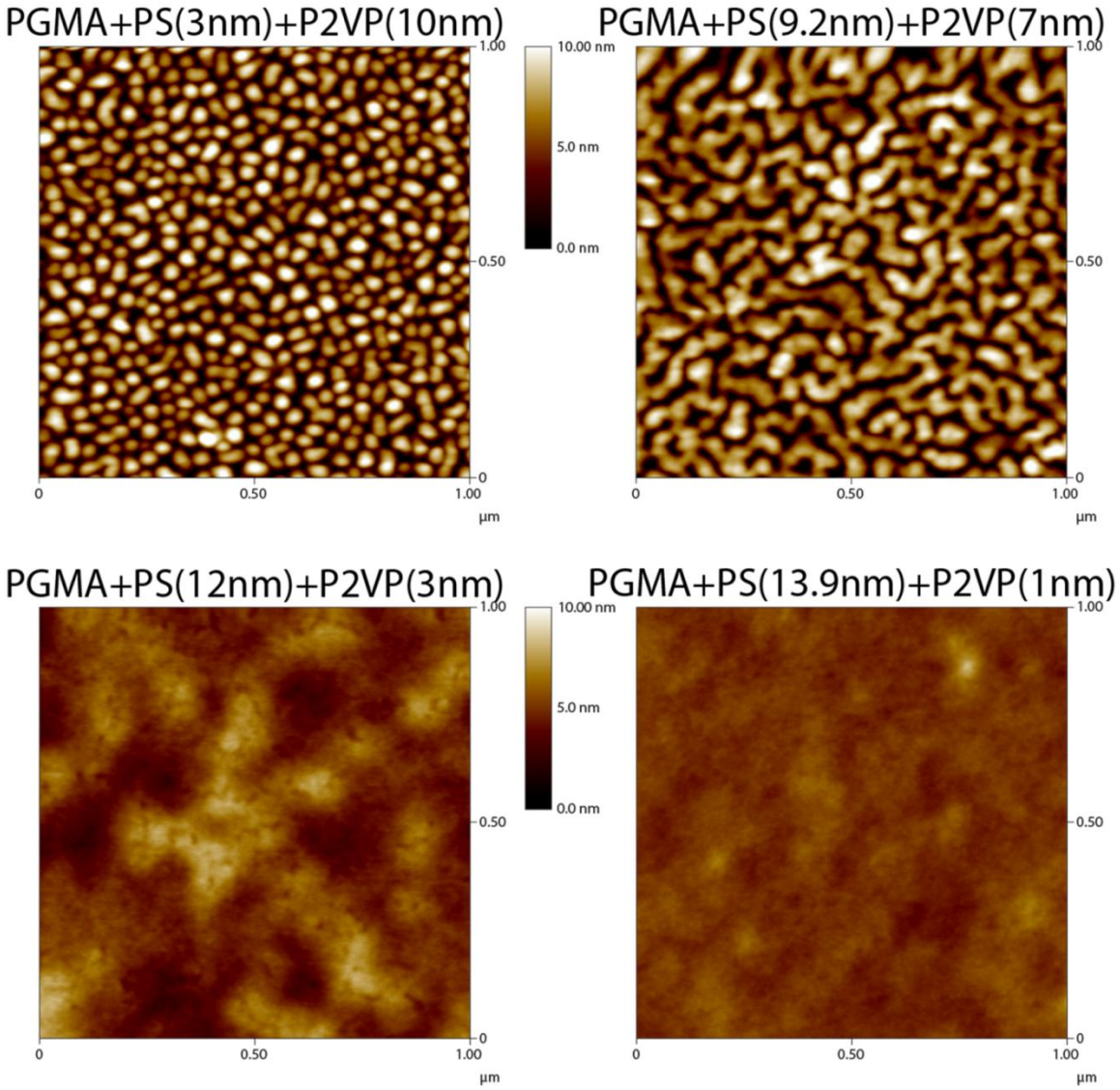


**Figure 7.4.** AFM images of mixed layers of PS-P2VP grafted to the surface of 6.5 nm thick PGMA-RhB film at various ratios after treatment with chloroform.

### 7.3.3. Fluorescent measurements

#### 7.3.3.1. Variations in the grafted layers thickness

Fluorescent emission of the PGMA-RhB films modified with PS and P2VP at different grafting densities and mixed layers of these polymers was measured in both the

dry state and the saturated vapor of several solvents using spectrophotometry. To compare the effect of grafting density variations on the signal change during vapor intake, chloroform and acetone were selected. The relative intensity change was calculated as described in **Section 5.3.7.2.3.**Results for the swelling of PS and P2VP modified PGMA-RhB films in chloroform are shown in **Figure 8.5.** It can be seen from the figure that as the amount of the grafted polymer increases, the relative intensity change decreases. However, for both polymers there is a small initial increase in intensity. Such behavior can be explained by the presence of the two competing effects of brush grafting on emission intensity.

As discussed in **Section 6.3.11.**, the first effect is related to the increase in the PGMA-RhB films rigidity upon grafting of the polymer layer. Increased rigidity lowers the chains mobility in the swollen state, thus reducing the emission intensity drop upon film swelling. The second effect is related to the presence of monomeric units of the grafted polymer, which can influence fluorescence in the swollen state in good solvents when polymer chains are mobile.

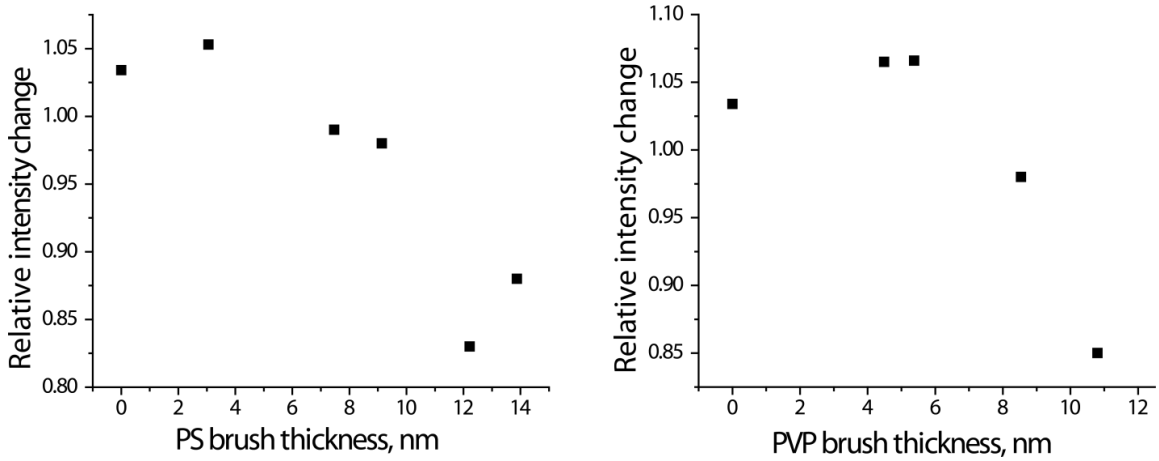


**Figure 7.5.** Relative intensity change in saturated acetone vapor vs. thickness of the grafted layer of PS (left) and P2VP (right) grafting to 6.5 nm thick PGMA-RhB film.

When a smaller amount of polymers is grafted to the PGMA-RhB film, the penetration depth for the grafted layers is low (**Figure 7.3.**) so there is little change in the RhB molecules immediate environment. However, small increase in the polymer networks rigidity cause small intensity increase. When more polymer is grafted (**Figure 7.5)** for both grafted polymers, the intensity goes down, which indicates that upon swelling more PS and P2VP monomeric units decrease chloroform contact with RhB molecules, decreasing the intensity of the emission. It needs to be pointed out that since both polymers have very similar physical properties and have a similar affinity to the PGMA and chloroform, the relative intensity changes dependence on thickness is quite similar for these two polymers.

The relative intensity change in the acetone vapor for the same modified films is shown in **Figure7.6.** It can be seen that the results are similar to the relative intensity change induced by chloroform vapors (**Figure 7.5.**). When no polymer is grafted to the PGMA-RhB system, the relative intensity change is smaller than that of chloroform

vapor due to the lower quantum yield (**Section 5.3.7.3.**) and higher affinity of RhB for acetone (**Section 5.3.8.**). Again, at a low grafting density there is not much variation in the relative intensity change with brush thickness for both polymers. At a high grafting density, due to the chains penetration into the PGMA-RhB network in swollen state mobile chains of P2VP and PS change the local environment of RhB molecules and intensity goes down. However, as opposed to the previous case, there is a difference in the behaviors of the PGMA-RhB-PS and PGMA-RhB-P2VP systems. It can be seen that for the PGMA-RhB-PS system, the signal change stays almost constant and starts decreasing at the maximum PS grafting, whereas for PGMA-RhB-P2VP, the gradual decrease starts at very low levels of P2VP grafting. This could be related to the fact that swelling of the PS in acetone is smaller than that of P2VP. Since the penetration depth for PS is also small and the affinity of the RhB molecules to the acetone is high, the presence of PS does not affect emission intensity up to high levels of grafting.

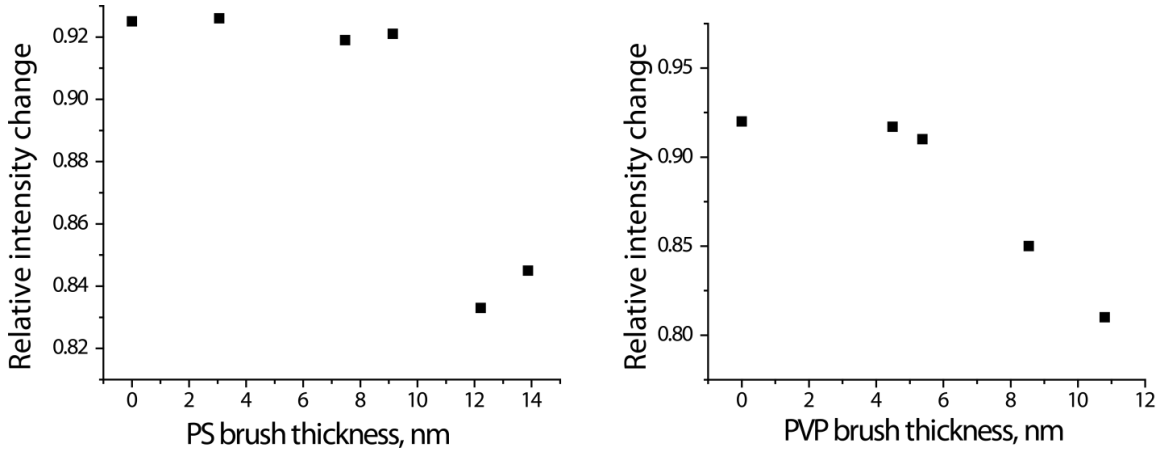


**Figure 7.6.** Relative intensity change in saturated acetone vapor vs. thickness of the grafted layer of PS (left) and P2VP (right) grafting to 6.5 nm thick PGMA-RhB film.

Changes in intensity were measured for the PGMA-RhB-PS films in the good solvent for PS. In **Figure 7.7**,results of the experiment on cyclohexane vapor are shown. It can be seen from the figure that as opposed to the case of PGMA-RhB-PS swelling in chloroform and acetone, emission intensity decreases even at a low PS layer thickness. This is the result of the high affinity of PS to cyclohexane. PS chains attract cyclohexane molecules to the PGMA-RhB network. Due to the low quantum yield of RhB in cyclohexane, the emission intensity decreases rapidly.

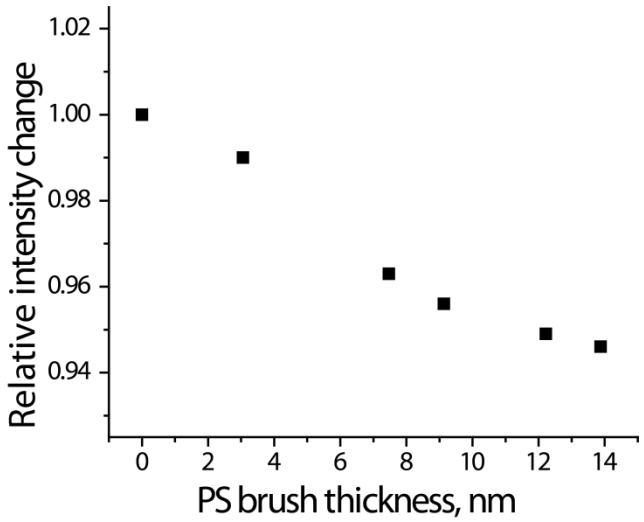


**Figure 7.7.** Relative intensity change in saturated cyclohexane vapor vs. thickness of the grafted layer of PS to 6.5 nm thick PGMA-RhB film.

#### 7.3.3.2. Mixed polymer layer grafting

Fluorescent response of the PGMA-RhB films modified with mixed PS-P2VP polymer layers was studied using the same procedure as for the case of grafting density variations. In **Figure 7.8.**,results of relative intensity change measurements for these films in acetone and chloroform vapor are presented. The x-axis shows the thickness of

the PS component in the PS-P2VP layer. On each plot, the left point corresponds to the relative intensity change for the PGMA-RhB film with a one-component grafted P2VP layer and the right point represents a one-component PS grafted layer. It can be seen that for chloroform (**Figure 7.8.left**), there is no particular trend in the signal change as the ratio between the polymers in the mixture changes. This can be explained by the systems similarity in physical properties: in the swollen state, physical properties of the films are nearly identical since PS and P2VP have similar swelling ratios in chloroform. In addition, intensity change dependence on the grafted layer thickness is close for both polymers. However, due to the phase separation between PS and P2VP in the dry state, the intensity change varies based on the thickness of the PS component in the mixture.

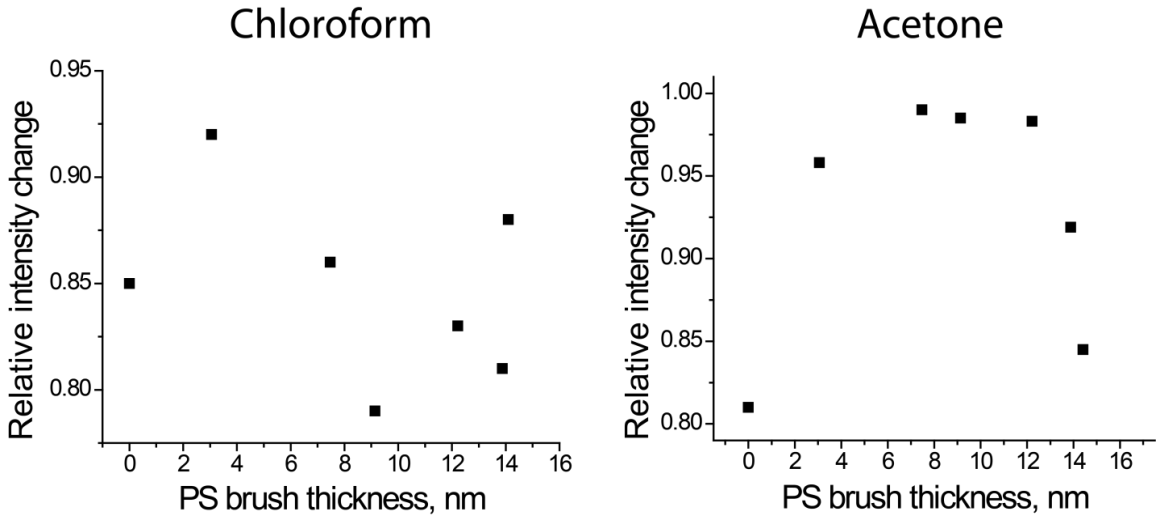


**Figure 7.8.** Relative intensity change in saturated chloroform (left) and acetone (right) vapor for PGMA-RhB film with mixed P2VP-PS grafted layers as a function of the thickness of the PS component of the brush.

In the acetone vapor (Figure 7.8. right), the relative intensity change first increases with PS content up to approximately 50% of PS and then goes down. Such behavior can be the result of the small influence of both PS and P2VP on PGMA-RhB

intensity at low grafting levels, as shown in Figure 7.6.Since P2VP is grafted through already attached PS chains, the depth of P2VP chains penetration is decreased for the mixed brush system as compared to the one-component P2VP grafting. Therefore, emission intensity is only influenced by the grafted layers for the samples with high PS or P2VP content.

However, since mixed polymer layer grafting has very complex effects, additional experiments such as swelling of the PGMA-RhB films with mixed grafted polymer layers are required to fully understand the behavior of the mixed system.

### 7.4. Tuning of fluorescent emission intensity response with gold nanoparticles

One of the possible ways of enhancement of the magnitude of fluorescent emission intensity changes is gold nanoparticle incorporation. It is known, that gold can quench fluorescent emission by electron transfer [13]. This effect in known to be distance dependent [14], changing significantly over the extremely short distances in order of several nanometers.

This phenomenon can be used to tune the fluorescent emission intensity response in the following way. If the gold nanoparticles are attached to the non-fluorescent layer grafted to the PGMA-RhB film fluorescent emission of the RhB molecules will be quenched, if the thickness of the non-fluorescent layer is small enough. However when the polymer film will swell in the vapor of organic solvent, thickness of non-fluorescent polymer layer will increase, separating the gold nanoparticles from fluorescent layer. The

efficiency of the electron transfer between the RhB molecules and the gold nanoparticles will decrease, increasing the emission intensity of the PGMA-RhB film.

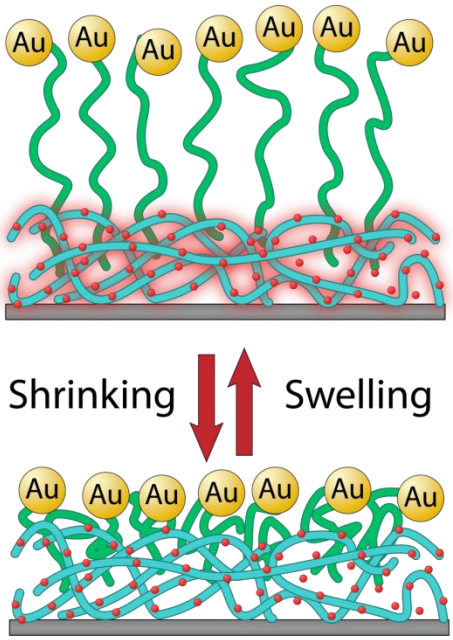


**Figure 7.9.** Schematic of the principle of the gold nanoparticle effect on the fluorescent emission of RhB units of PGMA.

### 7.4.1. Preliminary results of the influence of attached gold nanoparticles on the fluorescent emission intensity of PGMA-RhB film.

After the gold particle application the intensity of the emission of the sample in the dry state decreased for all the samples, as shown in **Figure 6.11**. It can be seen that the decrease in the emission intensity is around 40% for each of the films. This confirms the nanoparticle attachment to the surface of PGMA-RhB-P2VP, considering the quenching of the fluorescent emission from the RhB units of the PGMA-RhB-P2VP film by gold. The measurement of the emission intensity upon exposure of the film to the chloroform vapors showed emission intensity increase in comparison to the dry state for

all samples, as shown in **Figure 6.11**. Effect of fluorescent emission intensity change by grafting of the P2VP layer, discussed in the **Section 7.3.3.1.** is shown in **Figure 6.11.** for comparison.

It can be seen that the two opposite effects are happening at the same time. As P2VP swells gold nanoparticles are pushed back from the PGMA-RhB layer, increasing the emission intensity as the quenching intensity decreases. At the same time flexible monomeric units of P2VP decrease quantum yield of RhB units of PGMA-RhB in swollen state. Both effects change with the amount of the P2VP grafted to the surface of PGMA-RhB. When the thickness of P2VP layer equals 8.5 nm the net effect produces total fluorescent emission intensity increase in 21.8%.

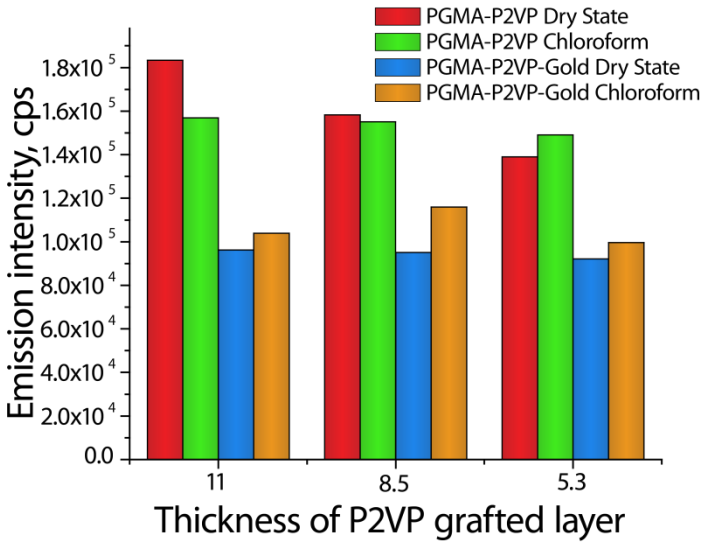


**Figure 7.10.** Emission intensity measured for the PGMA-RhB-P2VP film with attached gold nanoparticles in the dry state and in saturated chloroform vapor.

## 7.5. Conclusions

In conclusion, layers with different grafting densities and mixed polymer layers of PS and P2VP at various ratios were grafted to the PGMA-RhB films. The thickness of the grafted layers as well as the ratio between PS and P2VP in mixed systems was well controlled by the time of annealing.

Fluorescent measurements in saturated vapors of chloroform, acetone, and cyclohexane showed that in addition to the variations in the relative intensity change by non-fluorescent polymer grafting, additional tuning of the signal from PGMA-RhB film can be achieved by attaching the polymers at various grafting densities and through the use of mixed polymer grafting.

## 7.5. References


1. Toal, S. J.; Trogler, W. C., Polymer sensors for nitroaromatic explosives detection. *Journal of Materials Chemistry* **2006,** *16* (28), 2871-2883.

2. Liu, T.; He, G.; Yang, M.; Fang, Y., Monomolecular-layer assembly of oligothiophene on glass wafer surface and its fluorescence sensitization by formaldehyde vapor. *Journal of Photochemistry and Photobiology A: Chemistry* **2009,** *202* (2вЂ“3), 178-184.

3. Ionov, L.; Zdyrko, B.; Sidorenko, A.; Minko, S.; Klep, V.; Luzinov, I.; Stamm, M., Gradient Polymer Layers by "Grafting To" Approach. *Macromolecular Rapid Communications* **2004,** *25* (1), 360-365.

4. Sperling, L. H., *Introduction to physical polymer science*. Wiley: New York, 1986.

5. Gilmore, P. T.; Falabella, R.; Laurence, R. L., Polymer/Polymer Diffusion. 2. Effect of Temperature and Molecular Weight on Macromolecular Diffusion in Blends of Poly(vinyl chloride) and Poly(Oμ-caprolactone). *Macromolecules* **1980,** *13* (4), 880-883.

6. Zhao, B.; Zhu, L., Mixed Polymer Brush-Grafted Particles: A New Class of Environmentally Responsive Nanostructured Materials. *Macromolecules* **2009,** *42* (24), 9369-9383.

7. Draper, J.; Luzinov, I.; Minko, S.; Tokarev, I.; Stamm, M., Mixed Polymer Brushes by Sequential Polymer Addition:вЂ‰ Anchoring Layer Effect. *Langmuir* **2004,** *20* (10), 4064-4075.

8. Uhlmann, P.; Merlitz, H.; Sommer, J.-U.; Stamm, M., Polymer Brushes for Surface Tuning. *Macromolecular Rapid Communications* **2009,** *30* (9-10), 732-740.

9. Minko, S.; Luzinov, I.; Luchnikov, V.; MГјller, M.; Patil, S.; Stamm, M., Bidisperse Mixed Brushes:вЂ‰ Synthesis and Study of Segregation in Selective Solvent. *Macromolecules* **2003,** *36* (19), 7268-7279.

10. Liu, Y.; Klep, V.; Zdyrko, B.; Luzinov, I., Synthesis of High-Density Grafted Polymer Layers with Thickness and Grafting Density Gradients. *Langmuir* **2005,** *21* (25), 11806-11813.

11. Jones, R. A. L.; Lehnert, R. J.; SchГ¶nherr, H.; Vancso, J., Factors affecting the preparation of permanently end-grafted polystyrene layers. *Polymer* **1999,** *40* (2), 525-530.

12. Blank, W.; He, Z.; Picci, M., Catalysis of the epoxy-carboxyl reaction. *Journal of Coatings Technology* **2002,** *74* (926), 33-41.

13. Griffin, J.; Singh, A. K.; Senapati, D.; Rhodes, P.; Mitchell, K.; Robinson, B.; Yu, E.; Ray, P. C., Size- and Distance-Dependent Nanoparticle Surface-Energy Transfer (NSET) Method for Selective Sensing of Hepatitis C Virus RNA. *Chemistry – A European Journal* **2009,** *15* (2), 342-351.

14. Schneider, G.; Decher, G.; Nerambourg, N.; Praho, R.; Werts, M. H. V.; Blanchard-Desce, M., Distance-Dependent Fluorescence Quenching on Gold Nanoparticles Ensheathed with Layer-by-Layer Assembled Polyelectrolytes. *Nano Letters* **2006,** *6* (3), 530-536.

# CHAPTER EIGHT

# FLUORESCENT LAYERS ON ROUGH SURFACES AND NANOSCALE OBJECTS

## 8.1. Introduction

As discussed earlier, fluorescent PGMA films could be straightforwardly bonded to the surfaces of glass slides and silicon wafers. These films showed the ability to sense changes in the environment, evidenced by variations in their fluorescent responses, making fluorescent PGMA-RhB films good candidates for sensing applications. It should be pointed out that due to the high reactivity of PGMA, virtually any substance can be covered with fluorescent film as long as it has the necessary groups that are reactive with PGMA on its surface[1].

To this end, in this chapter the possibility of applying the PGMA-RhB fluorescent film to the different types of substrates is investigated. Specifically, nanoparticles and woven fabrics were targeted for PGMA-RhB deposition.

There are many means of incorporating rigid organic dye into nanoparticles including, but not limited to: dye incorporation into polymer latex beads[2] or microgels[3], pores[4], shells[5], or surfaces[6] of silica nanoparticles, or surfaces of magnetic[7] or noble metal[8] nanoparticles. Of all the carrier materials, silica nanoparticles attract great attention in the field of nanotechnology due to their ease of separation, biocompatibility, and stability[9]. They have no swelling or porosity changes associated with pH variations[10]. Due to the listed advantages, silica was selected as the carrier material.

For the preparation of fluorescent nanoparticles, the core-shell structure was selected, as schematically shown in **Figure 8.1.**In such architecture, organic fluorophores are covalently attached to the reactive polymer film that covers the surface of silica nanospheres. The method for nanoparticle synthesis was developed several years ago in our group[11].

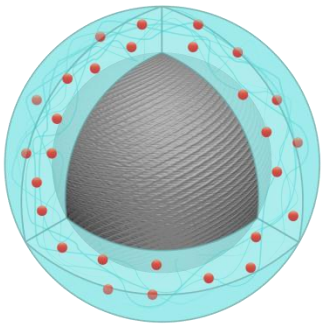

**Figure 8.1.** Schematic of the nanoparticle with the core-shell structure. The core of the particle is a silica sphere and the shell consists of fluorescent material.

Due to the presence of epoxy groups in each monomeric unit, the surface of the particle is still reactive after the fluorescent polymer layer is attached. These groups allow the application of additional functionalities to the particle's surface[12]. For example, a pH-responsive mixed P2VP-PEG polymer brush can be anchored to the surface of the particles using the "grafting to" technique[13]. Nanoparticles functionalized in such a way that they are fully stable at pH<4 undergo fully reversible aggregation upon pH increases to pH>6. It was also shown that the fluorescent emission intensity changed when the pH of the aqueous solution varied. This suggests the possibility of sensing applications for such core-shell nanoparticles.

In the present chapter, we show the results on the investigation of the sensitivity of silica nanoparticles covered with a fluorescent PGMA-RhB shell to the nature of the particle environment by changing the solvent for the nanoparticle dispersion. To make the nanoparticles stable indifferent solvents, the surface of the particles was modified with a PEG polymer brush using the "grafting to" method. Particles functionalized in this way can be easily dispersed in the most common organic solvents and water[14], permitting emission intensity measurements in chloroform, acetone, toluene, cyclohexane, and water. The measurements, performed using a fluorescent spectrophotometer, showed the fluorescent signals sensitivity from the particles to the solvent. Such surface functionalization also provides biocompatibility for the colloid system, since PEG is known for its biocompatibility and is widely used for drug delivery[15] and as a gene carrier[16]. In addition, the magnetic properties were introduced to the fluorescent nanoparticles by attaching paramagnetic $Fe_3O_4$ nanoparticles to the surface of PAA grafted to the PGMA-RhB.

For the deposition of the PGMA-RhB layers onto the rough surface, PET fabric was selected as a substrate. Fabric treatment with fluorescent film has several advantages over flat silicon wafers or glass slides treatment. Fluorescent fabrics can be used in smart textile applications, where the sensitivity is provided for daily use textiles. They can be also used in low-cost detection devices in the medical and defense industries[17]. Overall, the main advantages of the textile materials are their low cost, flexibility, and high surface to volume ratio that greatly enhances the sensitive region of the material[18]. Again,

due to PGMA reactivity, the fluorescently modified fabrics can be post-treated to achieve any desirable surface functionality.

Aside from the fluorescent nanoparticle suspension and directly modified fabrics, a mixed approach was tested in the present research. In this approach, advantages of both types of substrates are combined to achieve flexible material with fluorescent activity, a high surface to volume ratio of the sensitive region, and the ability to change the fluorescent emission upon exposure to the analytes in the vapor phase. In this method of deposition, PGMA-RhB coated fluorescent core-shell nanoparticles were applied to the surface of activated PET fabrics. This system showed higher sensitivity to the vapors of analytes than the flat PGMA-RhB films and the ability to tune that sensitivity with grafting of non-fluorescent polymers.

## 8.2. Experimental

### 8.2.1. Modification of nanoparticles

PGMA-RhB film was used as the fluorescent polymer for the surface modification of the nanoparticles and fabric samples. The preparation and properties of the fluorescent PGMA-RhB are described in detail in **Chapter 1**.

#### 8.2.1.1. Surface modification of $SiO_2$ spheres with PGMA

Deposition of the PGMA-RhB layer was performed using the technique reported elsewhere [11]. Briefly, water suspension of (10% w/vol) $SiO_2$spherical nanoparticles of 150 nm in diameter was used. To start, $SiO_2$ particles were transferred to the THF as

follows. One ml of the initial suspension was added dropwise to the 10 ml of THF under constant sonication. Suspension was purified from water via three subsequent centrifugations for 30 min at 5000 rpm. THF suspension of the $SiO_2$ spheres was added dropwise to the 3 % w/vol PGMA-RhB (Mn=405,000 g/mol with polydispersity 3.81) solution (25 ml) in THF under constant sonication. The mixture then was rotary evaporated and a flask with residuals was placed in an oven at 100 °C for 35 minutes to allow PGMA to attach to the surface of the nanoparticles. After annealing, PGMA-RhB-modified $SiO_2$ spheres were put in acetone and purified via three subsequent centrifugations for 30 min at 5000 rpm. PGMA-RhB film on the surface of the nanoparticles was investigated with TEM. For this purpose the particle suspension in acetone was drop casted onto the copper TEM grids. The thickness of the PGMA-RhB layer was measured using the acquired pictures.

#### 8.2.1.2. Surface modification of silica nanoparticles with the PGMA-RhB layer

To test the possibility of grafted layer deposition onto the PGMA-RhB layer anchored to nanoparticles, grafting of PAA (Mw=100,000 g/mol) and PEG (Mn=5,000 g/mol) was performed. At each step of new layer deposition, the particle agglomeration and the grafting thickness were studied by TEM. In addition, spectrophotometry measurements of the nanoparticle suspension were conducted to ensure that the fluorescent properties were retained after polymer grafting.

#### 8.2.1.2.1. Surface modification of the PGMA-RhB layer with PEG grafting

Suspension of PGMA-RhB modified $SiO_2$ spheres in acetone (100 mg in 5 ml) was added dropwise to the PEG solution in acetone (0.75 g in 20 ml) under sonication. The mixture was then rotary evaporated and placed in the oven at 120°C overnight. Particles then were put in methanol and purified via three subsequent rinses and centrifugations for 30 min at 5000 rpm.

#### 8.2.1.2.2. Surface modification of PGMA-RhB-covered spheres with PAA

To modify the PGMA-RhB layer with PAA, PGMA-RhB-modified $SiO_2$ spheres were transferred to N-Methyl-2-pyrrolidone(NMP) (10 ml) and shaken overnight in a shaker. PAA solution (0.2 g in 5 ml of NMP) was added to the particle suspension dropwise under sonication. Then, the mixture was heated to 70°C for 1 h to allow the PAA to attach to PGMA. After the reaction, NMP was substituted with same amount of ethanol. Particles showed no coagulation, confirming the PGMA-RhB layers surface modification with PAA. Ethanol was evaporated from the flask overnight and residuals were annealed (1h at 70°C) to conduct further attachments of PAA to the fluorescent polymer shell of the $SIO_2$ particle. Particle suspension was purified from unattached PAA via three subsequent rinses and centrifugations for 30 min at 5000 rpm.

#### 8.2.1.2.3. Decoration of PGMA-RhB-PAA with $Fe_3O_4$ nanoparicles

Suspension of PGMA-RhB-PAA modified $SiO_2$ spheres (5 ml) in ethanol was added dropwise to the 40 ml suspension of $Fe_3O_4$ (0.5 mg/ml) nanoparticles in water under sonication. The mixture was left for 1 h on the shaker to allow magnetic nanoparticles to attach to the PAA layer. Modified SiO2 spheres were recovered from the $Fe_3O_4$ suspension via three subsequent rinses and centrifugations for 30 min at 5000 rpm.

### 8.2.2. Studies of the fluorescent sensitivity of nanoparticles in suspension

Fluorescent emission sensitivity for PGMA-RhB-PEG covered nanoparticles was studied in various environments. Particles were transferred to five different solvents (chloroform, water, cyclohexane, toluene, and acetone) from methanol by addition of 1 ml of suspension dropwise to the 10ml of solvent of interest under sonication. This suspension was then purified from methanol via centrifugation 30 min at 5000 rpm. Quartz 1 cm cuvettes were used for the spectrophotometry measurements. Fluorescent emission intensity was scaled with concentration to allow signal comparison.

### 8.2.3. PGMA-RhB layer deposition onto the surface of PET fabrics

The cleaned PET fabric (cleaning procedure is described in detail in **Section 3.4.2.**) was used for PGMA-RhB deposition. The PGMA-RhB solution in chloroform (2% w/vol) was drop casted onto the fabric samples. After evaporation of the solvent

samples were annealed in the oven under vacuum at 100°C for 3 h. Unattached polymer chains were removed via rinsing in chloroform three times for 30 min.

### 8.2.4. Modification of PET fabric with the PGMA-RhB layer

PAA (Mw=100,000 g/mol) and carboxyl terminated versions of PS (Mn=48,000g/mol with polydispersity 1.05), P2VP (Mn=53,000g/mol with polydispersity 1.06) and PEG (Mn=5,000 g/mol) were used as a second layers in grafting experiments. PET fabric coated with a PGMA-RhB layer was dipcoated into the 1% w/w solution of the polymer used for grafting (PAA in methanol, PS in chloroform, P2VP in chloroform, PEG in methanol). After the dipcoating fabric was annealed in an oven under vacuum (PAA at 40°C for 2h; PEG, PS, P2VP at 120°C for 8h). After the annealing, unattached polymer chains were removed via rinsing the fabric samples in the good solvent for the polymer used for grafting: chloroform for PS and methanol for P2VP, PAA, and PEG. Rinsing was performed three times for 30 min each. Brush attachment was qualitatively confirmed by contact angle measurements. Fluorescent response of the fabric samples was measured by spectrophotometry.

### 8.2.5. Decoration of the PET fabric with nanoparticles

Attachment of PGMA-RhB-modified core-shell nanoparticles was conductedusing a procedure reported elsewhere[19]. PGMA-RhB coated silicon dioxide nanoparticles were deposited on to the surface of PET fabrics from suspension. A cleaned and activated piece of PET fabric was put into the 0.03% w/w suspension of PGMA-

RhB-modified spheres in acetone. A vial with the fabric and nanoparticle suspension was heated to 55°C in a water bath and held under constant stirring for 36h. Then, the nanoparticle adsorption fabrics were annealed under the vacuum at 100 °C for 3h, with subsequent rinsing in acetone to remove unattached nanoparticles. Particle attachment was confirmed by TEM imaging. Fluorescent properties of the fabric were studied using spectrophotometry.

### 8.2.6. Grafting of the polymer layer to the PGMA-RhB covered fabric

The polymer layer was grafted to the PGMA-RhB-covered nanoparticles attached to the PET fabric by the method described in **Section 8.2.1.2.1.** PET fabric with PGMA-RhB modified nanoparticles was dip coated into the 1% w/w solution of the polymer used for the grafting (PAA in methanol, PS in chloroform, P2VP in chloroform, PEG in methanol). After the dipcoating fabric was annealed in an oven under vacuum (PAA at 40°C for 2h; PEG, PS, P2VP at 120°C for 8h). After the annealing, unattached polymer chains were removed via rinsing the fabric samples in a good solvent for the polymer used for grafting: chloroform for PS and methanol for P2VP, PAA, and PEG. Rinsing was performed three times for 30 min each. Fluorescent properties were measured using the spectrophotometer. The samples with PEG grafting showed very low emission intensity, suggesting that PEG grafting cleaved the nanoparticles from the PET fibers' surface, so the PEG modified samples were discarded.

### 8.2.7. Fluorescent property measurements for fabric samples

Fluorescent emission intensity was studied by spectrophotometry using the same cuvette as for the fluorescent polymer films on the surface of the glass slide (see **Section 5.2.3.**). Stretched fabric coated with fluorescent polymer was placed into the cuvette and sealed with the clean glass microscope slide.

## 8.3. Results and discussion

### 8.3.1. Modification of nanoparticles with the PGMA-RhB layer

As discussed in previous chapters, PGMA-RhB films attached to the flat substrates showed fluorescent emission sensitivity to environmental changes. To expand the possible applications of such fluorescent polymer coating, the PGMA-RhB layer was deposited onto the surface of silicon dioxide nanoparticles. Since the surface chemistry of the nanoparticles does not differ significantly from the surface of glass slides used in the previous chapters, the same annealing procedure was selected. However, prior to annealing, it was necessary to perform the deposition of the PGMA-RhB layer onto the surface of silicon nanoparticles. To do that, both nanoparticles and polymer should be mixed together. THF was selected for this purpose as a solvent, since it provides stability to the nanoparticle suspension, and at the same time, it is a good solvent for PGMA-RhB. To cover particles uniformly, PGMA-RhB was provided in excess. After solvent evaporation, nanoparticles were annealed for the same amount of time and at the same temperature (100°C for 30 min) as was used for the PGMA-RhB attachment to the flat substrates (see **Section 5.2.1.**). After the annealing, unattached polymer chains have to

be removed from the suspension. The most convenient way to separate the particles is by utilizing centrifugation since the density of the silicon dioxide particles is greater than that of the acetone.

### 8.3.2. Characterization of nanoparticles modified with PGMA-RhB

Since the annealing time/temperature and surface chemistry were the same as for the flat substrates, it was anticipated that the same PGMA-RhB layer thickness would be achieved by using the deposition method presented above. The thickness of the obtained PGMA-RhB layer was measured by TEM. The typical image of silica nanoparticles covered with PGMA-RhB is shown in **Figure 8.2.** Since the density of the polymer is different from the density of silica, the TEM produces sufficient contrast between inorganic core and the polymer shell[20].

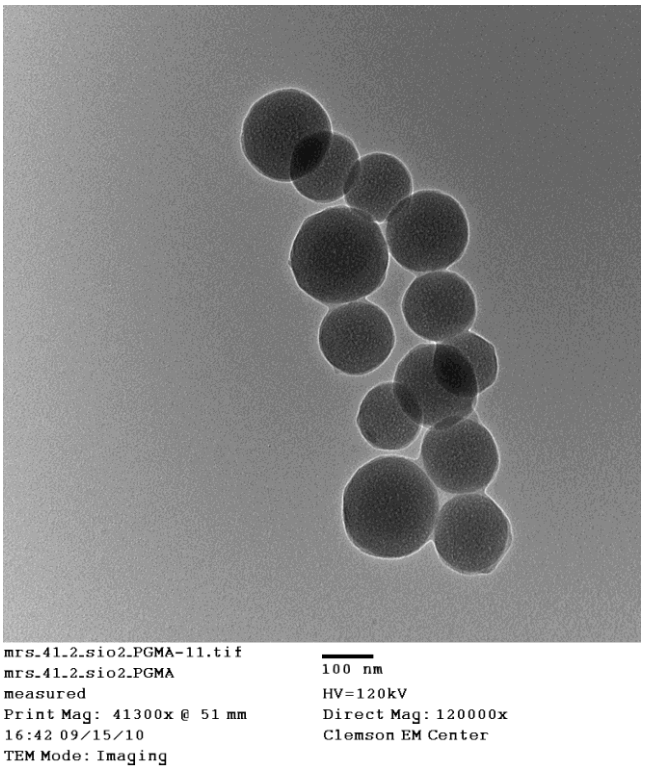


**Figure 8.2.** TEM image of the silica nanoparticles with the PGMA-RhB layer.

It can be seen from the image that there is a planar agglomeration of the particles on the TEM grid. Such one-layer agglomeration confirms the stability of the particle solution: during the evaporation of the acetone when the suspension droplet is deposited onto the TEM grid, the capillary forces bring the particles together; however, since no multilayer agglomerates are present, the particles were stabilized in the solution prior to deposition[21].

Using ImageJ software, the attached polymer layers thickness was extracted. To accomplish this, the shape of the particles with and without PGMA-RhB was traced in the images using the circles. Next, the film thickness was calculated from the difference in area of the circles representing the nanoparticles before and after the PGMA-RhB

attachment. Using the method described above, the PGMA-RhB layer thickness was estimated to be 4.8±1.2 nm. This value is close to the thickness of the PGMA-RhB created using the flat substrates in the same annealing condition. Nanoparticles dispersed in the acetone showed a high fluorescent signal even upon simple exposure of the particle suspension to the green laser pointer beam.

### 8.3.3. Modifications of PGMA-RhB-covered nanoparticles

The next step was to investigate the possibility of surface modification and the effects of this modification on fluorescent properties of the nanoparticles in the solution. For this purpose, two polymers were selected for the grafting: PAA and PEG.

#### 8.3.3.1. Deposition of the PAA layer

As in the case of PGMA attachments, to deposit the PAA onto the surface of PGMA-RhB covered nanoparticles, both PAA and nanoparticles need to be placed in the same solvent. NMP was used for this purpose since this PAA solvent provides stability for the nanoparticles' suspension. However, in this case, simple evaporation of the solvent prior to the annealing would take an extensive amount of time due to the low volatility on NMP[14]. Instead, the suspension with PAA in excess was heated to allow some adsorption of PAA onto the surface of PGMA-RhB covered nanoparticles. Then, the solvent was substituted with ethanol. Ethanol is a bad solvent for PGMA, but no nanoparticle agglomeration was observed following the substitution. This indicated that

PAA chains attached to the surface of PGMA creating a thin PAA layer as an outer shell. Next, the ethanol was evaporated and the annealing was performed in the same conditions as for the PAA attachment to the PGMA in case of flat substrates (**Section 6.2.1.**).

#### 8.3.3.2. Decoration of nanoparticles covered by PAA with $Fe_3O_4$ nanoparticles

It known that PAA has the ability to attract the iron oxide nanoparticles[22]. This feature of PAA allows PGMA-RhB covered silicon dioxide nanospheres to be decorated in a form of raspberry-like magnetic nanoparticles[23], as schematically shown in the **Figure 8.3.left**. Due to the paramagnetic properties of the iron oxide nanoparticles, such decoration will give the nanoparticles magnetic properties, allowing particle manipulation using a magnetic field[24].

The attachment of the $Fe_3O_4$ nanoparticles was conducted in suspension. Decorated nanoparticles were extracted from suspension via centrifugation. The resulting suspension was exposed to the magnetic field using a permanent magnet. It was observed that the nanoparticles followed the magnetic field, gathering at the side of the vial. As soon as the magnetic influence was removed, the nanoparticle cluster was easily separated into a stable suspension by shaking the vial.

Nanoparticle suspension was examined by TEM and spectrophotometry. TEM imaging (**Figure 8.3. right**)showed that $Fe_3O_4$ nanoparticles uniformly cover the surface of PGMA-RhB+PAA modified silica spheres. There was almost no aggregation of the

nanoparticles observed. Spectrophotometry of the nanoparticle suspension in water showed strong fluorescence, indicating that after PAA deposition and decoration with $Fe_3O_4$, nanoparticles retained their fluorescent ability.

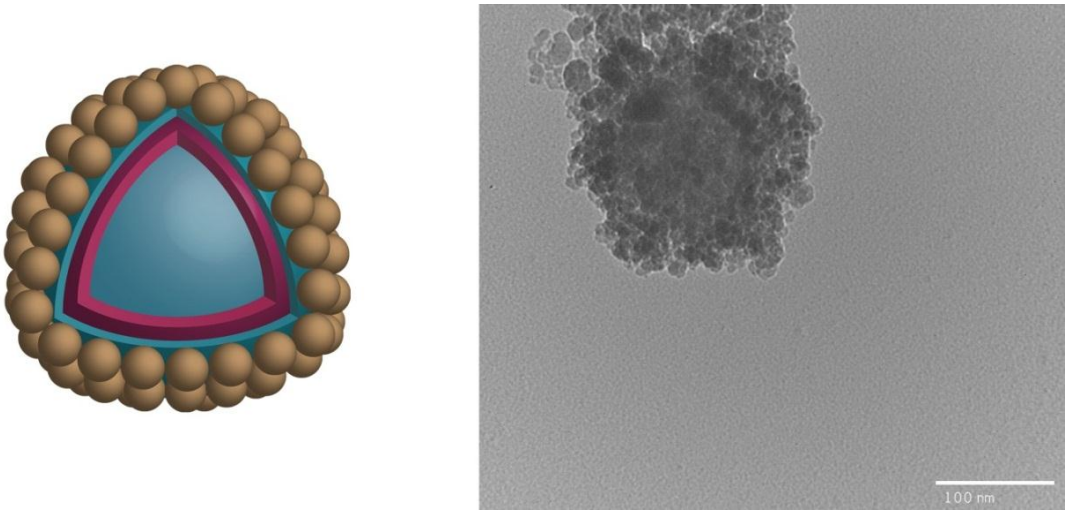


**Figure 8.3.** PGMA-RhB-PAA covered silica nanosphere decorated with $Fe_3O_4$ nanoparticles: Schematic representation (left) and TEM image of the nanoparticle on TEM grid (right)

#### 7.3.3.3. Deposition of PEG

Another polymer used for the grafting was PEG. This polymer was applied as a second layer to PGMA-RhB-covered nanoparticles as schematically shown in **Figure 8.4.**This polymer has the unique feature of being able to dissolve in most solvents[14]; therefore, PEG coating provides the nanoparticles with the ability to be dispersed in a variety of solvents. The procedure of PEG grafting was almost the same as for the PGMA-RhB layer deposition. After the PEG anchoring, the particles' suspension showed

good stability in a number of solvents, including water. Since it is known that PGMA dissolves poorly in water, this confirms the PEG layer's attachment to the nanoparticles.

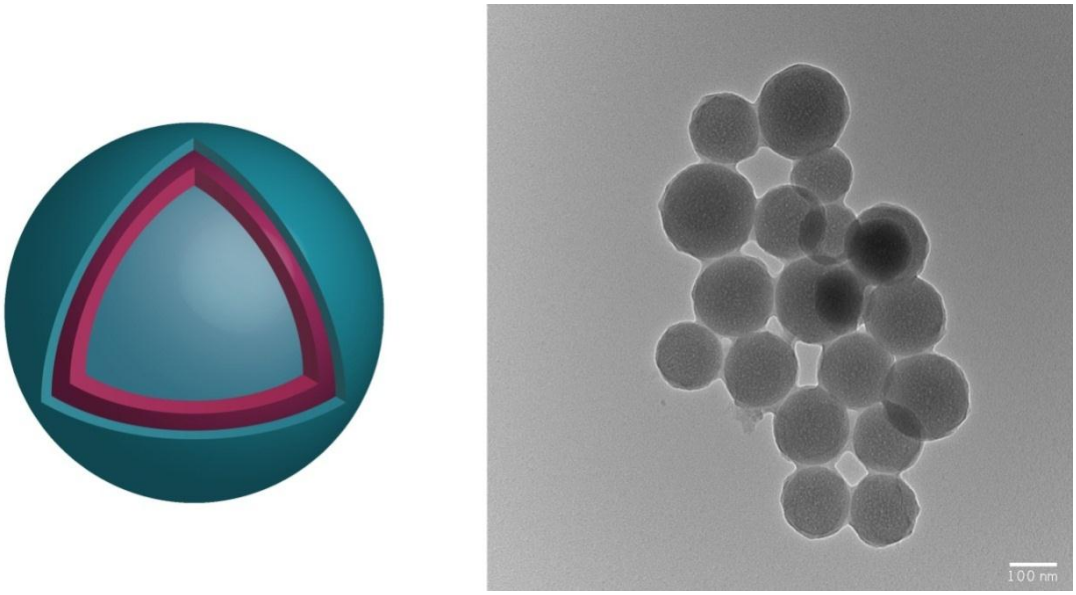


**Figure 8.4.** PGMA-RhB-PEG covered silica nanosphere: Schematic representation (left) and TEM image of the nanoparticles on TEM grid (right)

Suspension of the nanoparticles in water was studied by TEM imaging .**Figure 8.4.**shows that there is almost no out of plane clustering of the nanoparticles, confirming good stability of the suspension. The PEG layers thickness was estimated from the TEM images by the above mentioned procedure as 5.2±2 nm.

#### 8.3.3.4. Environmental sensitivity of the PGMA-RhB+PEG layer

The spectrophotometry of water suspension of the PGMA-RhB-PEG modified nanoparticles showed a strong fluorescent signal, meaning that the nanoparticles retained their fluorescent properties upon grafting of PEG. To assess the environmental sensitivity of the PGMA-RhB-PEG modified nanoparticles, small amounts of organic contaminants

were added to water. First, the fluorescent signal of two separate nanoparticle suspensions of the same concentration in water was recorded. Next, 1% of acetone and 1% of chloroform was added to the each of the suspensions, and the changes in fluorescent signal were observed. **Figure 8.5.left**shows the results of the measurements. It can be seen from the figure that the signal decreased significantly with the addition of chloroform and increased when the acetone was added.

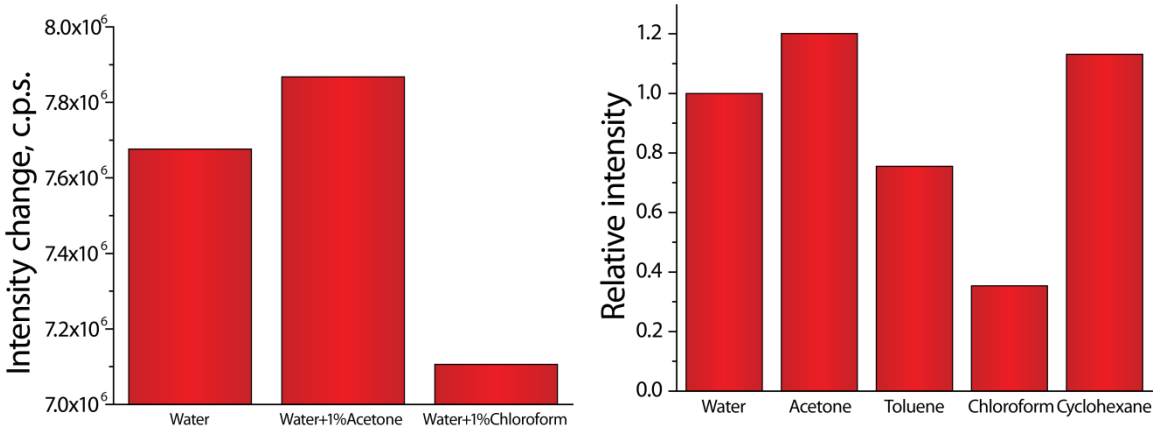


**Figure 8.5.** Intensity change for the suspension of PGMA-RhB-REG-covered nanoparticles in water after the addition of 1 % of acetone and 1 % of chloroform (left); Relative intensity of the fluorescent emission collected from the suspension of PGMA-RhB-REG-covered nanoparticles in water, acetone, toluene, chloroform, and cyclohexane (right).

Since the nanoparticle suspension appeared to be sensitive to the environment, measurements of the fluorescent emission of the same nanoparticle concentration in various solvents were recorded. Results are presented in **Figure 8.5.right**. It can be seen by comparison with the results in **Figure 6.6.right** that the signal variation for the nanoparticle system is much higher than that of the grafted layers on the flat substrates. This can be explained by the fact that during the measurements of the signal changes for

the films on flat substrates, analytes were introduced in the vapor phase; therefore, the flat films were less exposed to the molecules of the analyte.

### 8.3.4. PET fabric modification

#### 8.3.4.1. Deposition of the PGMA-RhB layer

The previous statement gives rise to the following question: How high would the amplitudes of the signal change be if a similar system with a high surface to volume ratio was exposed to the same analyte in the vapor phase? To answer this question, the surface of the PET fabric was covered with fluorescent polymer film, the same surface modification was performed, and the fluorescent characteristics of these textiles were studied. The surface of PET is known to be easily activated using plasma or base treatment[19]. Such activation brings hydroxylic and carboxylic groups to the surface of the yarn fibers, making yarn surface reactive with PGMA.

For surface activation base treatment was chosen instead of plasma treatment, because it is produces more uniform results than plasma. A short activation time was chosen to keep the fabrics undamaged. After the treatment, fabric samples soaked up more water, which confirms surface activation.

After the PGMA-RhB deposition and annealing, the fabrics showed strong fluorescent emission under the fluorescent microscope (**Figure 8.6. left**). Spectrophotometry measurements of the PGMA-RhB covered fabric fluorescent emission confirmed a strong fluorescent signal. In fact, the signal was several times higher than that of the 120 nm thick PGMA-RhB film deposited onto the surface of the glass slide.

This could be explained by the high surface to volume ratio of the PET fabric structure. The fluorescent intensity changes in several solvents varied significantly and showed signal changes that differed according to the nature of the solvent(**Figure 8.6. right**). The signal variation was different from the one observed for the 5 nm thick PGMA-RhB layer on the glass slides (**Figure 5.15.**). This difference may be explained by the presence of PET, which may modify the affinity of the PGMA-RhB system to the solvents used in the study by swelling in the solvents used.

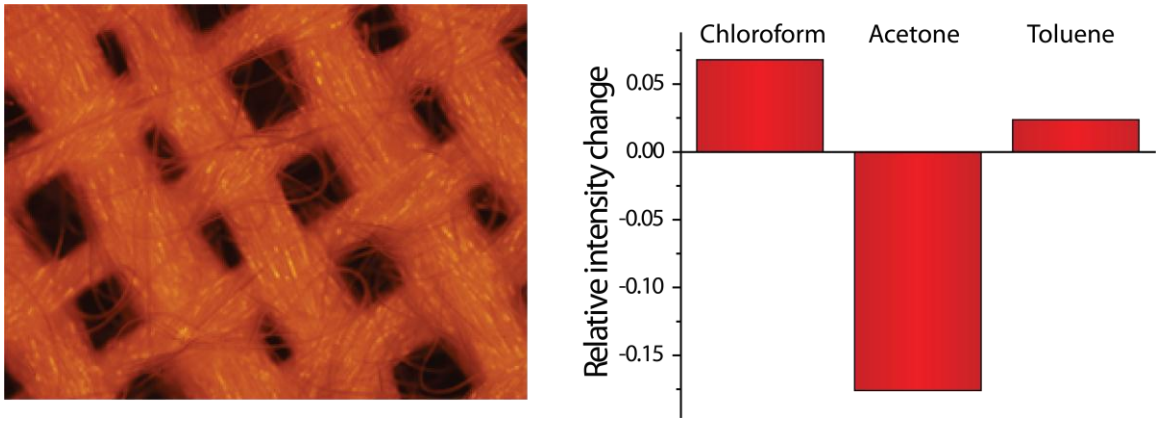


**Figure 8.6.** Fluorescent microscopy image of the PET fabric covered with the PGMA-RhB layer (left); Relative intensity change in chloroform, acetone, and toluene measured for the PET fabric covered with PGMA-RhB (right).

### 8.3.4.2. Grafting of the non-fluorescent polymer layer to the fabric covered with PGMA-RhB

Since measurements of the fluorescent intensity discussed aboveindicated signal changes upon variation of the solvent nature, it was decided to continue with non-fluorescent polymer grafting for the tuning of the signal changes, as reported in **Chapter 6**. For this purpose, the fabric was coated with a reactive polymer and annealed. After the

annealing and surface cleaning, the fabric samples modified with P2VP, PEG, and PAA showed wetting with water, while PS modification made fabrics hydrophobic, confirming the polymer attachment.

Spectrophotometry measurements for two layer films on the surface of fabric in saturated vapors of chloroform, acetone, toluene, water, and cyclohexane was performed using a spectrophotometer. The fluorescent emission intensity of the dry film did not decrease upon the second layer grafting. However, when chloroform vapor was introduced to the system, the change of the signal exhibited by different grafting layers was nearly identical (**Figure 8.7.**).

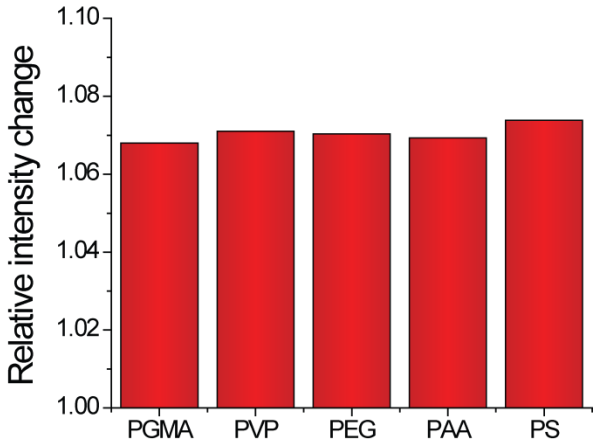


**Figure 8.7.** Relative intensity change measured for fabrics with PGMA-RhB, PGMA-RhB-P2VP, PGMA-RhB-PEG, PGMA-RhB-PAA, and PGMA-RhB-PS in chloroform vapor

This result indicates that the amount of the PGMA-RhB grafted to the textile surface is very high compared to the non-fluorescent polymer layer. A high amount of the PGMA-RhB is also the reason for the high fluorescent signal magnitude observed by the spectrophotometry of the dry fabrics. This important result confirms the proposed hypothesis of the fluorescent response changes of the PGMA-RhB films following non-

fluorescent polymer grafting, as discussed in **Chapter 3**. If the thickness of the PGMA-RhB layer is much greater than that on the non-fluorescent polymer, the influence of the grafted layer is not sufficient to tune the fluorescent emission of the PGMA-RhB film.

### 8.3.5. PET fabricmodified with nanoparticles covered with PGMA-RhB

#### 8.3.5.1. Deposition of the nanoparticles

Since the grafting of the second layer was not able to change the fluorescent response of the film, the amount of PGMA-RhB was decreased relative to the amount of non-fluorescent polymer grafted. However, instead of decreasing the amount of PGMA-RhB attached to the PET surface by decreasing annealing times, silica nanoparticles modified with PGMA-RhB were attached to the surface of the fabric, as shown schematically in **Figure 8.8.**

This method has several advantages over the simple PGMA-RhB layer thickness variation. First, since the method of depositing a 5 nm thick PGMA-RhB layer onto the silica nanoparticles has already been developed, this ensures the thickness of the non-fluorescent layer will be comparable with the PGMA-RhB layer, as shown in **Chapter 6**. The second advantage is the fact that the thickness of both fluorescent and non-fluorescent layers is the same for all nanoparticles in the solution, whereas for the fabrics this is probably not the case due to the high roughness of the fibers, and there are non-predictable and non-measurable thickness variations through the sample. In addition, if a high attachment density of nanoparticles is achieved, the surface to volume ratio for the sensitive layer should be also enhanced.

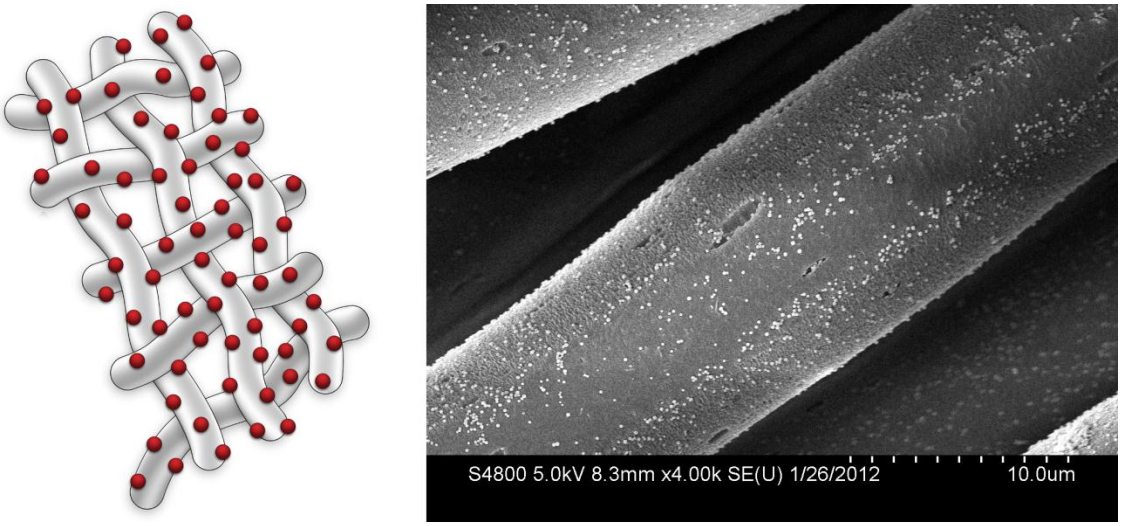


**Figure 8.8.** Schematic of PET fabric structure with attached PGMA-RhB covered silica nanoparticles (left); TEM image of the PET fabric covered with PGMA-RhB modified silica nanoparticles (right).

Attachment of the nanoparticles to the fabric samples was performed from suspension. The same PGMA-RhB modified nanoparticles as were discussed in **Section 8.3.2.**were used for the deposition. A single piece of fabric was used for the attachment and cut into smaller pieces for further modification after the particles were attached to the material. This was done to prevent the yarns from becoming entangled during the stirring and to ensure there was no stacking of the fabric pieces, in which case it would be more difficult for the particles to get through the fabrics to the grafting sites. TEM imaging was performed to confirm the nanoparticle attachment. **Figure 8.8.right** shows the uniform coverage of the surface of the fibers with the nanoparticles.

#### 8.3.5.2. Characterization of fabric modified with fluorescent nanoparticles

##### 8.3.5.2.1. Fluorescent properties of the PGMA-RhB layer

The fluorescent signal from the fabric was measured by spectrophotometry. **Figure 8.9.left** shows the measured values of the fluorescent emission intensity changes for the fabric samples covered with the fluorescent core-shell nanoparticles. Measurements of the intensity change for the 5 nm thick PGMA-RhB layer on the glass slide, discussed in Chapter 5, are shown in **Figure 8.9.right** for comparison. Results presented in **Figure 8.9.left** show the grafted layer high sensitivity to the solvent in the vapor phase. It can be seen by comparison with **Figure 8.9.right** that the magnitude of signal changes is much greater for the fabric samples. This can be explained by the fact that there is a much greater surface to volume ratio for the nanoparticles on fabric, and consequently, more RhB molecules are affected by the absorbing solvent. The direction of the signal change for the flat PGMA-RhB film in most solvents is the same for the nanoparticles on fibers. Specifically, the signal increases in chloroform and cyclohexane vapors, and it decreases in acetone and water. However, toluene induces an increase in the signal for the nanoparticles on fibers, as opposed to the flat films where the intensity decreases in toluene. This might be caused by the presence of the PET, in which an affinity to the solvent influences environment of the fluorescent PGMA-RhB layer. It is also known that due to the small interfiber space in the fabric's structure, condensation of the solvent may occur between the fibers[25], increasing the influence of the solvent of the PGMA-RhB emission.

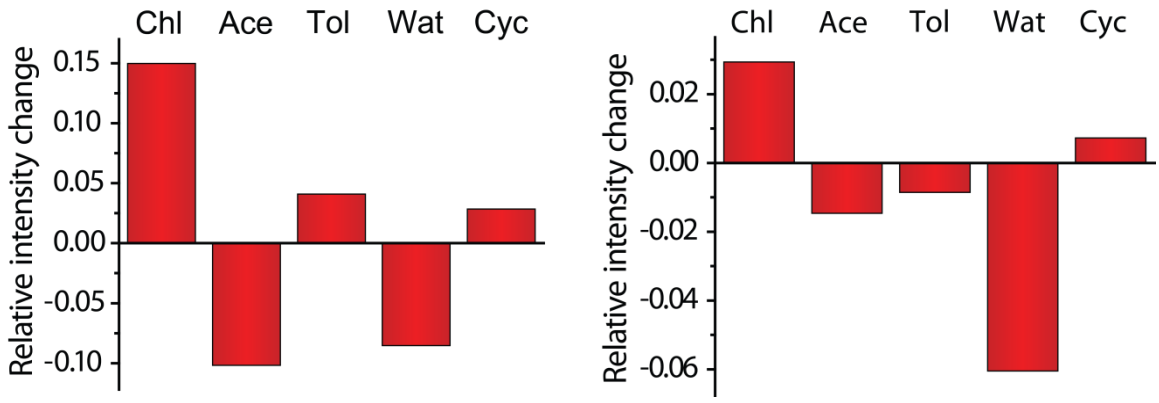


**Figure 8.9.** Relative intensity changes for the PET fabric covered with PGMA-RhB modified silica nanoparticles (left); Relative intensity change for the 5 nm thick PGMA-RhB layer on the surface of the glass slide (right). Relative intensity changes were induced by the saturated vapor of organic solvents: chloroform, acetone, toluene, water, and cyclohexane.

#### 8.3.5.2.2. Grafting of the non-fluorescent polymer layer

After measuring the emission intensity of the single PGMA-RhB layer for nanoparticles on the fabric system, the grafting of the second layer was performed. Since there is no chemical reaction between the PET itself and the polymer being grafted, whole fabric samples can be covered with the polymer, and then unattached polymer chains can be easily removed from the PET surface. After the second layer grafting, fluorescent measurements were performed. All dry films showed strong fluorescent signals except for the nanoparticles covered with PGMA-RhB-PEG. In fact, after PEG was grafted to the sample with PGMA-RhB modified nanoparticles, fluorescence of the fabric sample was about 20 times lower than that of the original PGMA-RhB layer.

This result could be explained if one considers the PEG reaction with PGMA in detail. It is known that relatively short PEG chains are able to penetrate through the PGMA network, thereby expanding it[12]. In the case of PGMA-RhB on the flat surface of the wafer or the glass slide, this network deformation is not enough to detach films from the surface. Conversely, the nanoparticles are attached to the surface of the PET by the small number of chemical bongs. When the PET enters the PGMA-RhB network, the expansion is so great that the particles become cleaved from the surface of the fibers.

#### 8.3.5.2.3. Environmental sensitivity of fabric with core-shell nanoparticles

Considering this phenomenon only, PS, P2VP, and PAA grafting was studied in this section. Measurements of the fluorescent emission changes during solvent absorption showed vast changes in fluorescent responses of the samples, as shown in **Figure 8.10.** Again, the amplitude of observed changes is much greater than that observed for the flat films (**Figure 6.10.**). The response for each analyte was unique, so the solvents used through the research can be easily distinguishable.

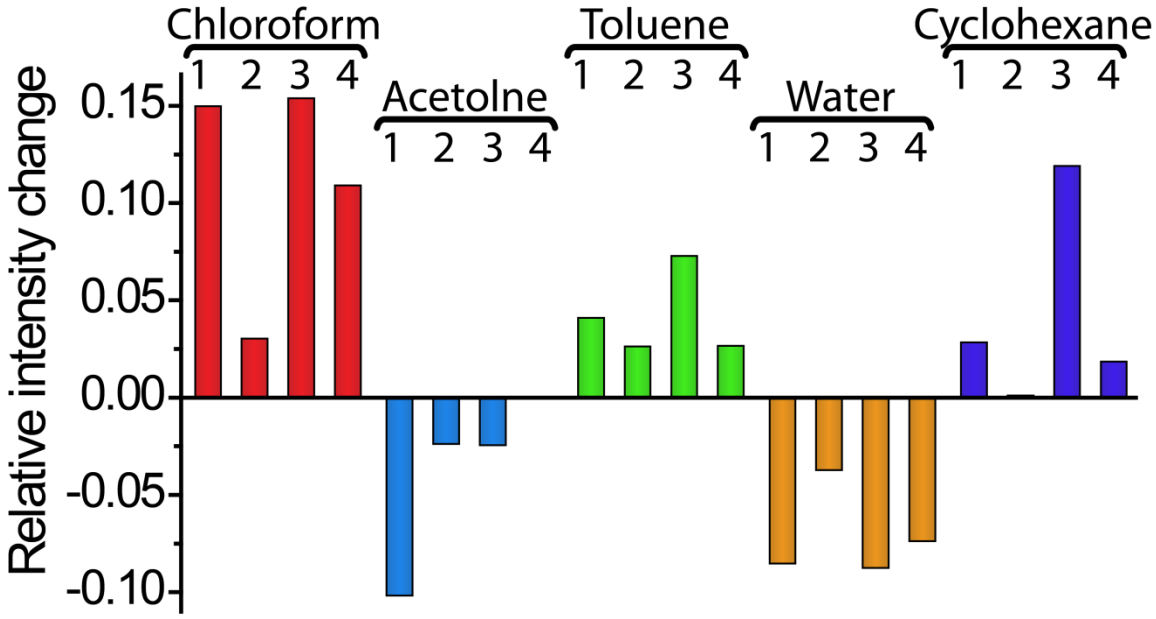


**Figure 8.10.** Relative intensity change for PET fabrics modified with fluorescent core-shell nanoparticles grouped by the solvents used in the measurements. The fluorescent shells used in the experiments were: 1 – PGMA-RHB, 2 – PGMA-RhB-PAA, 3 – PGMA-RhB-PS, and 4 – PGMA-RhB-P2VP.

### 8.4. Conclusions

The fluorescent PGMA-RhB layer was obtained on the surface of the silica nanoparticles. The amount of grafted polymer was consistent with that of the flat substrates after the same annealing process. Nanoparticles were highly fluorescent and showed sensitivity to the solvent in suspension.

The PEG and PAA layers were grafted to the nanoparticles, showing the tunability of the fluorescent nanoparticles surface chemistry. Attachment of iron oxide nanoparticles to the PGMA surface provided magnetic properties to the nanoparticles in suspension, with almost no effect on the fluorescent properties of the PGMA-RhB layer.

After the deposition of PEG on the surface of the nanoparticles, the suspension was stable in several solvents, producing unique fluorescent responses for each of them.

PET fabric samples were coated with PGMA, showing high fluorescent emission. However, this emission was not tunable by non-fluorescent polymer grafting due to large quantities ofthe fluorescent polymer.

To achieve tunability nanoparticles were attached to the fibers surface, allowing the nanoparticle system to sense solvents in the vapor phase. Grafting several different polymers to the nanoparticles surface allowed the fluorescent emission response of the film to be tuned. The response patterns for the solvents have higher signal change amplitudes than those of the flat polymer films and are unique and distinguishable from each other.

## 8.5. References


1. Iyer, K. S.; Zdyrko, B.; Malz, H.; Pionteck, J.; Luzinov, I., Polystyrene Layers Grafted to Macromolecular Anchoring Layer. *Macromolecules* **2003,** *36* (17), 6519-6526.

2. Taylor, J. R.; Fang, M. M.; Nie, S., Probing Specific Sequences on Single DNA Molecules with Bioconjugated Fluorescent Nanoparticles. *Analytical Chemistry* **2000,** *72* (9), 1979-1986.

3. Graf, C.; Schartl, W.; Fischer, K.; Hugenberg, N.; Schmidt, M., Dye-Labeled Poly(organosiloxane) Microgels with Core-Shell Architecture. *Langmuir* **1999,** *15* (19), 6170-6180.

4. Giri, S.; Trewyn, B. G.; Stellmaker, M. P.; Lin, V. S. Y., Stimuli-Responsive Controlled-Release Delivery System Based on Mesoporous Silica Nanorods Capped with Magnetic Nanoparticles. *Angewandte Chemie International Edition* **2005,** *44* (32), 5038-5044.

5. Gao, F.; Chen, X.; Ye, Q.; Yao, Z.; Guo, X.; Wang, L., Core-shell fluorescent silica nanoparticles for sensing near-neutral pH values. *Microchimica Acta* **2011,** *172* (3), 327-333.

6. Mader, H.; Li, X.; Saleh, S.; Link, M.; Kele, P.; Wolfbeis, O. S., Fluorescent Silica Nanoparticles. *Annals of the New York Academy of Sciences* **2008,** *1130* (1), 218-223.

7. Sahoo, Y.; Goodarzi, A.; Swihart, M. T.; Ohulchanskyy, T. Y.; Kaur, N.; Furlani, E. P.; Prasad, P. N., Aqueous Ferrofluid of Magnetite Nanoparticles: Fluorescence Labeling and Magnetophoretic Control. *The Journal of Physical Chemistry B* **2005,** *109* (9), 3879-3885.

8. Aslan, K.; Gryczynski, I.; Malicka, J.; Matveeva, E.; Lakowicz, J. R.; Geddes, C. D., Metal-enhanced fluorescence: an emerging tool in biotechnology. *Current Opinion in Biotechnology* **2005,** *16* (1), 55-62.

9. Wang, L.; Tan, W., Multicolor FRET Silica Nanoparticles by Single Wavelength Excitation. *Nano Letters* **2005,** *6* (1), 84-88.

10. Jain, T. K.; Roy, I.; De, T. K.; Maitra, A., Nanometer Silica Particles Encapsulating Active Compounds: A Novel Ceramic Drug Carrier. *Journal of the American Chemical Society* **1998,** *120* (43), 11092-11095.

11. Tsyalkovsky, V.; Klep, V.; Ramaratnam, K.; Lupitskyy, R.; Minko, S.; Luzinov, I., Fluorescent Reactive Core–Shell Composite Nanoparticles with A High Surface Concentration of Epoxy Functionalities. *Chemistry of Materials* **2007,** *20* (1), 317-325.

12. Zdyrko, B.; Swaminatha Iyer, K.; Luzinov, I., Macromolecular anchoring layers for polymer grafting: comparative study. *Polymer* **2006,** *47* (1), 272-279.

13. Tsyalkovsky, V.; Burtovyy, R.; Klep, V.; Lupitskyy, R.; Motornov, M.; Minko, S.; Luzinov, I., Fluorescent Nanoparticles Stabilized by Poly(ethylene glycol) Containing Shell for pH-Triggered Tunable Aggregation in Aqueous Environment. *Langmuir* **2010,** *26* (13), 10684-10692.

14. Brandrup, J.; Immergut, E. H., *Polymer handbook*. Wiley: New York, 1989.

15. Harris, J. M., *Poly(ethylene Glycol) Chemistry: Biotechnical and Biomedical Applications*. Plenum Press: 1992.

16. Lee, M.; Kim, S. W., Polyethylene Glycol-Conjugated Copolymers for Plasmid DNA Delivery. *Pharmaceutical Research* **2005,** *22* (1), 1-10.

17. Reches, M.; Mirica, K. A.; Dasgupta, R.; Dickey, M. D.; Butte, M. J.; Whitesides, G. M., Thread as a Matrix for Biomedical Assays. *ACS Applied Materials & Interfaces* **2010,** *2* (6), 1722-1728.

18. Stavis, S. M., A glowing future for lab on a chip testing standards. *Lab on a Chip* **2012**.

19. Ramaratnam, K.; Iyer, S. K.; Kinnan, M. K.; Chumanov, G.; Brown, P.; Luzinov, I., Ultrahydrophobic textiles: Lotus approach. *AATCC Rev. AATCC Review* **2008,** *8* (1), 42-48.

20. Williams, D. B.; Carter, C. B., *Transmission electron microscopy : a textbook for materials science*. Plenum Press: New York, 1996.

21. Balandin, A. A.; Kang, L. W., *Handbook of semiconductor nanostructures and devices*. American Scientific Publishers: Los Angeles, CA, 2005.

22. Gebhardt, J. E.; Fuerstenau, D. W., Adsorption of polyacrylic acid at oxide/water interfaces. *Colloids and Surfaces* **1983,** *7* (3), 221-231.

23. Wang, C.; Yan, J.; Cui, X.; Wang, H., Synthesis of raspberry-like monodisperse magnetic hollow hybrid nanospheres by coating polystyrene template with Fe3O4@SiO2 particles. *Journal of Colloid and Interface Science* **2011,** *354* (1), 94-99.

24. Vatta, L. L.; Sanderson, R. D.; Koch, K. R., Magnetic Nanoparticles: Properties and Potential Applications. *ChemInform* **2007,** *38* (4), no-no.

25. Butt, H.-J.; Graf, K.; Kappl, M., *Physics and chemistry of interfaces*. Wiley-VCH: Weinheim, 2006.

# CHAPTER NINE

## SUMMARY

The work presented here provided results on synthesis of and characterization of thin fluorescent polymer films with tunable properties, sensitive to the environment. The outlined results provide a basis for possible application of proposed methods of variation of fluorescent response in chemical sensing.

### 9.1. Synthesis of thin poly(glycidyl methacrylate films)

Thin film of poly(glycidyl methacrylate) (PGMA) fluorescently labeled with Rhodamine B (RhB) was used in this study as a main sensitive layer. Designed labeling method yielded approximately one RhB molecule per 311 PGMA monomeric units. Relatively thick crosslinked PGMA-RhB films were synthesized from the PGMA-RhB solution. Spin coating was used as a deposition technique and silicon wafers and glass slides were chosen as substrates.

The variation of the PGMA-RhB concentration used for the deposition allowed flexibility in the created film thickness in the tens to hundreds of nanometers range. Synthesized polymer films were characterized with AFM and ellipsometry. Spectrophotometry measurements as well as TIRF measurements confirmed that RhB molecules retained their fluorescent properties upon attachment to PGMA and subsequent PGMA-RhB polymer film deposition on the flat substrate. Both methods showed that the fluorescent characteristics of RhB molecules are not affected by film thickness.

### 9.2. Environmental sensitivity of the fluorescent emission of PGMA-RhB film

Ellipsometry measurements in the presence of saturated chloroform vapor vere performed usind specially designed transparent cuvette. These measurements revealed that the PGMA-RhB film is able to absorb solvent from the vapor phase. The relative thickness change upon liquid absorption was not varied for films of different thicknesses, suggesting the same crosslinking density of the PGMA-RhB film produced with the proposed deposition technique.

Using the TIRF apparatus sensitivity of the fluorescent emission of PGMA-RhB molecules was saturated chloroform vapor vas confirmed. As the PGMA-RhB film was subjected to chloroform vapor, prominent reversible and repeatable fluorescent emission intensity changes were observed. Emission intensity was found to have linear dependence on the thickness of the film, indicating that it is linearly proportional to the number of emitting RhB molecules.

### 9.3. Synthesis of nanoscale PGMA-RhB films

Ultrathin PGMA-RhB films (5 nm thick) were synthesized on the surface of silicon wafers and glass slides. To decrease the thickness of the synthesized polymer film the annealing time and temperature were decreased compared to the synthesis of thick PGMA-RhB films. The films were characterized using ellipsometry and AFM. It was found that the properties of these films are similar to the properties of the PGMA-RhB films with thickness in the order hundred nanometers.

After substantial decrease in the thickness the films were able to retain the ability to absorb solvents from the vapor phase. However, it was observed that thickness change during the vapor uptake is faster than for the thicker films, which can be used as advantage in sensing applications. Also, several different solvents (chloroform, acetone, toluene, cyclohexane and water) were used for the swelling measurements. The thickness change was found to be different for each solvent used in the study. From these measurements effective interaction parameter, which accounts for the affinity of the solvent for the polymer film, was calculated.

### 9.4. Quantum yield calculations

To find out the effect of the solvents, used as analytes for the detection on the fluorescent emission intensity of the RhB fluorescent unit of the PGMA-RhB quantum yield measurements were performed. Since the RhB itself does dissolve in some f the solvents used in the study Octadecyl Rhodamine B (R18) was used instead.

The measurements were done using relative quantum yield calculation method. The accuracy of this technique was confirmed by the measurements of the fluorescent material with known quantum yield prior to the measurements of R18. Obtained data was used in the investigations of the driving force for the relative intensity changes of the ultrathin PGMA-RhB films.

### 9.5. Fluorescent properties of nanoscale PGMA-RhB films

The fluorescent emission changes were recorded using spectrophotometry and TIRF measurements and also showed distinctive responses to the analytes. Both methods showed diverse fluorescent signal variations for the ultrathin PGMA-RhB layers exposed to the solvent. Such variations allow distinguishing between different analytes, confirming the sensitivity of the PGMA-RhB film to the environment. Quantum yield calculations for R18 and fluorescent emission changes in the vapor of different analytes were compared together in order to understand the driving force for the fluorescent emission intensity change during the solvent uptake. It was revealed that there is an effect of PGMA chain conformation of to the changes of fluorescent emission intensity of RhB fluorescent unit. This observation leaded to the conclusion, that grafting of non-fluorescent polymer to the surface of PGMA-RhB could influence the fluorescent response of the film.

### 9.6. Surface modification of ultrathin PGMA-RhB films for fluorescent property tuning

Thin grafted layers were deposited onto the surface of ultrathin PGMA-RhB films via dip coating. The deposited layers had low roughness and evenly covered the surface of the PGMA-RhB film. From the swelling experiments, solvent affinity to the polymers used in the study was calculated in terms of the effective interaction parameter. Calculations involving polymer-polymer interactions leaded to the estimation of the thickness of the interpenetration region in the two-layer modified PGMA-RhB films.

The spectrophotometry measurements for the modified PGMA-RhB films confirmed the hypothesis that non-fluorescent polymer films grafted to the surface of ultrathin fluorescent films influence the emission of the fluorophores embedded in the prime layer. Close studies on the nature of the fluorescent emission changes revealed complex influence of the solvent-dye and solvent-polymer interactions of the fluorescent emission of the modified films. Changes in the affinity of the PGMA-RhB film to the solvent, caused by the surface modification, strongly influenced the fluorescent response of the film.

Another important result was the uniqueness of the pattern of responses for each of the analytes (**Figure 10.1.**). This feature allows the use of presented response-tuning technique for substance identification applications.

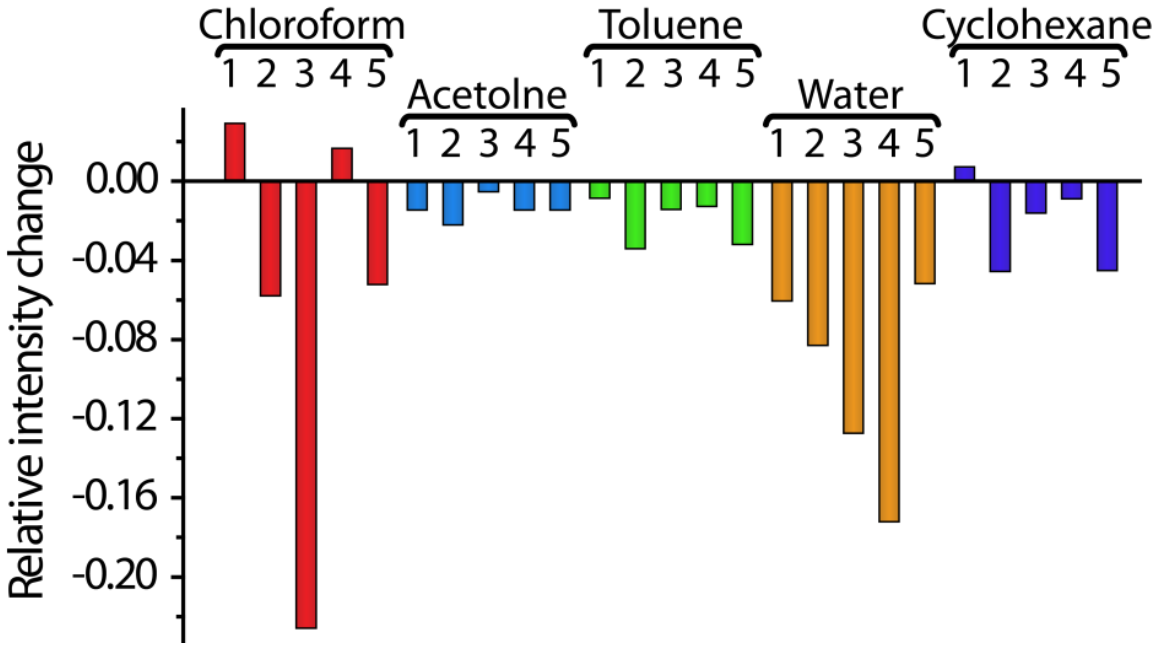


**Figure 10.1.**Relative intensity change grouped by the solvents used in the measurements. The fluorescent films used in the experiments were: 1 – PGMA-RhB, 2 – PGMA-RhB-P2VP, 3 – PGMA-RhB-PEG, 4 – PGMA-RhB-PAA, 5 – PGMA-RhB-PS.

## 9.7. Effect of the grafting layer properties on the fluorescent emission response of PGMA-RhB layer

To study effect of the grafting layer properties on the fluorescent emission response of PGMA-RhB film, layers with different grafting densities and mixed polymer layers of PS and P2VP at various ratios were grafted to the PGMA-RhB films. The thickness of the grafted layers as well as the ratio between PS and P2VP in mixed systems was well controlled by the time of annealing.

Fluorescent measurements in saturated vapors of chloroform, acetone, and cyclohexane showed that in addition to the variations in the relative intensity change by non-fluorescent polymer grafting, additional tuning of the signal from PGMA-RhB film can be achieved by attaching the polymers at various grafting densities and through the use of mixed polymer grafting.

## 9.8. Deposition of fluorescent PGMA-RhB films on nanoscale objects and rough surfaces

The fluorescent PGMA-RhB layer grafted to the surface of the silica nanoparticles. The amount of grafted polymer was consistent with that of the flat substrates after the same annealing process. After the PGMA-RhB grafting nanoparticles became highly fluorescent and showed sensitivity to the solvent in suspension.

The PEG and PAA layers were grafted to the nanoparticles, showing the tunability of the fluorescent nanoparticles surface chemistry. Attachment of iron oxide

nanoparticles to the PGMA surface provided magnetic properties to the nanoparticles in suspension, with almost no effect on the fluorescent properties of the PGMA-RhB layer. After the deposition of PEG on the surface of the nanoparticles, the suspension was stable in several solvents, producing unique fluorescent responses for each of them.

Polyethylene terephthalate (PET)fabric samples were coated with PGMA, showing high fluorescent emission. However, this emission was not tunable by non-fluorescent polymer grafting due to large quantities of the fluorescent polymer.

To achieve tunability of the fluorescent response nanoparticles were attached to the fibers surface, allowing the nanoparticle system to sense solvents in the vapor phase. Grafting several different polymers to the nanoparticles surface allowed the fluorescent emission response of the film to be tuned. The response patterns for the solvents have higher signal change amplitudes than those of the flat polymer films and are unique and distinguishable from each other.

### 9.9. Publications and presentations

Chyasnavichyus, M.; Tsyalkovsky, V.; Zdyrko, B.; Luzinov, I., Tuning Fluorescent Response of Nanoscale Film With Polymer Grafting. Macromolecular Rapid Communications 2012, 33 (3), 237-241.

M. Chyasnavichyus, V. Tsyalkovsky, B. Zdyrko, I. Luzinov, Environment sensitive fluorescent nanoparticles with tunable properties, Poster, The 242th ACS National Meeting, Denver, CO, 2011

M. Chyasnavichyus, V. Tsyalkovsky, B. Zdyrko, I. Luzinov, Tuning fluorescent response of ultrathin sensoric film with polymer grafting, Oral Presentation, The 242th ACS National Meeting, Denver, CO, 2011

M. Chyasnavichyus, V. Tsyalkovsky, B. Zdyrko, I. Luzinov, Fluorescent sensing array based on grafted polymer layers, Poster, The The 240th ACS National Meeting, Boston, MA, 2010

M. Chyasnavichyus, B. Zdyrko, V. Tsyalkovsky, V. Klep, I. Luzinov, Reactive fluorescent ultrathin films for sensor application, Poster, The 238th ACS National Meeting, Washington, DC, 2009

M. Chyasnavichyus, V. Tsyalkovsky, B. Zdyrko, V. Klep, I. Luzinov, Thin fluorescent films for sensor application, Poster, The 237th ACS National Meeting, Salt Lake City, UT, 2009

# APPENDIX

A MATLAB program was written to calculate the parameters of the film, its thickness and refractive index using the data collected by the ellipsometer.

The values collected by the ellipsometer, Ψ and Δ are bounded by the equation:

$$tan(\Psi)e^{i\Delta} = R_p/R_s \qquad \textbf{Eq.A.1}$$

where $\boldsymbol{R_p}$ and $\boldsymbol{R_s}$ can be calculated using Fresnel equations [1]. These equations include parameters describing the ellipsometer setup (angle of incidence and wavelength of the light beam) and parameters describing the properties of the film (its thickness, refractive index and absorption coefficient).

Two different cases are described in the present study. The first case is the case of the single layer polymer film deposited on the substrate with known properties. The structure of the film is shown schematically in **Figure A1**:

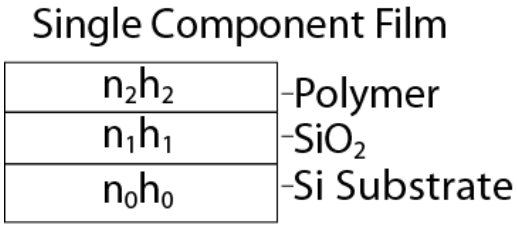


**Figure A1.** Schematic of the single component polymer film structure

For such structure only the thickness and refractive index of the polymer layer will be changing during the swelling of the polymer film. The properties of the silicon substrate are known (its thickness assumed to be infinite and the refractive index is

n=3.839+i0.014).The refractive index for silicon dioxide is n=1.457 and the thickness of this layer is measured prior to the polymer film deposition.

The optical properties of the polymer film in the dry state are measured using the technique described in the **Section 3.5.2.** Therefore, prior to the swelling measurements parameters of the system in the dry state were fully described.

Algorithm for the calculations of the parameters of the polymer film during the polymer film swelling for the films with thickness higher than 30 nm is presented in **Figure A2**.

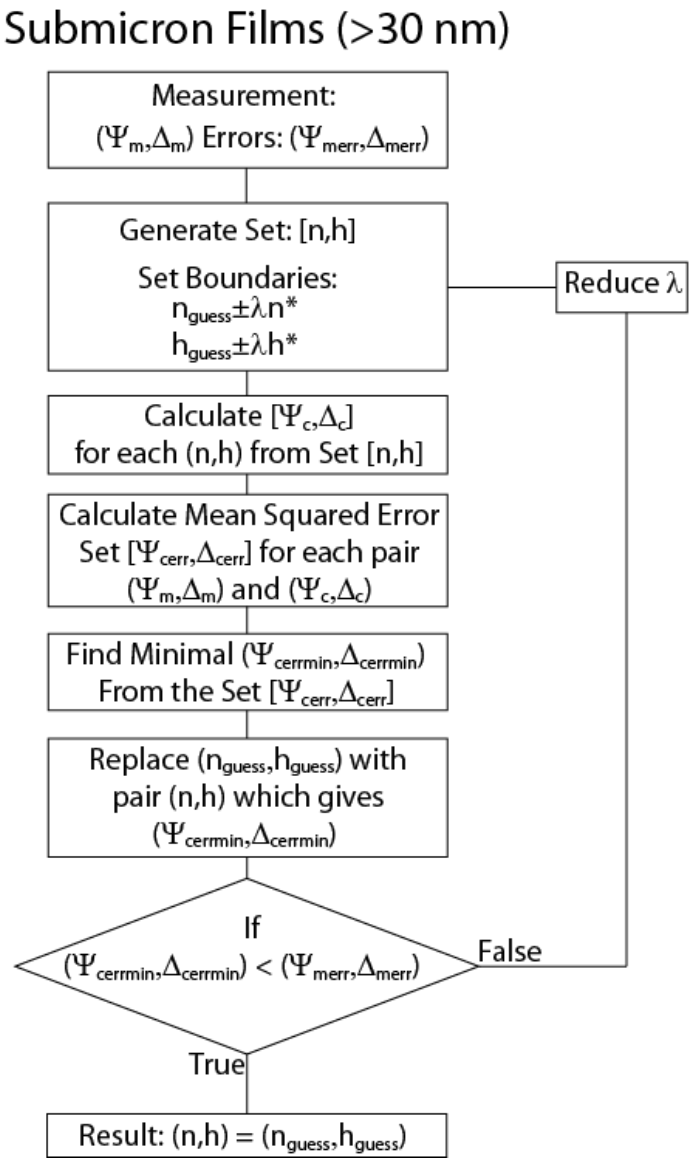


**Figure A2.** Algorithm for calculations of the thickness and refractive index of the polymer film during the swelling from ellipsometry data

The calculations were performed for each measured pair of $(\Psi, \Delta)$. The errors for $(\Psi, \Delta)$ measurements were taken from the program supplied with the device.

For the films with lower thickness errors of the measured $(\Psi, \Delta)$ were higher due to the decreased precision of the device in this region of thickness. To improve the results

of the calculations EMA (described in the **Section 5.3.4.1.**) was employed to find the thickness and refractive index of the polymer film. The algorithm with EMA embedded is presented in the **Figure A3**.

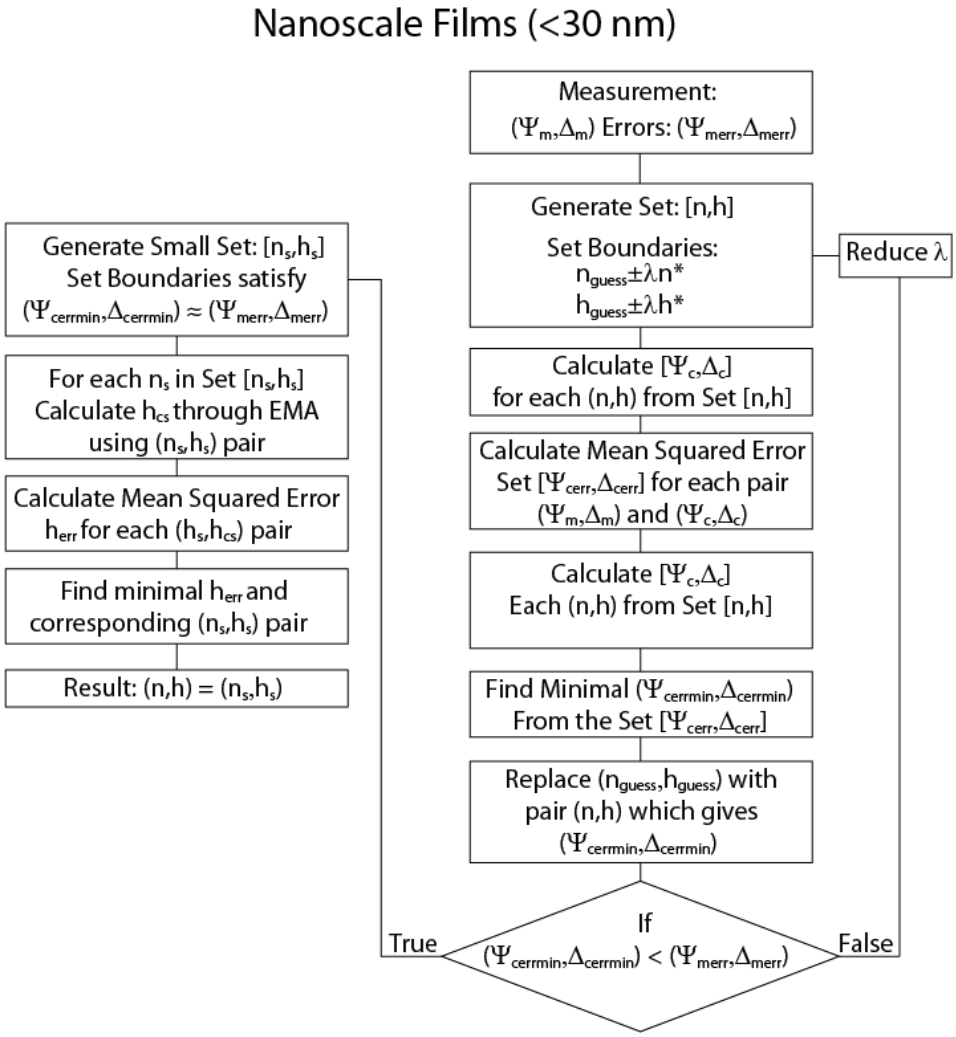


**Figure A3.** Algorithm for calculations of the thickness and refractive index of the ultrathin polymer film during the swelling from ellipsometry data

For the two layer polymer films proposed calculation technique cannot be used. **Figure A4** shows structure of two component polymer film. It can be seen from the figure, that during the swelling the four variables will change independently during the

polymer film swelling. Since the **Eq.A1** can be solved for only two independent variables, the full set of system's parameters cannot be found from ellipsometric measurements at any given state during the polymer film swelling.

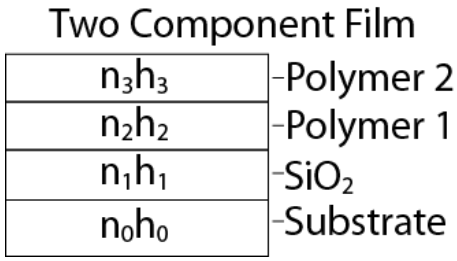


**Figure A4.** Schematic of the single component polymer film structure

However for the equilibrium state the parameters of the system can be estimated. For this estimation several assumptions are made. First assumption is that the swellings of polymer layers are independent from each other. Second assumption is that the swelling of the grafted polymer layer is the same as the swelling of single layer composed of this polymer. This means that the swelling ratio for the grafted polymer layer in equilibrium can be found using the method presented in **Figure A2.** Thus for the two component polymer film in the equilibrium state only the change of the base polymer layer thickness and refractive index becomes unknown and can be found using **Eq.A1.**

**References**

1. Fujiwara, H., *Spectroscopic ellipsometry : principles and applications*. John Wiley & Sons: Chichester, England; Hoboken, NJ, 2007.